SPRINGER SERIES ON CHEMICAL SENSORS AND BIOSENSORS 06

Series Editor G. Urban
Volume Editors G. Gerlach · K.-F. Arndt

Hydrogel Sensors and Actuators

Engineering and Technology

Springer

6
Springer Series on Chemical Sensors and Biosensors

Methods and Applications

Series Editor: G. Urban

Springer Series on Chemical Sensors and Biosensors

Series Editor: G. Urban

Recently Published and Forthcoming Volumes

Hydrogel Sensors and Actuators
Volume Editors: Gerlach G., Arndt K. -F.
Vol. 6, 2009

Piezoelectric Sensors
Volume Editors: Steinem C., Janshoff A.
Vol. 5, 2006

Surface Plasmon Resonance Based Sensors
Volume Editor: Homola J.
Vol. 4, 2006

Frontiers in Chemical Sensors
Novel Principles and Techniques
Volume Editors: Orellana G., Moreno-Bondi M. C.
Vol. 3, 2005

Ultrathin Electrochemical Chemo- and Biosensors
Technology and Performance
Volume Editor: Mirsky V. M.
Vol. 2, 2004

Optical Sensors
Industrial, Environmental and Diagnostic Applications
Volume Editors: Narayanaswamy R., Wolfbeis O. S.
Vol. 1, 2003

Hydrogel Sensors and Actuators

Volume Editors: Gerald Gerlach • Karl-Friedrich Arndt

With contributions by

K.-F. Arndt · K. Engelmann · U. Freudenberg · G. Gerlach · T. Götze
M. Guenther · F. Krahl · D. Kuckling · M. Nitschke · O. Okay
A. Richter · S. Richter · G. Steiner · G. A. Urban · M. Valtink
T. Wallmersperger · T. Weiss · P. Welzel · C. Werner · A. Zieris

Springer

Chemical sensors and biosensors are becoming more and more indispensable tools in life science, medicine, chemistry and biotechnology. The series covers exciting sensor-related aspects of chemistry, biochemistry, thin film and interface techniques, physics, including opto-electronics, measurement sciences and signal processing. The single volumes of the series focus on selected topics and will be edited by selected volume editors. The Springer Series on Chemical Sensors and Biosensors aims to publish state-of-the-art articles that can serve as invaluable tools for both practitioners and researchers active in this highly interdisciplinary field. The carefully edited collection of papers in each volume will give continuous inspiration for new research and will point to existing new trends and brand new applications.

ISSN 1612-7617
ISBN 978-3-540-75644-6 e-ISBN 978-3-540-75645-3
DOI: 10.1007/978-3-540-75645-3

Springer Heidelberg Dordrecht London New York

Library of Congress Control Number: 2009927282

© Springer-Verlag Berlin Heidelberg 2009
This work is subject to copyright. All rights are reserved, whether the whole or part of the material is concerned, specifically the rights of translation, reprinting, reuse of illustrations, recitation, broadcasting, reproduction on microfilm or in any other way, and storage in data banks. Duplication of this publication or parts thereof is permitted only under the provisions of the German Copyright Law of September 9, 1965, in its current version, and permission for use must always be obtained from Physica-Verlag. Violations are liable to prosecution under the German Copyright Law.
The use of general descriptive names, registered names, trademarks, etc. in this publication does not imply, even in the absence of a specific statement, that such names are exempt from the relevant protective laws and regulations and therefore free for general use.

Cover design: WMXDesign GmbH, Heidelberg

Printed on acid-free paper

Springer-Verlag Berlin Heidelberg (www.springer.com)

Series Editor

Prof. Dr. Gerald Urban

IMTEK - Laboratory for Sensors
Institute for Microsystems Engineering
Albert-Ludwigs-University
Georges-Köhler-Allee 103
79110 Freiburg
Germany
urban@imtek.de

Volume Editors

Prof. Dr. Gerald Gerlach

TU Dresden
Electrical and Computer Science Department
Solid State Electronics Laboratory
Helmholtzstr. 18
01069 Dresden
Germany
gerald.gerlach@tu-dresden.de

Prof. Dr. Karl-Friedrich Arndt

TU Dresden
Chemistry and Food Chemistry Department
Institute of Physical Chemistry and Electrochemistry
Bergstr. 66 B
01069 Dresden
Germany
karl-friedrich.arndt@chemie.tu-dresden.de

Springer Series on Chemical Sensors and Biosensors Also Available Electronically

For all customers who have a standing order to Springer Series on Chemical Sensors and Biosensors, we offer the electronic version via SpringerLink free of charge. Please contact your librarian who can receive a password or free access to the full articles by registering at:

springerlink.com

If you do not have a subscription, you can still view the tables of contents of the volumes and the abstract of each article by going to the SpringerLink Homepage, clicking on "Chemistry and Materials Science", under Subject Collection, then "Book Series", under Content Type, and finally by selecting Springer Series on Chemical Sensors and Biosensors.

You will find information about the series at springer.com using the search function.

Preface

Polymer gels, which have both solid- and liquid-like properties, are an astonishing and fascinating material. At a first glance, they are just composed of a cross-linked polymer network and interstitial fluid. The ability of cross-linked water-soluble polymers to absorb large amounts of water and to form hydrogels makes them ideal vehicles for the storage or transport of active ingredients. Polyelectrolyte gels have been developed as superabsorbent materials in diapers and for moisture control. These gels can contain over 99% water. The water uptake, the swelling process, is associated with a respective volume change. Hydrogels became part of our workaday life. Applications of hydrogels have become extraordinarily widespread, notably in food processing, cosmetics, pharmaceuticals, bio-technology, agriculture, and paint manufacturing.

Apart from the swelling, two other properties make hydrogels attractive.

First, a strong volume change can be excited by a large spectrum of different physical and chemical factors such as temperature, electrical voltage, pH, concentration of organic compounds in water, and salt concentrations. The possibility of a first-order volume phase transition in gels was suggested by K. Dušek and D. Patterson in 1968 based on an analysis of Flory–Rehner theory. It took ten years for the phenomenon to be experimentally observed after prediction. It was found by T. Tanaka that, when a critical amount of an organic solvent was added to a water-swollen poly(acrylamide) gel, the gel collapses. Many gels of synthetic and natural polymers have been studied. Subsequent experiments showed that a volume phase transition (swelling/collapse) could also be brought about by changes in other environmental parameters such as pH, ionic strength, and temperature.

Second, volume change due to these physical or chemical stimuli is reversible. Hence, hydrogels are chemomechanical transducers converting chemical energy into mechanical energy and vice versa. This offers a huge potential for new sensor and actuator principles especially for applications in all fields where aqueous solutions play a decisive role, e.g., in process engineering, fluidics, chemistry, cell biology, and drug delivery, and makes them real "smart" materials. Artificial muscles are another field where ionic hydrogels are getting more and more attention.

Most of the authors of this book are scientists from the Technische Universität Dresden, having been involved in the "hydrogel business" for many years. One of

the roots for that was the Collaborative Research Center "Reactive Polymers" (spokesman: Prof. Hans-Jürgen Adler) established in 1996 at the TU Dresden and funded by the German Research Foundation (DFG Deutsche Forschungsgemeinschaft). One of the foci of this centre was to investigate the chemistry and the physics of hydrogels, their synthesis, and their integration into engineering solutions. The close collaboration between chemists, physicists, and engineers was the prerequisite to get a profound understanding of the complex interactions within smart hydrogels and their prospects for new sensor and actuator systems.

Undoubtedly, a single institution is not capable of dealing with all aspects of such a complex matter. This is the reason why we were strongly interested in enlisting colleagues from the Universities of Stuttgart and Freiburg as well as from the Max Bergmann Centre, Dresden, as experts for several aspects with important relevance to hydrogel sensors and actuators. We are deeply indebted to them.

The book is organized in the following manner. After a short introduction of the general properties of hydrogels, Chap. 2 discusses the fabrication of hydrogels. Afterward, Chap. 3 introduces the thermodynamic processes down to the molecular level taking place in hydrogels during swelling and shrinkage. Since Chaps. 2 and 3 describe the complex chemical, physical, and physicochemical properties of hydrogels, their number of pages is larger than that of the following chapters. We did not take them to pieces to show the interactions and relationships in its complexity, but we structured the text in subchapters such that each of them has its own reference list.

Based on the understanding of the chemical and physical effects, the chemo-electro-mechanical coupling in hydrogels will be presented in Chap. 4. To predict the functioning of hydogel-based devices, models are needed to describe the complexity of occurring interactions and to enable the simulation of technical devices. The following three chapters (Chaps. 5–7) focus on the application of hydrogels in chemical and biosensors and for actuators. Finally, Chap. 8 shows a particular application of hydrogels in cell biology as cell culture carriers.

The editors of this book hope that the contents depict the most recent progress in hydrogel research for sensor and actuator devices. As it can be seen, it still needs a lot of efforts to bridge the gap between state-of-the-art research and existing demands for a future market introduction. However, there are plenty of ideas to overcome the still remaining problems. Let the book be an inspiration to all the colleagues involved in hydrogel research and development!

We thank all our coauthors who have contributed their comprehensive knowledge with their particular competence to this book. We also thank those companies and institutions that allowed us to use figures and material and which are named in the captures of the individual figures. Furthermore, we thank Springer-Verlag and in particular Thomas Lehnert and Ulrike Butz for the cordial cooperation and also for the patience when faced with repetitive delays due to the authors' workload. We are deeply grateful to the Springer staff for their support during the entire process, from the first idea all the way through to the final book.

Dresden, January 2009

Gerald Gerlach
Karl-Friedrich Arndt

Contents

General Properties of Hydrogels

O. Okay

Abstract In the application areas of polymer hydrogels, precise information on their molecular constitution as well as their elastic properties is required. Several interesting molecular features control the elastic properties of the hydrogels. In this chapter, we describe general properties of hydrogels formed by free-radical cross-linking copolymerization of vinyl/divinyl monomers in aqueous solutions. Special attention is paid to the relationships between the formation conditions of hydrogels and their properties such as swelling behaviour, elastic modulus, and spatial inhomogeneity. New developments achieved in the design of hydrogels with a good mechanical performance and a fast response rate is also presented.

Keywords Hydrogels • Elasticity • Swelling • Inhomogeneity

Contents

Abbreviations

AAm	Acrylamide
AMPS	Na sodium salt of 2-acrylamido-2-methylpropane sulfonic acid
DMSO	Dimethylsulfoxide

O. Okay
Department of Chemistry, Istanbul Technical University, Istanbul, Turkey
e-mail: okayo@itu.edu.tr

G. Gerlach and K.-F. Arndt (eds.), *Hydrogel Sensors and Actuators*,
Springer Series on Chemical Sensors and Biosensors 6,
DOI: 10.1007/978-3-540-75645-3_1, © Springer-Verlag Berlin Heidelberg 2009

FH	Flory–Huggins
MBAAm	*N*,*N*-methylene bisacrylamide
PAAc	Poly(acrylic acid)
PAAm	Poly(acrylamide)
PDMAAm	Poly(*N*,*N*-dimethylacrylamide)
PEG-300	Poly(ethylene glycol) of molecular weight 300 g mol^{-1}
PNIPAAm	Poly(*N*-isopropyl acrylamide)
TBA/AAm	Poly(*N*-*t*-butylacrylamide-co-AAm)

Symbols

C_o	Initial monomer concentration (g monomer / 100 mL solution)
f	Effective charge density of the network
G_r	Reduced elastic modulus
G_o	Modulus of elasticity after gel preparation
N_s	Number of segments between two successive cross-links
Q_v	Volume swelling ratio (swollen gel volume / dry gel volume)
$R_{ex,q}$	Excess scattering intensity at the scattering vector q
V	Gel volume at a given degree of swelling
V_{eq}	Equilibrium swollen normalized gel volume
V_o	Gel volume in after-preparation state
V_r	Normalized gel volume
V_{sol}	Equilibrium swollen gel volume in solution
V_w	Equilibrium swollen gel volume in water
x_i	Ionic monomer mole fraction in comonomer feed
α	Linear deformation ratio
ΔG_{el}	Gibbs free energy of elastic deformation
ΔG_{ion}	Ionic contribution to Gibbs free energy
ε_{xl}	Cross-linking efficiency of cross-linker
φ_2	Volume fraction of cross-linked polymer in gel
φ_2^0	Volume fraction of cross-linked polymer after gel preparation
ν_c	Effective cross-link density

1 Introduction

Hydrophilic gels called hydrogels are cross-linked materials absorbing large quantities of water without dissolving. Softness, smartness, and the capacity to store water make hydrogels unique materials (Tanaka 1981; Shibayama and Tanaka 1993). The ability of hydrogels to absorb water arises from hydrophilic functional groups attached to the polymer backbone while their resistance to dissolution arises

from cross-links between network chains. Water inside the hydrogel allows free diffusion of some solute molecules, while the polymer serves as a matrix to hold water together. Another aspect of hydrogels is that the gel is a single polymer molecule, that is, the network chains in the gel are connected to each other to form one big molecule on macroscopic scale. It is natural to expect that the conformational transitions of the elastically active network chains become visible on the macroscopic scale of hydrogel samples. The gel is a state that is neither completely liquid nor completely solid. These half liquid-like and half solid-like properties cause many interesting relaxation behaviours that are not found in either a pure solid or a pure liquid. From the point of view of their mechanical properties, the hydrogels are characterized by an elastic modulus which exhibits a pronounced plateau extending to times at least of the order of seconds, and by a viscous modulus which is considerably smaller than the elastic modulus in the plateau region (Almdal et al. 1993).

Hydrogels may exhibit drastic volume changes in response to specific external stimuli, such as the temperature, solvent quality, pH, electric field, etc. (Dusek and Patterson 1968; Tanaka 1978). Depending on the design of the hydrogel matrices, this volume change may occur continuously over a range of stimulus level, or, discontinuously at a critical stimulus level. The volume transition behaviours of hydrogels received considerable interest in the last three decades and large parts of the work have been collected in different reviews (Shibayama and Tanaka 1993; Khokhlov et al. 1993).

Polymeric hydrogel networks may be formed by various techniques, however the most common synthetic route is the free-radical cross-linking copolymerization of a hydrophilic non-ionic monomer such as acrylamide (AAm) with a small amount of a cross-linker, e.g., *N*,*N*'-methylenebis(acrylamide) (MBAAm). In order to increase their swelling capacity, an ionic comonomer is also included into the reaction mixture. Since the monomers for hydrogel preparation are usually solid at the usual polymerization temperature, it is necessary to carry out the polymerization reactions in an aqueous solution. Hydrogel structure and, thus, the hydrogel properties are closely related to the conditions under which the hydrogels are formed, i.e., the cross-linker concentration, the initial degree of dilution of the monomers and the chemistry of the units building the network structure. The understanding of the formation mechanism of hydrogels under various experimental conditions is of great interest to predict their physical properties.

2 Swelling and Elasticity of Hydrogels

The equilibrium swelling degree and the elastic modulus of hydrogels depend on the cross-link and charge densities of the polymer network as well as on the cross-linked polymer concentration after the gel preparation. Although the theories predict the swelling properties and the elastic behavior of hydrogels formed under various conditions, the agreement between theory (see Chap. 3 Sect. 1.2) and experiments is only qualitative. Figure 1 illustrates the characteristic features of

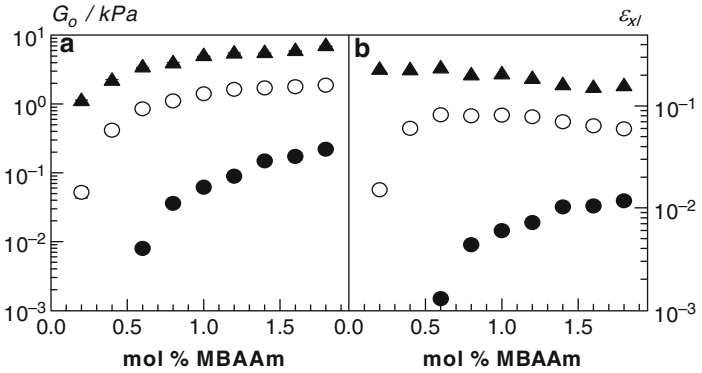

Fig. 1 The elastic modulus G_o of PAAm hydrogels after preparation (**a**) and the cross linking efficiency ε_{xl} (**b**) shown as a function of MBAAm concentration. Initial monomer concentration $C_o = 3$ (*filled circle*), 5 (*open circle*), and 7 w/v % (*filled triangle*). Reprinted from Orakdogen and Okay (2006a) with kind permission of Springer Science + Business Media

poly(acrylamide) (PAAm) hydrogels prepared from AAm and MBAAm in aqueous solutions (Kizilay and Okay 2003a; Orakdogen and Okay 2006a). In Fig. 1a, the modulus of elasticity after the gel preparation, G_o, is plotted against the cross-linker (MBAAm) content for three series of gels prepared at various initial monomer concentration C_o. Hydrogels exhibit elastic moduli in the range of 0.01 to 10 kPa, which are much smaller than the calculated values from their cross-linker contents. The initial period of the G_o versus MBAAm % plots can be used to estimate the lower limit of the cross-linker concentration required for the onset of gelation. The best-fit curves through the G_o versus % MBAAm data intersect with the positive abscissa at 0.03, 0.19, and 0.55 mol % MBAAm for $C_o = 7$, 5, and 3 %, respectively (Orakdogen and Okay 2006a). Thus, the larger the dilution degree of the reaction system, the higher is the threshold concentration of MBAAm for the formation of an infinite network. Figure 1b shows cross-linker concentration dependence of the cross-linking efficiency ε_{xl} of MBAAm, that is the fraction of MBAAm forming effective cross-links. ε_{xl} is less than 20% and, it further decreases below 1% as the initial monomer concentration is decreased. This is a consequence of the increase of probability of cyclization and multiple cross-linking reactions as the initial monomer concentration decreases (Funke et al. 1998).

The polymer network concentration at the state of gel preparation (index o), represented by the cross-linked polymer volume fraction φ_2^0, also alters significantly the hydrogel structure and, in turn, alters the hydrogel properties. The effect of φ_2^0 on the hydrogel properties is illustrated in Fig. 2 for polyacrylic acid (PAAc) hydrogels prepared at various φ_2^0 (Yazici and Okay 2005). In Fig. 2a, the modulus of elasticity G_o and the effective cross-link density ν_c of PAAc hydrogels are plotted against φ_2^0. Figure 2b shows φ_2^0 dependence of the swelling ratio of PAAc gels in terms of the volume swelling ratio Q_v (volume of swollen gel in water / volume of dry gel). G_o increases from 1.4 kPa to 50 kPa as φ_2^0 is increased. The inset to Fig. 2a shows that the modulus data can be described by a power law

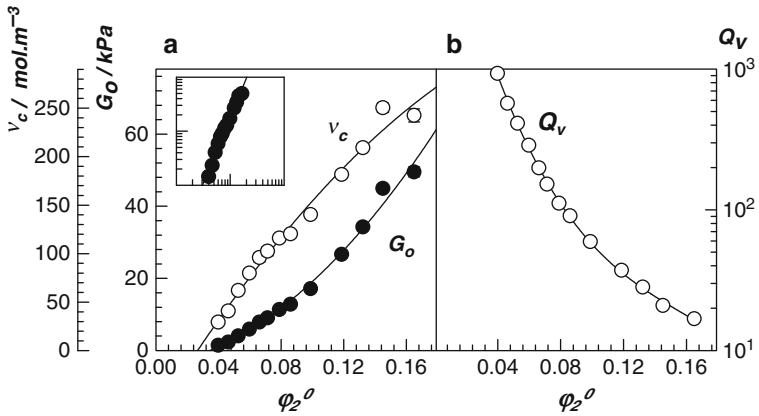

Fig. 2 The modulus of elasticity G_o, the effective crosslink density v_c (**a**) and the volume swelling ratio Q_v of PAAc hydrogels in water (**b**) as function of the polymer network concentration φ_2^0; 1.2 mol % MBAAm. The inset to Fig. 2a shows a double logarithmic G_o vs. φ_2^0 plot. Reprinted from Yazici and Okay (2005) with kind permission from Elsevier

$G_0 \propto \left(\varphi_2^0\right)^x$ where $x = 2.1 \pm 0.1$. The exponent is much larger than the linear dependence ($x = 1$) predicted by the theory of rubber elasticity (Flory 1953; Treloar 1975), and indicates existence of non-idealities during the gel formation process. Increasing number of wasted MBAAm molecules in cycles on raising the dilution of the reaction solution explains this discrepancy (Naghash and Okay 1996). Indeed, ν_c is an increasing function of φ_2^0 (Fig. 2a), that is, the higher the initial monomer concentration, the larger the effective cross-link density of the hydrogels and the smaller their swelling capacity (Fig. 2b).

Increasing number of ionic groups in hydrogels is known to increase their swelling capacities. This is mainly due to the simultaneous increase of the number of counterions inside the gel, which produces an additional osmotic pressure that swells the gel (Flory 1953). The excess swelling over the swelling of the corresponding non-ionic hydrogels can be suppressed with increasing salt concentration in the external solution, which decreases the concentration difference of the counterions between the inside and outside the gel phase. Figure 3 illustrates the typical swelling behaviour of ionic PAAm hydrogels of various charge densities in water and in aqueous NaCl solutions (Durmaz and Okay 2000). The ionic comonomer used in the hydrogel preparation is sodium salt of 2-acrylamido-2-methylpropane sulfonic acid (AMPS Na). AMPS Na units dissociate completely over the entire pH range so that AMPS Na containing hydrogels exhibit pH-independent swelling. Increase of the AMPS Na content from 0 to 80 mol % results in a 27-fold increase in the hydrogel volume in water. In 1.0 M NaCl solution, the swelling ratio is almost independent on the ionic group content due to screening of charge interactions within the hydrogel.

Since ionic hydrogels are highly swollen in water, their swelling equilibrium is mainly determined by the mixing entropy of the counterions, which is balanced by the gel´s rubberlike elasticity. According to the theory of rubber elasticity of

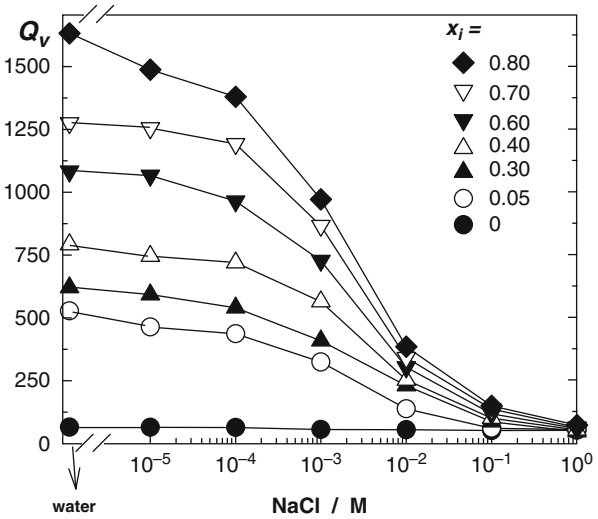

Fig. 3 Equilibrium volume swelling ratio Q_v of ionic PAAm hydrogels shown as function of the NaCl concentration in the external solution;1.2 mol % MBAAm. AMPS Na mole fraction x_i in the comonomer mixtures is indicated. Reprinted from Durmaz and Okay (2000) with kind permission from Elsevier

Gaussian chains (Flory 1953), the Gibbs free energy of elastic deformation ΔG_{el} scales with the deformation ratio as

$$\Delta G_{el} \approx N_s^{-1} \alpha^2, \tag{1}$$

where N_s is the number of segments between two successive cross-links, and α the linear deformation ratio. α is related to the normalized gel volume V_r by the equation $\alpha = (V/V_o)^{1/3} = V_r^{1/3}$, where V is the gel volume at a given degree of swelling and V_o is the gel volume in the reference state, i.e., at the state after preparation. On the other hand, the existence of fixed ions on the network chains results in an unequal distribution of mobile counterions between the inside and outside of the gel. The ionic contribution to the Gibbs free energy ΔG_{ion} may be written as

$$\Delta G_{ion} \approx f \ln\left(f \varphi_2^0/\alpha^3\right), \tag{2}$$

where f is the effective charge density of the network (Flory 1953). Balancing the two opposite free energy contributions represented by ΔG_{el} and ΔG_{ion} by minimizing their sum with respect to α, one obtains[1]

[1] To minimize the energy function, one needs to take the derivatives of the energy contributions with respect to α, and set the sum of the derivatives to zero. Thus, since $\partial \Delta G_{el}/\partial \alpha \approx N_s^{-1} \alpha$ and $\partial \Delta G_{ion}/\partial \alpha \approx f/\alpha$, one obtains $\alpha \approx (f N_s)^{1/2}$, i.e., (3) in the text.

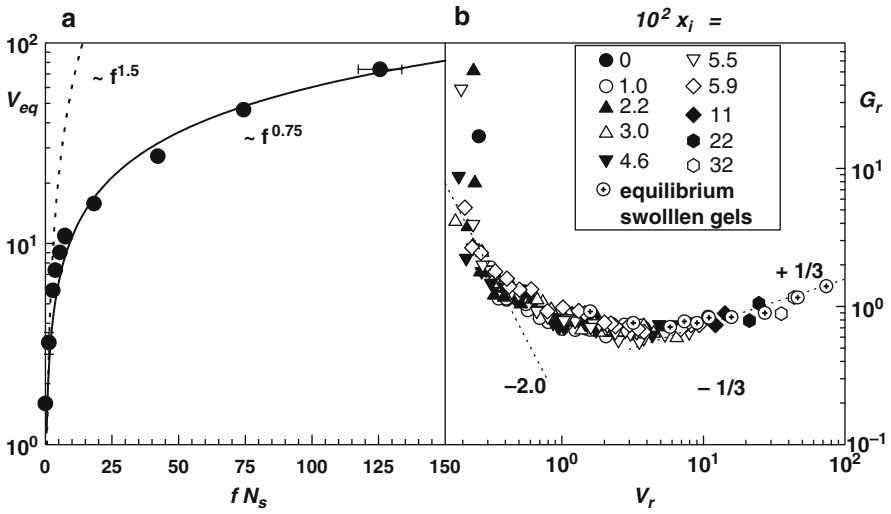

Fig. 4 The equilibrium swollen normalized gel volume V_{eq} of ionic PNIPAAm hydrogels as function of the number fN_s of charges per network chain (see (3)) (**a**) Reduced modulus G_r of ionic PNIPAAm hydrogels as function of the normalized gel volume V_r (**b**) The mole fractions x_i of AMPS Na are indicated in the figure. Reprinted from Gundogan et al. (2002) with permission of American Chemical Society

$$V_{eq} \approx (fN_s)^{3/2}, \tag{3}$$

which indicates a scaling parameter of 3/2 between the equilibrium swollen normalized gel volume V_{eq} and the number of charges per network chain fN_s.

Figure 4a shows the double-logarithmic plot of V_{eq} against fN_s. Experimental data are for poly(*N*-isopropyl acrylamide) (PNIPAAm) hydrogels prepared in the presence of the ionic comonomer AMPS Na (Gundogan et al. 2002). The dotted curve in the Figure represents the prediction of (3), i.e., Flory–Huggins (FH) theory with a scaling parameter of 3/2. The solid curve is the best fitting curve to the experimental swelling data, which gives a scaling relation $V_{eq} \approx (fN_s)^{3/4}$. The scaling parameter 3/4 is much smaller than the predicted value of 3/2 of the FH theory. An exponent between 0.6 and 0.8 has been reported for both weak and strong polyelectrolyte hydrogels equilibrium-swollen in water (Durmaz and Okay 2000; Silberberg-Bouhnik et al. 1995; Bromberg et al. 1997; Melekaslan and Okay 2000).

The discrepancy between theory and experiment is related to the non-Gaussian behaviour of fully swollen hydrogels in water. The theory (3) assumes that the polymer network is a collection of Gaussian chains, which can be extended to infinity. However, the network chains in the equilibrium swollen ionic hydrogels as given in Fig. 4a are three to nine times as elongated as in the dry state. At such high swelling ratios, deviation from the Gaussian statistics may appear due to the finite extensibility of the network chains. A further evidence for the non-Gaussian behaviour of the network chains in the swollen hydrogels comes from the elasticity

data. In Fig. 4b, the dependence of the reduced modulus G_r of ionic PNIPAAm hydrogels is shown as a function of the normalized gel volume V_r (Gundogan et al. 2002). The reduced modulus G_r is defined as the ratio of the elastic modulus of the gel at a given degree of swelling $Q_v = 1/\varphi_2$ to that one of the same gel after its preparation. G_r is given for a network of Gaussian chains by (Flory 1953)

$$G_r = G(\varphi_2)/G\left(\varphi_2^o\right) = {V_r}^{-1/3}. \quad (4)$$

However, Fig. 4b shows that the dependence of the reduced modulus on the gel volume cannot be described by a single scaling exponent. For the gel volumes V_r of less than 0.4, the reduced modulus G_r decreases sharply with increasing volume V_r. The rapid decrease of G_r with increasing gel volume V_r in the first regime is usually interpreted as the transition of the polymer from the glassy to the rubbery state by addition of solvent (Gundogan et al. 2002). In the range of the gel volume V_r between 0.4 and 3.5, the slope of G_r versus V_r plot is -0.32, close to the theoretical value of $-1/3$. Thus, PNIPAAm hydrogels in this regime behave as Gaussian. For gel volumes larger than 3.5, the reduced modulus G_r starts to increase with increasing gel volume with a slope of 0.22 which is an indication of the limited extensibility of the network chains and is connected with the high stretching of the network chains.

Swelling behaviour of hydrophobically modified hydrogels has also received considerable attention due both to fundamental and to technological interests (Hirotsu 1993). Such hydrogels generally exhibit a temperature sensitivity, which is associated with the temperature dependence of hydrogen bonding and hydrophobic interactions (Hirotsu 1993; Arndt et al. 2001). A phenomenon called reentrant swelling transition was also observed in hydrophobically modified hydrogels immersed in aqueous solutions of organic solvents or linear polymers (Katayama et al. 1984; Melekaslan and Okay 2001; Okay and Gundogan 2002). In such a transition, the gel first collapses and then reswells if a particular external parameter such as the organic solvent or linear polymer concentration is continuously varied. As a consequence, the organic solvent (or linear polymer) first flows from the gel to the solution phase but then reenters the gel phase at higher concentrations. Examples of such transitions are illustrated in Fig. 5 for PNIPAAm, poly(*N*,*N*-dimethylacrylamide) (PDMAAm), and poly(*N*-*t*-butyl-acrylamide-co-AAm) (TBA/AAm) hydrogels immersed in aqueous solutions of poly(ethylene glycol) of molecular weight 300 g mol^{-1} (PEG-300), acetone, and dimethylsulfoxide (DMSO), respectively (Melekaslan and Okay 2001; Orakdogen and Okay 2006b; Ozmen and Okay 2003). The competing attractive forces between the gel components are responsible for the reentrant transition behavior of hydrophobically modified hydrogels.

3 Inhomogeneity of Hydrogels

Another non-ideal feature of hydrogels is the so-called spatial gel inhomogeneity (Shibayama 1998; Bastide and Candau 1996). In contrast to ideal gels with a homogeneous distribution of cross-links, hydrogels always exhibit an inhomogeneous

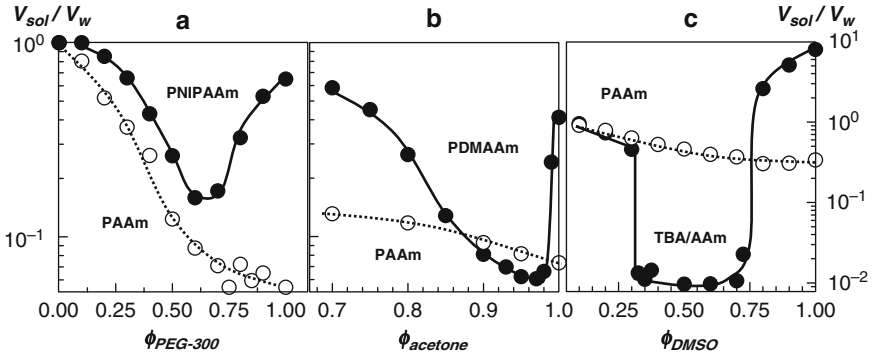

Fig. 5 Variation of the volume ratio V_{sol}/V_w (equilibrium swollen gel volume in solution / equilibrium swollen gel volume in water) of PNIPAAm, PDMAAm, and TBA/AAm (60/40 by mole) hydrogels (*filled symbols*) and PAAm hydrogels (*open symbols*) with the volume fraction Φ of PEG-300, acetone, and DMSO in the outer aqueous solution. (**a**) reproduced from Melekaslan and Okay (2001) with permission from Wiley-VCH Verlag GmbH & Co. KGaA; (**b, c**) reproduced from Orakdogen and Okay (2006b) and Ozmen and Okay (2003) with permissions from Elsevier

cross-link density distribution, known as the spatial gel inhomogeneity. The spatial inhomogeneity is undesirable because it dramatically reduces the optical clarity and strength of hydrogels. Since the gel inhomogeneity is closely connected to the spatial concentration fluctuations, scattering methods such as light scattering, small angle X-ray scattering, and small angle neutron scattering have been employed to investigate the spatial inhomogeneities. The gel inhomogeneity can be manifested by comparing the scattering intensities from the gel and from a semi-dilute solution of the same polymer at the same concentration (Lindemann et al. 1997). The scattering intensity from gels is always larger than that from the polymer solution. The excess scattering over the scattering from polymer solution is related to the degree of the inhomogeneities in gels.

In general, the spatial inhomogeneity increases with the gel cross-link density due to the simultaneous increase of the extent of network imperfections producing regions more or less rich in cross-links. On the other hand, the inhomogeneity decreases with the ionization degree of gels due to the effects of the mobile counter ions, electrostatic repulsion and the Donnan potential (Kizilay and Okay 2003b). The degree of swelling of gels subjected to scattering measurements also affects the scattering intensities (Kizilay and Okay 2004; Gundogan et al. 2004; Orakdogen et al. 2005). The scattering intensity at low scattering vectors is enhanced as the swelling degree is increased. This behaviour was interpreted as the enhancement of the difference of polymer concentration between the more and the less cross-linked regions. The initial monomer concentration used in the gel preparation significantly affects the scattering intensities (Kizilay and Okay 2003a, 2004; Gundogan et al. 2004). An inflection point was observed in the excess scattering versus monomer concentration plot, at which the inhomogeneity attained a maximum value.

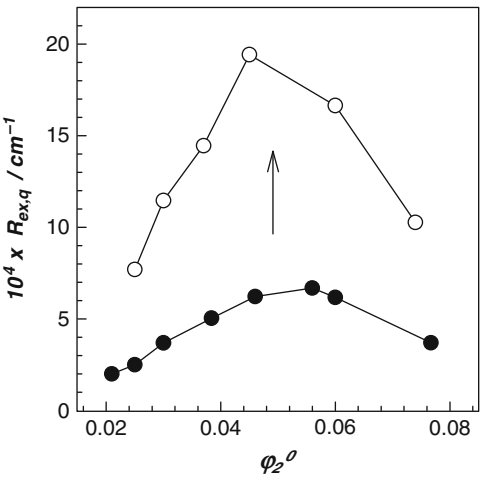

Fig. 6 Excess scattering intensities from PAAm hydrogels $R_{ex,q}$ measured at the scattering vector $q = 1 \times 10^{-2}$ nm $^{-1}$ shown as function of φ_2^0. The filled and open symbols represent results of measurements after gel preparation and after equilibrium swelling in water, respectively; 1.5 mol % MBAAm. Reprinted from Kizilay and Okay (2004) with permission from Elsevier

Figure 6 shows excess scattering intensity $R_{ex,q}$ plotted as a function of φ_2^0 for PAAm hydrogels with 1.5 mol % MBAAm cross-linker (Kizilay and Okay 2004). $R_{ex,q}$ significantly increases as the gel swells beyond its swelling degree after preparation. Moreover, PAAm gels at both states exhibit a maximum scattering intensity at a critical polymer network concentration. As the monomer concentration is increased, the effective density of cross-links also increases (Fig. 1), so that the spatial inhomogeneity becomes larger. Opposing this, increasing monomer concentration, i.e., decreasing the degree of swelling of the gels after preparation reduces progressively the concentration difference between densely and loosely cross-linked regions of gel, so that the apparent inhomogeneity decreases. The interplay of these two opposite effects determines the inhomogeneity in PAAm gels and results in the appearance of a maximum gel inhomogeneity at a critical monomer concentration.

4 Hydrogels with Improved Properties

The design of hydrogels with a good mechanical performance is of crucial importance in many existing and potential application areas of soft materials. Several attempts, such as topological gels and double network gels, have been made in recent years to design hydrogels with even better mechanical performance (Tanaka et al. 2005). The nanoscale dispersion of layered silicates or clays in polymer networks is one of the techniques offering significant enhancements in the material properties of hydrogels. Haraguchi et al. prepared such nanocomposite hydrogels starting from AAm-based monomers together with Laponite as a physical cross-linker, replacing the traditional chemical cross-linkers (Haraguchi and Takehisa

2002). Laponite, a synthetic hectorite clay, when suspended in water, forms disc-like particles with a thickness of 1 nm, a diameter of about 25 nm, and a negative surface charge density stabilizing dispersions in water. Formation of a cross-linked polymer network using a small amount of Laponite indicates that these nanoparticles act as a multifunctional cross-linker with a large effective functionality (Okay and Oppermann 2007).

A fast response of hydrogels to the external stimuli is also a requirement in many application areas of these materials. However, the kinetics of hydrogel volume change involves absorbing or desorbing solvent by the polymer network, which is a diffusive process. This process is slow and even slower near the critical point of volume phase transition (Shibayama and Tanaka 1993). Increasing the response rate of hydrogels has been one of the challenging problems in the last 25 years (Arndt Schmidt et al. 2004). In order to increase their response rate, several techniques were proposed (see also Chap. 3 Sect. 3.2):

- Submicrometer-sized gel particles: Since the rate of response is inversely proportional to the square of the size of the gel (Shibayama and Tanaka 1993), small hydrogel particles respond to the external stimuli more quickly than bulk gels (Oh et al. 1998).
- Gels having dangling chains: Attachment of linear polymer chains on the gel particles is another approach to increase the response rate of hydrogels (Yoshida et al. 1995). Dangling chains in a gel easily collapse or expand upon an external stimulus because one side of the dangling chain is free.
- Macroporous gels: Another technique to obtain fast-responsive hydrogels is to create voids (pores) inside the hydrogel matrix, so that the response rate becomes a function of the microstructure rather than the size or the shape of the gel samples (Okay 2000). For a polymer network having an interconnected pore structure, absorption or desorption of water occurs through the pores by convection, which is much faster than the diffusion process that dominates the non-porous hydrogels.

The basic technique to produce macroporous hydrogels involves the free-radical cross-linking copolymerization of the monomer-cross-linker mixture in the presence of an inert substance (the diluents), which is soluble in the monomer mixture (Okay 2000). In order to obtain macroporous structures, a phase separation must occur during the course of the network formation process so that the two-phase structure formed is fixed by the formation of additional cross-links. After polymerization the diluent was removed from the network, leaving a porous structure within the highly cross-linked polymer network. Thus, the inert diluent acts as a pore-forming agent and plays an important role in the design of the pore structure of cross-linked materials. Another technique to create a macroporous network structure is the use of inert templates in the preparation of hydrogels. By this technique, the polymer formation reactions are carried out in the presence of templates; a macroporous structure in the final hydrogel matrix appears after extraction of template materials. For example, by the cryogelation technique, the polymer formation reactions are carried out below the bulk freezing temperature of the

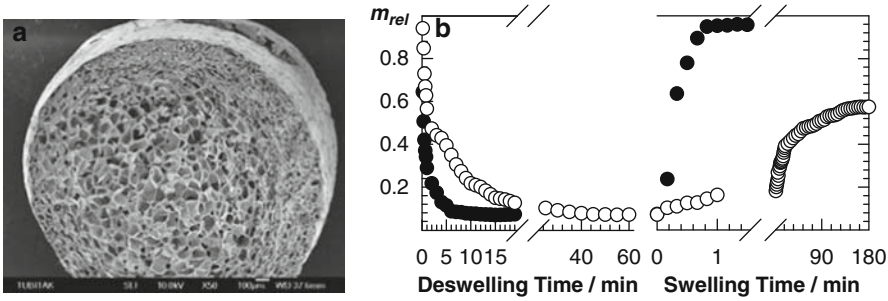

Fig. 7 (**a**) SEM of PAAm network prepared by cryogelation at −18 C. $C_o = 3$ w/v %; 1.2 mol % MBAAm; magnification 50; scaling bar 100 μm. Reprinted from (Ozmen et al.2007) with permission from Taylor & Francis Group. (**b**) Swelling and deswelling kinetics of PAAm hydrogel in water and in acetone, respectively, shown as variation of the relative weight swelling ratio m_{rel} with time of swelling or deswelling. $C_o = 3$ w/v %; 1.2 mol % MBAAm; polymerization temperature − 18 °C (*filled circle*) and + 21 °C (*open circle*). Reprinted from Dinu et al. (2007) with permission from Elsevier

reaction system (Lozinsky 2002). The essential feature of such reaction systems is that the monomers and the initiator are concentrated in the unfrozen microzones of the apparently frozen system. The polymerization and cross-linking reactions proceed in the unfrozen microzones of the reaction system. A macroporous structure in the final material appears due to the existence of solvent crystals acting as a template for the formation of the pores. The advantage of these so-called "cryogels" compared to the macroporous hydrogels obtained by phase separation is their high mechanical stability (Dinu et al. 2007). They are very tough and can withstand high levels of deformations, such as elongation and torsion; they can also be squeezed under mechanical force to drain out their solvent content. A typical SEM image of such materials in their dried state is shown in Fig. 7a illustrating their honeycomb morphology. These materials respond against the external stimuli such as the solvent composition change immediately (Fig. 7b).

References

Almdal K, Dyre J, Hvidt S, Kramer O (1993) What is a gel? Makromol Chem Macromol Symp 76:49–51

Arndt Schmidt T, Richter A, Kuckling D (2004) High response smart gels. Synthesis and applications. Macromol Symp 207:257–268

Arndt K-F, Schmidt T, Menge H (2001) Poly(vinyl methyl ether) hydrogel formed by high energy irradiation. Macromol Symp 164:313–322

Bastide J, Candau SJ (1996) Structure of gels as investigated by means of static scattering techniques. In: Cohen Addad JP (ed) Physical properties of polymeric gels. Wiley, New York

Bromberg L, Yu GA, Matsuo ES, Suzuki Y, Tanaka T (1997) Dependency of swelling on the length of subchain in poly(N, N-dimethylacrylamide)-based hydrogels. J Chem Phys 106: 2906–2910

Dinu MV, Ozmen MM, Dragan ES, Okay O (2007) Freezing as a path to build macroporous structures: superfast responsive polyacrylamide hydrogels. Polymer 48:195–204
Durmaz S, Okay O (2000) Acrylamide/2-acrylamido- 2- methyl propane sulfonic acid sodium salt–based hydrogels: synthesis and characterization. Polymer 41:3693–3704
Dusek K, Patterson D (1968) Transition in swollen polymer networks induced by intramolecular condensation. J Polym Sci A 2(6):1209–1216
Flory PJ (1953) Principles of polymer chemistry. Cornell University Press, Ithaca, NY
Funke W, Okay O, Joos-Muller B (1998) Microgels – intramolecularly crosslinked macromolecules with a globular structure. Adv Polym Sci 136:139–234
Gundogan N, Melekaslan D, Okay O (2002) Rubber elasticity of poly(*N*-isopropylacrylamide) gels at various charge densities. Macromolecules 35:5616–5622
Gundogan N, Okay O, Oppermann W (2004) Swelling, elasticity and spatial inhomogeneity of poly(N, N-dimethylacrylamide) hydrogels formed at various polymer concentrations. Macromol Chem Phys 205:814–823
Haraguchi K, Takehisa T (2002) Nanocomposite hydrogels: a unique organic-inorganic network structure with extraordinary mechanical, optical and swelling/deswelling properties. Adv Mat 14:1120–1124
Hirotsu S (1993) Coexistence of phases and the nature of first-order transition in poly(*N*-isopropylacrylamide) gels. Adv Polym Sci 110:1–26
Katayama S, Hirokawa Y, Tanaka T (1984) Reentrant phase transition in acrylamide-derivative copolymer gels. Macromolecules 17:2641–2643
Khokhlov A, Starodubtzev S, Vasilevskaya VV (1993) Conformational transitions in polymer gels: theory and experiment. Adv Polym Sci 109:123–172
Kizilay MY, Okay O (2003a) Effect of initial monomer concentration on spatial inhomogeneity in poly(acrylamide) gels. Macromolecules 36:6856–6862
Kizilay MY, Okay O (2003b) Effect of hydrolysis on spatial inhomogeneity in poly(acrylamide) gels of various crosslink densities. Polymer 44:5239–5250
Kizilay MY, Okay O (2004) Effect of swelling on spatial inhomogeneity in poly(acrylamide) gels formed at various monomer concentrations. Polymer 45:2567–2576
Lindemann B, Schroder UP, Oppermann W (1997) Influence of crosslinker reactivity on the formation of inhomogeneities in hydrogels. Macromolecules 30:4073–4077
Lozinsky VI (2002) Cryogels on the basis of natural and synthetic polymers: preparation, properties and application. Russ Chem Rev 71:489–511
Melekaslan D, Okay O (2000) Swelling of strong polyelectrolyte hydrogels in polymer solutions: effect of ion pair formation on the polymer collapse. Polymer 41:5737–5747
Melekaslan D, Okay O (2001) Reentrant phase transition of strong polyelectrolyte poly(*N*-isopropylacrylamide) gels in PEG solutions. Macromol Chem Phys 202:304–312
Naghash HJ, Okay O (1996) Formation and structure of polyacrylamide gels. J Appl Polym Sci 60:971–979
Oh KS, Oh JS, Choi HS, Bae YC (1998) Effect of crosslinking density on the swelling behavior of NIPA gel particles. Macromolecules 31:7328–7335
Okay O (2000) Macroporous copolymer networks. Prog Polym Sci 25:711–779
Okay O, Gundogan N (2002) Volume phase transition of polymer networks in polymeric solvents. Macromol Theory Simul 11:287–292
Okay O, Oppermann W (2007) Polyacrylamide – clay nanocomposite hydrogels: rheological and light scattering characterization. Macromolecules 40:3378–3387
Orakdogen N, Okay O (2006a) Correlation between crosslinking efficiency and spatial inhomogeneity in poly(acrylamide) hydrogels. Polym Bull 57:631–641
Orakdogen N, Okay O (2006b) Reentrant conformation transition in poly(N, N-dimethyl acrylamide) hydrogels in water- organic solvent mixtures. Polymer 47:561–568
Orakdogen N, Kizilay MY, Okay O (2005) Suppression of inhomogeneities in hydrogels formed by free-radical crosslinking copolymerization. Polymer 46:11407–11415

Ozmen MM, Okay O (2003) Swelling behavior of strong polyelectrolyte poly(*N*-*t*-butylacrylamide-co-acrylamide) hydrogels. Eur Polym J 39:877–888
Ozmen MM, Dinu MV, Dragan ES, Okay O (2007) Preparation of macroporous acrylamide-based hydrogels: cryogelation under isothermal conditions. J Macromol Sci Part A 44:1195–1202
Shibayama M (1998) Spatial inhomogeneity and dynamic fluctuations of polymer gels. Macromol Chem Phys 199:1–30
Shibayama M, Tanaka T (1993) Phase transition and related phenomena of polymer gels. Adv Polym Sci 109:1–62
Silberberg-Bouhnik M, Ramon O, Ladyzhinski I, Mizrahi S (1995) Osmotic deswelling of weakly charged poly(acrylic acid) solutions and gels. J Polym Sci Polym Phys 33:2269–2279
Tanaka T (1978) Collapse of gels and the critical end point. Phys Rev Lett 40:820–823
Tanaka T (1981) Gels. Sci Am 244:110–123
Tanaka Y, Gong JP, Osada Y (2005) Novel hydrogels with excellent mechanical performance. Prog Polym Sci 30:1–9
Treloar LRG (1975) The physics of rubber elasticity. Oxford University Press, Oxford
Yazici I, Okay O (2005) Spatial inhomogeneity in poly(acrylic acid) hydrogels. Polymer 46: 2595–2602
Yoshida R, Ushida K, Kaneko Y, Sakai K, Kikuchi A, Sakurai Y, Okano T (1995) Comb-type grafted hydrogels with rapid deswelling response to temperature changes. Nature 374:240–242

Synthesis of Hydrogels

Dirk Kuckling, Karl-Friedrich Arndt, and Sven Richter

Abstract In order to tailor hydrogels for the application as actuator-sensor microsystems based on the responsive behaviour of smart gels, a general strategy has to be developed. Since the phase transition phenomenon of hydrogels is theoretically well understood advanced materials based on the predictions can be prepared. The requirements for applying hydrogels can be summarized as follows:

- Development of novel sensitive polymers: Polymer networks with a large volume transition in combination with a sufficient high elastic modulus and short response times have to be prepared.
- Definition of the stimulus: Responsive behaviour of the gels towards relevant stimuli (e.g. temperature, pH value, solvent composition, low molecular weight solutes etc.) has to be realized. The hydrogels have to show a strong, non-linear response towards these stimuli. The defined adjustment of the stimuli must be possible.
- Speed of response: The response time of the smart hydrogels have to be decreased by some orders of magnitude compared with conventional gels. Fast responsive hydrogels are necessary to obtain sufficient fast cycle times.

D. Kuckling (✉)
Department of Chemistry, University of Paderborn, D-33098 Paderborn
e-mail: dirk.kuckling@uni-paderborn.de

K.-F. Arndt
Department of Chemistry and Food Chemistry, Physical Chemistry of Polymers, TU Dresden, 01062 Dresden, Germany
e-mail: karl-friedrich.arndt@chemie.tu-dresden.de

S. Richter
Leibniz Institute of Polymer Research Dresden, Hohe Straβe 6, D-01069 Dresden, Germany
e-mail: richter-sven@ipfdd.de

G. Gerlach and K.-F. Arndt (eds.), *Hydrogel Sensors and Actuators*,
Springer Series on Chemical Sensors and Biosensors 6,
DOI: 10.1007/978-3-540-75645-3_2, © Springer-Verlag Berlin Heidelberg 2009

- Specific stimulation: The subsequent adjustment of the transition by modification (e.g. changing the pH value) of the applied polymers must be possible. The external stimulation (e.g. by photo-switching) is desirable. Advanced materials will show multi-sensitive behaviour.

Since the volume phase transition of hydrogels is a diffusion-limited process the size of the synthesized hydrogels is an important factor. Consistent downscaling of the gel size will result in fast smart gels with sufficient response times. In order to apply smart gels in micro-systems, new preparation techniques for hydrogels have to be developed. For the up-coming nano-technology, nano-sized gels as actuating material would be of great interest.

An often applied method for the synthesis of hydrogels, especially for applications in medicine and pharmaceutics, is based on radiochemistry. The hydrogel can be formed by irradiation of monomers, polymers dissolved in water, or polymers in dry state. Electrons of different energies or γ-rays are used as high-energy radiation. The possibilities of the radiation-chemical synthesis of smart hydrogels are discussed on different examples. The technique is applied to bulk polymers, to micro- and nanogel particles, and to patterned layers on different materials. The basics and fundamentals of irradiation techniques as well as the equipment are described.

In addition to synthesis of hydrogels, the theory of thermoreversible gelation and the gel point itself, the determination of the gel point on gelatin by using dynamic light scattering (DLS), oscillatory shear rheology as well as nuclear magnetic resonance (NMR) diffusion experiments will be described. Special attention has been devoted to the comparison of the results each methods have been provided when monitoring the gelatin gelation process. Furthermore, an important point is the estimation of the critical dynamical exponents in DLS and rheology at the gel point and their comparison with the theoretical prediction, which was given by Doi and Onuki.

Keywords Patterning • Stimuli-responsive • Cross-linking • Radiation • Gel point

Contents

Abbreviations

2VP	2-vinyl pyridine
AAmPA	3-acrylamido propionic acid
ATR-FTIR	Attenuated total reflection Fourier transform infra red
DI	De-ionized
DLS	Dynamic light scattering
DMAAAm	2-(dimethylamino)-*N*-ethyl acrylamide
DMAAm	*N*,*N*-dimethylacrylamide
DMIAAm	2-(dimethyl maleimido)-*N*-ethyl-acrylamide
DSC	Differential scanning calorimetry
EBL	Electron beam lithography
FESEM	Field emission scanning electron microscopy
HCl	Hydrochloric acid
HPC	Hydroxypropylcellulose
LBG	Locust bean gum
LCST	Lower critical solution temperature
MBAAm	*N*,*N*-methylene bisacrylamide
MWD	Molecular weight distribution
NIPAAm	*N*-isopropyl acrylamide
NMR	Nuclear magnetic resonance
OWS	Optical waveguide spectroscopy
P2VP	Poly(2-vinyl pyridine)
P4VP	Poly(4-vinyl pyridine)
PAAc	Poly(acrylic acid)
PEO	Poly(ethylene oxide)
PFG-NMR	Pulsed field gradient nuclear magnetic resonance
PNIPAAm	Poly(N-isopropyl acrylamide)
PPO	Poly(propylene oxide)
PVA	Poly(vinyl alcohol)
PVCL	Poly(vinyl caprolactam)
PVDF	Poly(vinyliden fluorid)
PVME	Poly(vinyl methyl ether)

PVP	Poly(vinyl pyrrolidone)
SEM	Scanning electron microscopy
SPR	Surface plasmon resonance
TCF	Time correlation function
UV	Ultraviolett
XG	Xanthan gum

Symbols

A	Area
c_P	Concentration of polymer solution
d	Diameter in equilibrium state
d_0	Diameter at preparation
d_f	Fractal dimension of the critical gel
D	Diffusion coefficient
D	Irradiation dose
D_{av}	Average dose
D_g	Gelation dose
D_p	Fractal exponent
D_V	Virtual dose
g	Gel fraction
$g_1(q,t)$	Electric field correlation function
$g_2(q,t)$	Time-intensity correlation function
$G(t)$	Shear stress relaxation modulus
$G'(\omega)$	Shear storage modulus
$G''(\omega)$	Shear loss modulus
$I(t)$	Scattering intensity at time t
l	Layer thickness
l_0	Layer thickness in dry state
M_n	Number-averaged molecular weight
M_w	Weight-averaged molecular weight
n	Critical exponent in shear rheology
n	Refractive index
p_0	Average number of main chain scissions per monomer unit and per unit dose
q	Scattering vector
q_0	Proportion of monomer units cross-linked per unit dose
Q	Degree of swelling
Q_m	Weight degree of swelling
s	Sol fraction
S	Gel stiffness

$S(q,t)$	Dynamic structure factor
t	Time
T	Temperature
T_c	Critical temperature
T_{syn}	Synthesis temperature
$u_{2,0}$	Weight-averaged degree of polymerisation of the polymer before irradiation
U_B	Acceleration voltage
V	Volume in equilibrium state
V_0	Volume at preparation
W_d	Weight of dry network
W_t	Weight of swollen network at time t
β,μ	Critical exponents in DLS
ΔT_c	Width of temperature induced transition
θ	Scattering angle
ω	Shear frequency
ω	Rotational speed
$<\tau>$	Mean relaxation time

1 Chemical Cross-Linking

Stimuli-responsive hydrogels change their volume and elasticity in response to a change in the properties of the liquid phase such as temperature, pH, solvent composition and ionic strength (Okuzaki and Osada 1995; Matsukata et al. 1998; Inomata et al. 1995; Kabra and Gehrke 1991; Feil et al. 1991). Depending on the chemical compositions of gels and liquids and on experimental conditions, the volume change occurs either continuously or discontinuously. These polymers have promising potential to achieve smart chemo-mechanical valves, pumps, sensors etc. because they may be utilized e.g. for the automatic regulation of a flow.

1.1 Temperature Dependent Swelling

A common method to vary the degree of swelling and the transition temperature T_c of temperature-responsive hydrogels, e.g. based on poly(*N*-isopropyl acrylamide) (PNIPAAm), is the incorporation of a weak acid or base component into the network (Hirotsu 1993; Velada et al. 1998; Liu et al. 1999; Champ et al. 2000; Shibayama et al. 1996a; Stile et al. 1999). Using this method, it is possible to obtain gels with temperature as well as pH sensitivity (Yu and Grainger 1993; Brazel and Peppas 1995; Yoshida et al. 1995a). Such behaviour can be obtained in interpenetrating polymeric networks, too (Zhang and Peppas 2000). Due to

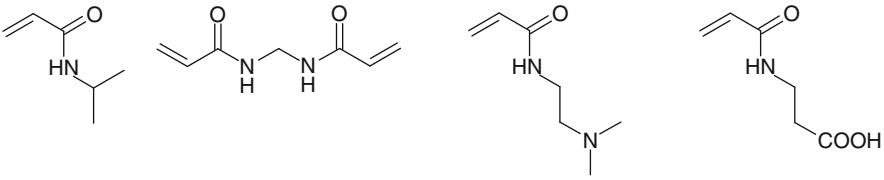

Fig. 1 Structure of the monomers for the synthesis of PNIPAAm homo- and copolymers

protonation-deprotonation reactions altering the pH value of the swelling medium, the network changes from a non-ionic to an ionic state and vice versa. The critical behaviour of these polymers is very sensitive to changes in the hydrophilic/hydrophobic balance of the macromolecules. In the ionic state the network is much more hydrophilic and the degree of swelling and the transition temperature is increased (Hirotsu 1993; Shibayama et al. 1996b). With a random distribution of the acidic or basic comonomers it is not possible to vary the comonomer content in order to modify the degree of swelling below T_c without also changing T_c itself (Kuckling et al. 2000). For this purpose, the components have to be separated into blocks (Vakkalanka and Peppas 1996). A suitable method to prepare cross-linked polymers with blocked components is the preparation of graft copolymer gels. Those structures were realized in order to enhance the response time of PNIPAAm gels (Chen and Hoffman 1995; Yoshida et al. 1995b; Kaneko et al. 1998).

PNIPAAm homo- and copolymer gels with different feed compositions can be prepared by free-radical cross-linking polymerization with the monomers 2-(dimethylamino)-*N*-ethyl acrylamide (DMAAAm) and 3-acrylamido propionic acid (AAmPA) as well as the cross-linker *N*,*N*-methylene bisacrylamide (MBAAm) (Fig. 1).

The weight degree of swelling Q_m is defined as the mass of absorbed water, as calculated from the weight of swollen networkW_t, per mass of dried copolymer W_d network:

$$Q_{\mathrm{m}} = (W_{\mathrm{t}} - W_{\mathrm{d}})/W_{\mathrm{d}} \tag{1}$$

The volume swelling ratio for smaller gel cylinders can be expressed as ratio of gel volume in equilibrium state (V) to volume at preparation (V_0) measured as the ratio of the respective diameter of the cylinder in equilibrium state (d) to the diameter at preparation (d_0):

$$V/V_{\mathrm{o}} = (d/d_{\mathrm{o}})^3 \tag{2}$$

The lower critical solution temperature (LCST) of the pure, weakly cross-linked PNIPAAm gel is 34°C determined by the swelling method (Shibayama et al. 1994). In order to increase the mechanical properties hydrogels with higher cross-linking densities can be prepared. In Fig. 2 the temperature-dependent swelling behaviour

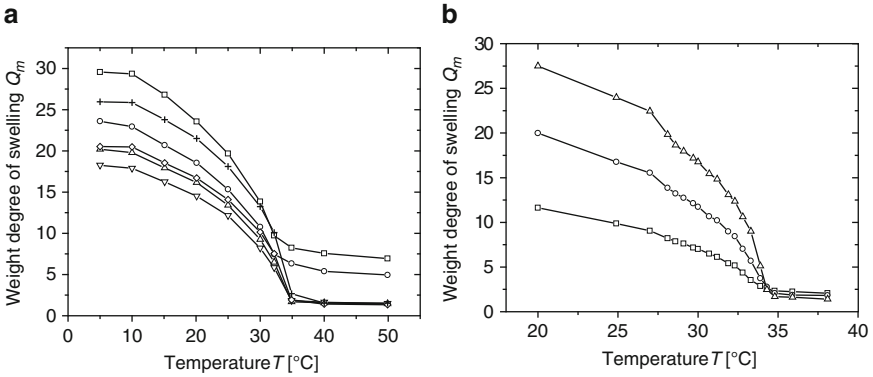

Fig. 2 Temperature dependence of the degree of swelling of PNIPAAm homo-polymer gels (a) with different cross-linker contents (T_{syn} = 20°C) (*open square* - MBAAm 1, *open circle* - MBAAm 2, *open triangle* - MBAAm 4, *open down triangle* - MBAAm 6, *open diamond* - MBAAm 8, + − MBAAm10). (b) synthesized at different temperatures (MBAAm 4) (*open square* − 10°C, *open circle* − 20°C, *open triangle* − 30°C)

for PNIPAAm homopolymer gels with different cross-linker content (e.g. MBAAM 1 corresponds to 1 mol-% MBAAm) is shown. With increasing the cross-linker content (MBAAm 1–MBAAm 6) the maximum degree of swelling is decreased. For very high cross-linker content (MBAAm 8, MBAAm 10) the hydrogels show improved swelling properties. This is due to a change of the network structure. At low cross-linker content (MBAAm 1, MBAAm 2) the gels are homogeneous and transparent. With an increase of the cross-linker content the gels get first slightly cloudy (MBAAm 4, MBAAm 6) and then opaque and heterogeneous (MBAAm 8, MBAAm 10). The equilibrium degree of swelling for the latter gels is lower than the polymer concentration in the reaction mixture. Cross-linking under these conditions leads to a porous but highly cross-linked sample. A change of the network structure can also be obtained by an increase of the synthesis temperature (T_{syn}) (Fig. 2). At 10°C and 20°C the prepared gels are homogeneous. At 30°C near the phase transition temperature heterogeneous gels are obtained. The difference between T_{syn} and the phase transition temperature is important for the properties of the gels (Kabra and Gehrke 1991; Gotoh et al. 1998). Gels synthesized at temperatures above the phase transition temperature are characterized by a very weak mechanical stability, but due to their highly heterogeneous and porous structure also by a fast speed of shrinking and swelling. Heterogeneous, porous networks consist of two phases, a swollen polymer phase and a pure solvent phase. In conclusion, the swelling properties of the hydrogels can be adjusted by the content of the cross-linker and T_{syn}. The phase transition temperature is not affected, which could be proven by differential scanning calorimetry (DSC) measurements, too (Shibayama et al. 1996c).

In Fig. 3 the temperature-dependent swelling behaviour for PNIPAAm copolymer gels with different amounts of acidic comonomer (e.g. AAmPA 2 corresponds to 2 mol-% of AAmPA) is shown. In de-ionized (DI) water the comonomer is partly

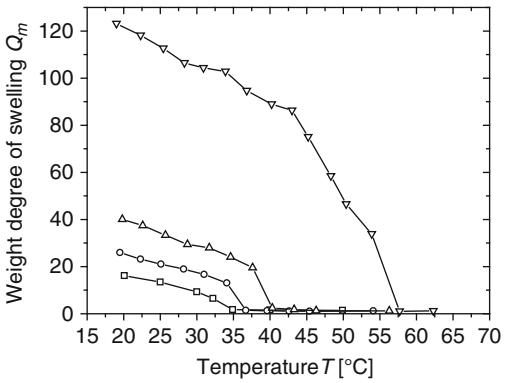

Fig. 3 Temperature dependence of the degree of swelling of PNIPAAm copolymer gels with ifferent contents of an acidic monomer (*open square* – PNIPAAm, *open circle* - AAmPA 2, *open triangle* - AAmPA 5, *open down triangle* - AAmPA 10)

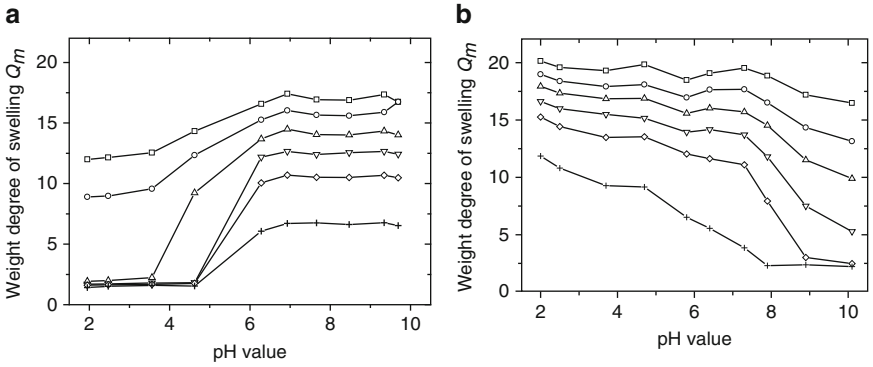

Fig. 4 pH dependence of the degree of swelling. (**a**) acidic PNIPAAm copolymer gels for AAmPA 5 (*open square* - 20°C, *open circle* − 25°C, *open triangle* − 30°C, *open down triangle* − 35°C, *open diamond* − 40°C, + − 50°C). (**b**) basic PNPAAm copolymer gels for DMAAAm 10 (*open square* − 20°C, *open circle* − 25°C, *open triangle* − 30°C, *open down triangle* − 35°C, *open diamond* − 40°C, + − 50°C)

charged. This results in an additional part of osmotic pressure to the swelling pressure of the gels. The degree of swelling in the swollen state increases with increasing the amount of comonomer. An increase of the hydrophilic content of the gels also increases the phase transition temperature. The behaviour is more pronounced for the acidic comonomer than for a basic comonomer, suggesting a higher degree of ionization for the acidic comonomer in DI water (Kuckling et al. 2000).

1.2 pH-Dependent Swelling

In Fig. 4 the pH-dependent degrees of swelling of PNIPAAm hydrogels with 5 mol-% of the AAmPA comonomer are shown. Increased comonomer content increased the step height of the pH curve (Kuckling et al. 2003a). The pH sensitivity

comes up to the maximum at temperatures just above the phase transition temperature for the non-charged hydrogels. At these temperatures it is possible to switch the hydrogels between the collapsed state at around pH 4 and the completely swollen state at around pH 6. At lower temperatures the differences are only caused by the extra portion of osmotic pressure due to the deprotonation of the carboxyl group. At higher temperatures the differences decrease due to the temperature dependence of the degree of swelling at higher pH values.

Like PNIPAAm and some other acrylamide derivative polymer gels, the poly (NIPAAm-co-AAmPA) gels swell at low temperature and de-swell at elevated temperature. At pH 2.1.5 the comonomer is completely protonated. The hydrophilicity of the comonomer is very similar to *N*-isopropyl acrylamide (NIPAAm). No differences in the swelling curves could be seen. At pH 7.7 the comonomer is charged. The degree of swelling is strongly affected by the copolymerization ratio. The transition behaviour under these circumstances is not very well pronounced (Beebe et al. 2000).

The phase transition behaviour of poly(NIPAAm-co-DMAAAm) gels in buffer solutions can be seen in Fig. 4. The degree of swelling of the gel in buffer solutions is much lower than that in water due to the high ionic strength in the buffer solutions. Generally, the swelling ratio is higher in a smaller pH value buffer solution at the same temperature. At around 35°C an inverted pH response between pH 7 and pH 9 can be obtained. The influence of the basic comonomer on the swellability in buffer solutions is again less pronounced than of the acidic comonomers.

1.3 Bi-Responsive Materials

In order to prepare bi-responsive materials different monomers have to be separated in different blocks. Hence, the combination of temperature-sensitive PNIPAAm with a pH-sensitive component poly(2-vinyl pyridine) (P2VP) leads to polymers possessing both of these properties. PNIPAAm aggregates while increasing the temperature to above the phase transition temperature, which lies generally at approx. 34°C (Shibayama et al. 1994). P2VP is soluble in aqueous media at low pH due to the protonation of the basic aromatic nitrogen and aggregates at higher pH. The critical pH value for the transition from hydrophilic to hydrophobic macromolecule lies at approx. 5.5.

Graft copolymer gels with different compositions were prepared by radical polymerization in dioxane from NIPAAm and P2VP macromonomers with 1 mol-% MBAAm as the cross-linking agent (Fig. 1) (Wohlrab and Kuckling 2001; Kuckling and Wohlrab 2002). The compositions of the graft copolymer gels (CPNI and CPNIPY 1-3) are listed in Table 1. The polymerization can be performed in small capillaries (diameter $d_0 = 775$ µm). After removing the gels from the capillaries and subsequent washing with 0.05 N HCl to remove unreacted chemicals the gels are equilibrated in different buffer solutions. Assuming a full conversion as well as a random distribution of the monomers, an average distance between two

Table 1 Composition of the graft copolymer gels

Gel	Ratio of repeating units in the gel NIPAAm:2VP[a]	Average distance between two P2VP side chains [NIPAAm repeating units][b]
CPNI	1:0	–
CPNIPY 1	10.9:1	280
CPNIPY 2	4.5:1	116
CPNIPY 3	1:1	26

[a]estimated from the feed composition and the degree of functionalization for P2VP macromonomers; [b]estimated from the ratio of repeating units and the degree of polymerization for P2VP macromonomers

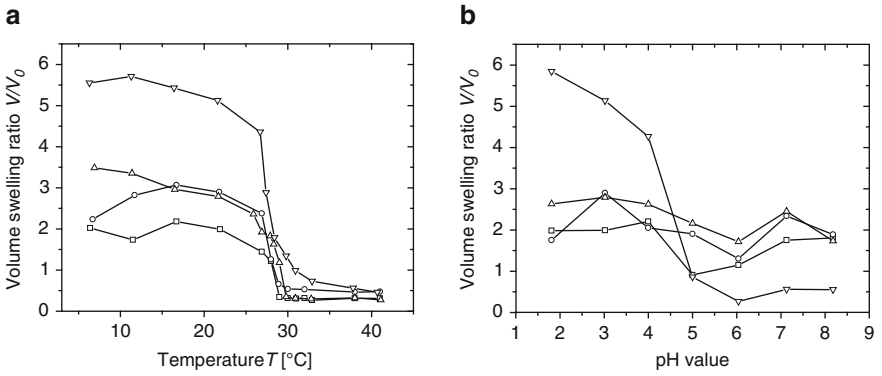

Fig. 5 Volume swelling ratio of graft copolymer gels: (**a**) in response to temperature at constant pH (pH=3) (*open square*: CPNI; *open circle*: CPNIPY1; *open triangle*: CPNIPY2; *open down triangle*: CPNIPY3); (**b**) in response to pH at constant temperature ($T = 22°C$) (*open square*: CPNI; *open circle*: CPNIPY1; *open triangle*: CPNIPY2; *open down triangle*: CPNIPY3)

P2VP side chains can be estimated from the NIPAAm/P2VP macromonomer ratio. The temperature-dependent swelling curves of the graft copolymers at different pH values are shown in Fig. 5.

The graft copolymer gels show the typical swelling behaviour for PNIPAAm gels. Independent from the composition T_c is around 28°C. The shift of T_c towards lower values as compared with the behaviour of PNIPAAm gels in water can be explained by the influence of the buffer solution (electrolyte effect). At pH 3 at lower temperatures an increase of the P2VP content increases the volume swelling ratio of the gels due to an increased electrostatic repulsion of the charged P2VP side arms. Interestingly at higher temperatures all networks collapse to nearly the same swelling ratio. A dependence of the volume swelling ratio on the P2VP content can not be observed. It seems that the attractive force of the collapsed network backbone is much stronger than the repulsive force of the charged side arms. At pH 7 the P2VP side arms are in their non-charged, hydrophobic form. A difference in the swelling curve due to additional hydrophobic interactions can only be observed at the highest P2VP content. There is no pH effect on the swelling behaviour of CPNI gels.

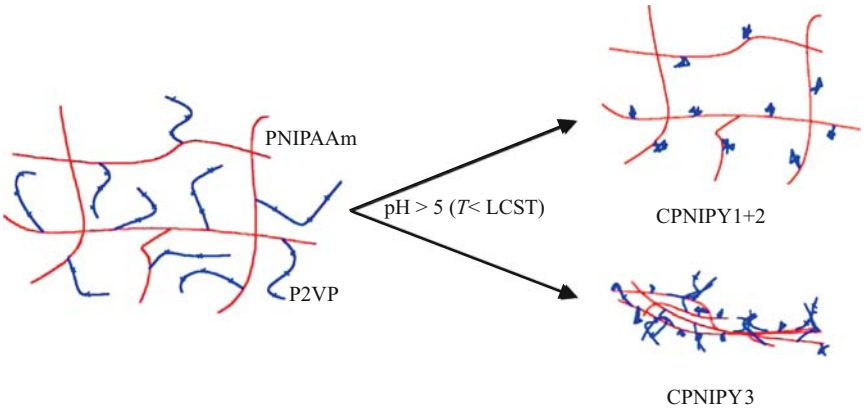

Fig. 6 Scheme of the deswelling of graft copolymer gels in response to a pH increase

The pH dependent volume swelling ratio of the graft copolymer gels at temperatures below T_c is shown in Fig. 5. In contrast to the temperature-dependent measurements only the graft copolymer with the highest P2VP content showed a pronounced swelling transition on changing pH value. The volume swelling ratios of the other gels remained nearly constant, approx. 2 at low temperatures and approx. 0.2 at high temperatures. The difference between the volume swelling ratios only corresponds to the transition of the PNIPAAm backbone.

The different behaviour of graft copolymer gels with low and high P2VP contents might be explained as followed. The different side arms are only able to interact and form additional junction points at the highest graft density. In this case an additional effect on the degree of swelling was observed (Fig. 6). At lower graft densities the side arms are spatially separated. In the case of a transition of the side arms they are too far from another for aggregation. Thus, the influence on the volume swelling ratio is only marginal. The swelling of the gels is dominated by the PNIPAAm backbone.

1.4 Polymerisation and Cross-Linking

Responsive hydrogels can undergo a volume change in response to stimuli from their local environment. Such hydrogels can be used e.g. as actuators for flow control in drug delivery systems (Zhang et al. 2004). The characteristic response time is inversely proportional to the square of the smallest dimension of the gels (for details see Section 3.2.5). Thus, the decrease of the gel size will be favourable for the response time of polymer actuators and applications with downsized hydrogel dimensions should be targeted. Several methods are known for the fabrication of microfluidic devices, e.g. rapid prototyping, microinjection molding and microfluidic tectonics. Microfluidic tectonics involves development

of patterns in responsive hydrogel component in microfluidic network as well as fabrication of these networks with non-responsive pre-polymers. The photo polymerization technique for fabricating microfluidic networks can open new possibilities for creating drug delivery devices as well (Eddington and Beebe 2004a; Eddington and Beebe 2004b; Beebe et al. 2000a). Hydrogels can either be synthesized outside the system needing manual manipulation to incorporate them whereas in situ polymerization will occur inside microfludic channels by liquid-phase photo polymerization.

Although polymerization of NIPAAm has been extensively investigated in the past using free radical initiator, this method can not be used for the preparation of thin films. Thin hydrogels films can find applications as microfluidic devices for sensors and actuators in case patterning is possible. This problem can be solved by preparing gel films from narrowly distributed microgel particles (Zhou and Wu 1996) or branching of the sensitive polymer onto the surface (Yoshioka et al. 1993). The photo polymerization/photo cross-linking is a more suitable method for microsystem technology and there is an increased interest in this method (Nakayama and Matsuda 1992; Kuckling et al. 2003b). The preparation of hydrogels by photo cross-linking by using water-soluble photo initiator or ammonium persulphate (Ikkai and Adachi 2004) and their photo lithographic patterning (Chen et al. 1997; Ito et al. 1997; Lesho and Sheppard 1996) has been investigated with this respect (Singh et al. 2006).

Conditions of polymerization like temperature (≈7°C or ≈40°C what means below or above the phase transition temperature in pure water), nature of solvent (water or water/ethanol 50/50 mixture to use hydrophilic or more hydrophobic photo initiators), amount of cross-linker and monomer concentration can be varied to investigate the effect of reaction conditions on the swelling behaviour, phase transition temperature and morphology. Photo patterning of hydrogels can be done in the presence of an adhesion promoter on glass substrate (Singh et al. 2006).

1.4.1 Effect of Synthesis Temperature

Samples prepared under different conditions can be differentiated visually. PNIPAAm hydrogels prepared using water as solvent at ≈7°C were transparent (homogeneous condition), whereas those prepared using water at ≈40°C or water/ethanol mixture at ≈7°C were opaque or translucent (heterogeneous condition). The latter conditions favour the precipitation of PNIPAAm chains once they are formed after initiation. Thus, cross-linking is performed in a two-phase system leading to heterogeneous gels. The swelling was dependent upon the polymerization conditions and it was found to be stronger for hydrogels prepared at low temperature. This might be due to the precipitation or additional cross-linking in case of samples prepared at ≈40°C. Increased reaction temperature increases the rate of transfer reaction during the photo polymerization leading to more cross-links and, thus, lower swelling. At the same time polymerization is faster and cross-linking more efficient even under heterogeneous conditions.

1.4.2 Effect of Solvent

Swelling behaviour is significantly different when water is replaced partially by ethanol (water/ethanol 50/50). Similar behaviour has been observed on replacing water by methanol, acetone, tetrahydrofuran, or dimethyl sulfoxide, respectively (Schild et al. 1991). Maximum shrinkage is observed as a function of temperature in samples prepared using water/ethanol (50/50, ≈7°C) as solvent. These samples show much higher swelling at all levels of cross-linking compared to samples prepared in DI water. This behaviour is due to the co-nonsolvency effect as reported (Schild et al. 1991).

The rate of polymerization in the water/ethanol system is lower as compared to the other heterogeneous system, thus, polymers can phase-separate and cross-linking occurs in the separated phase mostly. Since the rate of transfer reaction should be almost the same as for the pure water system, no additional cross-links are formed. Thus, the swelling of water/ethanol gels are mostly governed by the expansion of the macroporous network.

1.4.3 Effect of Cross-Linker Concentration

PNIPAAm films can prepared by varying cross-linker concentration (e.g. from 1 to 4 wt.-%). As expected, the degree of swelling decreases as the cross-link density increases. However, water/ethanol samples showed a significant decrease in swelling as MBAAm concentration increases from 1 to 2 wt.-%. Further increase in MBAAm (4 wt.-%) does not show much effect. A marginal decrease is observed in samples prepared under homogeneous conditions as MBAAm concentration is increased from 1 to 4 wt.-%. The reason for this behaviour might be the high monomer concentration used for network formation. The network is formed at a concentration above the overlap concentration of PNIPAAm in water. Fixing this structure by cross-linking leads to networks with additional junction points due to entanglements. In those systems the influence of the cross-linking agent is suppressed.

1.4.4 Effect of Monomer Concentration

A significant increase in swelling is observed below phase transition temperature for samples prepared at 7 wt.-% monomer concentration (instead of 14.3 wt.-%). Higher swelling in case of low monomer concentration is due to fewer entanglements. However, PNIPAAm films with lower monomer concentration (7 wt.-%) showed bubble formation during shrinkage, which leads to fast shrinkage. When gels are in the fully shrunken state, the bubbles disappear. This might happen because at low monomer concentration there will be a large number of loops and polymeric chains will shrink like those with free ends. No bubble formation is observed in PNIPAAM films with higher monomer concentration of 14.3 wt.-%.

In general, DSC scans of PNIPAAm films showed, that as cross-linker concentration was increased, transition temperature regions broadened and shifted to lower

temperature. T_c calculated from the shrinkage study by fitting with a sigmoidal curve (Harmon et al. 2003a) showed good agreement with the results obtained from DSC.

1.4.5 Morphological Characterization and Photo Patterning

Hydrogels show great morphological differences when reaction conditions are varied. Samples prepared at high temperature (≈40°C using water as solvent) or by using the water/ethanol mixture as solvent (at ≈7°C) show the formation of heterogeneous systems with significant differences in morphology. Scanning electron microscopy (SEM) images show that the size of cavities holding water decreases as cross-link density increases (Fig. 7). Samples prepared under heterogeneous conditions showed the formation of sponge-like structures and the mesh size is highly dependent on the MBAAm concentration. This further supports the results of swelling behaviour.

The glass substrate after treatment with adhesion promoter can be used for photo patterning (Singh et al. 2006). The reactor is filled with monomer solution together with MBAAm and photo initiator and covered with the treated glass plate followed by a mask having desired patterns. The polymer solution was irradiated with UV light up to 25 min. After 25 min of irradiation under the present conditions of experiment, all patterns vanish. By prolonged reaction times radicals are able to diffuse into dark areas and also initiate the polymerization in the unexposed areas. Desired patterns are formed within 6–10 min of irradiation. These patterns are attached to the glass surface through covalent bonds. The unexposed areas are etched out by washing with water to get the required patterns. These patterns have sizes of about 500 μm in the dried state.

1.5 Generation of Hydrogel Patterns

The swelling behaviour of smart hydrogels makes them very attractive for (micro-) actuator and sensor applications. One key point in the employment of smart

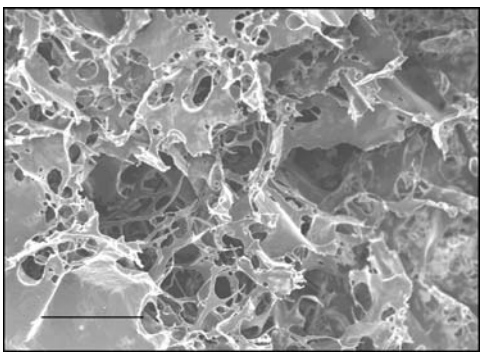

Fig. 7 SEM image of a PNIPAAM hydrogel prepared in a water/ethanol mixture as solvent at ≈7°C (scale bar 50 m)

polymers is their customizing to microsystems with its standard techniques. This requires the following:

- Cross-linking in the applied state (e.g. by photo cross-linking),
- High resolution and contrast
- Influence on the patterning through the irradiation process (adjustment of the cross-linking density and generation of a cross-linking gradient)
- Fast cross-linking reaction
- Good adhesion to the substrate

Bulk gels (i.e. gel samples in the mm-range) can easily be prepared and modified and the effects of changes in the environmental parameters can be investigated. But the kinetics of swelling and de-swelling in these gels are typically governed by diffusion-limited transport of the polymeric components of the network in water, the rate of which is inversely proportional to the square of the smallest dimension of the gel. Thus, the response times of the gels are very slow. The de-swelling kinetics are also affected by the gel thickness due to the "skin" formation phenomenon (Park and Hoffman 1994). However, it is possible to decrease the response time, e.g. by changing the synthesis conditions. The formation of a porous structure has been shown to effectively enhance the de-swelling rate of PNIPAAm gels.

Most of the PNIPAAm systems were prepared via free radical polymerizations yielding voluminous gel samples (Schild 1992). However, it is rather difficult using this method to prepare the thin films, which are necessary for applications in microsystems, e.g. with integrated valves or pumps based on polymeric actuators. Typical monomers for smart polymers are non-film-forming monomers, thus, polymerization in "dry" thin films is not possible. For solution polymerization special closed cavities have to be designed on the target, which is highly unprofitable. Photo cross-linking of a polymer film is a more suitable method for microsystem technology and increasing interest is being shown in this method. Photo cross-linking of thin films of hydrophilic polymers is a convenient pathway to the preparation of network layers with µm-dimensions.

Photo cross-linkable co- and terpolymers of *N*-isopropylacrylamide (NIPAAm), 2-(dimethyl maleimido)-*N*-ethyl-acrylamide (DMIAAm) as the chromophore, and *N*,*N*-dimethylacrylamide (DMAAm) can be prepared by free-radical polymerization (Harmon et al. 2003a; Kuckling et al. 2002a; Pareek et al. 2006). Aqueous solutions of the co- and terpolymers show LCST behaviour, and the corresponding phase transition temperature T_c can be detected by DSC. T_c decreased with increasing amount of DMIAAm, as low as 24.7°C for 9.2 mol-% DMIAAm, and increased with increasing DMAAm content, as high as 59.5°C for 52.6 mol-% DMAAm. The resulting polymers are shown to be photo cross-linkable, and the sensitivity of the polymers towards UV light was studied by monitoring the photo cross-linking reaction with (attenuated total reflection-Fourier-transform infrared) ATR-FTIR spectroscopy. With 2 wt-% thioxanthone as the photo sensitizer, nearly full conversion could be achieved with 10 min of irradiation even though the photo cross-linking was performed in the glassy state. By using an appropriate mask, this same approach can be used to pattern hydrogel layers (Fig. 8) (Singh et al. 2006).

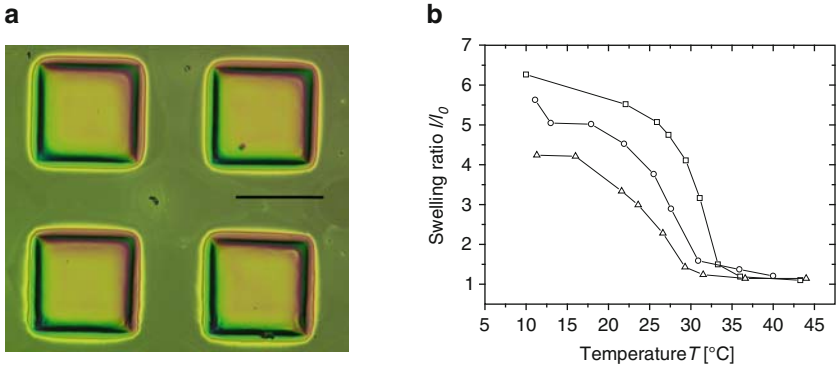

Fig. 8 (**a**) Pattern of photo cross-linked hydrogel structures (dry state, scale bar 250 μm). (**b**) Swelling ratio (l/l_0) of photo cross-linked hydrogel layers measured by SPR (*open square*: 2.4 mol% DMIAAm, *open circle*: 4.5 mol% DMIAAm, *open triangle*: 9.2 mol% DMIAAm)

Surface plasmon resonance (SPR) spectroscopy in combination with optical waveguide spectroscopy (OWS) and optical microscopy has been reported to obtain information about the swelling behaviour of thin smart hydrogel films (Harmon et al. 2003a; Kuckling et al. 2002a; Harmon et al. 2003b). SPR devices are based on the detection of refractive index changes in a thin dielectric layer on top of a noble metal surface and probed by the evanescent field of a laser beam. The reflected intensity of the beam is recorded as a function of incident angle and decreases dramatically as the light couples into the plasmon mode of the metal or the waveguide modes of the dielectric. The evanescent tail of the plasmon decays exponentially into the dielectric and is therefore very surface-sensitive. Hence, SPR has been proven to be successful in a variety of sensor applications. The method is non-destructive, does not require labelling, is suited for solid-air or solid-liquid interfaces including non-transparent media (as run in reflection mode), and allows for the real-time analysis of changes in the probed zone. In order to fit the SPR data with a simple box model, the cross-linked gel films must consist of a thin layer with uniform thickness. Spin coating provides very precise control over film thickness, and with a suitable solvent and spin speed, results in uniform films. The PNIPAAm copolymer films are then vacuum-dried and photo cross-linked. This produces a dry film thickness l_0 in the range of 9 nm–2.3 μm. In the SPR scans the plasmon resonance minimum and the first waveguide mode were fit to Fresnel calculations to determine the refractive index n and the layer thickness l of the hydrogel. The volume degree of swelling Q can be calculated from the refractive index, and the swelling ratio can be calculated from the layer thickness (Fig. 8). Changes in the degree of swelling, T_c and the width of the transition ΔT_c are observed by changing the chromophore content and, as a result, the gel cross-linking density. For a hydrogel film with a dry thickness of 200 nm, the collapsed film thickness above T_c is around 220 nm and depends only weakly on the chromophore content. However, at temperatures below T_c, the swollen film

thickness is strongly dependent on the chromophore content and ranges from 1,200 nm for 2.4 mol-% DMIAAm to 800 nm for 9.2 mol-% DMIAAm. The reverse is true for the refractive index, which increases as the film thickness decreases. A comparison of volume degree of swelling and swelling ratio might be utilized to demonstrate the high anisotropy of swelling in these hydrogel layers that are physisorbed to the substrate and therefore constrained from expanding or contracting laterally. The swollen film expands 9.5% laterally as compared to the dry film, and this value appears to be independent of temperature. The swelling perpendicular to the substrate ranges from 6.4 % for 9.2 mol-% DMIAAm at temperatures above T_c to 630 % for 2.4 mol-% DMIAAm at temperatures below T_c. However, the swelling of surface-attached networks is larger than that suggested by simple geometric considerations for swelling in one dimension. The results are in qualitative agreement with Flory-Rehner theory extended to one-dimensional swelling (Toomey et al. 2004).

Photo cross-linkable co- and terpolymers of NIPAAm, DMIAAm as the photo sensitive component, and 3-acryloylaminopropionic acid (AAmPA) or *N*-(2-dimethylamino-ethyl)acrylamide (DMAAAm) as ionizable comonomers are able to respond to both pH and temperature, which provides two independent parameters that can be used to control the properties of the resulting gels (Singh et al. 2006). This contributes to the "smart" behaviour of the gel, and the exact temperature and pH of the response can be tailored to specific applications. The gels were shown to be both temperature- and pH-responsive with a transition temperature ranging from 25.3°C to 44.9°C for films with a 200 nm dry film thickness. The transitions of the photo cross-linked samples in DI water are sharper (ΔT_c is smaller) than the samples measured in buffer solution, and there is also a difference between the two buffer solutions, with higher ΔT_c values at pH 10 than at pH 3. This is similar to the behaviour of ionized bulk gels where the ions in the salt solution screen the interactions within the gel and act as structure breakers to reduce the entropic penalty of solution. Another trend is the increase in the transition temperature as the polymers become more hydrophilic with the introduction of charged comonomers. The acidic AAmPA comonomer becomes ionized at high pH while the basic DMAAAm comonomer becomes ionized at low pH.

2 Cross-Linking and Patterning by Irradiation

2.1 Sol-Gel Analysis

High energy radiation splits covalent bonds into unpaired radicals, which can then recombine randomly. Depending upon the relative rates of recombination and scission, an irradiated polymer can be cross-linked or it degrades into low- molecular weight fragments. Simple rules can be formulated to estimate the influence of radiation on polymers:

Table 2 Influence of high-energy radiation on polymers under inert atmosphere

Polymers prone to scission	Polymers prone to cross-linking
Poly(isobutylene)	Poly(ethylene)
Poly(tetrafluoroethylene)	Poly(styrene)
Poly(methyl methacrylate)	Poly(vinyl alcohol)
Poly(acrylnitrile)	Poly(butadiene)
Poly(methacrylamide)	Poly(acrylates)
Cellulose and derivatives	Poly(acrylamide)
Poly(α-methylstyrene)	Poly(dimethylsiloxane)
Poly(vinyliden fluoride)	Poly(urethanes)
-[CH_2 -CR´R´´]-	Natural rubber -[CH_2 -CHR]-

- For polymers with quaternary C-atoms in the backbone, chain scission will occur
- Unsaturated bonds reinforce the tendency to cross-linking
- Aromatic groups in the polymer chain reduce the influence of radiation
- The atmosphere at radiation plays an important role, especially the influence of oxygen. Polymers which can cross-link under inert atmosphere can degrade under oxygen atmosphere
- The temperature during irradiation has an influence on the reaction: The mobility of the polymer chains is hindered at a temperature lower than the glass transition temperature. As a consequence, cross-linking might be suppressed

Table 2 gives an overview of the influence of high-energy radiation on different polymers.

A cross-linking reaction has great influence on polymer properties. Typically, a cross-linked polymer is insoluble. During the cross-linking reaction the amount of polymer chains being connected by chemical bonds increases. The determination of the insoluble fraction and the soluble fraction of a polymer is done by the sol-gel analysis.

The determination of the soluble part of a polymer sample, the so-called sol fraction (s) or sol content, in contrast to the insoluble part, the gel fraction (g) or gel content, gives the possibility to distinguish between polymers, which can be cross-linked by irradiation and polymers which are not cross-linkable by radiation techniques. The sum of s and g amounts to unity,

$$s = 1 - g. \tag{3}$$

Charlesby and Pinner first obtained a simple expression relating the sol fraction to the absorbed dose D[1] of radiation (Charlesby and Pinner 1959).

$$s + \sqrt{s} = \frac{p_0}{q_0} + \frac{2}{q_0\, u_{2,0}\, D} \tag{4}$$

[1]The term dose means here the quantity of radiation applied to or absorbed accidentally by a given volume or mass of sample. The absorbed dose is measured in Gray (Gy), 1 Gy = 1J/kg.

where p_0 is the degradation density, i.e. the average number of main chain scissions per monomer unit and per unit dose, q_0 the cross-linking density, i.e. proportion of monomer units cross-linked per unit dose, and $u_{2,0}$ is the weight averaged degree of polymerisation of the polymer before irradiation. This equation was derived on example of a polymer with a most-probable molecular weight distribution (MWD) and with $M_w = 2\ M_n$, where M_n is the number-averaged molecular weight and M_w the weight-averaged molecular weight.

Plotting $s + s^{1/2}$ against the reciprocal of the dose D gives a straight line. We can calculate the value q_0 from its slope and the ratio p_0/q_0 from the intercept at $1/D=0$. Values of p_0/q_0 above unity mean that degradation is preferred, whereas values smaller than unity tell us that cross-linking reaction is preferred.

An important characteristic value is the gelation dose D_g. If the absorbed dose D is smaller than the gelation dose ($D < D_g$), then no cross-linking occurs. If the absorbed dose equals the gelation dose, then at first time a network is formed. The gel point is crossed and the weight-averaged molecular weight is infinite, (for details of the gelation process and the gel point see Sect. 2.3). For $D > D_g$, the amount of polymer chains which have reacted with the network increases, and therefore the gel fraction increases, whereas the sol fraction decreases.

The gelation dose D_g can be determined by means of the Charlesby-Pinner Eq. (4) (Charlesby and Pinner 1959; Charlesby 1960), see Fig. 9.

$$1/D = 1/D_g \text{ at } s = 1 \text{ or } s + s^{1/2} = 2 \tag{5}$$

Many authors proposed deviations from the simple Charlesby-Pinner-Eq. (5). The experimental data do not fit the straight line predicted by Charlesby and Pinner. This can not be ascribed to structural effects of the polymer, but rather to the

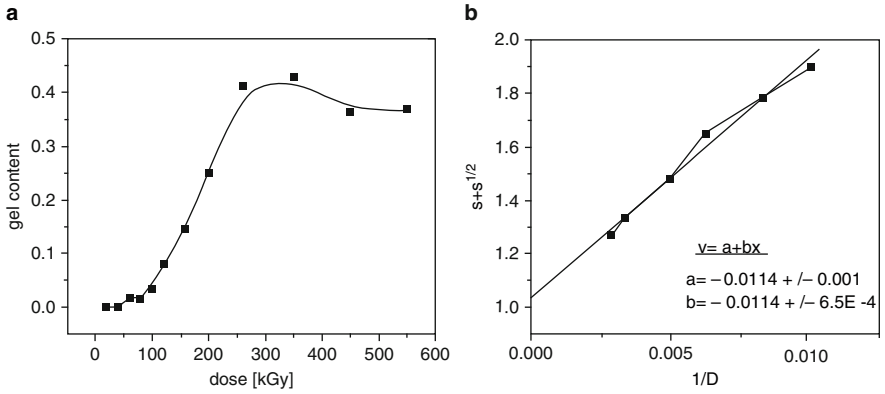

Fig. 9 Sol-gel analysis of PVP gel. (**a**) Gel content versus radiation dose (e-beam); (**b**) Charlesby–Pinner plot (with regression line).The gelation dose is determined to $D_g = 94$ kGy; from the intercept follows $p_0/q_0 = 1.03$. Reprinted from Burkert et al. (2007a), p. 1326. Copyright (2007), with permission from Elsevier

deviation of the real MWD of the polymer from the most-probable MWD and to other relations between M_n and M_w.

For evaluating experiments we mostly used a modified equation, firstly reported by Rosiak, often named as Charlesby-Pinner-Rosiak Eq. (Rosiak 1998):

$$s + \sqrt{s} = \frac{p_0}{q_0} + \left(2 - \frac{p_0}{q_0}\right)\left(\frac{D_V + D_g}{D_V + D}\right) \tag{6}$$

where D_V is the virtual dose[2].

If M_n and M_w of the polymer under investigation are known, D_V can be calculated from the following equation:

$$D_V = \frac{4}{3\,q_0}\left(\frac{1}{2\,M_n} - \frac{1}{M_w}\right) \tag{7}$$

Otherwise, it can be determined from the modified Charlesby-Pinner plot using an appropriate computer algorithm. The fit of measured sol fraction in dependence on dose D enables us to calculate D_V, D_g, and $p_0\,/q_0$.

Often, so-called G-values are reported for different radiochemical yields, e.g. (Perera and Hill 1999). The G-values are defined as the yield of individual atomic or molecular events for 100 eV (or molecular events in mole per J) of energy absorbed by the system. The number of moles of cross-linking bonds G_x per Joule (no chain scission) can be calculated from D_g (in Gy):

$$G_x = \frac{0.5 \cdot 10^{-3}}{M_{w,0}\,D_g} \tag{8}$$

with $M_{w,0}$ as the weight-averaged molecular mass of the uncross-linked polymer.

2.2 Radiation Source

Radiation cross-linking affects different characteristics of polymers like mechanical behaviour, chemical stability, thermal and flame resistance. Until now, radiation cross-linking is limited to only a few industrial applications: cross-linking of rubber or polymers for tyres, cables, pipes (e.g. in under floor heating systems), and heat-shrinkable tubes. Nevertheless, there exist industrial facilities like electron accelerators and gamma plant. Some of these radiation sources are operated by research institutes.

[2]The virtual dose is required for changing the MWD of the polymer in such a way that $M_w = 2\,M_n$. If the polymer under investigation has a broader distribution, then $D_V > 0$, or if it has a narrower distribution, then $D_V < 0$.

As high-energy radiation, γ-rays (electromagnetic radiation emitted by a source of a radioactive isotope, mostly cobalt 60) or electron beams (electron accelerator of low energies, 0.1–3 MeV; or high-energy electron accelerator, 10 MeV) are available.

In general, outstanding features of radiochemical cross-linking processes are:

- Easy process control by simple switching on and off the cross-linking reaction.
- Degree of cross-linking is correlated with the applied dose.
- No necessity to add any initiators, cross-linkers etc.; the mostly of used low-molecular weight additives are harmful and difficult to remove.
- Possibility of joining hydrogel formation and sterilization in one technological step, what is advantageous for hydrogels in medical applications.
- Relatively low running costs.

We used different radiation sources in our experiments with following characteristics:

Gamma irradiation: The isotope Co^{60} is used as radiation source[3]. A typical dose rate is 2 kGy/h. The dose is controlled by the exposure time and measured with a dosimeter.

Electron accelerator: To generate electrons of high energy it is necessary to accelerate the electrons leaving a cathode. The experiments described here were performed with an ELV-2 (Budker Institute of Nuclear Physics, Novosibirsk, Russia). The accelerator was a LINAC (linear accelerator) working in the energy range from 0.6 to 1.5 MeV. The maximum beam current and beam power were 25 mA and 20 kW, respectively. The dimensions of the beam extraction windows (50 μm titanium foil) are 980 mm in length and 75 mm in width. Typically applied experimental parameters for hydrogel synthesis were 1.5 MeV and 4 mA, respectively.

The dose was regulated by the exposure time and measured with a dosimeter.

Several experiments were performed at the experimental facility ANDREA 1 (Fraunhofer Institut für Elektronenstrahl- und Plasmatechnik, Dresden, Germany). The accelerator voltage in the range from 90 to 120 kV resulted in smaller penetration depths (10–80 μm). The applied radiation dose was adjusted to several hundred kGy at different dose rates by changing the beam current (2–20 mA) and the exposure time (Dänhardt et al. 2002).

Especially for the synthesis of nanogels[4] (e.g. by intramolecular cross-linking of polymer molecules with high molecular weights), the method of pulse irradiation is useful, see Fig. 10. The polymer is dissolved and the solution, flowing through a quartz irradiation cell (effective volume about 1 ml), is pulse-irradiated with electrons of several MeV (in our experiments 6 MeV) generated by a linear accelerator (ELU-6, Eksma, Russia). Pulse frequency of 5.0 Hz and pulse duration of 3 μs were applied at a flow rate of 5.0 ml/s.

[3] Co^{60} is formed in atomic reactors under the bombardment with neutrons: ${Co_{27}}^{59} + {n_0}^1 \rightarrow {Co_{27}}^{60} + \gamma$

[4] The term nanogel is used for intramolecularly cross-linked polymers. For intermolecularly cross-linked gels in the range of several 100 nm, the term microgel is used.

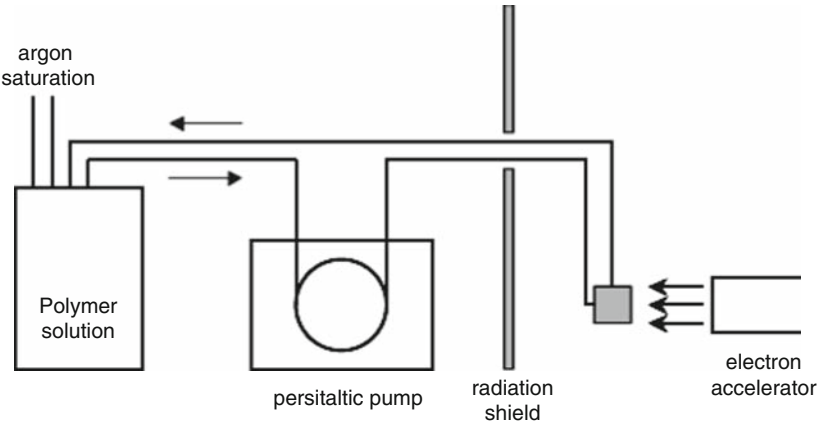

Fig. 10 Closed-loop system for pulse irradiation. Reprinted from Schmidt et al. (2005), p. 9909. Copyright (2005), with permission from Elsevier

Electron beam lithography (EBL): Some applications of responsive hydrogels require patterns of a sensitive polymer on a substrate. Applying electron beams for cross-linking enables two possibilities for patterning:

- The polymer film is exposed to high energy irradiation through a mask.
- Writing of patterns into a film of uncross-linked polymer with a focused electron beam.

Some electron beam sources (electron beam guns) work with a low beam power (acceleration voltage $U_B < 40$ kV, $p < 100$ W) but with a high power density and a high precision (diameter about 10 μm) of the beam. They were mostly used in thermal processing (Dänhardt et al. 2002). With such equipment it should be possible to write patterns with a size of several 10 μm. A further reduction of the hydrogel structures on a substrate is possible by using focused electron beams with a typical beam diameter of 10 nm and smaller. The electron beam is moved in a linear pattern across the sample and deflected to a defined extent in *x*- and *y*-direction. Often, scanning microscopes are modified for electron beam lithography.

For a patterning in the sub-μm range, the microscope S-4500 from Hitachi Ltd., Japan, with a cold field emission cathode was modified. Beam steering is decoupled from the microscope and is carried out with an adapted electronic device (ELPHY plus, Raith GmbH, Dortmund, Germany). The properties of the electron beam can be adjusted. The main influencing factors are acceleration voltage, sample current, beam diameter, dwell time (time the electron beam dwells on one pixel), and step size. The beam current (electron energy 20 keV) was typically chosen as (8–15) pA.

The patterns were generated by an arrangement of exposure points. The structural design is converted pixel-wise into "Yes" (electron beam hits the sample) or

"No" (electron beam does not hit the sample) decisions. The position of the electron beam (deflection in *x*- and *y*-directions by a coil system) and the dwell time (beam blanker, on–off) for each pixel were controlled by an ELPHY data acquisition and control computer system (Raith GmbH Dortmund, Germany). To increase precision when fabricating larger structures, the unit is equipped with a sample holder controlled by laser interferometry. Positioning accuracy amounted to about 10 nm ranges. Different patterns like individual points, stripes (linear sequence of points), pads (two-dimensional array of exposure points), and more complicated geometrical figures have been be generated by electron beam lithography. The irradiation experiments were performed under high vacuum (10^{-4} Pa). The average dose D_{av} for an exposure is given by

$$D_{\mathrm{av}} = \frac{I\,t\,N}{A}, \tag{9}$$

where I is the beam current, t the dwell time per pixel (in our experiment 8 ms) and N the number of pixel in the area A. The dose is measured in $\mu C/cm^2$; a typical value used for cross-linking is about 100 $\mu C/cm^2$.

EBL exhibits both, advantages and disadvantages. Main advantages are (Liu et al. 1999):

- Geometric structure size of down to a few nm, depending on the properties of the polymer.
- Structures of different polymers can be created consecutively.
- By varying the dose above the minimum cross-linking dose, areas with different degrees of cross-linking can be produced which can cause different swelling patterns.
- The location of the structures can be defined very precisely.

Main disadvantages are:

- Beam-borne and, hence, slow process;
- Exposure area of the electron beam is limited in size ($< 1 \times 1 mm^2$, depending on the magnification selected during exposure on many commercial microscopes). To create larger structures, substructures have to be lined up and exposed consecutively. This requires a very precise control of the sample holder.

During exposure the electrons penetrate the polymer layer and lead to a modification of the polymer. Depending on the acceleration voltage in particular, the electrons also penetrate the substrate material and are scattered. Thus, they can influence the polymer again by the so-called back scattering. Using Monte Carlo simulations it is possible to describe energy deposition and electron scattering within a polymer layer and the substrate. Simulations results showed that the spatial energy distribution depends strongly on the acceleration voltage. The higher the acceleration voltage is the larger hydrogel thicknesses are possible.

Table 3 Comparison of electron beam and gamma irradiation

Radiation	Electron beam	Gamma irradiation
Source	Electron accelerator	Radioactive isotopes (mostly $^{6\circ}$Co)
Depth of penetration	mm range	cm range
Reaction time	1–2 min	Several hours
Reaction condition	Only thin films, thicker films need higher beam energy (penetration profile!)	Diffusion of oxygen must be prevented
Critical process conditions	Variation in cross-linking density, gradient of cross-linking density, heating effects	Long reaction time
Advantages	Short reaction time, beam focusing	Homogeneously cross-linked samples, no restrictions regarding dimension

2.3 Radiochemical Synthesis of Hydrogels

The history of radiation chemistry of polymers started in the early 1950s (Chapiro 1962; Charlesby and Alexander 1955). Poly(*N*-vinyl pyrrolidone) (PVP) was and still is an often applied polymer, also as hydrogel, in medicine and pharmacy. In 1955 Charlesby and Alexander first reported on cross-linking of PVP (Charlesby and Alexander 1955). Since then various other water soluble polymers have been radiochemically cross-linked, even for creating new biomaterials (Hoffman 1981). Hydrogels can be synthesized by radiation techniques in different ways:

- Irradiation of monomers (in bulk or in solution). Polymerization takes place in the first stage of the process, followed by a cross-linking of the formed polymer chains. This way is the most common one if the monomer is easily available. It is frequent practice to add some bi-functional monomers to increase the efficiency of cross-linking. For biomedical use, all non-reacted monomers and residues have to be extracted.
- Irradiation of polymers in aqueous solution. The polymer is dissolved in water and the aqueous solution is irradiated. Such systems do not contain monomers or a cross-linking agent; therefore, hydrogels formed by this procedure are suitable for biomedical applications. The structure of the formed hydrogel depends on the concentration of the polymer see Sect. 2.4 a. The concentration influences the cross-linking efficiency. It is easy to degas the solution and to prevent the disturbing influence of oxygen. In some cases it is necessary to remove reactive species, formed during irradiation, by proper washing the gel. Hydroxyl radicals, hydrated electrons, and hydrogen atoms are the dominant species formed by irradiation of aqueous polymer solutions. The former two are the main species. Their yield can be enhanced in the presence of N_2O.

- Irradiation of dry polymers (often as film). The gelation dose is higher than for cross-linking dissolved polymers, because the amount of formed radicals during irradiation is small. From this it does not follow, that the energy must be higher than for the irradiation of a solution. It may be difficult to remove the oxygen fully. In general, the cross-linking efficiency is lower and the gel fraction is smaller. For our own experiments we irradiated dry thin films of smart polymers on different substrates. The patterning experiments were performed also at the dry state.

The extent of reaction as well as the cross-linking density is determined by the irradiation dose. In general, the cross-linking density increases and the sol content decreases with increasing dose. But it is necessary to determine these correlations for each polymer at the conditions during irradiation.

In the following we discuss the radiation-chemical synthesis of non-sensitive and smart hydrogels. The aim was to synthesize hydrogels of different sensitivities as bulk material. Usually, we used these experiments to determine the characteristic parameters of the cross-linking process (p_0/q_0; D_g, $g = \mathrm{f}(D)$, see Eq. (4)). For technical applications we need polymers from the mm- via the μm-down to the nm-range, e.g. as particles or as thin films. Procedures to patterning smart hydrogel layers on different substrates (glass, silicon wafer) are described below. The radiochemical approach offers possibilities to fix structures which were formed in solution, e.g. complexes, aggregates, or micelles. Polymers of different size can be filled with ferroelectric or ferromagnetic particles and afterwards cross-linked.

2.4 Examples of Gel Synthesis

a) Influence of concentration and temperature

Poly(vinyl methyl ether) (PVME) is known as a temperature-sensitive polymer. The polymer finds industrial application as adhesive in packaging and is produced in industrial scale. PVME was obtained from the BASF AG as aqueous solution (Lutonal M40, 50 wt.-%). The molecular weight was determined by static light scattering in 2-butanone as $M_w = 57{,}000$ g/mol. The polydispersity, determined by GPC in THF using universal calibration, is $M_w/M_n = 2.3$. The phase transition temperature was analyzed by DSC measurements at $c_p = 5.0$ g/l as $T_{cr} = 37°\mathrm{C}$. Aqueous solutions of PVME were prepared by diluting the concentrated solutions ($c_p = 0.01$–5.0 g/l). Prior to the irradiation the solutions were degassed to remove oxygen by purging argon through the solution. The parameters of Charlesby-Pinner Eq. (4) (e-beam irradiation) in our experimental setup were determined as $D_g = 21$ kGy (gelation dose) and $p_0/q_0 = 0.36$, respectively. The cross-linking dominates the chain scission reaction.

As mentioned above, a typical cross-linking procedure starts with the irradiation of an aqueous solution of the polymer with electrons or γ-rays. The structure of the formed gel depends on polymer concentration. If the conformation of the polymer

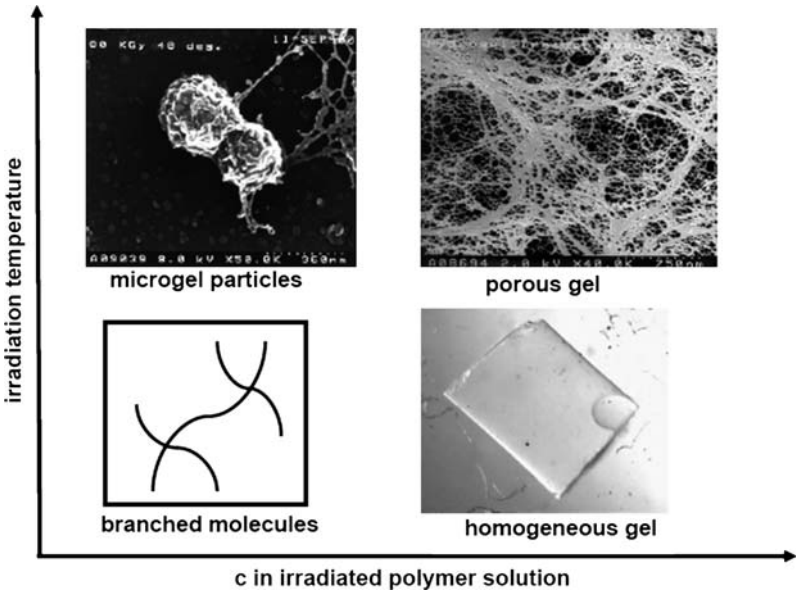

Fig. 11 Influence of temperature and polymer concentration c on the structure of PVME as example of a stimuli-responsive gel

chain depends on temperature, then the morphology of the formed gel is influenced by T. It is worth to mention that in case of electron beam irradiation, it is difficult to prevent a change in temperature, due to the high amount of absorbed energy and the short irradiation time. In comparison to γ-cross-linked gels, the resulting gel is mostly heterogeneous; often it is sponge-like.

Fig. 11 shows schematically the relation between gel structure, concentration and temperature exemplarily for PVME.

Depending on temperature, different mechanisms occur:

- Low temperature: The polymer is in a good solution state and possesses the shape of an expanded coil. At low concentration, the polymer molecule has no contact with other molecules (single polymer chain). If the diluted solution is irradiated, radicals were produced and some polymer chains react. Molecules with high molecular weight, mostly branched, are formed (Querner et al. 2004). Irradiation of a higher-concentrated polymer solution (semi-diluted polymer solution with concentration above the overlap concentration[5]), results in a homogeneous macroscopic (bulky) gel.

[5]The overlap concentration c^* is that concentration where contacts between the polymer chains occur. c^* depends on molecular weight; the higher M is, the smaller is c^*. At $c > c^*$, the polymer chains form an entanglement (physical) network with elastic properties. It can be destroyed by adding solvent.

- High temperature: At a temperature above the critical temperature of the polymer phase separation occurs. At low concentration the polymer chains tend to aggregate. The formed aggregates have a molecular weight of several million g/mol. They can be cross-linked by irradiation; the structure formed by phase separation is fixed. Size and morphology of the gel particles is determined by the aggregation process, e.g. the heating conditions, and by the applied irradiation technique and irradiation conditions. Continuous irradiation of the solution results in particles of a diameter in the range of about 100 nm (Arndt et al. 2001a). Fig. 11 shows a single PVME particle with a diameter of about 300 nm at 40°C in the collapsed state. The particles were used as a template for dispersion polymerization of the electro-conductive polymer poly(pyrrole). The polymer forms needles (Pich et al. 2002). The size of the formed gel particles at pulse irradiation was (10–30) nm. It is possible to introduce cross-links into a single chain with high molecular weight (intra-molecular cross-linking). Under conditions of chain degradation, these intra-molecular cross-linked molecules are more stable than uncross-linked polymer molecules. Degradation does not reduce the molecular weight.

Irradiation of a high concentrated solution (again above overlap concentration) yields to a porous sponge-like macroscopic gel. Gels with high porosity show a fast swell kinetic (Arndt et al. 2001b).

Fig. 12 shows micro-gel particles cross-linked by irradiation of a phase- separated solution in the two differently swollen states, at 25°C in a highly-swollen state and at 40°C at low degree of swelling. For details see (Arndt et al. 2001a). Irradiation of a high concentrated solution results in a bulky hydrogel with typical dimension in the cm-range. The sponge-like structure of the formed PVME hydrogel (irradiation of a PVME-solution in the phase-separated state) at different temperatures (swollen above and below the volume phase transition temperature) is shown in Fig. 13. The irradiation dose was 50 kGy.

Radiation-induced cross-linking gives the possibility to synthesize gels in a broad range of dimension, a broad variety of geometries, and of different composition. This is discussed on selected examples (see Sect. 2.4b–2.4e).

b) PVME films

For some applications, e.g. for sensors, cell adhesion or cell detachment, microfluidic application or for smart coatings, it might be useful to synthesize cross-linked films or to cross-link a layer of the stimuli-responsive hydrogel on different substrates. On example of PVME we demonstrated the possibilities of radiation chemistry to achieve films with thicknesses in the range of microns. In a first step, a substrate is coated with the uncross-linked polymer by spin-coating. The thickness d of the polymer layer depends on the concentration c_P of the polymer solution and the rotational speed ω. It can be adjusted to a predetermined value. The substrate is irradiated after drying. We used the following radiation parameters: radiation source ANDREA 1, dose (150–450) kGy at different dose rates, E=(90–120) keV (Hegewald et al. 2005; Hegewald et al. 2006). The

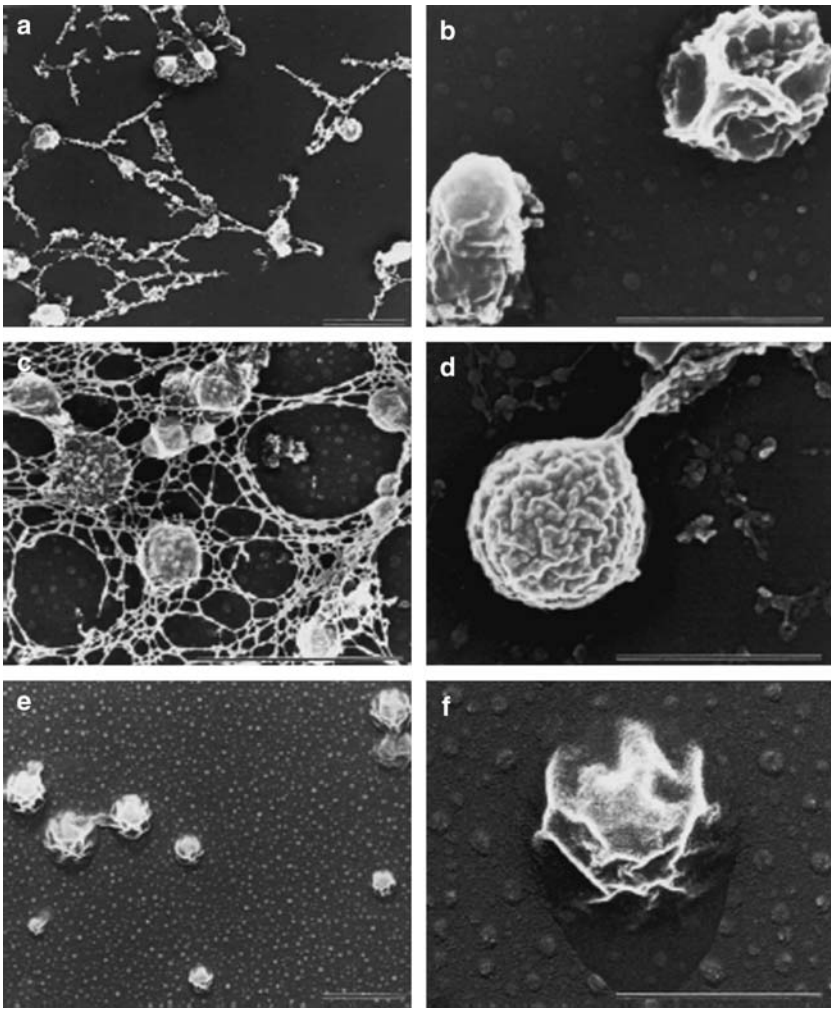

Fig. 12 Secondary electron micrographs of microgels in (**a**, **b**) swollen, (**c**, **d**) shrunken, and (**e**, **f**) dry state. The microgels were formed by irradiation (dose 80 kGy) of a diluted PVME solution (PVME from Aldrich). (**a**) Globular particles bound to polymeric net showing different sizes and shapes, (**b**) individual sponge-like microgels at high magnification, (**c**) polymeric net, formed by the sol content, with microgel particles, (**d**) single particle at high magnification, (**e**) particles in the dry state; the particles were flattened due to the surface tension, (**f**) individual flattened particle at high magnification. Scale bars correspond to 1 m (**a**, **c**, **e**) and 0.5 m (**b**, **d**, **f**), respectively. Reprinted from Arndt et al. (2001a), p. 6790. Copyright (2001), with kind permission from Elsevier.

irradiation was performed in inert atmosphere; the samples were placed into poly (ethylene) bags, which were purged with N_2. The remaining O_2 content was (50–100) ppm. A scheme of the preparation procedure is shown in Fig. 14.

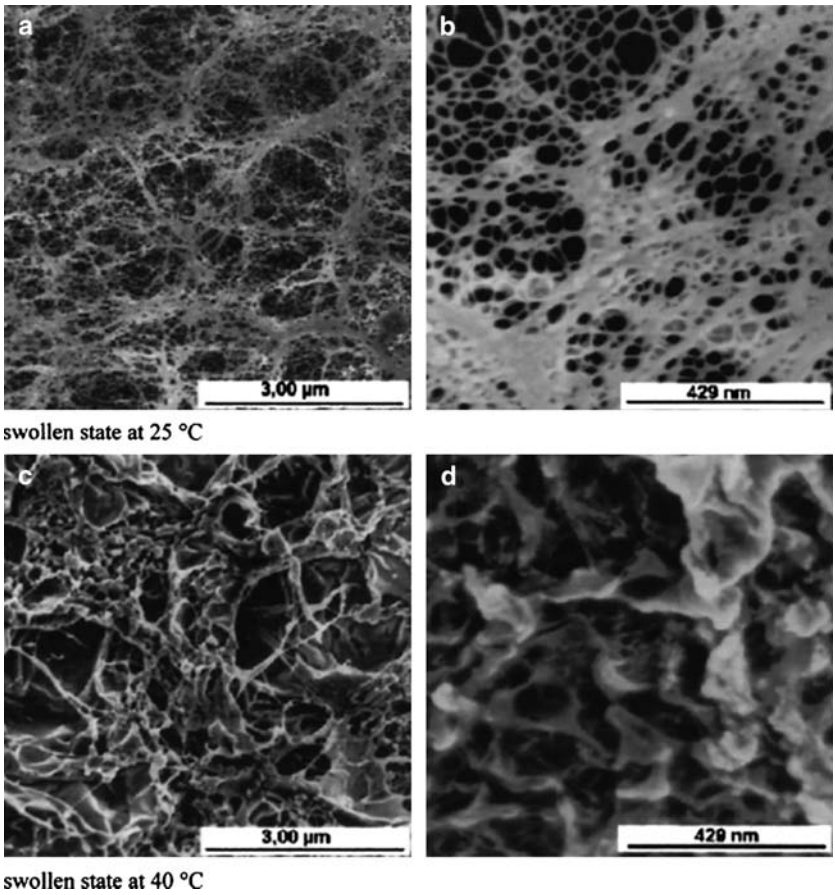

Fig. 13 Secondary electron micrographs of PVME hydrogel in different states at different magnifications. (**a**, **b**) Gel at high degree of swelling (25°C, temperature below volume phase transition temperature); (**c**, **d**) Gel at small degree of swelling (40°C, temperature above the volume phase transition). Reprinted from Arndt et al. (2001b), p. 321. Copyright Wiley-VCH & Co. KGaA. Reproduced with permission

The thickness d of the polymer film is given by

$$d \propto c_P/\sqrt{\omega} \tag{10}$$

After drying the film is irradiated. The non-irradiated polymer as well as the sol content is washed out by a good solvent, here water. The thickness of the dry layer after irradiation is smaller than before irradiation due to the sol content. The higher the dose is, the smaller is the sol content.

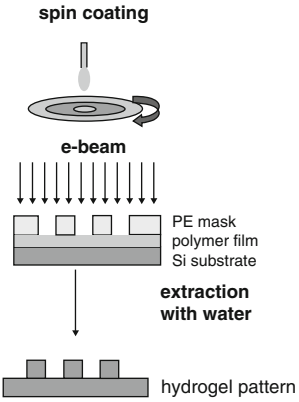

Fig. 14 Preparation scheme of a patterned PVME structure on silicon substrate by e-beam irradiation through a PE mask.

The swelling behaviour was investigated by measuring the thickness of the cross-linked layer and the concentration of the swelling agent inside the layer by ellipsometry. The thickness ratio measured in the highly swollen state at low temperature and the shrunken state at high temperature was equal to the volume degree of swelling. That means that thin layers deposited on a substrate swell only unidirectional out-of-plane.

A gradient in cross-linking density and therefore regions with different swelling behaviour can be generated by a consecutive spatially localized irradiation of a precross-linked layer through a mask.

The synthesis of a bilayer, e.g. of an environmentally sensitive polymer and of a non-sensitive polymer with special properties (e.g. biocompatibility), is possible by coating a low cross-linked polymer layer with a second polymer and applying an additional irradiation step (Hegewald 2004).

c) Blends

An advantage of radiochemical induced cross-linking is the possibility to combine polymers with different properties. For that purpose, the polymers were separately dissolved in water. The solutions were mixed and irradiated. (Gottlieb et al. 2005) describes the synthesis of temperature-sensitive hydrogel blends of PVME (as thermo-sensitive polymer) and the radiation-cross-linkable polymer PVP (a polymer that is applied in pharmaceutics). The experiments show that the gelation dose of the blend is between the gelation doses of the two pure polymers.

Another way to synthesize gels of different composition is the irradiation of a mixture of polymers and monomers (Licea-Claverie et al. 2008). In comparison to other methods of macromolecular synthesis the radiochemical route seems to be easier, but a drawback of the method is that the reaction is less controllable and the formed polymer is less defined in its structure.

d) Filled hydrogels

Filling of polymers is a common technique to improve their properties. For examples, hydrogel can be filled with ferroelectric substances to obtain

electro-rheological properties (Gao and Zhao 2004) or with ferromagnetic material. Ferroelectrical particles were aligned in the hydrogel matrix under an externally applied electrical DC field. The alignment increases the elastic modulus. It was found, that the modulus of the elastomer cured under an electrical field is larger than that without an electrical field. The modulus increases proportional to the increasing field. Gels filled with magnetic particles can be deformed by magnetic fields (Zrinyi 2008; Filipcsei et al. 2007). The magnetic gels and elastomers (magneto-elasts) consist of small magnetic particles (in the nm- to μm-range) dispersed in an elastic polymeric matrix. The magnetic particles couple the shape and the elastic modulus with the external magnetic field.

Ferroelectric and ferromagnetic materials can generate heat in an AC field due to their hysteretic materials properties. The thermal energy can be used to heat the gel and to induce the phase separation process in a temperature-sensitive hydrogel. Different particles were suspended in a solution of PVME. Films of the filled polymer were casted and cross-linked by irradiation. Due to the cross-linking process, the particles are fixed in the polymer structure. Fig. 15 shows FESEM micrographs of such a filled hydrogel. The films show ferroelectric or ferromagnetic properties (Theiss et al. 2005).

e) Complexes, micelles

Cross-linked particles with dimensions in the range of (10–100) nm are needed for biomedical application, e.g. as drug carrier. A suitable route to synthesize such particles is given by fixing aggregated structures which were formed in a polymer solution. Polymers can form intermolecular and intramolecular complexes (Tsuchida and Abe 1982), e.g. hydrogen-bonded complexes are formed between proton acceptors and proton donators. These complexes can be applied as drug carriers or for drug delivery (Lele and Hoffman 2000), especially if one of the complex-forming agents is a polymer-drug conjugate. It is an interesting fact that the conditions of the volume phase transition of a sensitive polymer were influenced by polymer complexation. If measurements were done at constant environmental conditions, then the concentration of the complexing polymer induces the transition (Yu et al. 1992).

The procedure for a radiation-induced cross-linking of intermolecular complexes is demonstrated in the following exemplarily for polyvinylpyrrolidone and polyacrylic acid as complexing polymers. Both polymers are often used in pharmaceutical application.

Spontaneous formation of interpolymer complexes with a weak polyacid (like PAA) can be observed below a certain pH value (critical pH). Aqueous solutions of both polymers were mixed. At a pH below 4.0 [6] complexes were formed. Irradiation of the diluted complex-containing solution results in an intermolecular cross-linking of the complexes at low radiation doses. Irradiation at higher doses generates simultaneously more than one radical on a chain. The formation of covalent bonds

[6] PAA: $pK_a = 4.7$, Yu et al. (1992).

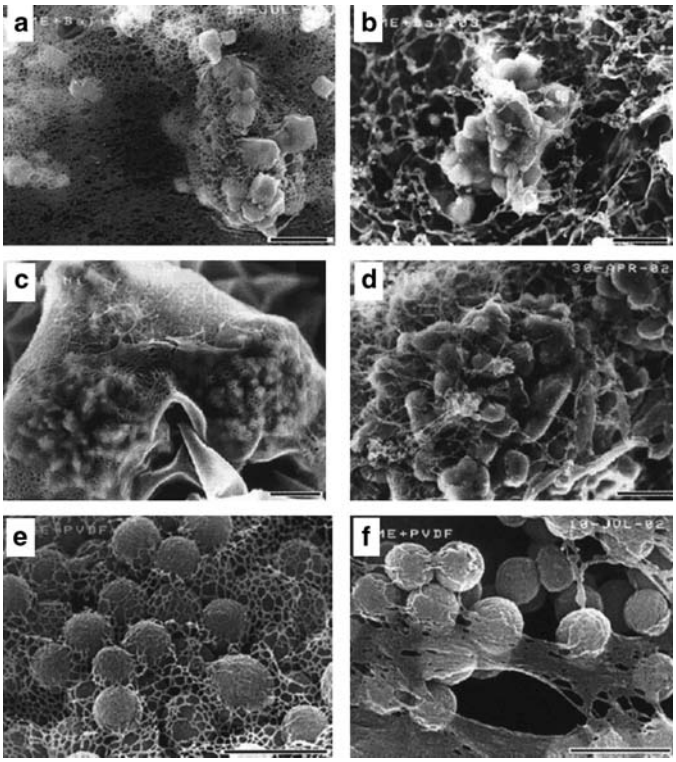

Fig. 15 FESEM micrographs of PVME filled with (**a**, **b**) ferroelectric $BaTiO_3$ particles, (**c**, **d**) ferromagnetic nickel particles and (**e**, **f**) ferroelectric poly(vinylidene fluoride). The figures show the filled hydrogel in the swollen state (**a**, **c**, **d**) low temperature,) and shrunken state (**b**, **d**, **f**) high temperature). The bars correspond to (**a**–**d**) 1 μm and (**e**, **f**) 500 nm. Reprinted from Theiss et al. (2005), p. 2262 . Copyright John Wiley & Sons Inc. Reproduced with permission

between chain segments leads to compact structures and a decrease of size with increasing radiation dose. Typically, the radius of gyration of the formed intramolecular complexes was (20–50) nm. The Fig. 16 shows a scheme of the complex formation.

The molecules of a block copolymer can micellize in an aqueous solution. A well-known example is Pluronic® F127, a PEO-PPO-PEO block-copolymer from BASF AG, Germany. This polymer is cross-linkable by irradiation and, therefore, the micelles formed in aqueous solution can be fixed by irradiation.

2.5 Patterning

Many applications of hydrogels need a patterned layer on a substrate. Different techniques were used for patterning in different regions of dimension (Table 2).

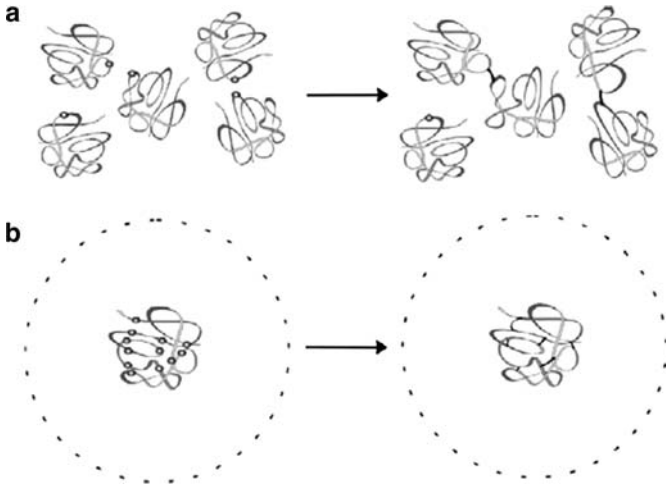

Fig. 16 Scheme of radiation-induced (**a**) intermolecular and (**b**) intramolecular cross-linking processes. The dots denote mid-chain polymer radicals. Reprinted from Henke et al. (2005), p. 395. Copyright (2005), with permission from Elsevier

Table 4 Overview of patterning techniques and applications of patterned hydrogels

Patterning techniques	Applications
• Micro-contact printing (Xia and Whiteside 1998)	• Cell adhesion/detachment devices (Lutolf et al. 2003; Koh et al. 2003)
• Photolithography (Chen et al. 1998; Ward et al. 2001)	
• Surface-initiated polymerization of brushes (Milner 1991; Zhao and Brittain 2000; Rühe et al. 2004)	• Protein adsorption (Hong et al. 2004)
	• Micro-reactors (Harmon and Tang 2003)
• "dip-pen" nano-lithography (Wounters and Schubert 2003)	• Automated fluidic valves (Beebe et al. 2000; Richter et al. 2003)
• Plasma immobilization (Schmaljohann et al. 2005)	• Sensors (Marshall et al. 2003; Richter et al. 2004a)
• Ink-jet printing (de Gans et al. 2004)	

The most commonly practiced means for fabricating micro-patterned hydrogels is based on in-situ photo-polymerization and photo cross-linking using UV light in a liquid phase. A drawback of this method is that the prepolymer or polymer solution has to be brought into the irradiation set-up. An alternative approach is to cross-link a prefabricated dry film of the sensitive polymer.

Patterning is possible for polymers which can be cross-linked even in a dry state. The polymer layer, typically with thicknesses in the 100 nm range, is formed e.g. by spin-coating on a substrate and irradiated by an electron beam in the dry state. Different patterns with high resolution (down to the 10 nm range) are possible. The dose needed for cross-linking the dry polymer is higher than for the same polymer

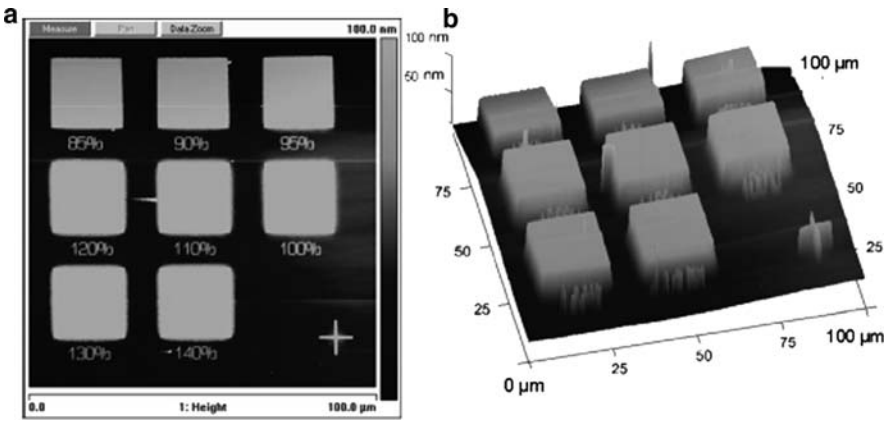

Fig. 17 AFM image of irradiated PVP dots in the dry state on a Si substrate. (**a**) Irradiation pattern; (**b**) 3-D visualization. The values in Fig. 9a corresponds to the particular percentage of the irradiation dose (100 % = 100 µC/cm^2). Reprinted from Burkert et al. (2007b), p.536. Copyright John Wiley & Sons Inc. Reproduced with permission

in the dissolved state. The radiation dose influences the sol content: the higher the dose is, the lower is the sol content. After irradiation the sol is washed out. Therefore, the thickness of the dry pattern depends on the dose. This is shown in Fig. 17 on the example of dots of PVP cross-linked with an electron beam. The 3-D visualization of the patterns shows a change of the dot thickness from 50 nm at low doses to 100 nm at high doses.

Due to the back-scattering of the electrons on the substrate, the adhesion of the cross-linked polymer is very good (Krsko et al. 2003). Hence, in most cases an adhesion promoter is not necessary.

More complex pattern can be written by electron beam lithography. This is shown on example of the thermo-sensitive polymer PVME deposited on a silicon substrate in Fig. 18. The patterns attached to the substrate show the same sensitivity as bulk polymer networks.

The resolution and the sharpness of the patterns were strongly influenced by the irradiation conditions. On example of the temperature-sensitive polymer hydroxypropylcellulose (HPC; LCST in water of 41°C (Kley 1971)) and PNIPAAm, we investigated the influence of the acceleration voltage on the back-scattering and the proximity effect (Arndt et al. 2009). In closely packed patterns, the primary beam generates back-scattered electrons causing an over- or under-exposure in the resulting pattern. The so-called proximity effect is seen in the contour line in Fig. 19. It influences the spatial resolution of the structure.

To create ideal structures, one thing which needs to be determined in particular is the ideal dose depending on the acceleration voltage, the structural geometry and

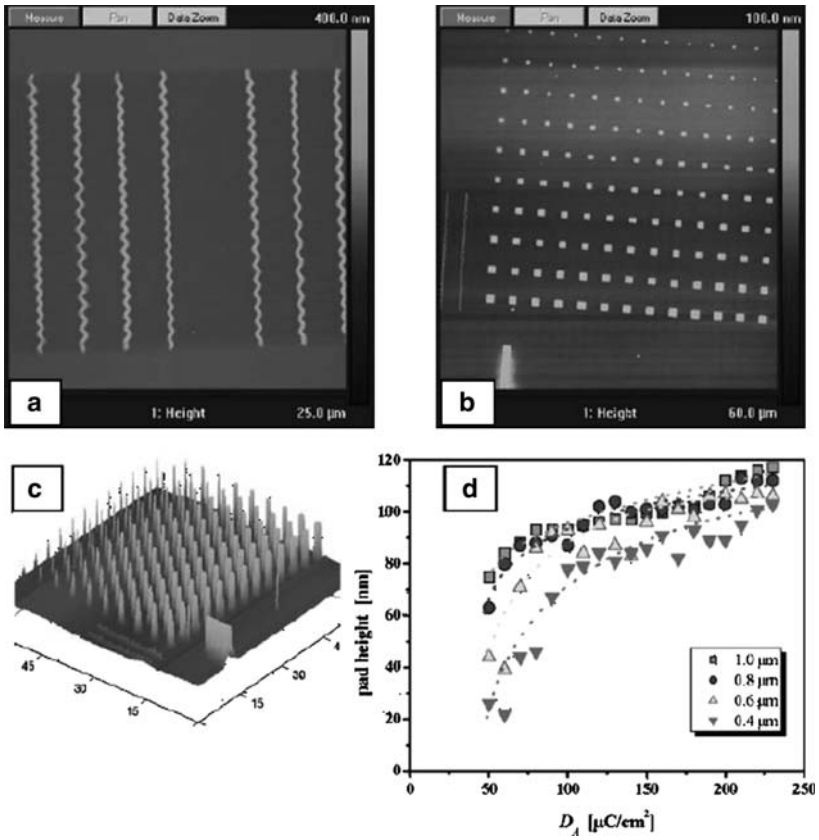

Fig. 18 (**a**) AFM image of irradiated stripes (thickness 250 nm, line width 150 nm; dose $D < 100$ µC/cm^2). Swelling and deswelling result in a wave-like structure at these doses. Stripes irradiated with a higher dose show no influence of swelling/deswelling cycles on topography; (**b**) AFM image and (**c**) 3-D plot of irradiated squares, pad with lateral size ranging from (1.2×1.2) µm^2 to (250×250) µm^2 at various irradiation doses; (**d**) pad height as function of size and applied radiation dose. Due to the decreasing sol content with increasing dose, the height of the pads increases with dose. The spin-coated dry PVME layer was 150 nm thick. All images were taken in dry state. Reprinted from Schmidt et al. (2006), p. 757, Copyright Wiley-VCH & Co. KGaA. Reproduced with permission

the structural surroundings. Often, special test structures are used to determine the particular exposure parameters.

Like for the creation of separated structures, e-beam lithography can be used to generate cross-linking gradients or small areas with different cross-linking density and therefore swelling degree in a geometrically larger hydrogel structure. The last technology uses a two-irradiation step procedure, where a pre-irradiated layer is locally irradiated again forming the resulting structure, see Fig. 20. The first and

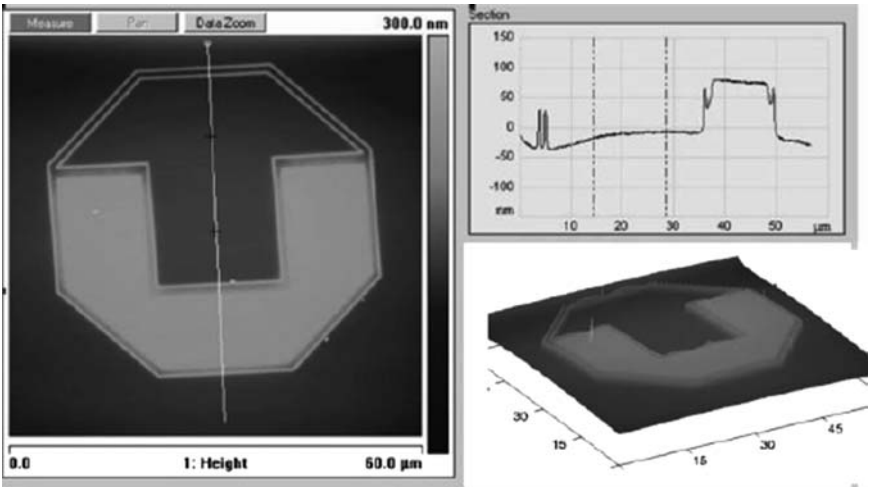

Fig. 19 PVP film patterned as TU Dresden logo by electron beam lithography. The contour plot demonstrates the influence of the proximity effect on the spatial resolution. Reprinted from Burkert et al. (2007b), p. 537. Copyright Wiley. Reproduced with permission

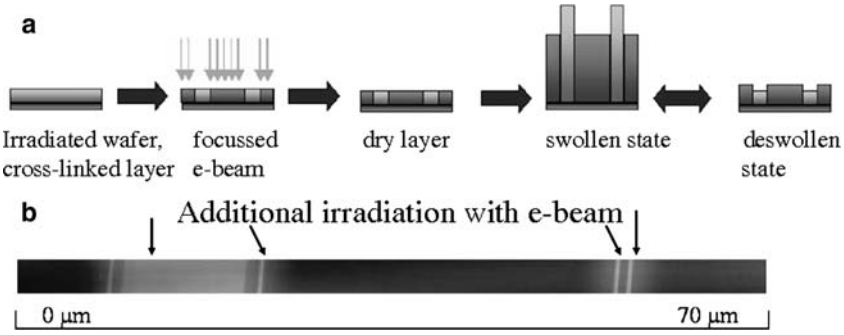

Fig. 20 Two-step irradiation of a cross-linked PVP layer with an electron beam. (**a**) Principal sketch of the irradiation procedure. (**b**) Three lines of 0.4 µm and one line of 14 µm were written into a PVP square of about 60 µm width. The degree of swelling Q of the pre-irradiated PVP was 10 and of the double irradiated $Q = 6$. For details see Burkert et al. (2007b)

second irradiation can be carried out by two electron beam lithography steps or as a combination of EBL and another irradiation method.

As mentioned above, structures of different polymers like bilayers can be produced by coating a cross-linked layer with another polymer and a consecutive irradiation. EBL can also be used to generate complex structures from several different hydrogels located next to one another. This was shown exemplarity for

the HPC (thermo-sensitive) and P4VP (pH-sensitive) hydrogels (Arndt et al. 2009; Kaiser 2007).

3 Gel Point Determination of the Reversible Gelatin Gelling System

3.1 Gel Point

The sol-gel transition (Winter and Mours 1997; Stauffer 1998; Stauffer et al. 1982; Adam and Lairez 1996) of polymers is a very important branch of critical phenomena. Its kinetics characterizes the chemistry and physics of gelation. The determination of the gelation threshold is an important parameter to control the mechanical properties of a gelling system in polymer industry. In the sol-gel phase transition, an infinitely large macromolecule is formed, which can only swell but cannot be dissolved in a solvent. Critical phenomena are those which occur exactly in the phase transition or asymptotically close to it.

Branching models are based on multifunctional molecules of different types between which covalent bonds are formed to yield a network structure. One of the multifunctional molecules is required to carry at least three functional groups, whereas the other one can have two functional groups. The overall extent of reaction p equals the *a priori* probability that any given functional group has condensed. The earliest of these branching theories was developed by Flory (Flory 1941) and Stockmayer (Stockmayer 1943). Using combinatorial approaches, both derived an expression for the molecular weight distribution and subsequently the critical extent of reaction p_c at which the molecular weight diverges ($M_w \rightarrow \infty$: gel point). Their approach includes several simplifying assumptions, which are usually not valid in real systems, i.e.

- The reactivities of all functional groups of the same type are equal and independent of each other
- No intramolecular reactions between functional groups on the same cluster (loop formation) are allowed
- The cross-links are randomly formed between any pair of functional groups that can form a bond, and
- Point-like monomers are assumed (no steric hindrance and excluded volume effects)

More advanced branching models are the so-called recursive theory by Miller and Macosko (Macosko and Miller 1976) and the cascade theory by Gordon (Gordon 1962). Both are able to include nonidealities such as cyclization and long-range substitution effects. All branching theories are mean-field theories and

yield the same simple expression for the critical extent of reaction (for the same chemical model) depending on the geometry of the network.

Percolation theory (Stauffer and Aharony 1995) describes the random growth of molecular clusters on a *d*-dimensional lattice. It is intended to describe gelation in a better way then classical statistical methods (which in fact are equivalent to percolation on a Bethe lattice or Cayley tree) because it overcomes limitations regarding mean-field assumptions like unlimited mobility and accessibility of all groups (Stauffer et al. 1982; De Gennes 1979).

There is a big difference between chemical and physical gels. Chemical gels are irreversible and their cross-links have an infinite lifetime resulting in mechanically strong gels. In physical gels (Te Nijenhuis 1997a) various forces such as van der Waals forces, electrostatic attraction or hydrogen bonding can be employed to bind polymer chains together to form a reversible gel network, in which the cross-links have a finite lifetime, breaking and reforming continuously. Most of such reversible gels consist of double- or triple-helical sections (junction zones) where the chain length of the macromolecule is much larger than these ordered sections (Burchard et al. 1998). Such reversible gels are never true solids; but if the association lifetime is sufficiently long enough, they appear to be solid for a certain time. That means, whether a physical gel is weak or strong, it depends on the time scale on which it is observed.

3.2 Gel Point Determination Methods

3.2.1 Dynamic Light Scattering

The in-situ dynamic light scattering (DLS) technique is very suitable to study the gelation process without disturbing the gelling system. It is also worth mentioning, that the DLS method has the advantage to have access to shorter time scales than in-situ rheology.

Scattering signals in a gelling solution are dominated by interference between different clusters evolving by gelation. This interference conceals structural information on individual clusters. Hence, in order to investigate the spatial correlation of concentration fluctuations, a scattering experiment was carried out on a diluted system.

A lot of studies on the sol-gel transition by light scattering methods have been carried out in the past, see (Richter 2007) and the references cited therein.

When an infinite network is formed, the polymer chains in the network lose their freedom to move and are in a limited space. This results in non-cancellation of concentration fluctuations and in the emergence of position-dependent concentration fluctuations (i.e. frozen inhomogeneities). According to Shibayama et al. (Shibayama and Norisuye 2002; Shibayama 2006) there are four types of such frozen inhomogeneities in the gel state: spatial, topological, mobility and connectivity

inhomogeneities and four physical properties for determining the gelation threshold by DLS:

1. The change in the scattered intensity (occurence of speckle patterns)
2. The power-law behaviour in the time intensity correlation function (TCF)
3. The characteristic broadening of the decay time distribution function obtained by inverse Laplace transform of the TCF, and
4. The suppression of the initial amplitude of the TCF

These methods are nondestructive and no dilution of the sample is required. Each of these methods is a phenomenon based on the characteristic features of gels, i.e. (1) inhomogeneity, (2, 3) connectivity divergence and (4) nonergodicity.

The spatial inhomogeneities are nonrandom spatial variations of the cross-link density in a gel, which result in anomalous scattering. The topological inhomogeneities represent defects of the network such as dangling chains, loops, chain entrapment, etc. They affect the dynamics and swelling behaviour of gels. The connectivity inhomogeneities depend on cluster size, distribution and architecture of polymer chains. They govern the dynamics of the system and determine the sol–gel transition threshold as critical dynamic property. The mobility inhomogeneities correspond to variations of the local degree of mobility due to emerging cross-links. The mobility inhomogeneities are the reason why scattering speckles appear exclusively in the gel state. For gels, the scattering intensity strongly fluctuates with sample position. Each speckle corresponds to a time-average scattering intensity $\langle I \rangle_T$. On the other hand, an ensemble-average scattering intensity $\langle I \rangle_E$ is obtained by averaging over sample position. The inequality $\langle I \rangle_T \neq \langle I \rangle_E$ is a characteristic feature of gels due to their nonergodic nature.

At the gelation threshold, a clear power law behaviour for the TCF occurs:

$$g_2(q,t) - 1 = \frac{\langle I(q,0) \times I(q,t) \rangle}{\langle I(q,0) \rangle^2} - 1 \propto t^{-\mu} \tag{11}$$

with $0.19 \leq \mu \leq 0.9$ as reported by different authors (Richter 2007; Shibayama and Norisuye 2002; Shibayama 2006; Geissler 1993; Martin and Adolf 1991). Here, $\langle I(t) \rangle$ is the scattering intensity at time t and given scattering vector q with respect to $t = 0$. $< \bullet \bullet \bullet >$ denotes the time average. The power-law behaviour, which possesses no characteristic relaxation time, is self-similar, implying a fractal structure of the clusters forming the critical gel (Geissler 1993).

3.2.2 Oscillatory shear rheology

Winter et al. (Winter and Mours 1997) reported at first a power law behaviour for the shear moduli (storage $G'(\omega)$ and loss modulus $G''(\omega)$) over a wide range of shear frequencies of a permanently gelling system. They found experimentally for poly(dimethylsiloxane) samples a scaling law $G'(\omega) = G''(\omega) \propto \omega^{1/2}$ at the gel point and later generalized it to

$$G'(\omega) \propto G''(\omega) \propto \omega^n \quad \text{with} \quad 0 < n < 1 \tag{12}$$

or

$$\frac{G''(\omega)}{G'(\omega)} = \tan\delta = \tan\left(\frac{n\pi}{2}\right) \tag{13}$$

for all gelling systems. The Eq. (12) as well as the frequency independence of the loss tangent tan δ in the vicinity of the gel point has been widely examined for chemical and physical gels and has also been employed to determine the gel point in an exact rheological manner (Winter and Mours 1997).

On the other hand, a power law relaxation in rheology cannot be a sure indication for a gelation threshold. Self-similar relaxations has been associated with self-similar structures on the molecular and supermolecular level as well as for suspensions and emulsions (Winter and Mours 1997). Similarities between gelation and long-chain branching viscoelastic behaviour have been also discussed (García-Franco et al. 2001).

A liquid-solid transition requires additional characteristics such as the lacking of a upper time limit for the self-similar region, stretching out of the spectrum at the approach of the gel point and shrinking beyond the gel point and different curvature of the storage modulus before and after the gel point (Winter and Mours 1997). For other systems, including heat-set globular proteins, G' appears to be larger than G'' well before gelation and no cross-over or power law is observed due to the highly ordered structure before gelation (Ikeda and Nishinari 2001).

3.3 Gelatin as Example for Reversible Gelation

Gelatin is a biopolymer made from collagen through a hydrolysis process. The native conformation of collagen molecules is a triple helix formed by three individual molecular strands held together by interchain hydrogen bonding (Guo et al. 2003a, 2003b; De Carvalho and Djabourov 1998; Te Nijenhuis 1997b). Gelatin dissolves in water at temperatures above the melting temperature and consists of flexible individual random coils in solution. By cooling below the melting temperature, ordered structures of the gelatin molecules are formed. It has been shown that the ordered gelatin structures have the same conformation as collagen (Guo et al. 2003a, b). Gelatin molecules partially revert to the ordered helical collagen-like sequences, separated along the gelatine molecular chain by peptide residues in the disordered random coil conformation. While the coil-helix reversion is predominantly intramolecular through a back-refolding of the single chains at very low concentrations of about 0.01–0.1 wt-%, it becomes increasingly intermolecular as concentration is raised. This leads to gelation at concentrations above 0.5–1 wt-% caused by the formation of an infinite network of intermolecularly connected

molecules. The gelation of gelatin was found to obey the general scheme of percolation, and gelatin exhibits a gel point that depends only on the amount of renatured helices (fraction of reacted bonds) (De Carvalho and Djabourov 1998). The elastic moduli versus helix amount follows the predicted scaling laws (De Carvalho and Djabourov 1998). At the gel point, the helix amount is only a few percent (De Carvalho and Djabourov 1998).

3.3.1 Critical Dynamical Exponents for the Gelation Threshold of Gelatin

Because DLS is sometimes called micro-rheology, one can assume, that the exponent μ in Eq. (11) should be in relation with the viscoelastic exponent n from Eq. (12). The shear stress relaxation modulus $G(t)$ at the gel point shows a power law distribution of relaxation modes

$$G(t) = S\,t^{-n} \quad \text{for} \quad \lambda_0 < t < \propto \tag{14}$$

with S being the gel stiffness and t the relaxation time (Winter and Mours 1997). The upper cut-off is infinite because the longest relaxation time diverges to infinity at the gel point. The parameters S, n, λ_0 depend on the material structure at the transition point. Stiff critical gels have a small n value ($n \rightarrow 0$) and a large S value, while the critical gels are very soft and fragile, with a large relaxation exponent n ($n \rightarrow 1$) and a small front factor S (Winter and Mours 1997).

On the other hand, Doi and Onuki (Doi and Onuki 1992) proposed both a dynamic structure factor $S(q,t)$ and a time-dependent modulus $G(t)$, considering the dynamic coupling between stress and composition in polymer solutions and blends:

$$g_1(q,t) = S(q,t)/S(q,0) \cong (\xi^2 q^2/\Gamma_q \eta)\, G(t) \tag{15}$$

with ξ as the characteristic correlation length and Γ_q the thermal decay rate without the viscoelastic effect. Eq. (15) describes a correlation between the electric field correlation function $g_1(q,t)$ and shear stress relaxation modulus $G(t)$. At the gelation threshold, they obtained a decay both for the dynamic structure factor $S(q,t)$ and the time-dependent modulus $G(t)$, with the same power law exponent (cp. Eqs. (5.25) and (5.35) in (Doi and Onuki 1992)):

$$g_1(q,t) \propto S(q,t) \propto G(t) \propto t^{-\beta} \tag{16}$$

with $\beta = 0.2$–0.4 over a very wide region of t.

Because the shear relaxation modulus $G(t)$ with both its storage $G'(\omega)$ and loss parts $G''(\omega)$ of the complex modulus are connected by Fourier transform it follows

$$G(t) \propto t^{-\beta} \Leftrightarrow G'(\omega) \propto G''(\omega) \propto \omega^{n} \tag{17}$$

That implies that the critical exponents β and n have the same value (and probably the same physical origin) at the gel point: $n=\beta$.

If you take $g_2(t) - 1$, because of the Siegert relation (Geissler 1993) between $g_1(q,t)$ and $g_2(q,t)$, it follows that

$$n = \beta = {}^1\!/_2\mu. \tag{18}$$

$G(t)$ and TCF can be expressed as a sum of exponential terms, characterizing the relaxation time of different molecular processes.

As a consequence, a similar behaviour, not only at the gel point, but also over the whole range of extent of cross-linking for permanently cross-linked as well as for physical clustered systems, can be expected.

Since $G(t)$ and TCF are connected via the longitudinal modulus and the cooperative diffusion coefficient (Geissler 1993; Candau et al. 1982; Lang and Burchard 1991), it was shown that also the TCF shows a power law behaviour in the critical region (Martin and Adolf 1991; Lang and Burchard 1991). Coviello and Burchard (Coviello and Burchard 1992) could show as a first example on a thermoreversibly gelling polysaccharide that both physical quantities gave a power law behaviour at the same temperature in the critical region. The shear moduli gave also a power law behaviour in the critical region on schizophyllan gels, whereas in DLS no power law of the TCF was observed (Richtering et al. 1998; Fuchs et al. 1997).

This problem of comparing of the dynamic exponents μ and n seems to be not settled at all and is still a controversial issue. It must be emphasized that in several studies (Takeda et al. 2000; Norisuye et al. 1999, 2000) the power law exponent in DLS was discussed in the inconsistent context to the viscoelastic exponent n, while no rheological experiments were performed. To demonstrate this we carried out oscillatory shear rheology experiments. In Figure 21 the frequency-dependent storage and loss moduli for three selected temperatures are shown. The power law behaviour regarding Eq. (12) ($G'(\omega) \propto \omega^{0.71}$; $G''(\omega) \propto \omega^{0.65}$) can be observed at 25°C with an averaged exponent of $n \approx 0.7$.

In-situ DLS experiments were performed at several temperatures at a scattering angle of $\theta=90°$ during cooling. Selected TCF values $g_2(t) - 1$ are shown in Figure 22. At 24.5°C in a delay time window of $t = 0.05$–250 ms (solid line), a power law Eq. (11) with an exponent $\mu = 0.21$ was found.

Recently, Matsunaga and Shibayama (Matsunaga and Shibayama 2007) investigated also the sol-gel transition of gelatin with both methods and found that the fractal exponent D_p in their notation, ($g_2(t)-1 \propto t^{-(1-Dp)}$ and $G' \propto G'' \propto \omega^{n}$ with $D_p \approx n \approx 0.73$) both was angular- and concentration-independent. In our notation, $\mu = 1 - D_p$ holds. One can conclude, shown on several gelling systems (see below) studied here, that an equality of the exponents $D_p = n$ (with $\mu = 1 - D_p$) cannot be generally adopted.

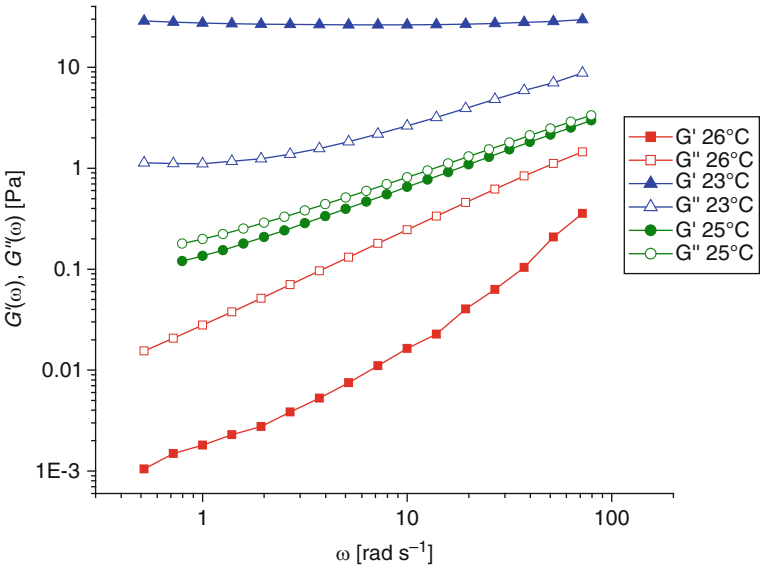

Fig. 21 Double-logarithmic plot of $G'\omega$) and $G''(\omega)$ of a gelatin sample at three selected temperatures in a cooling regime. Reproduced from Brand et al. (2006) with kind permission from American Chemical Society

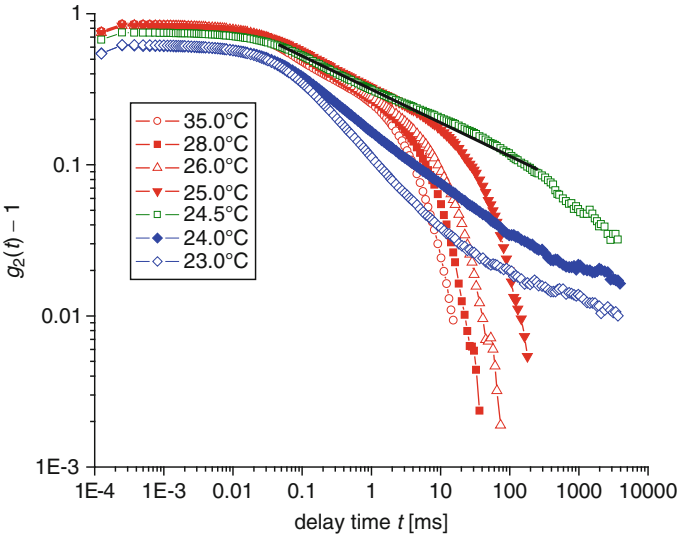

Fig. 22 Double-logarithmic plot of the TCFs versus delay time t during gelatin gelation. Reproduced from Brand et al. (2006) with kind permission from American Chemical Society

Corresponding DLS and rheology studies to prove the validity of the Eq. (18) were performed on another thermoreversible system (three mixtures made of xanthan gum and locust bean gum (XG/LBG) (Richter et al. 2004b, 2005) and on the irreversibly radical chemical cross-linking system (*N*-vinylcaprolactam/2-hydroxylethyl- methacrylate/allylmethacrylate) (Richter et al. 2004c).

The advantage of studying thermoreversible gelation during radical cross-linking reactions is that the gelation process is only influenced by temperature, which can be held constant to have enough measuring time for rheological and DLS investigations. Similar dynamical power scaling in DLS and rheology were consequently observed over several decades (not shown here). The following critical exponents were estimated from the experiments on the system XG/LBG: $n_1 = 0.62$, $\mu_1 = 0.36$; $n_2 = 0.67$, $\mu_2 = 0.32$; $n_3 = 0.59$, $\mu_3 = 0.41$.

For the radical cross-linking system (Richter et al. 2004c), the exponents were estimated as $n_4 \approx 0.75$, $\mu_4 = 0.62$. As a general result, the prediction of Eq. (18) as well as the relation $(1 - n) = \mu$ is in practice not valid at all.

It must be mentioned that the difference in the estimated gelation temperature (power law behaviours of Eqs. (11–12) on all mixtures made of xanthan gum and locust bean gum was 5–7 K (Richter et al. 2004b, 2005). The higher sol-gel transition temperature indicated by the power law scaling was always estimated by rheology measurement. The reasons for this unusual behaviour, which was observed by the authors for the first time are given in detail in (Richter et al. 2005).

For gelatin were similar gelation threshold temperatures (in a cooling regime at about 25°C) was found in rheology, DLS and NMR diffusion experiments (Brand et al. 2006). Here, for the first time, pulsed field gradient (PFG) NMR experiments have been used to determine the gel point of gelatin. From the TCFs one can calculate the mean relaxation times $\langle\tau\rangle$ which are inversely proportional to the diffusion coefficients D with $\langle\tau\rangle \propto 1/(D\,q^2)$. $\langle\tau\rangle$ is known to diverge (or at least pass a maximum) at the gelation point (Coviello and Burchard 1992). Therefore, D can be expected to show a minimum at the gelation point. We have found, that the maximum of $\langle\tau\rangle$ in DLS coincided very well with the measured minimum in the self-diffusion coefficients estimated by NMR at the gelling temperature (Brand et al. 2006). The hysteresis effects of the gelatin gelation process could also be confirmed (Fig. 23).

4 Conclusions

Oscillatory shear rheology and DLS studies have been performed on gelatin and several other gelling systems (Richter 2007). The occurrence of a power law behaviour observed with both methods was mostly assigned to the gel point. The physical meaning of μ and, as a consequence, the physical origin of the power law behaviour in DLS seems to be not completely understood in detail and is therefore

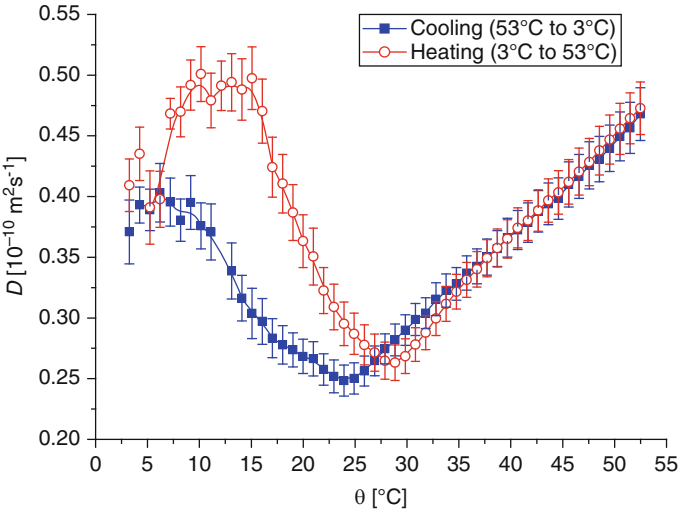

Fig. 23 Temperature dependence of the (apparent) diffusion coefficient D measured with PFG-NMR obtained by fitting the integrals of the most shielded methyl signal for the cooling and the heating regime. The error bars correspond to the statistical error of D obtained during the fitting procedure. For the other spectral regions (amide and aliphatic region) similar behaviour was observed. Reproduced from Brand et al. (2006) with kind permission from American Chemical Society.

different from that of the rheological exponent n. It was shown that up to now in each investigated case the relation $n > \mu$ at the gel point is valid but no fixed mathematical relation exists between them. A general trend in the direction of values of n (where a lucid imagination in the critical gel stiffness exists) and μ is also not observable comparing different systems. Therefore, the results of Doi and Onuki (Doi and Onuki 1992) have to be reconsidered taking into account the results presented here.

Here, the discussion of the viscoelastic exponent n in relation to the assumed gelation model (e.g. electrical analogy percolation or Rouse model), as well as the fractal dimension d_f of the critical gel (Muthukumar and Winter 1986; Muthukumar 1989) will be ignored. The reader is referred e.g. to (Adam and Lairez 1996; Martin and Adolf 1991). It has been also shown, that stoichiometry, molecular weight and concentration have an impact on the critical gel properties (Winter and Mours 1997).

In general, the small-amplitude oscillatory shear experiment seems to be the more sensitive method for a safe detection of the gel point, formed by the incipient infinite percolated cluster for thermoreversible systems. Sometimes it is difficult to decide which of the TCFs during a temperature scan has the most linear behaviour in the observed delay time window. As it was shown in (Richter et al. 2004b; Richter et al. 2005), the effect in rheology is more pronounced, such that 1–2 K

below or above the gelation threshold may influence the formed gel and pre-gel structures in the frequency dependence, and the values of $G'(\omega)$ and $G''(\omega)$ are stronger than in the shape of the TCFs. The DLS method seems not generally be able to detect the gelation threshold, and DLS measures concentration fluctuations rather than the shear response.

For thermoreversible systems like (poly(vinyl alcohol)/Congo Red) (Ikkai and Shibayama 1999) and gelatin (Ren et al. 1992) a power law in DLS was observed not only at the gelation threshold but also for gels. The same behaviour was found for silica gels (Martin et al. 1991). During the gelation to a homogeneous and speckle-free chemical gel, however, no power law was observed (Ngai et al. 2004). It has been shown, that the power law behaviour is not restricted to incipient gels but can also arise in moderately viscous solutions of a Pluronic (Nyström and Kjøniksen 1997).

One can say generally, that a power law scaling in DLS means any self-similarity, but strictly speaking not necessarily a gel point. At the critical point no characteristic length dominates, thus the power law is a requirement. Since other situations and structures can give rise to a power law, its observation cannot prove that the system is at the critical gelation condition. This may be also due to the inherent degeneracy between a spatial distribution of scatterers and the resulting scattering function. The averaging process removes any knowledge of position and phase, therefore the sample distribution cannot be reconstituted from the scattering spectrum. Furthermore, the tilting test of the light scattering cuvette cannot be a sure evidence for a gelation threshold in an exact rheological framework.

There is also a difference whether natural physical gels (with their extended heterogeneities arising form large pregel clusters already in the solution state, polydispersity effects and very high molecular weights), low molecular weight gelators (superposition with crystallization effects) or chemical gels with a different cross-linking mechanism and often fast reaction rates were studied.

Most of the gelation studies in the literature have the shortcoming that usually only one typical characterization method was used. But it must be also taken into account, that by introducing shear into the system, the gelation process can be induced or impeded. Organogelator gels are very brittle and rheological methods for the gel point determination are failing because shear load destroys the incipient gel. A very recent example for the gel point determination of a gelator using the non-destructive PFG-NMR method has been published by Brand et al. (2008).

The advantage of using DLS instead of rheology is that it can be used for systems with fast reaction rates without disturbing them. In case of doubt, both methods should be applied and compared with respect to response frequency and system size.

Acknowledgments The authors are grateful to Dr. I. Mönch (IFW Dresden) for the ELB-experiments and to Dr. U. Gohs (IPF Dresden) for the irradiation experiments with the electron accelerator.

The financial support by the DFG (grants no. RI 1079/1-1, RI 1079/1-2) is gratefully acknowledged.

References

Adam M, Lairez D (1996) Sol-gel transition. In: Cohen Addad JP (ed) The physical properties of polymeric gels. Wiley, Chichester

Arndt K-F, Schmidt T, Reichelt R (2001a) Thermo-sensitive poly(methyl vinyl ether) micro-gel formed by high energy radiation. Polymer 42:6785–6791

Arndt K-F, Schmidt T, Menge H (2001b) Poly(vinyl methyl ether) hydrogel formed by high energy irradiation. Macromol Symp 164:313–322

Arndt K-F, Richter A, Mönch I (2009) Synthesis of stimuli-sensitive hydrogels in the μM and sub-μM range by radiation techniques and their application. In: Barbucci R (ed) Hydrogels, biological properties and application. Springer, Berlin

Beebe DJ, Moore JS, Bauer JM, Yu Q, Lui RH, Devadoss C, Jo BH (2000) Functional hydrogels for autonomous flow control inside microfluidic channels. Nature 404:588–590

Brand T, Richter S, Berger S (2006) Diffusion NMR as a new method for the determination of the gel point of gelatin. J Phys Chem B 110:15853–15857

Brand T, Nolis P, Richter S, Berger S (2008) NMR study of the gelation of a designed gelator. Magn Reson Chem 46:545–549

Brazel CB, Peppas NA (1995) Synthesis and characterization of thermomechanically and chemomechanically responsive poly(*N*-isopropylacrylamide-co-methacrylic acid) hydrogels. Macromolecules 28:8016–8020

Burchard W, Aberle T, Fuchs T, Richtering W, Coviello T, Geissler E, Schulz L (1998) Steps to a deeper understanding of gels and physical networks. In: te Nijenhuis K, Mijs WJ (eds) The Wiley Polymer Networks Group Review Series, vol 1. Wiley, New York

Burkert S, Schmidt T, Gohs U, Dorschner H, Arndt K-F (2007a) Cross-linking of poly (N-vinylpyrrolidone) films by electron beam radiation. Radiat Phys and Chem 76:1324–1328

Burkert S, Schmidt T, Gohs U, Mönch JI, Arndt K-F (2007b) Patterning of thin poly(N-vinyl pyrrolidone) films on silicon substrates by electron beam lithography. J Appl Polymer Sci 106:534–539

Candau S, Bastide J, Delsanti M (1982) Structural, elastic, and dynamic properties of swollen polymer networks. Adv Polym Sci 44:27–71

Champ S, Xue W, Huglin MB (2000) Concentrating aqueous solutions of water soluble polymers by thermoreversible swelling of poly[(*N*-isopropylacrylamide)-co-(acrylic acid)] hydrogels. Macromol Chem Phys 201:931–940

Chapiro A (1962) Radiation chemistry of polymeric systems. Interscience, New York

Charlesby A (1960) Atomic radiation and polymers-radiation effects in materials. Pergamon Press, London

Charlesby A, Alexander P (1955) Reticulation of polymers in aqueous solution by γ-rays. Journal de Chimie Physique et de Physico-Chimie Biologique 52:699–709

Charlesby A, Pinner SH (1959) Analysis of the solubility behaviour of irradiated polyethylene and other polymers. Proc Royal Soc A 249:367–386

Chen G, Hoffman AS (1995) Graft-copolymers that exhibit temperature-induced phase-transitions over a wide-range of pH. Nature 373:49–52

Chen G, Imanishi Y, Ito Y (1997) Micropattern immobilization of a pH-sensitive polymer. Macromolecules 30:7001–7003

Chen C, Imanishi Y, Ito Y (1998) Photolithographic synthesis of hydrogels. Macromolecules 31:4379–4381

Coviello T, Burchard W (1992) Criteria for the point of gelation in reversibly gelling systems according to dynamic light scattering and oscillatory rheology. Macromolecules 25:1011–1012

Dänhardt J, Panzer S, Bartel R (2002) Eine neue Elektronenstrahltechnologie für die Mikrosystemtechnik. FEP Annual Report 26–33

De Carvalho W, Djabourov M (1998) Gelation under shear: a dynamic phase transition. In: te Nijenhuis K, Mijs WJ (eds) The wiley polymer networks group review Series, vol 1. Wiley, New York

de Gans BJ, Duineveld PC, Schubert US (2004) Inkjet printing of polymers: state of the art and future developments. Adv Mater 16:203–213

De Gennes PG (1979) Scaling concepts in polymer physics. Cornell University Press Ithaca, New York

Doi M, Onuki A (1992) Dynamic coupling between stress and composition in polymer solutions and blends. J Phys II France 2:1631–1656

Eddington DT, Beebe DJ (2004a) Flow control with hydrogels. Adv Drug Delivery Rev 56:199–210

Eddington DT, Beebe DJ (2004b) A valved responsive hydrogel microdispensing device with integrated pressure source. J Microelectoromech Sys 13:586–593

Feil H, Bae Y, Feijen J, Kim S (1991) Molecuar separation by thermosensitive hydrogel membranes. J Membr Sci 64:283–294

Filipcsei G, Csetneki I, Szilagyi A, Zrinyi M (2007) Magnetic field-responsive smart polymer composites. Adv Polym Sci 206:137–189

Flory PJ (1941) Molecular size distribution in three dimensional polymers. I. Gelation. J Am Chem Soc 63:3083–3090

Fuchs T, Richtering W, Burchard W, Kajiwara K, Kitamura S (1997) Gel point in physical gels: rheology and light scattering from thermoreversibly gelling schizophyllan. Polym Gels Networks 5:541–559

Gao L, Zhao X (2004) Electrorheological behaviors of barium titanate/gelatin composite hydrogel elastomers. J Appl Polym Sci 94:2517–2521

García-Franco CA, Srinivas S, Lohse DJ, Brant P (2001) Similarities between gelation and long chain branching viscoelastic behaviour. Macromolecules 34:3115–3117

Geissler E (1993) Dynamic light scattering from polymer gels. In: Brown W (ed) Dynamic light scattering. Clarendon Press, Oxford

Gordon M (1962) Good's theory of cascade processes applied to the statistics of polymer distributions. Proc Roy Soc London A 268:240–256

Gotoh T, Nakatani Y, Sakohara S (1998) Novel synthesis of thermosensitive porous hydrogels. J Appl Polym Sci 69:895–906

Gottlieb R, Schmidt T, Arndt K-F (2005) Synthesis of temperature-sensitive hydrogel blends by high energy irradiation. Nucl Instr Methods Phys Res B 236:371–376

Guo L, Colby RH, Lusignan CP, Whitesides TH (2003a) Kinetics of triple helix formation in semidilute gelatin solutions. Macromolecules 36:9999–10008

Guo L, Colby RH, Lusignan CP, Howe AM (2003b) Physical gelation of gelatin studied with rheo-optics. Macromolecules 36:10009–10020

Harmon ME, Tang MF (2003) A microfluidic actuator based on thermosensitive hydrogels. Polymer 44:4547–4556

Harmon ME, Kuckling D, Frank C (2003a) Photo cross-linkable PNIPAAm copolymers 2: effects of constraint on temperature and pH-responsive hydrogel layers. Macromolecules 36:162–172

Harmon ME, Kuckling D, Pareek P, Frank CW (2003b) Photo cross-linkable PNIPAAm copolymers 4. Effects of copolymerization and cross-linking on the volume phase transition in constrained hydrogel layers. Langmuir 19:10947–10956

Hegewald J (2004). Strahlenchemische Synthese und Charakterisierung dünner, temperatursensitiver PVME-Schichten. Diploma thesis, TU, Dresden

Hegewald J, Schmidt T, Gohs U, Günther M, Reichelt R, Stiller B, Arndt K-F (2005) Electron beam irradiation of poly(vinyl methyl ether) films: 1. Synthesis and film topography. Langmuir 21:6073–6080

Hegewald J, Schmidt T, Eichhorn K, Kretschmer K, Kuckling D, Arndt K-F (2006) Electron beam irradiation of poly(vinyl methyl ether) films: 2 Temperature-dependent swelling behavior. Langmuir 22:5152–5159

Henke A, Kadłubowski S, Ulański P, Rosiak JM, Arndt K-F (2005) Radiation-induced cross-linking of polyvinylpyrrolidone-poly(acrylic acid) complexes. Nucl Inst Meth Phys Res B 236:391–398

Hirotsu S (1993) Coexistence of phases and the nature of 1st-order phase-transition in poly (*N*-isopropylacrylamide) gels. Adv Polym Sci 110:1–26

Hoffman AS (1981) A review of the use of radiation plus chemical and biochemical processing treatments to prepare novel biomaterials. Radiat Phys Chem 18:323

Hong Y, Krsko P, Libera M (2004) Protein surface patterning using nanoscale PEG hydrogels. Langmuir 20:11123–11126

Ikeda S, Nishinari K (2001) Structural changes during heat-induced gelation of globular protein dispersions. Biopolymers 59:87–102

Ikkai F, Adachi E (2004) Novel method of producing polymer gels in aqueous solution using UV irradiation. Macromol Rapid Commun 25:1514–1517

Ikkai F, Shibayama M (1999) Static inhomogeneities in thermoreversible physical gels. Phys Rev Lett 82:4946–4949

Inomata H, Wada N, Yagi Y, Goto S, Saito S (1995) Swelling behaviors of N-alkylacrylamide gels in water–Effects of copolymerization and cross-linking density. Polymer 36:875–877

Ito Y, Chen G, Guan Y, Imanishi Y (1997) Patterned immobilization of thermoresponsive polymer. Langmuir 13:2756–2759

Kabra B, Gehrke S (1991) Synthesis of fast response, temperature-sensitive poly(N-isopropylacrylamide) gel. Polymer 32:322–323

Kaiser C (2007) Strahlenchemische Synthese und Charakterisierung dünner Hydrogel-Multi-Schichten. Diploma thesis, TU, Dresden

Kaneko Y, Nakamura S, Sakai K, Aoyagi T, Kikuchi A, Sakurai Y, Okano T (1998) Rapid deswelling response of poly(*N*-isopropylacrylamide) hydrogels by the formation of water release channels using poly(ethylene oxide) graft chains. Macromolecules 31:6099–6105

Kley ED (1971) Properties of water-soluble hydroxyalkyl celluloses and their derivates. J Polym Sci C 9:491–508

Koh WG, Revzin A, Siminian A, Reeves T, Pishko M (2003) Control of mammalian cell and bacteria adhesion on substrates micropatterned with poly(ethylene glycol) hydrogels. Biomed Microdev 5:11–19

Krsko P, Sukhishvili MM, Clancy R, Libera M (2003) Electron-beam surface-patterned poly (ethylene glycol) microhydrogels. Langmuir 19:5618–5625

Kuckling D, Wohlrab S (2002) Synthesis and characterization of multiresponsive graft copolymer gels. Polymer 43:1533–1536

Kuckling D, Adler H-J P, Arndt K-F, Ling L, Habicher WD (2000) Temperature and pH-dependent solubility of novel poly(*N*-isopropyacrylamide)-copolymers. Macromol Chem Phys 201:273–280

Kuckling D, Harmon M, Frank CW (2002a) Photo cross-linkable PNIPAAm copolymers 1: synthesis and characterization of constrained temperature-responsive hydrogel layers. Macromolecules 35:6377–6383

Kuckling D, Adler H-J, Arndt K-F (2002b) Poly(N-isopropylacrylamide) copolymers: Hydrogel formation via photocrosslinking. In: Bohindar HB, Dubin P, Osada Y (eds) Polymer gels: fundamentals and applications, ACS Symp Ser 833. ACS, Washington

Kuckling D, Richter A, Arndt K-F (2003a) Temperature and pH dependent swelling behavior of poly(*N*-isopropyl-acrylamide)-copolymer hydrogels and their use in flow control. Macromol Mater Eng 288:144–151

Kuckling D, Hoffman J, Plötner M, Ferse D, Kretschmer K, Adler HJP, Arndt KF, Reichelt R (2003b) Photo cross-linkable PNIPAAm copolymers 3: microfabricated temperature responsive hydrogels. Polymer 44:4455–4462

Lang P, Burchard W (1991) Dynamic light scattering at the gel point. Macromolecules 24: 814–815

Lele BS, Hoffman AS (2000) Mucoadhesive drug carriers based on complexes of poly(acrylic acid) and PEGylated drugs having hydrolyzable PEG-anhydride-drug linkages. J Controlled Release 69:237–248

Lesho MJ, Sheppard NF (1996) Adhesion of polymer films to oxidized silicon and its effect on performance of a conductometric pH sensor. Sens Actuators B 37:61–66

Licea-Claverie A, Salgado-Rodriguez R, Lugo-Medina E, Arndt K-F (2008) Incorporation of acid polymethacrylates into temperature sensitive hydrogels using electron beam irradiation. Polym Bull 60:701–712

Liu Y, Velada JL, Huglin MB (1999) Thermoreversible swelling behaviour of hydrogels based on *N*-isopropylacrylamide with sodium acrylate and sodium methacrylate. Polymer 40:4299–4306

Lutolf MP, Raeber GP, Zisch AH, Tirelli N, Hubbell JA (2003) Cell-responsive synthetic hydrogels. Adv Mater 15:888–892

Macosko CW, Miller DR (1976) A new derivation of average molecular weights of nonlinear polymers. Macromolecules 9:199–206

Marshall AJ, Blyth J, Davidson CAB, Lowe CR (2003) pH-sensitive holographic sensors. Anal Chem 75:4423–4431

Martin JE, Adolf D (1991) The sol-gel transition in chemical gels. Annu Rev Phys Chem 42: 311–339

Martin JE, Wilcoxon J, Odinek J (1991) Decay of density fluctuations in gels. Phys Rev A 43: 858–872

Matsukata M, Hirata M, Gong JP, Osada Y, Sakurai Y, Okano T (1998) Two step surfactant binding of solvated and cross-linked poly(N-isopropylacrylamide-co-(2-acrylamido-2-methyl propane sulfonic acid)). Colloid Polym Sci 276:11–18

Matsunaga T, Shibayama M (2007) Gel point determination of gelatin hydrogels by dyn-amic light scattering and rheological measurements. Phys Rev E 76:030401-1–030401-4

Milner ST (1991) Polymer brushes. Science 251:905–914

Muthukumar M (1989) Screening effect on viscoelasticity near the gel point. Macromolecules 22:4656–4658

Muthukumar M, Winter HH (1986) Fractal dimension of a cross-linking polymer at the gel point. Macromolecules 19:1284–1285

Nakayama Y, Matsuda T (1992) Preparation and characteristics of photocrosslinkable hydrophilic polymer having cinnamate moiety. J Polym Sci A, Polym Chem 30:2451–2457

Ngai T, Wu C, Chen Y (2004) Origins of the speckles and slow dynamics of polymer gels. J Phys Chem B 108:5532–5540

Norisuye T, Shibayama M, Tamaki R, Chujo Y (1999) Time-resolved dynamic light scattering studies on gelation process of organic-inorganic polymer hybrids. Macromolecules 32:1528–1533

Norisuye T, Inoue M, Shibayama M, Tamaki R, Chujo Y (2000) Time-resolved dynamic light scattering study on the dynamics of silica gels during gelation process. Macromolecules 33:900–905

Nyström B, Kjøniksen AL (1997) Dynamic light scattering of a poly(ethylene oxide)-poly(propylene oxide)-poly(ethylene oxide) triblock copolymer in water. Langmuir 13:4520–4526

Okuzaki H, Osada Y (1995) Role and effect of cross-linkage on the polyelectrolyte-surfactant interactions. Macromolecules 28:4554–4557

Pareek P, Adler H-J P, Kuckling D (2006) Tuning the swelling behavior of chemisorbed thin PNIPAAm hydrogel layers by N, N-dimethyl acrylamide content. Prog Colloid Polym Sci 132:145–151

Park TG, Hoffman AS (1994) Deswelling characteristics of poly(*N*-isopropylacrylamide) hydrogel. J Appl Polym Sci 52:85–89

Perera MCS, Hill DJT (1999) Radiation chemical yields: G values. In: Brandrup J, Immergut EH, Grulke EA (eds) Polymer handbook, 4th edn. Wiley-Interscience, New York

Pich A, Lu Y, Adler H-J, Schmidt T, Arndt K-F (2002) Dispersion polymerization of pyrrole in the presence of poly(vinyl methyl ether) microgels. Polymer 43:5723–5729

Querner C, Schmidt T, Arndt K-F (2004) Characterization of structural changes of poly(vinyl methyl ether) γ-irradiated in diluted aqueous solutions. Langmuir 20:2883–2889
Ren SZ, Shi WF, Zhang WB, Sorensen CM (1992) Anomalous diffusion in aqueous solutions of gelatin. Phys Rev A 45:2416–2422
Richter S (2007) Recent gelation studies on irreversible and reversible systems with dynamic light scattering and rheology–A concise summary. Macromol Chem Phys 208:1495–1502
Richter A, Kuckling D, Arndt K-F, Gehring T, Howitz S (2003) Electronically controllable microvalves based on hydrogels: magnitudes and potential applications. J Microelectromech Syst 12:748–753
Richter A, Bund A, Keller M, Arndt K-F (2004a) Characterization of a microgravimetric sensor based on pH sensitive hydrogels. Sens Actuat B 99:579–585
Richter S, Boyko V, Matzker R, Schröter K (2004b) Gelation studies: comparison of the critical exponents obtained by dynamic light scattering and rheology, 2A thermoreversible gelling system: mixtures of xanthan gum and locust-bean gum. Macromol Rapid Commun 25: 1504–1509
Richter S, Boyko V, Schröter K (2004c) Gelation studies on a radical chain cross-linking copolymerization process: comparison of the critical exponents obtained by dynamic light scattering and rheology. Macromol Rapid Commun 25:542–546
Richter S, Matzker R, Schröter K (2005) Gelation Studies, 4: Why do ''classical'' methods like oscillatory shear rheology and dynamic light scattering for characterization of the gelation threshold sometimes not provide identical results especially on thermoreversible gels? Macromol Rapid Commun 26:1626–1632
Richtering W, Fuchs T, Burchard W (1998) Dynamics during thermoreversible gelation of the polysaccharide schizophyllan. Ber Bunsenges Phys Chem 102:1660–1664
Rosiak JM (1998) Gel/sol analysis of irradiated polymers. Radiat Phys Chem 51:13–17
Rühe J et al (2004) Polyelectrolyte brushes. Adv Polym Sci 165:79–150
Schild HG (1992) Poly(N-isopropylacrylamide)–experiment, theory and application. Progr Polym Sci 17:163–249
Schild HG, Muthukumar M, Tirrell DA (1991) Cononsolvency in mixed aqueous-solutions of poly (*N*-isopropyacrylamide). Macromolecules 24:948–952
Schmaljohann D, Nitschke M, Schulze R, Eing A, Werner C, Eichhorn K-J (2005) In situ study of thermoresponsive behavior of micropatterned hydrogel films by imaging ellipsometry. Langmuir 21:2317–2322
Schmidt T, Janik I, Kadłubowski S, Ulański P, Rosiak JM, Reichelt R, Arndt K-F (2005) Pulsed electron beam irradiation of dilute aqueous poly(vinyl methyl ether) solutions. Polymer 46:9908–9918
Schmidt T, Mönch JI, Arndt K-F (2006) Temperature-sensitive hydrogel pattern by electron-beam lithography. Macromol Mater Eng 291:755–761
Shibayama M (2006) Universality and specificity of polymer gels viewed by scattering methods. Bull Chem Soc Jpn 79:1799–1819
Shibayama M, Norisuye T (2002) Gel formation analyses by dynamic light scattering. Bull Chem Soc Jpn 75:641–659
Shibayama M, Morimoto M, Nomura S (1994) Phase-separation induced mechanical transition of poly(*N*-isopropyacrylamide) water isochore gels. Macromolecules 27:5060–5066
Shibayama M, Fujikawa Y, Nomura S (1996a) Dynamic light scattering study of poly(*N*-isopropylacrylamide-co-acrylic acid) gels. Macromolecules 29:6535–6540
Shibayama M, Mizutani SY, Nomura S (1996b) Thermal properties of copolymer gels containing N-isopropylacrylamide. Macromolecules 29:2019–2024
Shibayama M, Norisuye T, Nomura S (1996c) Cross-link density dependence of spatial inhomogeneities and dynamic fluctuations of poly(*N*-isopropylacrylamide) gels. Macromolecules 29:8746–8750
Singh D, Kuckling D, Choudhary V, Adler H-J, Koul V (2006) Synthesis and characterization of poly(*N*-isopropylacrylamide) films by photo polymerization. Polym Adv Technol 17:186–192

Stauffer D (1998) Gelierungstheorie. Versäumte Zusammenarbeit von Physik und Chemie. Ber Bunsenges Phys Chem 102:1672–1678
Stauffer D, Aharony A (1995) Perkolationstheorie–Eine Einführung. VCH, Weinheim
Stauffer D, Coniglio A, Adam M (1982) Gelation and critical phenomena. Adv Polym Sci 44: 103–158
Stile RA, Burghardt WR, Healy KE (1999) Synthesis and characterization of injectable poly (*N*-isopropylacrylamide)-based hydrogels that support tissue formation in vitro. Macromolecules 32:7370–7379
Stockmayer WH (1943) Theory of molecular size distribution and gel formation in branched-chain polymers. J Chem Phys 11:45–55
Takeda M, Norisuye T, Shibayama M (2000) Critical dynamics of cross-linked polymer chains near the gelation threshold. Macromolecules 33:2909–2915
Te Nijenhuis K (1997a) Thermoreversible networks. Introduction. Adv Polym Sci 130:1–12
Te Nijenhuis K (1997b) Thermoreversible networks. Gelatin. Adv Polym Sci 130:160–193
Theiss D, Schmidt T, Dorschner H, Reichelt R, Arndt K-F (2005) Filled temperature-sensitive poly(vinyl methyl ether) hydrogels. J Appl Polym Sci 98:2253–2265
Toomey R, Freidank D, Rühe J (2004) Swelling behavior of thin, surface-attached polymer networks. Macromolecules 37:882–887
Tsuchida E, Abe K (1982) Interactions between macromolecules in solution and intermacromolecular complexes. Adv Polym Sci 45:1–130
Vakkalanka SK, Peppas NA (1996) Swelling behavior of temperature- and pH-sensitive block terpolymers for drug delivery. Polym Bull 36:221–225
Velada JL, Liu Y, Huglin MB (1998) Effect of pH on the swelling behaviour of hydrogels based on *N*-isopropylacrylamide with acidic comonomers. Macromol Chem Phys 199:1127–1134
Ward JH, Bashir R, Peppas NA (2001) Micropatterning of biomedical polymer surfaces by novel UV polymerization techniques. J Biomed Mater Res 56:351–360
Winter HH, Mours M (1997) Rheology of polymers near liquid-solid transitions. Adv Polym Sci 134:165–234
Wohlrab S, Kuckling D (2001) Multisensitive polymers based on 2-vinylpyridine and *N*-isopropylacrylamide. J Polym Sci A, Polym Chem 39:3797–3804
Wounters D, Schubert US (2003) Nanolithography and nanochemistry: probe-related patterning techniques and chemical modification for nanmeter-sized devices. Angew Chem Int Ed 43: 2480–2495
Xia Y, Whiteside GM (1998) Soft lithography. Angew Chem Inter Ed 37:550–557
Yoshida R, Ichijo H, Hakuta T, Yamaguchi T (1995a) Self-oscillating swelling and deswelling of polymer gels. Macromol Rapid Commun 16:305–310
Yoshida R, Uchida K, Kaneko Y, Sakai K, Kikuchi A, Sakurai Y, Okano T (1995b) Comb-type grafted hydrogels with rapid de-swelling response to temperature-changes. Nature 374:240–242
Yoshioka H, Mikami M, Mori Y, Tsuchida E (1993) Preparation of thermoresponsive surfaces using polyvinylchloride-graft-poly(*N*-isopropylacrylamide). Polym Adv Technol 4:519–521
Yu H, Grainger DW (1993) Thermosensitive swelling behavior in cross.linked N-isopropylacrylamide networks–cationic, anionic, and ampholytic hydrogels. J Appl Polym Sci 49:1553–1563
Yu X, Tanaka A, Tanaka K, Tanaka T (1992) Phase transition of a poly(acrylic acid) gel induced by polymer complexation. J Chem Phys 97:7805–7808
Zhang J, Peppas NA (2000) Synthesis and characterization of pH- and temperature-sensitive poly (methacrylic acid)/poly(*N*-isopropylacrylamide) interpenetrating polymeric networks. Macromolecules 33:102–107
Zhang XZ, Wu DQ, Chu CC (2004) Synthesis, characterization and controlled drug release of thermosensitive IPN-PNIPAAm hydrogels. Biomaterials 25:3793–3805
Zhao B, Brittain WJ (2000) Polymer brushes: surface-immobilized macromolecules. Progr Polym Sci Jpn 25:677–710

Zhou SQ, Wu C (1996) In-situ interferometry studies of the drying and swelling kinetics of an ultrathin poly(*N*-isopropylacrylamide) gel film below and above its volume phase transition temperature. Macromolecules 29:4998–5001

Zrinyi M (2008) Magnetic polymeric gels as intelligent artificial muscles. In: Shahinpoor M, Schneider HJ (eds) Intelligent Materials. Royal Society of Chemistry, Cambridge, UK

Swelling-Related Processes in Hydrogels

K.-F. Arndt, F. Krahl, S. Richter, and G. Steiner

Abstract The swelling equilibrium of gels can be explained by the Flory-Rehner theory. The FR theory calculates the difference of the chemical potential of a solvent inside a gel to the surrounding pure solvent as a sum of the mixing and the elastic part. The first is based on the Flory–Huggins theory, the second on the rubber elasticity theory (Sect. 1). An important role for gels with volume phase transition plays the Flory–Huggins interaction parameter and its dependencies on temperature and concentration. In a system with specific interactions between the solvent and the network, additional contributions to the chemical potential have to be taken into consideration. The application of hydrogels is based on changes of the gel properties, mostly the dramatic change of their swollen volume, in response to specific environmental stimuli. The velocity of changes of the degree of swelling is of outstanding importance. The kinetics of swelling and shrinking is determined by different diffusion processes (Sect. 2). The cooperative motion of the net chains is characterized by a cooperative diffusion coefficient D_{coop}. The time dependence of the degree of swelling for gels of different geometries is followed and D_{coop} calculated. Processes happening at the volume phase transition were discussed. Section 3 introduces then the fundamental concepts of the spectroscopic characterization of hydrogels. The focus of Sect. 3.1 is a practical hands-on advice that everyday practitioners of infrared and Raman spectroscopy will find useful. The reader will be introduced to

K.-F. Arndt (✉) and F. Krahl
Department of Chemistry and Food Chemistry, Physical Chemistry of Polymers, TU Dresden, 01062, Dresden, Germany
e-mail: karl-friedrich.arndt@chemie.tu-dresden.de

S. Richter
Leibniz Institute of Polymer Research Dresden, Hohe Straße 6, 01069, Dresden, Germany
e-mail: richter-sven@ipfdd.de

G. Steiner
Medical Faculty Carl Gustav Carus, Clinical Sensoring and Monitoring, TU Dresden, 01307, Dresden, Germany
e-mail: gerald.steiner@tu-dresden.de

G. Gerlach and K.-F. Arndt (eds.), *Hydrogel Sensors and Actuators*,
Springer Series on Chemical Sensors and Biosensors 6,
DOI: 10.1007/978-3-540-75645-3_3, © Springer-Verlag Berlin Heidelberg 2009

spectroscopic methods and to sample preparation techniques. More advanced techniques like imaging spectroscopy and chemometric data analysis are discussed. Section 3.2 discusses the NMR imaging technique as an important method to visualize swelling-related processes in hydrogels.

Keywords Swelling • Thermodynamic • Cooperative diffusion • Spectroscopic methods • Imaging

Contents

Abbreviations

AMTIR-1	Ge33As12Se55 glass
ANN	Artificial neural network
ATR	Attenuated total reflectance
BaF_2	Barium fluoride glass
CA	Cluster analysis
CaF_2	Calcium fluoride glass
CCD	Charge-coupled device
CH_3OD	Per-deuterated methanol
D_2O	Deuterium oxide (heavy water)
DC	Direct current
DLS	Dynamic light scattering
EWF	Equilibrium water fraction
FA	Factor analysis
FESEM	Field emission scanning electron microscopy
FPA	Focal plane array
FT-IR	Fourier transform infrared spectroscopy

GAR	Grazing angle reflectance
Ge	Germanium
IR	Infrared
KBr	Potassium bromide
LDA	Linear discriminant analysis
MBAAm	*N*,*N*'-methylene bisacrylamide
NMR	Nuclear magnetic resonance
PAAc	Poly(acrylic acid)
PCA	Principal components analysis
PEG	Poly(ethylene glycol)
PLS	Partial least squares
PNIPAAm	Poly(*N*-isopropyl acrylamide)
PVA	Poly(vinyl alcohol)
PVME	Poly(vinyl methyl ether)
PVP	Poly(vinyl pyrrolidone)
RET	Rubber elasticity theory
NMR	Nuclear magnetic resonance
Si	Silicon
UV	Ultraviolet
Vis	Visible
ZnS	Zinc sulfide
ZnSe	Zinc selenide

Symbols

A	Area
A_0	Structure factor (RET)
a_1	Correction term
B	Volume factor (RET)
B_0	Static magnetic field power
B_1	Intercept
c	Concentration
c^*	Overlap concentration
d	Diameter of gel cylinder
D	Diffusion coefficient
D_{coop}	Cooperative diffusion coefficient
d_p	Depth of penetration
E	Young's modulus
f	Functionality of junction points
f	Friction coefficient
f	Force
F	Free energy (intensive, with index)
G	Gradient of magnetic field

G	Free enthalpy (intensive, with index)
G	Shear modulus
$g^{(1)}(t)$	Electric field correlation function
$g^{(2)}(t)$	Intensity correlation function
H	Enthalpy
I_F	Scattering intensity for thermal fluctuations
k	Cylinder diameter; disc thickness
K	Bulk modulus
$K(\lambda)$	Hindrance of fluctuation (constraint function)
k_B	Boltzmann constant (1.381×10^{-23} J K^{-1})
m	Mass
M	Molecular weight
M_c	Molecular weight of network chain
n	Number of moles
n	Refractive index
n_S	Refractive index of the sample
n_C	Refractive index of the ATR crystal
N	Number of molecules or particles
N_0	Number of monomers
N_L	Avogadro number (6.022×10^{23} mol^{-1})
p	Pressure
q	Scattering vector
$q^{2/3}$	Memory-term
Q	Degree of swelling
Q_m	Mass degree of swelling
Q_v	Volume degree of swelling
R	Gas constant (8.314 J K^{-1} mol^{-1})
r	Radius
r	Rocking vibration
R_h	Hydrodynamic radius
S	Entropy (intensive)
s	Scissoring vibration
T	Tempereture
t	Delay time
t	Twisting vibration
T_1	Relaxation time
T_2	Relaxation time
T_c	Critical temperature
T_g	Glass transition temperature
t_{lag}	Time-lag
u	Displacement
$\overline{V_i}$	Partial molar volume of component i
V_i	Molar volume of component i
x,y,z	Space coordinate
X_P	Fraction of dynamically scattered light

$\langle\rangle$	Time average
$\langle I\rangle_{t,P}$	Total time-averaged scattering intensity at a constant sample position
α	angle of incidence
γ	Gyro-magnetic ratio
Γ	First cummulant
δ	Deformation vibration
$\delta(u)$	Displacement
Δ	Total change
Δx	Spatial resolution
$\Delta\omega$	Width of resonance line
η_s	Viscosity of solvent
Θ	Theta condition
θ	Scattering angle
λ	Extension ratio relative to isotropic state of reference
λ_0	Wavelength of the incident light
μ	Poisson´s ratio
μ_i	Chemical potential of component i
μ_J	Number of junction points
ν	Stretching vibration
ν	Wavenumber
ν_{as}	Antisymmetrical stretching vibration
ν_s	Symmetrical stretching vibration
ν_c	Cross-linking density (mol network chains / volume)
ξ	Cycle rank
ξ	Screening length
π	Osmotic pressure, swelling pressure
σ	Stress, force per area of un-deformed sample
τ	Relaxation time
φ_A	Volume fraction swelling agent
φ	Volume fraction
χ	Huggins interaction parameter
ω	Resonance frequency of the signal
ω	Wagging vibration

Indices

0	Reference state
1	Solvent
2	Polymer
c	Cross-linked
cr	Critical
d	Dry, unswollen
dry	Dry state
el	Elastic

exp	Measured quantity
lo	Longitudinal
m	Medium intensity of the vibration mode
m	Mixing
net	Network
P	Sample position
Q	Swollen state
s	Swollen
tr	Transversal
u	Uncross-linked
v	Strong intensity of the vibration mode
VPT	Volume phase transition temperature
vs	Very strong intensity of the vibration mode
w	Weak intensity of the vibration mode

1 Thermodynamics of Swelling

1.1 Chemical Potential and Equilibrium Degree of Swelling

In general, swelling means an increase in volume of a cross-linked polymer by uptake of solvent from a liquid or gaseous phase. We observe a transition from a dry polymer to a polymeric gel. Swelling in an extent of liquid gives us the possibility to determine the properties of a gel in equilibrium state, e.g., calculation of cross-linking density. The sorption of gels at different vapour pressures has been used to determine the thermodynamic properties of gels[1].

In thermodynamics, it is common to discuss the chemical potential of a component. It is possible to determine the chemical potential of the solvent by different methods, e.g., vapour pressure measurements. In the language of thermodynamics, swelling or shrinking (de-swelling) is a result of a difference of chemical potentials, or with other words, the driving force for the uptake of solvent (1) is a difference $\Delta\mu_1$ in chemical potentials of the solvent inside (μ_1) and outside ($\mu_{1,0}$) the polymeric phase.

The chemical potential μ_i of component i at a certain temperature T, pressure p, and constant number of moles n_j in the system is defined as:

$$\mu_i \equiv \left(\frac{\partial G}{\partial n_i}\right)_{T,p,n_{j\neq i}}. \tag{1}$$

[1] It was observed, that a gel swollen to equilibrium in the liquid solvent shrinks as soon as it is transferred to the vapour phase of the same solvent. This phenomenon is known as the "paradox of Schroeder" (Freundlich 1932). For a theory of swelling with solvents in various phases, see (Borchard & Steinbrecht 1991).

The Gibbs free energy G of a two component system is generally given by:

$$G = f(T, p, n_1, n_2). \tag{2}$$

Since μ_i is the partial derivative of the state function G it is also a state function itself and will depend on the same variables:

$$\mu_i = f(T, p, n_1, n_2). \tag{3}$$

Subscripts 1 and 2 denote solvent and polymer, respectively, n is the number of moles, T and p are temperature and pressure, respectively.

The change of volume due to swelling results in a deformation of the net chains and, therefore, in a change of their thermodynamic properties. The two competing processes taking place when an elastomeric polymer network comes into contact with a thermodynamically good solvent are:

- Entropy increase of the network-solvent system as a result of the introduction of solvent molecules in the network (mixing term)
- Entropy decrease (for entropy-elasticity) of the network chains as a result of the dilation (elastic deformation term).

The entropy of a network-solvent system will increase because of the tendency of the solvent molecules to disperse in the network. This is in analogy to thermodynamics of the dissolution process of macromolecules in a solvent. In reality, it is necessary to take into consideration the additional effect of interaction between polymer segments and solvent molecules, e.g., by introducing an interaction parameter. The dilation gives rise to an elastic response from the network chains which will oppose the tendency for dilation.

The swelling equilibrium occurs when these two opposing tendencies balance out each other. The difference of the above introduced difference of chemical potential equals to zero.

1.2 Flory–Rehner Theory, Mixing Part

The condition of swelling equilibrium can be calculated by means of two theoretical approaches. It is assumed that the chemical potential of mixing for a network is the same as the chemical potential of mixing an uncross-linked polymer of high molecular weight and of the same structure as the network polymer. The mixing term can be described by means of the Flory–Huggins (FH) equation. The calculation of the elastic deformation term is based on the rubber elasticity theory (RET).

Flory and Rehner have proposed that the free enthalpy change during swelling depends on two contributions, the free enthalpy of mixing network and solvent $\Delta G_m$and a contribution from elasticity, the free enthalpy of elastic deformation

ΔG_{el} (Flory 1944; Flory and Rehner 1943a, 1943b). A basic premise of the Flory–Rehner theory is the separability and additivity of both contributions:

$$\Delta G = \Delta G_m + \Delta G_{el} \tag{4a}$$

or

$$\Delta \mu_1 = \Delta \mu_{1,m} + \Delta \mu_{1,el} \tag{4b}$$

From a difference in chemical potential it is easy to calculate a clear quantity, the osmotic pressure. Flory has drawn the analogy between swelling equilibrium and osmotic equilibrium (Flory 1953). The difference between the osmotic pressure π_m and the elastic response π_{el} of the network chains in the swollen network is named swelling pressure π_{res}. It can be calculated as following:

$$\pi_{res} = \pi_m + \pi_{el} \tag{5}$$

$$\pi_m = -\left(N_L/\overline{V_1}\right) \Delta \mu_{1,m}\,, \quad \pi_{el} = -\left(N_L/\overline{V_1}\right) \Delta \mu_{1,el}\,, \tag{6}$$

with N_L the Avogadro number and $\overline{V_1}$ the partial molar volume of solvent.

Now it is clear that a network starting to swell or to shrink (it is not in a swelling equilibrium) generates a force. In equilibrium, the swelling pressure is zero. This is synonymous with the statement above, that the difference in chemical potentials of the two solvent phases, inside and outside the gel, is zero.

As shown by Flory and Huggins, the difference $\Delta \mu_1^u = \mu_1^u - \mu_{1,0}$ for a polymer solution (index u means uncross-linked) can be expressed as following (Flory 1942; Huggins 1941, 1943):

$$\Delta \mu_1^u = \mu_1^u - \mu_{1,0} = RT\left[\ln(1-\varphi_2) + \varphi_2\left(1 - \frac{1}{x}\right) + \chi\,\varphi_2^2\right], \tag{7}$$

where $\varphi_2$is the polymer volume fraction, χ the thermodynamic polymer-solvent interaction parameter (Flory-Huggins interaction parameter) and x the ratio of molar volume of polymer to that of the solvent given as:

$$x = \frac{V_2}{V_1} = \frac{M_2\,\rho_1}{M_1\,\rho_2} \propto M_2. \tag{8}$$

Since a network is considered to be one molecule of infinite molecular weight, it follows that $1/x$ must be equal to zero.

The polymer volume fraction φ_2 is defined as ratio of polymer volume to the sum of the volumes of polymer and solvent. To describe the swollen state of a cross-linked polymer, we introduce the volume degree of swelling Q_v as ratio of the

volume of swollen polymer to the volume of dry (unswollen) polymer. Comparing both yields to

$$\varphi_2 = 1/Q_{\mathrm{v.}} \tag{9}$$

The volume degree of swelling can be determined either by measuring the volume of swollen and dry sample (e.g., determination of sample height or thickness), or if the densities of the solvent ρ_1 and the dry polymer ρ_2 are known by weighing the swollen ($m_1 + m_2$) and dry (m_2) sample (10).

The ratio ($m_1 + m_2$)/m_2 is the mass degree of swelling Q_m [2] and the polymer volume fraction yields

$$\varphi_2 = 1 - \varphi_1 = 1 - \frac{\frac{m_1}{\rho_1}}{\frac{m_1}{\rho_1} + \frac{m_2}{\rho_2}} = \left(\frac{h_q}{h_0}\right)^{-3}, \tag{10}$$

where h_q and h_0 are the sample height in swollen and in the dry state, respectively (isotropic swelling).

The lattice model of Flory–Huggins calculates the entropic changes of the mixing process. The enthalpy effects are considered by the interaction parameter χ:

$$\chi = \frac{\Delta h - T\Delta s}{\mathrm{k_B}\, T}. \tag{11}$$

In real polymer-solvent systems, χ can be separated in two contributions, an enthalpic and an entropic part. In general, χ depends on temperature T and on polymer concentration.

It is remarkable, that the prediction of a volume phase transition of nonionic polymer gels was done by Dušek and Patterson by discussing the Flory–Rehner equation (Dušek and Patterson 1968)). They predicted that a strong concentration dependence of χ facilitates the occurrence of phase transition in polymer gels. The phase transition should be analogous to the "coil-globule" transition of a single polymer chain.

Polymer-solvent systems possessing an upper critical solution temperature (UCST, defined by phase separation at decreasing T) are characterized by positive values of the change of enthalpy Δh and the change of entropy Δs at the mixing processes while systems possessing a lower critical solution temperature (LCST) are characterized by negative values. For the NIPAAm-water system, Δh and Δs as

[2] Also, the swelling can be measured as the equilibrium water fraction *EWF*, defined as the wet weight fraction of swollen gel: $EWF = [(\text{weight of swollen gel}) - (\text{weight of dry gel})]/[\text{weight of swollen gel}]$; $\varphi_2 = (1 - EWF)\,\rho_1/[\rho_1 + EWF\,(\rho_2 - \rho_1)]$

well as the concentration dependence of χ were determined by swelling measurements on a network with known cross-linking density (Hirotsu 1991).[3]

$$\chi = \chi_1 + \chi_2 \varphi_2 \tag{12}$$

with

$$\chi_1 = (\Delta h + \Delta s)/\mathrm{k_B\,T}$$

$$\chi_2 = 0.518$$

$$\Delta h = -12.462\,10^{-21}\mathrm{J}$$

$$\Delta s = -4.717\,10^{-23}\mathrm{J/K}.$$

Different intermolecular forces, like van der Waals forces (e.g., for acrylamide gel in acetone/water), hydrophobic interaction (e.g., NIPAAm in water), hydrogen bonding (ionic repulsive, e.g., IPN acrylic acid-acrylamide in water), and electrostatic interaction (ionic attractive, e.g., polyampholytes (cation-anion) in water) contribute to the various types of phase transitions in polymer gels. Their influence on to free enthalpy must be taken into account by additional terms to ΔG (or to χ). Examples are:

- A polyelectrolyte gel (pH-dependent swelling) is immersed in a large solvent reservoir (pure solvent, no added ions). The system consists of three components: polymer ions, counter ions, solvent molecules. Each of them contributes to the chemical potential.
- Hydrophobic interactions occur at neutral polymers with hydrophobic and hydrophilic groups. The water molecules around the polymers are highly hydrogen bonded and form ordered structures (icebergs, similar to the structure of water molecules in ice). Enthalpy and entropy of mixing are lowered. The iceberg formation is exothermic. This effect is called hydrophobic interaction (energy in the order or smaller than that of hydrogen bonds, for details see (Saito et al. 1993)). The change of the free enthalpy can be described by a power series with, e.g.

$$\Delta G = C_1 + C_2 T + C_3 T^{-2} \tag{13}$$

[3] Other values for Δs and Δh were given in (Shibayama et al. 1994a): $\Delta s = -2.8\ 10^{-23}$ J/K; $\Delta h = -6.5\ 10^{-21}$ J

1.3 Flory–Rehner Theory, Elastic Part

a) Chemical Potential

The elastic response of the network contributes to the solvent chemical potential. Assuming isotropic dilation, which is typical in swelling experiments, $\Delta\mu_{1,el}$ is given by

$$\Delta\mu_{1,el} = \left(\frac{\partial \Delta G_{el}}{\partial \lambda}\right)_{T,P}\left(\frac{\partial \lambda}{\partial n_1}\right)_{T,P}. \tag{14}$$

The deformation λ due to swelling can be related to the volume of the swollen network V and to a reference volume V_0. If V_0 is the volume of the unswollen (dry) network, λ is also related to the volume fraction φ_2 of the polymer and to Q_V:

$$\lambda^3 = \frac{V}{V_0} = \frac{1}{\varphi_2} = Q_V \tag{15}$$

with $\lambda = \lambda_x = \lambda_y = \lambda_z$. Indices x, y, and z denote the different directions of deformation. Differentiating (14) with respect to the number of moles of solvent, one obtains:

$$\frac{\partial \lambda}{\partial n_1} = \frac{\overline{V_1}}{3V_0\lambda^2}, \tag{16}$$

where $\overline{V_1}$ is the partial molar volume of the solvent. Assuming that volume changes in the mixed phase are small and negligible then $\overline{V_1}$ is equal to the molar volume of the solvent V_1.

The calculation of the elastic term is based on the available theories of rubber-like elasticity, which calculate the change of elastic free energy [4] ΔF_{el} due to dilation λ. The elastic contribution to the chemical potential $\Delta\mu_{1,el}$, is then given by

$$\Delta\mu_{1,el} = \left(\mu_1 - \mu_{1,0}\right)_{el} = \left(\frac{\partial \Delta F_{el}}{\partial \lambda}\right)_{T,V}\left(\frac{\partial \lambda}{\partial n_1}\right)_{T,V}. \tag{17}$$

Combining (15) to (17) yields:

$$\Delta\mu_{1,el} = \left(\frac{V_A}{3V^{2/3}V_0^{1/3}}\right)\left(\frac{\partial \Delta F_{el}}{\partial \lambda}\right)_{T,V}. \tag{18}$$

[4] Changes in the Gibbs (G) and the Helmholtz ($F = f(T, V, n_1, n_2)$) free energies are assumed to be equivalent since the product $p\Delta V$ is small at low pressures.

b) Deformation Models

A network is formed by N_c network chains (N_c number of net chains) which are connected in the cross-links (junction points). The functionality f of cross-links (number of chains connected in a junction point) depends on their chemical nature, e.g., on the cross-linker. In a perfect network each network chain starts in one junction point and ends in another one. A real network is imperfect, but it can be described by two quantities, the network cycle rank ξ [5], and the number of junction points μ_J.

The theoretical approach for determining the deformation behaviour of a network due to swelling or due to a mechanical force (stress–strain measurements, compression experiment) is based on a hypothetical phantom network. A phantom network is, by definition, a network with the fictitious property that chains and junctions can move freely through one another without destroying the connectivity of the network. Usually, the network chains behave as Gaussian chains. Within the phantom network model, three network types can be distinguished:

- Free phantom network: Network without any constraints, which consequently collapses,
- Fixed phantom network: Some junctions are fixed in space. Such constraints do not occur in reality.
- Localised phantom network: The equilibrium position of all segments of the net chains is determined by suitable boundary conditions without any need for segments or junctions to be fixed.

According to Flory (Flory 1976), a real network shows behaviour between the two limiting cases:

- Free-fluctuation limit (localised phantom network),
- Limit of full suppression of junction fluctuation (fixed phantom network, affine network).

Both limits correspond to the classical approaches of phantom network theory.

The mean values of the chain end-to-end vectors are displaced affinely with the macroscopic extension in the James-Guth theory (James and Guth 1943). The fluctuations of the junctions are independent of the deformation of the sample. As a consequence, the end-to-end vectors are deformed not affinely. The free energy of elasticity of the free-fluctuation limit is

$$\Delta F_{el} = \frac{\xi \, k_B T}{2} \left(\lambda_x^2 + \lambda_y^2 + \lambda_z^2 - 3 \right) \tag{19}$$

with k_B the Boltzmann constant and $R = k_B N_L$. From this follows with $\lambda_x = \lambda_y = \lambda_z = \lambda$ for the isotropic swelling:

[5] The cycle rank ξ, or number of independent circuits, characterizes the network with greater generality, regardless of the nature of its imperfection. ξ is the minimum number of scissions required to reduce the network to a spanning tree.

$$\Delta\mu_{1,el} = \frac{\xi\, k_B T\, V_1}{V_0 \lambda}. \tag{20}$$

The basic assumption behind the second limit, the affine limit of rubberlike elasticity (sometimes also called the affine limit of a phantom network, Hermans–Flory–Wall (Wall 1942, 1943, 1951; Hermans 1947)), is that the cross-links are firmly embedded in their surroundings and, therefore, they do not fluctuate. Their position is transformed affinely with the macroscopic strain. The elastic part of free energy is given by

$$\Delta F_{el} = \frac{\xi\, k_B T}{2}\left(\frac{f}{f-2}\right)\left(\lambda_x^2 + \lambda_y^2 + \lambda_z^2 - 3\right) - \frac{\xi\, k_B T}{\frac{1}{2}f - 1}\ln\left(\lambda_x \lambda_y \lambda_z\right). \tag{21}$$

The second term on the right-hand side vanishes for incompressible networks. For deformations caused by swelling, the deformation is isotropic and thus

$$\lambda_x \lambda_y \lambda_z = \lambda^3 = V/V_0.$$

The volume of the deformed network is Q times larger than that one of the undeformed network (15) and the second term in (21) is not zero. From (15) and (21) it follows:

$$\Delta F_{el} = \frac{\xi\, 3\, k_B T}{2}\left(\frac{f}{f-2}\right)\left(Q^{2/3} - 1 - \frac{2}{3} B \ln Q\right) \tag{22}$$

with the volume factor B, here $B = 2/f$, and the functionality f. The elastic contribution to the chemical potential is given by

$$\begin{aligned}\Delta\mu_{1,el} &= \frac{\xi\, k_B T\, V_1}{V_0}\left(\frac{f}{(f-2)\lambda} - \frac{1}{\left(\frac{1}{2}f - 1\right)\lambda^3}\right)\\ &= \frac{\xi\, k_B T\, V_1}{V_0}\frac{f}{(f-2)\lambda}\left(1 - \frac{2}{f\lambda^2}\right).\end{aligned} \tag{23}$$

Substituting of λ by the volume degree of swelling Q results in

$$\Delta\mu_{1,el} = \frac{\xi\, k_B T\, V_1}{V_0}\frac{f}{(f-2)}\left(Q^{-1/3} - \frac{2}{f} Q^{-1}\right). \tag{24}$$

The fluctuation of the cross-links (junction points) depends on the deformation. Qualitatively, an increase of fluctuations is expected at higher deformation. The behaviour of a networks changes from an affine phantom network (Hermans–Flory–Wall) at small deformation (low degree of swelling, dry network) to a free-fluctuating network (James–Guth) at large deformation (high degree of swelling). This is

important for using the deformation experiments for determination of the molecular weight of the net chains. A function $K(\lambda)$ was introduced to describe the hindrance (constraints) of junctions fluctuations (Flory 1977a, b; Erman and Flory 1978).

Applying the constrained junction theory on a phantom network Erman and Flory (1978) obtained:

$$\Delta\mu_{1,el} = \left(\frac{\xi\, k_B\, T\, V_1}{V_0 \lambda}\right)\left[1 + \left(\frac{\mu_J}{\xi}\right) K(\lambda)\right]. \tag{25}$$

In case of the free-fluctuating limit of a phantom network, the fluctuations are not hindered. $K(\lambda)$ is equal to zero, leading to (20).

Since fluctuations are suppressed for affine deformation the function $K(\lambda)$ becomes

$$K(\lambda) = (1 - \lambda^{-2}). \tag{26}$$

c) Deformation of Perfect Networks

The cycle rank ξ is given by the difference of the number of net chains N_c and the number of junction point μ_J

$$\xi = N_c - \mu_J. \tag{27}$$

The number of net chains in a perfect network is

$$N_c = f\,\frac{\mu_J}{2} \tag{28}$$

and thus

$$\xi = \frac{\mu_J}{2}\,(f - 2)\,. \tag{29}$$

For a perfect tetra-functional ($f = 4$) it results in

$$\xi = \mu_J = \frac{N_c}{2}\,. \tag{30}$$

The network (20) for the free-fluctuating limit becomes

$$\Delta\mu_{1,el} = \frac{k_B T\, V_1}{V_0 \lambda}\,\frac{N_c}{2} = \frac{1}{2}\,\frac{k_B T\, V_1}{V_0}\, N_c\, Q^{-1/3}, \tag{31}$$

whereas (23) for affine networks becomes

$$\Delta\mu_{1,el} = \frac{k_B T V_1}{V_0 \lambda} N_c \left(1 - \frac{1}{2\lambda^2}\right) = \frac{k_B T V_1}{V_0} N_c \left(Q^{-1/3} - \frac{1}{2} Q^{-1}\right). \quad (32)$$

The cross-linking density cannot be estimated from the stoichiometric relation between monomer and cross-linker, e.g., NIPAAm and MBAAm, since the possibility of cyclization during NIPAAm polymerization is high (see Sect. 2, in chapter "General properties of hydrogels"). A more realistic number of net chains can be determined by compression or stress-strain measurements, preferred on a gel swollen in organic solvent.

The relation between stress and moderate uniaxial [6] mechanical deformation (in x– direction) is

$$\begin{aligned} \sigma(\lambda) &= f/A = \frac{1}{A}\frac{\partial}{\partial x}\Delta F_{el} = \frac{1}{A x_0}\frac{\partial}{\partial \lambda}\Delta F_{el} \\ &= \frac{N_c}{V_0 N_L} N_L k_B T (\lambda - \lambda^{-2}) \\ &= v_c R T A_0 q^{2/3} (\lambda - \lambda^{-2}) , \end{aligned} \quad (33)$$

where A_0 is the microstructure factor, $q^{2/3}$ the memory-term (see explanation at (39)), f the force, and A the area. The microstructure factor depends on the deformation model ($A_0 = 1$ for affine networks, $A_0 = (f\text{-}2)/f$ for free-fluctuating networks).

1.4 Discussion of Flory–Rehner Equation

Swelling a network to equilibrium allows one to determine the cross-linking density and the molecular weight M_c between cross-links. The cross-linking density v_c is defined as the number of net chains in mol per volume. The molecular weight of the net chains can be calculated by the cross-linking density and the density of the dry polymer network ρ_2 [7]. In case of a swollen network, the volume depends on the degree of swelling; therefore, it is useful to calculate the number of net chain N_c in mol per volume V_0 of the dry network [8]:

[6] Uniaxial means: $\lambda_x = \lambda$; $\lambda_y = \lambda_z = \lambda^{-1/2}$; $\lambda = x/x_0$ with x_0 the un-deformed and x the deformed length, respectively.

[7] The mole number of net chains is $n_c = N_c/N_L = m/M_c$, where m is the mass of the network. The density of the network is $\rho_2 = m/V_o$.

[8] It is possible to use the volume of the polymer in the state of preparing the network as a reference. The deformation of the network by swelling is then measured as the ratio of the swollen volume to the volume at preparation, see Chapter 1. This quantity is called as swelling ratio.

$$v_c = \frac{N_c}{V_0 \, \mathrm{N_L}} \; ; \qquad M_c = \frac{\rho_2}{v_c} \, , \tag{34}$$

where $\mathrm{N_L}$ is the Avogadro number. With $f = 4$ and $Q = 1/\varphi_2$, it follows with (31) and (32):

$$\Delta\mu_{1,el} = \frac{\mathrm{R}T V_1}{\lambda} \frac{v_c}{2} = \frac{1}{2} \, v_c \mathrm{R}T V_1 \, \varphi_2^{1/3} \tag{35}$$

and for the affine limit

$$\Delta\mu_{1,el} = \frac{\mathrm{R}\,T V_1}{\lambda} v_c \left(1 - \frac{1}{2\,\lambda^2}\right) = v_c \, \mathrm{R}\,T V_1 \left(\varphi_2^{1/3} - \frac{\varphi_2}{2}\right). \tag{36}$$

Flory–Rehner theory assumes that the mixing part of the chemical potential of the network is the same as the mixing part of the uncross-linked polymer with an infinite molecular weight:

$$\Delta\mu_{1,m} = \mathrm{R}\,T \left[\ln(1 - \varphi_2) + \varphi_2 + \chi \, \varphi_2^2\right]. \tag{37}$$

It follows from (4b), (34), (35) and (37) for the swelling equilibrium (Mark 1982):

$$M_c = \frac{-F_f \, \rho_2 V_1 \, \varphi_2^{1/3} \, q^{2/3}}{\ln(1 - \varphi_2) + \varphi_2 + \chi \, \varphi_2^2}, \tag{38}$$

where V_1 is the molar volume of the diluent, ρ_2 the polymer volume fraction in the network, ρ_2 the mass density of dry polymer network, and χ the diluent-polymer interaction parameter. F_f is given by

$$F_f = \left(1 - \frac{2}{f}\right)\left[1 + \left(\frac{\mu_J}{\xi}\right) K(\lambda)\right]. \tag{39a}$$

For a perfect network with the functionality of the junction points $f = 4$, it follows

$$F_{f=4} = \begin{cases} \left(1 - \dfrac{\varphi_2^{2/3}}{2}\right) & \text{affine limit} \qquad (39b) \\ \dfrac{1}{2} & \text{fluctuating limit} \qquad (39c) \end{cases}$$

If a polymer is cross-linked in the presence of an inert solvent it will show a topology (and properties) which differs from that one of a network prepared in bulk. This can be taken into consideration by introducing the so-called memory

term[9] $q^{2/3}$. q is the volume fraction of polymer present during cross-linking reaction (cross-linking in bulk: $q = 1$).

Sometimes it could be useful to discuss the influence of swelling as dependencies on the ratio of the current gel volume and the volume after the chemical synthesis of the gel (see Sect. 2 in chapter "General properties of hydrogels", normalized gel volume).

Determining M_c by means of (38), it is necessary to know the interaction parameter χ of the cross-linked polymer at concentration φ_2. χ is generally assumed to be the same for the cross-linked and uncross-linked polymer. From experiments follows a concentration-dependent χ. Mostly, χ increases with growing φ_2. Applying χ, which was measured in a dilute polymer solution in (38) can result in a large numerical error of M_c. Measuring M_c by uniaxial deformation at equilibrium swelling degree and applying (38) enables the determination of χ at this polymer concentration. Equation (38) can be applied to the free-fluctuating limit ($K(\lambda) = 0$, $F_f = 1 - 2/f$), without decisive loss in accuracy. Therefore, the M_c range can be determined by simple swelling measurements in the equilibrium state.

$$M_c(\text{free} - \text{fluctuating}) \leq M_c(\text{real network}) \leq M_c(\text{affine}).$$

For that, knowledge of the network structure is not needed at all.

In a good solvent and at the swelling equilibrium, the end-to-end-distance of a network chain scales with the number N_0 of monomers with about $N_0^{3/5}$ like that one of a free macromolecule of the same molecular weight in the same solvent. The cross-over volume fraction of polymer (overlap concentration) between dilute and semi-dilute regimes c^* is proportional to $1/Q_V$ (c^*-theorem). A series expansion of (38) ($\chi = \text{const.}$) results in a power law for the correlation between the degree of swelling Q_V and M_c:

$$Q_v \sim (M_c)^a. \tag{40}$$

The exponent a depends on the quality of solvent (good solvent with high degree of swelling: $a = 3/5$; poor solvent: $a = 3/8$).

At constant cross-linking density, the value of χ influences the equilibrium swelling degree: the smaller χ is for a given network and solvent the higher is the swelling degree. The concentration of polymer at cross-linking influences the degree of swelling. The degree of swelling of a network cross-linked in a dilute regime is higher than that of a polymer cross-linked in the dry state ($M_c = \text{const.}$). Decreasing the solvent quality or increasing χ results in a smaller equilibrium degree of swelling at constant cross-linking density. Changes in solvent quality can be achieved by changing the composition of solvent or the temperature. Calculation with the Flory–Rehner equation shows a corresponding continuous

[9] The memory term describes the changes of the network chain conformation in a solution at a concentration of the reacting system to the conformation in a dry state (reference state).

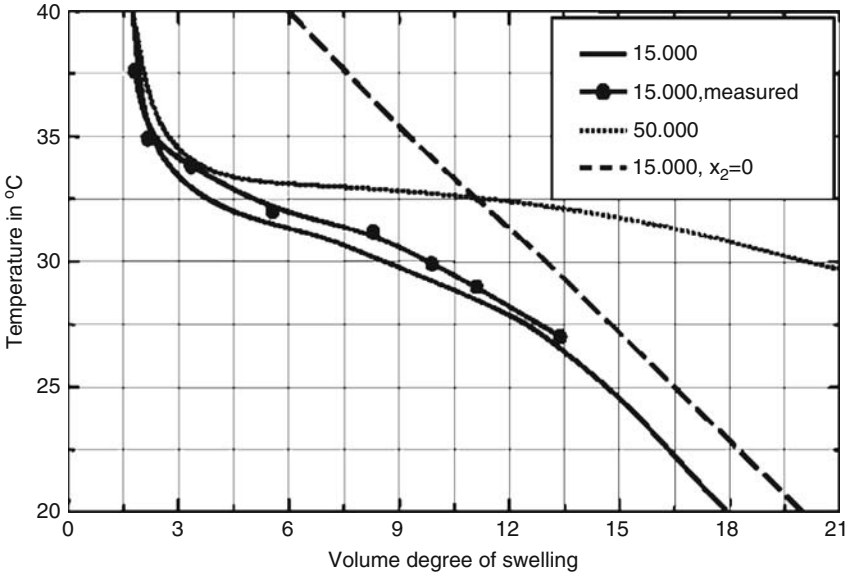

Fig. 1 Calculated and measured (•) swelling curves for PNIPAAm of different molecular weight- of the net chains M_c in g/mol. The Flory-Huggins interaction parameter χ was calculated using (12). The dashed curve was calculated considering only a temperature-dependent χ ($\chi_2 = 0$). The sharp decrease of the volume degree of swelling with temperature is only observed for concentration-dependent interactions. The sharpness of the curve is influenced by M_c

volume change. A discontinuous volume transition can cause by additional intermolecular forces. For neutral hydrogels like PVME or PNIPAAm, this happens at a constant temperature by adding an organic solvent to the surrounding water (e.g., water-acetone for PNIPAAm) or for constant solvent composition by changing the temperature.

The swelling curves show that the gel undergoes a sharp, but continuous volume phase transition (Fig. 1). By decreasing the cross-linking density, a first-order or discontinuous volume phase transition has also been observed.

The equilibrium degree of swelling or the gel volume of shows a large change in response to external conditions. Only when the volume change is discontinuously and the coexistence of two phases is experimentally proofed, we should use the term "phase transition". By applying the stability criteria on the Flory–Rehner equation one can calculate the conditions of phase transition (binodal and spinodal curve, critical point). For details see e.g. (Onuki 1993).

The application of smart hydrogels in actuator or in sensor systems is possible, even if the response of the degree of swelling and other gel properties on the environmental condition is continuously. For applications it is important that the gel properties are in a strong correlation to the properties of the surrounding liquid phase.

1.5 Mechanical Power Generation on Example of PVA-PAAc gel

The swelling or shrinking process of a gel as a result of the change between two different equilibrium states of swelling ($Q_{V,1} < Q_{V,2}$) can be used to generate a force. In the simplest case, a load is first put on a gel in the equilibrium degree of swelling $Q_{V,1}$. The gel is now allowed to swell to $Q_{V,2}$ while undergoing mechanical work. The load will be lifted.

As mentioned above and discussed in details in Sect. 1 in chapter "Synthesis of hydrogels" the swelling/deswelling can be induced by changes in the environment. In the following we will discuss qualitatively changes in electrostatic swelling forces via pH. We have determined the volume-related capability of work (working energy) during the change of pH value of the environment for a cross-linked PVA-PAAc blend as a function of the mechanical stress. The blend was synthesized as follows: PVA and PAAc were dissolved separately in water. Both solutions were mixed (80 wt.-% PVA, 20 wt.-% PAAc) and homogenized. Films were prepared from this mixture by evaporation of water. The dried films (thickness 0.1 . . . 0.2 mm) were cross-linked by annealing in an oven; for details see (Arndt et al. 1999).

The Fig. 2 shows a scheme of the test equipment. The sample is placed in a thermostated test chamber which is filled with the swelling agent of a constant pH. The sample is clamped on one side. The sample can be loaded with a constant force F. The change of length ds of the sample which is connected with the change of Q_V is recorded. The volume-specific working energy w_V is calculated by

$$w_V = \frac{1}{V_{swollen}} \int_{s_1}^{s_2} F\, ds. \tag{41}$$

The measured working energy as a function of stress $\sigma = F/A$ is shown in Fig. 3. The change of the degree of swelling was stimulated by changing the pH from pH = 11.5 to 7 and from pH = 7 to 2. The experiments show a maximum of working energy at a certain value of stress depending on the cross-linking density.

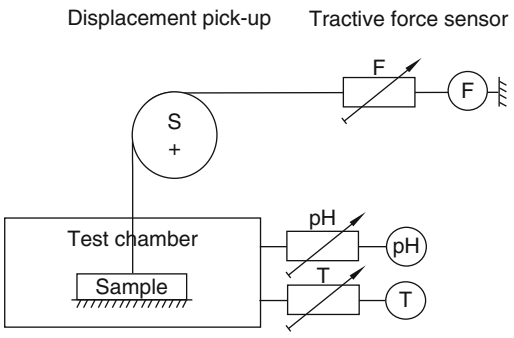

Fig. 2 Scheme of the set-up for measuring the working energy of a pH-sensitive hydrogel. Reprinted from ref. (Arndt et al. 1999), p. 384. Reproduced with kind permission of Wiley-VCH Verlag

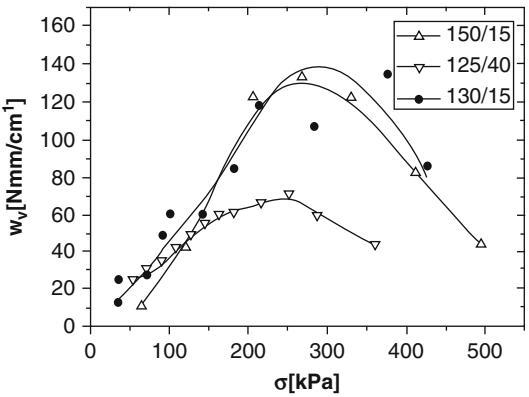

Fig. 3 Working energy of a PVA/PAAc network as a function of applied stress. A mixture of PVA/PAAc was thermally cross-linked under different conditions (temperature in °C/time in min). Reprinted from ref. (Arndt et al. 1999), p. 389. Reproduced with kind permission of Wiley-VCH Verlag

The working energy is a function of the applied stress. On one hand, w_V is restricted by the maximum change of the length of the gel. On the other hand, if the stress is too large then w_V is restricted by the maximum of the restoring force. A maximum value of $w_V = 135\ \mathrm{N\,mm/cm^3}$ follows from the curves in Fig. 3. Table 1 in Chapter 7 compares the working energies of different actuator principles.

2 Kinetics of Swelling

2.1 Diffusion

The kinetics of swelling determines time constants of the processes using the uptake or delivery of the swelling agent, or substances dissolved in the swelling agent. Because the application of hydrogels as sensors or actuators is based on a change of the degree of swelling, also the characteristic time for the response on changes in environmental conditions is determined by the swelling kinetics. In some applications the degree of swelling has to be controlled by a physical quantity, e.g., by temperature. The degree of swelling has to follow changes of temperature immediately. Therefore, it is of general interest which factors could be used to influence swelling kinetics.

In general, the swelling process can be described as a diffusion of different species. In case of swelling, a solvent (the swelling agent) has to diffuse into the polymer. The polymer chains change their conformation; they expand. The relation between the relative rate of penetrant diffusion and relaxation of the polymer chain can be used to distinguish different types of time-dependences of degree of swelling Q[10]. Alfrey Jr. et al. have proposed three models for the swelling process (Alfrey et al. 1966; George et al. 2004):

[10] The ratio of the characteristic relaxation time to the characteristic diffusion time is the so-called Deborah number (De). The smaller De is, the more fluidic the material appears.

- Case I or Fickian diffusion: The diffusion is significantly slower than the rate of relaxation of the polymer chains. The change of the degree of swelling is determined by the diffusion of the swelling agent. The mass uptake is proportional to the square root of diffusion time, $Q \sim t^{1/2}$ (see Fig. 4).
- Case II diffusion: The rate of penetrant diffusion is higher than the relaxation rate of polymer chains. Case II diffusion is characterized by a mass uptake that is proportional to the time, $Q \sim t^{1}$.
- Case III or anomalous diffusion: Both rates are comparable, $Q \sim t^{\alpha}$. The exponent of the time dependence amounts between 0.5 and 1.

The form of diffusion profile is related to the type of diffusion (Ghi et al. 1997). When a polymer is initially in the dry state, the solvent must penetrate into the network by diffusion. In case of a glassy polymer (starting from the dry state of a high T_g-polymer) the diffusion profile in Fickian diffusion decreases gradually from the swollen, rubbery region to the non-swollen, glassy inner part of the polymer. In case II diffusion, the rubbery, swollen outer part has a constant content of swelling agent and exhibits a sharp decrease in concentration at the interface to the inner glassy core. The rate of advance of the diffusion front shows the same t-dependences as the mass uptake (case I $\sim t^{1/2}$; case II $\sim t$). Because the swelling of glassy polymers is connected with the softening of the polymer, the change in mechanical properties inside the network during swelling shows the same time-dependence as the advance of the swelling front. The time dependence of Q can be a sigmoidal curve. The first part is related to the movement of the swelling front. The rigid inner

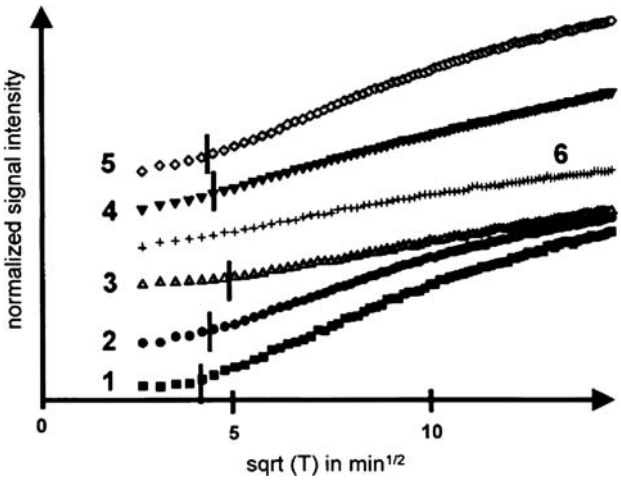

Fig. 4 Time dependence of solvent absorption inside a water-swollen PNIPAAm-gel. The normalized NMR signal of a 0.5 mm thin layer at a distance of 2.78 mm to the solvent-sample interface measures the solvent concentration. The curves are separated by a stepwise offset. 1: D_2O/H_2O; 2: 20 vol-% CH_3OD; 3: 40 vol-% CH_3OD; 4: 60 vol-% CH_3OD; 5: 80 vol-% CH_3OD; 6: 40-vol % CH_3OD, more cross-linked gel. The small vertical lines mark the end of time lag and the start of case I diffusion (if recognizable). Reprinted from (Knörgen et al. 2000), p. 77. Copyright (2000), with permission from Elsevier

core constrains swelling, permitting swelling only in the direction normal to the front. After the fronts meet, swelling is permitted in all directions, leading to an acceleration of the swelling kinetics, the second part of the sigmoidal curve. If glassy polymer networks of different thickness start to swell, the shape of swelling curves at the beginning of the solvent uptake are identical. The starting point for acceleration of the swell process depends on the thickness of the network sample. The thickest gel accelerates at last.

2.2 Cooperative Diffusion Coefficient

A variety of techniques are known to monitor the swelling/deswelling process. The simplest are based on the determination of degree of swelling in dependence on time. It is possible to measure the size change of a gel piece by optical methods or the increase in mass by weighing them.

These techniques monitor the macroscopic changes of size or weight. They do not allow a discussion of the microscopic processes during swelling, the shape of the diffusion profile as well as the location and concentration of the diffusing liquid. All this information is available and can be visualized time- and space-resolved by imaging techniques, e.g., NMR imaging; see Sect. 3.2.

The kinetics of swelling is successfully described as a collective diffusion process. Tanaka et al. (Tanaka et al. 1973) developed a theory for the dynamics of polymeric gels. They realized that the polymer chains are connected by chemical bonds and a gel has to be treated as a continuum. In addition, the network behaves as an assembly of springs due to their entropy elasticity.

Briefly, Tanaka et al. formulated an equation of motion for the displacement of a point of the network $\delta(u)$ from its average position, which depends on the friction coefficient f between network and solvent, the bulk and shear moduli K and G, respectively. The equation of motion has three solutions corresponding to one longitudinal (42) and two transverse modes (43), which can be expressed by diffusion equations:

$$\frac{\partial u_{lo}}{\partial t} = \frac{K + \frac{4}{3}G}{f} \frac{\partial^2 u_{lo}}{\partial x^2} \tag{42}$$

$$\frac{\partial u_{tr}}{\partial t} = \frac{\mu}{f} \frac{\partial^2 u_{tr}}{\partial x^2}, \tag{43}$$

where u_{lo} and u_{tr} are the components of the displacement vector in x-direction and perpendicular to x. According to this, the collective diffusion coefficient in longitudinal direction is given by

$$D = \frac{K + \frac{4}{3}G}{f}. \tag{44}$$

Equation (44) relates the diffusion coefficient to gel properties. From scaling laws applied to the conditions for overlap of random coils it is concluded that K and G as well as the friction coefficient f depend on the polymer concentration. In case of a swollen polymer, K, G, and f depend on the degree of swelling,

$$\begin{aligned} K, G &\propto Q^{-9/4} \\ f &\propto Q^{-3/2}. \end{aligned} \tag{45}$$

Therefore, also D depends on Q:

$$D \sim Q^{-3/4}.$$

The above introduced diffusion coefficient D, often termed as cooperative diffusion coefficient, can be measured directly by scattering experiments (e.g., dynamic light scattering). Based on the Tanaka theory, dynamic light scattering became one of the standard methods of studying polymer gels. The polymer chains undergo random thermal motion, which give rise to spatial and thermal fluctuations of polymer concentration. The light is scattered by density fluctuations. An analysis of the frequency distribution of the scattered light in comparison with the incident beam shows a line broadening. From this, a correlation function and diffusion coefficients can be calculated.

The diffusion coefficient D_o of a polymer in a dilute solution with a viscosity η_s of the solvent gives the hydrodynamic radius R_h of a single polymer chain:

$$D_o = \frac{k_B T}{6 \pi \eta_s R_h}. \tag{46}$$

This relation is used for the characterization of gel particles with diameters of $(10^2 \ldots 10^3)$ nm. The influence of T or pH etc. on the particle dimension can be investigated by changing the properties of the swelling agent.

If the concentration of polymer exceeds the so-called overlap concentration then the polymer chains are in contact and an entanglement network is formed. The diffusion coefficient increases with polymer concentration. In a system at high concentration it is assumed that the polymer chain can be described by a chain consisting of "blobs" (spheres with the diameter ξ, blob-chain model).The properties do not depend on the molecular weight of the polymer chain, but on the length or molecular weight of a sub-chain connecting two junctions. For a polymer network, ξ is the distance between two junction points. The diffusion coefficient of an entangled polymeric system or a swollen polymer gel, observed by DLS, is a cooperative diffusion coefficient D_{coop} since it represents the cooperative motion of chain segments within a blob of diameter ξ (correlation length or screening length):

$$D_{coop} = \frac{k_B T}{6 \pi \eta_s \xi}. \tag{47}$$

From scaling theory it follows a concentration dependence of the correlation length ξ. It decreases with increasing concentration, $\xi \sim c_2^{-3/4}$ (good solvent), and leads with (47) therefore to

$$D_{coop} \sim c_2^{3/4}.$$

Polymeric networks are inhomogeneous. The structural inhomogeneities are mainly dependent on how the gel was formed (cross-linker, concentration, solvent, conversion etc.). They are expected to affect the macroscopic properties of a gel. The in-homogeneities have a great influence on the scattering properties and make the exact determination of D_{coop} by DLS more difficult; for details see (Shibayama and Norisuye 2002). On the other hand, scattering methods provide information on the structural inhomogeneities of the gel. Several examples on that subject were given in (Shibayama 2006; Shibayama 1998). Examples for a DLS measurement and for determining of D_{coop} are given in Sect. 2.6.

2.3 Time Dependence of the Degree of Swelling

Another way to determine the cooperative diffusion coefficient is to measure the degree of swelling of a sample with a defined geometry as function of time. The experimental data were evaluated by a solution of the diffusion equation based on the equation of motion for a given sample geometry. In the following this is demonstrated on example of swelling of a spherically symmetrical gel (shear modulus $G = 0$).

The change of radius r of a sphere in dependence on time due to the swelling is given by (Tanaka and Fillmore 1979; Li and Tanaka 1990):

$$\frac{r(t=\infty) - r(t)}{r(t=\infty) - r(t=0)} = \frac{\Delta r(t)}{\Delta r_0} = \frac{6}{\pi^2} \sum_{n=1}^{\infty} n^{-2} \exp\left(-n^2 \frac{t}{\tau}\right). \tag{48}$$

For the long term ($t/\tau > 0.25$), when the first term $\exp(-t/\tau)$ of the sum is dominant over the higher order terms, the plot $\ln \frac{\Delta r(t)}{\Delta r_0}$ versus time delivers a straight line with the slope τ:

$$\ln \left. \frac{\Delta r(t)}{\Delta r_0} \right|_{t \to \infty} = \ln \frac{6}{\pi^2} - \frac{t}{\tau}. \tag{49}$$

The cooperative diffusion coefficient can be calculated according to

$$D_{coop} = \frac{r(t \to \infty)^2}{\pi^2 \tau}. \tag{50}$$

Equations (48) and (50) are valid only for a spherically symmetric gel. The specimens for swelling measurements are mostly cylinders or strips (slabs). In case of other specimen geometries, (50) has to be modified due to $G \neq 0$. Nevertheless, the proportionality between time constant τ and the square of dimension is independent of sample geometry.

For a sphere, the diffusion occurs in all three dimensions, for a cylinder of an infinite length in two dimensions, for a disk with infinite diameter in one dimension. For a long cylinder, any change in diameter is coupled to a change in length. It was shown experimentally, that the relative change of diameter and length are the same. The experimentally observed D_{exp} values are only two thirds of that one for a spherical gel with the same diameter:

$$D_{\text{exp}}\,(\text{cylinder}) = (2/3)\,D_{\text{coop.}}$$

D_{exp} of a large disk is only a third of that for a sphere with a diameter equal to the thickness of the disk:

$$D_{\text{exp}}(\text{disk}) = (1/3)D_{\text{coop}}.$$

From both equations it follows, that the relaxation time τ of a long cylinder is longer than that of a short cylinder with the same diameter:

$$\frac{\Delta u(k,\,t)}{\Delta u(k,\,t\,=\,0)} = \sum_{n=1}^{\infty} B_{\text{n}}\,\exp\left(-\,\frac{t}{\tau_n}\right) \tag{51}$$

with k as diameter for cylinders and thickness for discs, respectively, and

$$\Delta u(k,t) = u(k,t \to \infty) - u(k,t);$$

$$\Delta u(k,t=0) = u(k,t \to \infty) - u(k,t \to 0).$$

From the semi-logarithmic plot

$$\ln \left.\frac{\Delta\, u\,(k,\,t)}{\Delta\, u\,(k,\,t)_0}\right|_{t\to\infty} = \ln B_1 - \frac{t}{\tau} \tag{52}$$

the intercept B_1 and the slope τ can be found.

D_{coop} is then given by

$$D_{coop} = \frac{k\,(t \to \infty)^2\,c}{\text{a}_1^2\,\tau} \tag{53}$$

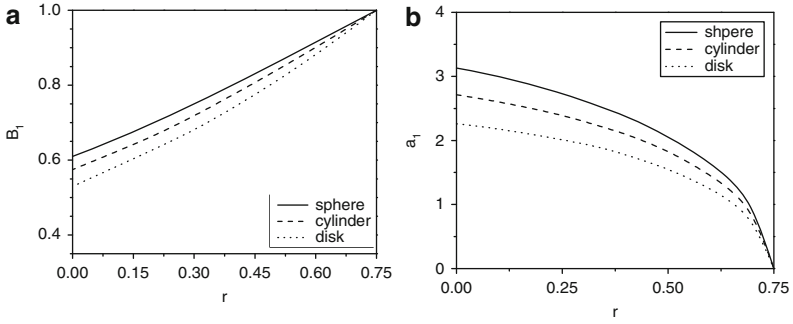

Fig. 5 Parameters a) B_1 and b) a_1 for (53). For details see (Eckert 2003)

with $c = 2/3$ for cylinders and 1/3 for disks. The correction term a_1 can be estimated graphically from B_1 (Fig. 5).

The swelling kinetics is determined by measuring the thickness of a gel strip or slab. Again, the diffusion occurs only in one dimension. The measured time-dependence is different for the thickness and the lateral (length l) dimension of the strip. In a first step of swelling the thickness (a, z-axis) increases up to a value higher than the thickness in the equilibrium. The second step is characterized by a decrease of thickness and a strong increase of sample length (l, x- and y-axes), to the equilibrium. The swelling is characterized by two different time constants, τ and τ_s. The former is related to the slower shear elongation of the x- and y-axes, and the latter to the faster dilation motion (z-axis) (Chiarelli et al. 1993):

$$l(t) = l(t \to \infty)\left[1 + \frac{4}{\pi}\,\varepsilon \sum \left(\frac{(-1)^n}{2n+1}\right) \exp\left(-\frac{(2n+1)^2}{\tau}\right)\right] \tag{54}$$

$$a(t) = a(t \to \infty)\left\{1 + \frac{8\,\varepsilon}{\pi}\sum_n (2n+1)^{-2}\left[3\exp\left(-\frac{(2n+1)^2\,t}{\tau_s}\right) - 2\exp\left(-\frac{(2n+1)^2\,t}{\tau}\right)\right]\right\} \tag{55}$$

with

$$\varepsilon = -\frac{l_\infty - l_0}{l_0}; \tag{56}$$

$$\tau = \frac{a^2}{\pi^2 D_{coop}}; \tag{57}$$

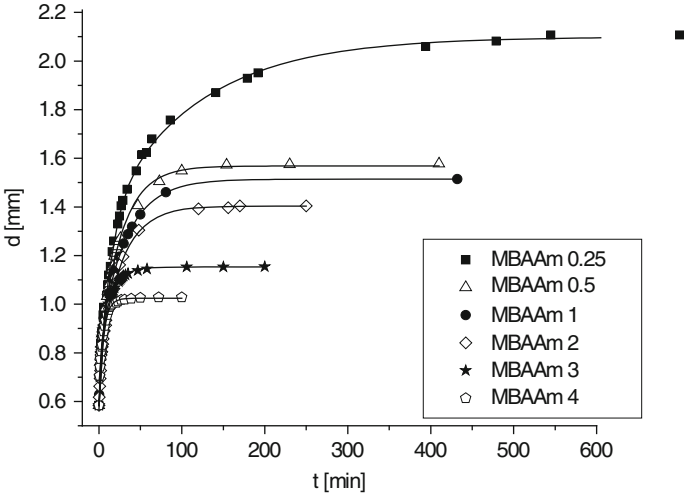

Fig. 6 Time dependence of thickness d of a gel cylinder. For details see (Eckert 2003)

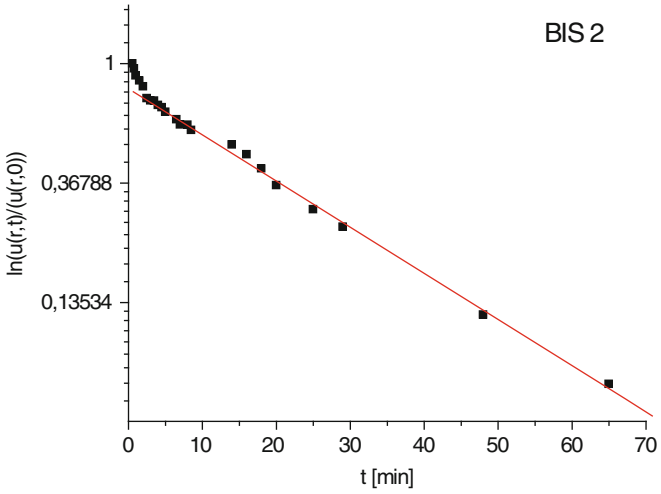

Fig. 7 Semi-logarithmic plot for determination of B_1 and τ. For details see (Eckert 2003)

$$\tau_s = \frac{a^2}{\pi^2 D_s} . \tag{58}$$

The differences in swelling parallel and perpendicular to the thickness causes stress in the inner part of the gel, which than could cause a fracture of the polymer sample, especially for very fast changes of the degree of swelling.

The Fig. 6 shows swelling curves of cross-linked polyacrylic acid (cross-linker MBAAm with different concentrations, in relation to the monomer acrylic acid) in

Table 1 Cooperative diffusion coefficients determined from the time dependence of gel geometry

MBAAm content mol-%	d_{dry} mm	$d\ (t=\infty)$ mm	B_1	r	a_1	τ min	D_{coop} 10^{-7} cm^2/s
0.25	0.584	2.107	0.6536	0.179	2.49	78.86	5.04
0.5	0.640	1.634	0.7252	0.314	2.28	31.63	9.02
1	0.937	1.875	0.7160	0.297	2.31	33.84	10.8
2	0.991	1.811	0.7398	0.339	2.22	29.88	12.4
3	0.745	1.315	0.6939	0.257	2.37	12.79	13.4
4	0.671	1.115	0.6552	0.182	2.49	7.60	14.7

water. The cooperative diffusion coefficient can be calculated from the semi-logarithmic plot in Fig. 7 (Eckert 2003), see Table 1.

2.4 Volume Phase Transition

As a model to understand and to describe the processes during the response of a smart gel on changes of environmental properties, a two-step mechanism can be assumed (Fig. 8). In a first step, the stimulus which triggers the swelling/shrinking must permeate the gel. Heat transfer for temperature-sensitive polymers or mass transfer (ions, organic solvents) determine the rate of the first step.

Typical diffusion coefficients are determined by the type of transport process:

- The stimulus is a change in temperature. The rate of heat transfer is given by the thermal diffusivity. In general, the thermal diffusivity of a solvent is in the order of 10^{-3} cm^2/s (Gehrke 1993), which is smaller than those of solids.
- The stimulus is a change in composition, e.g., diffusion of an organic component in a water-swollen gel. The diffusion coefficient for this transport is almost the same as in water, about 10^{-5} cm^2/s (Arndt et al. 2006).

Comparing both transport processes, it is evident, that thermo-sensitive gels can respond faster to the environmental change than chemo-sensitive gels.

The swelling/shrinking starts if thermodynamically conditions for a volume phase transition, e.g., temperature, pH, appropriate mixing ratio of water with a hydrophobic agent, like an organic solvent, are given.

This is followed by a change of the degree of swelling (second step), which is governed by the above discussed cooperative diffusion. Typically, the cooperative diffusion coefficient D_{coop} is in the order of 10^{-7} cm^2/s, i.e., about one hundredth of the mass transfer.

The mechanical properties of a gel are influenced by the degree of swelling. The volume phase transition and therefore the switching between two temperatures (above and below the temperature for volume phase transition) can be performed as a process under isobar or under isochoric conditions. For PNIPAAm, the bulk modulus shows a strong increase at 33 °C during heating. The abrupt change in the

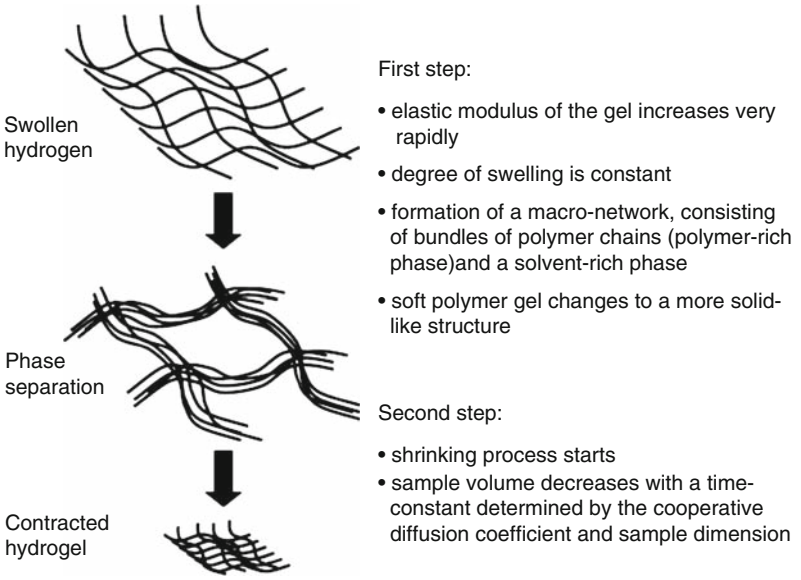

Fig. 8 Two-step mechanism of volume-phase transition

mechanical properties of an isobar gel could be ascribed to the volume transition (change of degree of swelling) taking place at the characteristic temperature.

In case of an isochore gel, we have to discuss the change in mechanical properties at a constant volume of gel (constant degree of swelling). An isochore gel can reach a new equilibrium state much faster than an isobar gel upon a change of temperature. Their equilibration is not accompanied by cooperative diffusion of network chains and solvent molecules. In practice, the above discussed first step can be assumed as an isochoric process. Due to constant polymer concentration classical network theories predict that the mechanical properties are nearly constant. Measurements under isochoric conditions show that during heating the bulk modulus (and similarly the Young´s modulus E) increases at the temperature of volume phase transition. An explanation for this behaviour was given by Shibayama et al. (Shibayama et al. 1994). For a polymer solution, phase transition means a separation in two phases, a polymer-rich phase and a polymer-poor phase. The polymer chains undergo a coil-globule transition. Network chains are connected in the junction by chemical bonds. A macroscopic phase transition like in a polymer solution is not possible. But the net chains can form a macro-network. It consists of bundles of polymer chains. The bundles comprise the polymer-rich phase which is surrounded by the polymer-poor phase. The increase in Young´s modulus can be estimated by the ratio of the degree of swelling, measured in isobar equilibrium, in the swollen ($T < T_c$) and shrunken ($T > T_c$) state.

With $E \propto \varphi_2^{\alpha}$ ($\alpha = 9/4$ for expanded polymer chains in a thermodynamically good solvent, $\alpha = 3$ for theta-solvent) it follows for the modulus E_{VPT} of the gel in the phase-separated state:

$$E_{VPT} = E_Q m^{\alpha - 1} \tag{59}$$

with m the ratio of degree of swelling in homogeneous state at $T < T_c$ to the degree of swelling in the phase-separated state. E_Q is the modulus of the swollen hydrogel. The strong increase in the modulus in the first step of volume phase transition plays an important role for the application of smart gels. The hydrogel gets stiffer, even at a high degree of swelling. The formation of the bundles in a macro-network means a reduction of chain mobility.

As discussed in Sect. 3.2, we can visualize the mobility of polymer chains by NMR-imaging. Fast heating of a PNIPAm gel shows that the net chains get immobile just before the shrinking starts; see Fig. 25 (Sect. 3.2).

Figure 9 shows the temperature dependence of the elastic part of the complex Young´s modulus $E'(\omega)$ for various poly(vinyl methyl ether) hydrogel samples in water at a selected frequency of 20.1 rad/s. The polymer was cross-linked by electron beam irradiation (see Sect. 2.4, chapter "Synthesis of hydrogels"). These data were compared with the temperature shrinking behaviour of sample PVME 20/80 .[11]

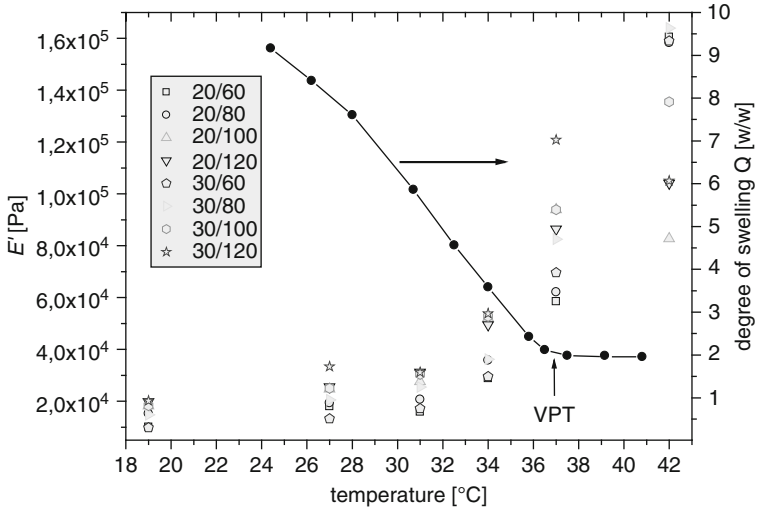

Fig. 9 Temperature dependence of the E' modulus of PVME hydrogel samples at $\omega = 20.1$ rad/s in water and the degrees of swelling Q of one selected hydrogel (PVME 20/80) in water at different temperatures. For details see (Richter 2006)

[11] A solution of 20 wt-% polymer in water was irradiated with a dose of 80 kGy.

For this given case on PVME hydrogels, a value of $\alpha \approx 2.5$ in (59) is assumed for the quality solvent. The ratio of degree of swelling $m \approx 4.5$ is given by the measured values of Q ($Q_v \approx 2$ at and above the temperature of transition VPT and $Q_v \approx 9$ below VPT at $T = 24\,°C$). Applying (59), a ratio of $E_{VPT}/E_0 \approx 9.7$ is obtained. For samples with a low radiation dose (PVME 20/60, PVME 20/80, PVME 30/60, PVME 30/80), the modulus rose to about 1.6×10^5 Pa at 42 °C. The ratio E_{VPT}/E_0 amounts to about 10 in these cases and confirms the calculations.

2.5 Gels with Fast Response

The swelling/shrinking rate dQ/dt and hence the response time τ for any application during volume phase transitions of smart hydrogels depends on the cooperative diffusion coefficient D_{coop} and on the square of their characteristic dimension l,

$$\tau \sim \text{length}^2/D_{coop}.$$

An effective reduction of response time is only possible by reducing the size of the gel using different techniques:

- Synthesis of porous or sponge-like gels (Dong and Hoffman 1990). The dimension of walls between the pores is crucial for the response time. Porous gels swell or shrink very fast compared with nonporous gels of the same size. The synthesis of porous gels is based on a cross-linking process in a phase-separated state. Yan and Hoffman (1995) have shown that polymerizing NIPAAm at temperatures above the volume phase transition results in gels having large pore sizes and faster swelling rates. Also the cross-linking by irradiation of a highly concentrated solution at high temperatures with γ- or electron rays results in porous gels (Gehrke 1993; Arndt et al. 2001; Gotoh et al. 1998; Suzuki and Hirasa 1993).
- Cross-linking of polymers in the presence of an inert substance yield to macro porous hydrogels. An example of the synthesis of a macro porous hydrogel as well as its swelling kinetics is shown in Sect. 3 in chapter "General properties of hydrogels" and Sect. 2.4 in chapter "Synthesis of hydrogels".
- Formation of hydrophobic clusters in a comb-grafted polymer gel leads to additional junction points and to an abrupt increase in the cross-linking density (Yoshida et al. 1995).
- Synthesis of gel particles in the μm-range (micro-gels) (Pelton 2000) using different techniques, e.g., thermo-sensitive micro-gels based on NIPAAm by inverse suspension polymerization (Bajpai et al. 2007) or inverse emulsion polymerization (Hirotsu et al. 1987).
- Cross-linking a spin-coated polymer thin films on a support using e.g., UV irradiation (photochemical cross-linking) (Kuckling et al. 2003) or high energy irradiation (γ-ray, e-beam; for details see Sect. 1.5 and 2.4 in chapter "Synthesis of hydrogels").

2.6 Determination of D_{coop} of Polyelectrolyte Hydrogels by DLS

Light scattered by dynamic concentration fluctuations is strongly heterodyned[12] due to the large scale heterogeneities of gels (see Sect. 3 in chapter "General properties of hydrogels" and Fig. 6). In contrast to the non-ergodic character of the static light, the movement of the polymer chains on a local scale ensures ergodic[13] behaviour. Therefore, to determine the contributions to the scattering from fluctuations of the network chains, it is sufficient to detect the light from a single sample position (P), avoiding ensemble averages. The resulting light intensity correlation function $g^{(2)}(t)$ which can be measured by dynamic light scattering is expressed in terms of the desired electric field correlation function $g^{(1)}(t)$ as follows:

$$g_P^{(2)}(q,t) = \frac{\langle I(0)I(t)\rangle_P}{\langle I(t)\rangle_P} = \left(X_P\, g^{(1)}(q,t)\right)^2 + 2X_p\left(1 - X_p\right) g^{(1)}(q,t) \; + \; 1. \quad (60)$$

Here X_P is the fraction of dynamically scattered light:

$$X_P = \frac{I_F}{\langle I\rangle_{t,P}} \quad (61)$$

with I_F as the scattering intensity for the thermal fluctuations of the network chains and $\langle I\rangle_{t,P}$ the total time-averaged scattering intensity at a constant sample position. q is the scattering vector:

$$q = \frac{4\pi n}{\lambda_0} \sin\left(\frac{\theta}{2}\right) \quad (62)$$

with n the refractive index of the solvent, λ_0 the wavelength of the incident light, and Θ the scattering angle. The brackets $\langle\rangle$denote time averages. Note that $g^{(2)}(t)$ as well as X_P depend on the sample position, denoted by the index P.

The value for X_P is found from the initial amplitude σ_P^2 of the measured intensity correlation function $g^{(2)}(t)$ by using the condition $g^{(1)}(t=0)=1$:

[12] A gel consists of polymer chains, cross-links and solvent. The polymer chains undergo Brownian motion while the cross-links remain at the same position. Light scattered from gels therefore has a dynamic and a static contribution. The scattering by chain segments resulting in an exponential decay of the scattering field is called homodyne scattering. Contrary, cross-links behave as local oscillators and do not produce any decay of the scattering field. This non-decaying component heterodynes with the decaying part and is called heterodyne scattering.

[13] For an ergodic system the long-time average is equal to the ensemble average – the average with respect to the configuration of the systems (average over all possible positions and shapes).

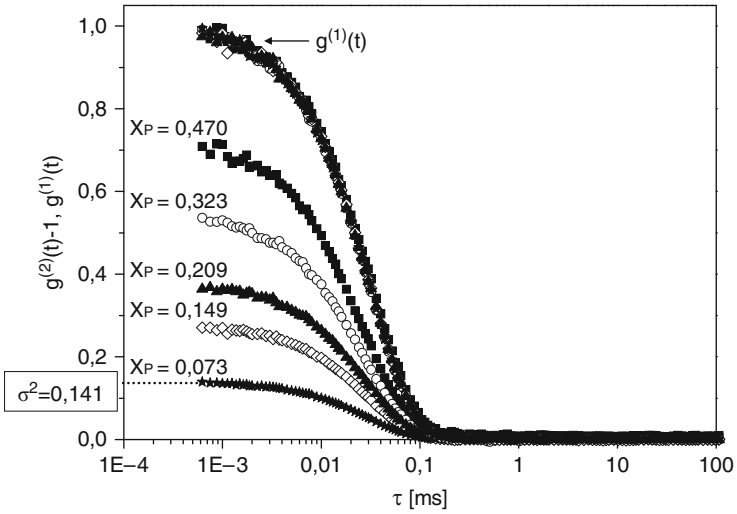

Fig. 10 Intensity correlation functions ($g^{(2)}(t)$-1) measured at five different sample position at $\theta = 90°$ in the swollen poly(acrylic acid) gel MBAAm-2. The corresponding field correlation function $g^{(1)}(t)$ is shown as one curve

$$\sigma_P^2 = g_P^{(2)}(q, t = 0) - 1 = X_P(2 - X_P). \tag{63}$$

σ^2 is less than unity and sample-position-dependent for gels due to the existence of frozen inhomogeneities.

The characteristic sample position dependency for the poly(acrylic acid) sample MBAAm-2 is illustrated in Fig. 10. Several measurements of $g^{(2)}(t)$ at different sample positions are shown (scattering angle $\theta = 90°$). After each measurement the sample was rotated in the measuring cell to adjust another position. Each position yields a different intensity correlation function $g^{(2)}(t)$ connected with a different value for X_P. The resulting field correlation functions represent the fully fluctuating component. They all are described by one curve $g^{(1)}(t)$.

It is convenient to describe the average decay rate of $g^{(1)}(t)$ by its first cummulant Γ which is correlated to the cooperative diffusion coefficient D_{coop} of the network chains:

$$\Gamma = -\left[\frac{d \ln g^{(1)}(q,t)}{dt}\right]_{t\to 0} \tag{64}$$

and

$$D_{coop} = \frac{\Gamma}{q^2}. \tag{65}$$

Table 2 Procedure for calculating the cooperative diffusion coefficient D_{coop} of a swollen hydrogel

No.	Step	Governing equations and example of Fig. 10, curve of filled stars
1	Calculation of the value of the fraction X_P of the dynamically scattered light from initial amplitude σ^2 of the intensity correlation function ($g^{(2)}(t) - 1$) using (63).	$\sigma^2 = 0.141 = X_P(2 - X_P)\ X_P^2 - 2X_P + \sigma^2 = 0$ $\rightarrow X_P = 1 - \sqrt{1 - \sigma^2} X_P = 0.073$
2	Calculation of the the field correlations function $g^{(1)}(t)$ for all delay times t using (60).	$g^{(1)}(q,t) = -\left(\frac{1-X_P}{X_P}\right) + \sqrt{\left(\frac{1-X_P}{X_P}\right)^2 + \frac{g_P^{(2)}(q,t)-1}{X_P^2}}$
3	Determination of Γ (in millisec^{-1}) from the initial decay of the semi-logarithmic plot $\ln g^{(1)}(t)$ vs. t using (64).	$\Gamma = -\left[\frac{d \ln g^{(1)}(q,t)}{dt}\right]_{t \rightarrow 0}$ $\Gamma = 13.87(\mathrm{ms})^{-1}$
4	The scattering vector q (in m^{-1}) is given by the experimental set-up ($n_{\text{water}} = 1.332$, $\lambda_0 = 632.8$ nm): (62)	$q = \frac{4\pi n}{\lambda_0} \sin\left(\frac{\theta}{2}\right) = \frac{4\pi 1.332}{632.810^{-9}\mathrm{m}} \sin(45°)$ $q = 1.87\ 10^7 \mathrm{m}^{-1}$
5	Calculation of D_{coop} from Γ and q^2 using (65).	$D_{coop} = \frac{\Gamma}{q^2} = \frac{13.87\,(\mathrm{ms})^{-1}}{3.498\ 10^{14}\mathrm{m}^{-2}}$ $= 3.97\ 10^{-14} \frac{\mathrm{m}^2}{(\mathrm{ms})} = 3.97\ 10^{-7} \frac{\mathrm{cm}^2}{\mathrm{s}}$

For a swollen polymer gel, D_{coop} describes the relaxation rate of concentration fluctuations caused by the collective motion that govern the swelling rate.

Compared to swelling-kinetic measurements DLS is a very fast method to determine D_{coop} of gels. Information about the network inhomogeneity can be drawn additionally.

A procedure for calculating the cooperative diffusion coefficient D_{coop} is shown in Table 2.

3 Characterization of Molecular Processes

3.1 Fourier Transform Infrared Spectroscopy and Raman Spectroscopy

3.1.1 Introduction

Infrared (IR) spectroscopy and Raman spectroscopy are both types of vibrational spectroscopy, providing the vibrational modes of a molecule. The vibrational spectrum of a molecule is composed of bands representing vibrations between atoms that depend on the masses of the atoms in the molecule, the strength of their chemical binding and the atomic environment. Molecular substituents, molecular

geometry and hydrogen bonding also affect the position of vibrations. Therefore, the vibrational spectrum of a molecule is considered to be an unique chemical fingerprint of the molecule. Consequently, each molecule has a specific vibrational spectrum and is useful in elucidating the molecular structure, conformation and intermolecular interactions of molecules (Smith 1996). Based on this background, IR and Raman spectroscopy are the most popular and cost-effective techniques for the structural elucidation of organic molecules as well as many polymers. The main difference between these two methods is that IR spectroscopy is sensitive to vibrations caused by changes of dipole moment of the molecule whereas Raman spectroscopy is sensitive to changes of molecular polarizability. Whether a vibrational mode is active or inactive in IR or Raman spectroscopy depends on the symmetry of the molecule. Since IR and Raman spectroscopy are based on different physical processes, the factors governing the intensity of different types of vibrational modes are different in the two types of spectroscopy. Vibrational modes related to high change of dipole moment during the vibration will have a large sensitivity in the IR spectrum, and vibrations with a small change of dipole moment are weak or even completely absent in the IR spectrum. Raman active vibrational modes are related to changes in polarizability during the vibration; as a result vibrations with a weak or no dipole moment change and a high degree of symmetry are favored. (Griffiths and de Haseth 2007; Kwak and Lafleur 2003)

Vibrations of atoms in a molecule can be divided in six different forms: symmetrical and antisymmetrical stretching, rocking, scissoring, twisting and wagging. Simple diatomic molecules have only one bond, and only one fundamental vibrational mode (the interatomic stretching mode) is seen in the spectrum. More complex molecules, such as hydrogels, have many bonds, and their vibrational spectrum is much more complex.

Water, one of the major components of swollen hydrogels, has very strong and broad absorption bands. Consequently, knowledge of spectral characteristics is important for choosing appropriate experimental conditions. Figure 1 displays the absorption spectrum of water. An isolated water molecule has three vibrational modes. These are: antisymmetric stretch at 3,750 cm^{-1}, symmetric stretch at 3,650 cm^{-1} and bending vibration at 1,630 cm^{-1}. The effect of hydrogen bonding is to shift each of these frequencies to a lower value.

Despite its apparent simplicity, the IR spectrum of liquid water is difficult to interpret exactly because of the effect of intermolecular interactions, especially hydrogen bonding. It should be also noted that the broad absorption band between 3,200 and 3,600 cm^{-1} has an additional component belonging to the overtone of the bending mode.

Molecules with polar groups such as H_2O exhibit very strong and often broad absorption bands in IR spectrum whereas they have weak bands in the Raman spectrum. A full theoretical discussion of the selection rules of IR and Raman spectroscopy can be found for example in (Smith 1979; Ferraro and Nakamoto 1994). IR and Raman spectroscopy tend to be complementary techniques. Moreover, both types of spectroscopy are required to measure the complete vibrational spectrum. Both these techniques are well developed, and instruments for carrying out each of the techniques are commercially available.

3.1.2 Fourier Transform Infrared Spectroscopy

Fourier transform infrared (FT-IR) spectrometers are by far the most popular type of instrument for the measurement of IR spectra. Most FT-IR spectrometers allow the spectral range from ca. 400 to 4,000 cm^{-1} (25. . ..2.5 μm), in which fundamental vibrations and associated rotational-vibrational structures occur, to be observed. One of the strengths of FT-IR spectroscopy is its capability to apply different sampling techniques to obtain spectra from a very wide range of samples. Probably the most popular way to obtain an IR spectrum is simply to pass the IR light through the sample, known as the transmission mode. Transmission spectra have usually a high signal-to-noise ratio and require no accessories other than a cell. To obtain a transmittance spectrum T, the ratio of the single-beam spectrum of the sample and that of an appropriate background must be calculated. The background spectrum is obtained either without a cell in the beam or with a cell containing only the solvent. The transmittance spectrum is usually then converted to absorbance ($-\log_{10}T$), since absorbance is proportional to the concentration of each component. One of the major problems of the transmission mode for hydrogels is that water is such a strong absorber. Hence, the thickness of the hydrogel film must be kept below 20 μm as the absorption of thicker samples in the region of the stretching and bending bands is too great to allow useful information to be obtained.

The attenuated total reflection (ATR) technique has become increasingly attractive to characterize hydrogels. ATR is a technique that requires no or little sample preparation and can be used for the quantitative and qualitative analyses. ATR is performed using a reflection accessory with a crystal of IR-transparent material of high refractive index. Typical materials and their relevant properties are listed in Table 3. When the angle of incidence of the beam at the inner surface of the crystal is greater than the critical angle, the beam is totally reflected. However, a standing wave, known as the evanescent field, extends beyond the surface, so that any material that is located in the evanescent field absorbs parts of the IR radiation at the frequencies of its absorption bands (Günzler and Gremlich 2002).

The depth of penetration d_p is defined as the distance from the surface at which the evanescent field has decayed to 1/e (ca. 37 %) of its value at the surface; d_p is given by the equation

$$d_p = \frac{\lambda}{2\pi\, n_C \sqrt{\sin^2(\alpha) - (n_S/n_C)^2}} \tag{66}$$

where λ is the vacuum wavelength, n_C the refractive index of the crystal, α the angle of incidence and n_S the refractive index of the sample. The wavelength in micrometers is 10^4 times the reciprocal of the wavenumber in cm^{-1}. As the equation (66) reveals, the penetration depth increases with the wavelength of the light. Thus, in comparison to the transmission spectra, ATR spectra exhibit absorption bands that are more intense at low wavenumber and less intense at high wavenumber. The refractive index of the crystal determines also the penetration depth. This fact is

Table 3 Materials for ATR crystals

Material	Refractive index	Transmission range, cm^{-1}	Hardness Knoop	Chemical properties
ZnSe	2.43	500–20,000 (0.5–20 μm)	150	slightly soluble in water, soluble in acids, sensitive against stretches, slightly toxic
ZnS	2.25	750–22,000 (0.9–13 μm)	355	slightly soluble in water, soluble in acids
Si	3.42	1,000–10,000 (1–10 μm)	1,150	insoluble in water, insoluble in most acids and bases, (not HF and HNO_3), hard
Ge	4.05	600–5,000 (2–16 μm)	550	insoluble in water, insoluble in most acids and bases, soluble in hot H_2SO_4,brittle
CaF_2	1.40	1,000–50,000 (0.2–10 μm)	158	insoluble in water, resists most acids and bases, soluble in solutions of ammonium salts, brittle
BaF_2	1.45	900–50,000 (0.2–11 μm)	82	slightly soluble in water, soluble in strong acids and solutions of ammonium salts
AMTIR-1 $Ge_{33}As_{12}Se_{55}$	2.50	900–11,000 (1.1–11 μm)	170	insoluble in water, soluble in bases, high homogeneity, sensitive against stretches, toxic
Diamond	2.40	100–45,000 (0.2–100 μm)	7,000	insoluble in water, insoluble in acids and bases, extremely hard

important when water-containing hydrogels are investigated since there is always a thin film of water between the crystal surface and the hydrogel network. For example, Ge with a refractive index of 4.0 has a shorter penetration depth than ZnSe. Therefore, for ATR spectroscopic studies of hydrogels, materials with low refractive index are recommended. The wavenumber-depending penetration depth for Ge and ZnSe is shown in Fig. 12.

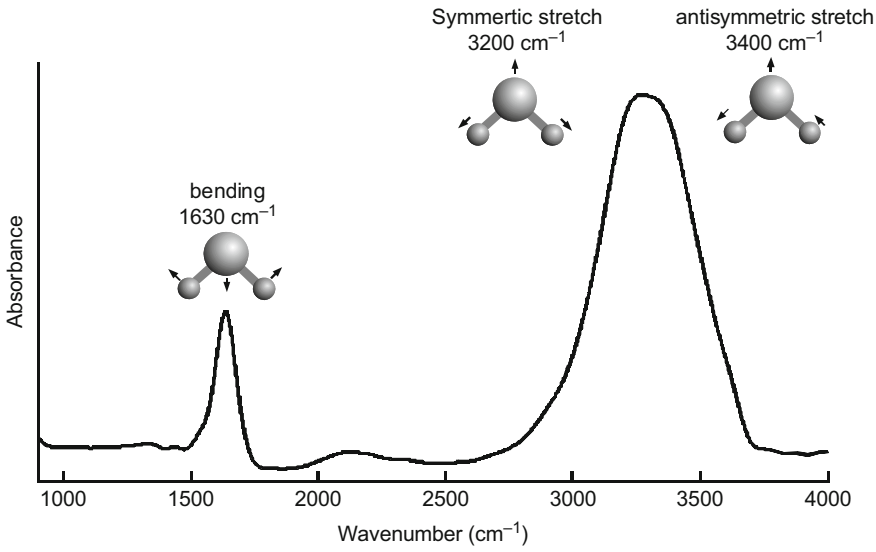

Fig. 11 Infrared absorption spectrum of water

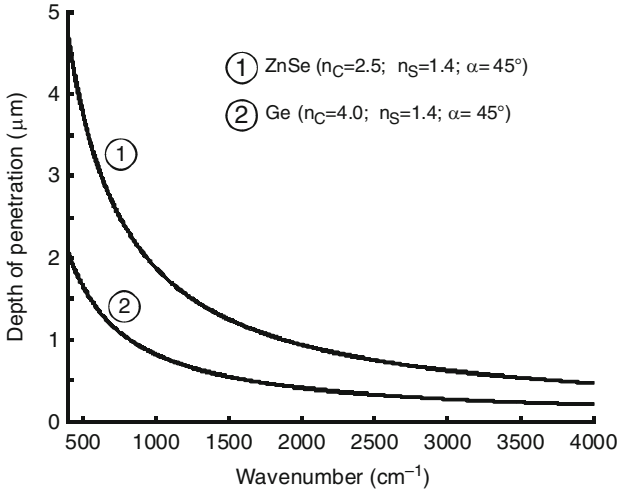

Fig. 12 Depth of penetration of the evanescent field vs. wavenumber for ATR crystals of ZnSe and Ge

Diamond is by far the best ATR crystal material because of its hardness and durability. However, the purchase cost is obviously higher than that of all other crystal materials. ZnSe and Si are also suitable but they can scratch and break with improper use.

The denominator in (66) also includes the angle of incidence α. Similar to the refractive index of the crystal, the penetration depth increase as α decreases. However, the most commercial ATR accessories are working with a fixed angle of incidence usually at 45°. Lastly, the refractive index of the sample has also an influence on the penetration depth. Fortunately, the refractive index of water-containing hydrogels are in a small range between 1.35 ... 1.4 whereas dry hydrogels may exhibit a refractive index higher than 1.5. Despite the complex theoretical relations, ATR is an easy and well-suitable technique for the investigation of hydrogels (Saiano et al. 2005). The thickness of the sample plays no role and even water-containing hydrogels might be investigated. Since ATR requires no sample preparation, it is the method of choice for in-situ investigations. Usually, the background spectrum is recorded from the dry and clean ATR crystal.

External reflection techniques like specular reflection and diffuse reflection are less suitable for studying hydrogels. There are a number of disadvantages of external reflection compared to transmission and ATR techniques. First, for the same acquisition time, the signal-to noise ratio is lower than in transmission or ATR. It is difficult to determine the path length of the light inside the sample making quantitative information difficult.

A special technique is the Grazing Angle ATR (GATR) FT-IR spectroscopy. The angle of incidence in GATR spectroscopy is much larger than in conventional ATR measurements, typically between 70° and 80°. This technique is ideal for analyzing very thin films of dry hydrogels on metal or semiconductor substrates.

3.1.3 Raman Spectroscopy

In Raman spectroscopy, a monochromatic light beam (almost invariably from a laser) excites the molecules of the sample residing in the ground vibrational and electronic states to a so-called virtual state. When the molecules relax back to the ground vibrational state, the energy is back-emitted at the same wavelength by a process known as Rayleigh scattering. A small portion of electrons relaxes to an excited vibrational state; in this case the emitted light is of lower energy and hence at longer wavelength. When the scattered radiation is shifted to lower frequency, this process is known as Stokes-shifted Raman scattering. When a small fraction of the molecules are originally in an excited vibrational state, those molecules that are raised to the virtual state can return to the ground vibrational state. In this case, the Raman-scattered radiation is higher in frequency than the incident laser frequency and the process is called anti-Stokes Raman scattering. The difference between the frequency of Raman-scattered radiation and the initial laser frequency is equal to the same vibrational energy gap that is excited in FT-IR spectroscopy. Raman spectroscopy is often considered as alternative to FT-IR spectroscopy for two reasons. First, water has the strongest absorption of all molecules in the IR spectrum whereas the water bands are weak in the Raman spectrum. Second, many bands that are weak in the IR spectrum are strong in the Raman spectrum (Maeda et al. 2003; Raasmark et al. 2005).

Raman spectrometers employ two techniques for the collection of spectra, dispersive Raman and Fourier Transform (FT) Raman spectroscopy. Dispersive Raman spectrometers incorporate a charge-coupled device (CCD) array detector and polychromator. Because silicon-based CCDs only respond to radiation of shorter wavelength than ~1,100 nm (9,100 cm^{-1}), and the Stokes-shifted Raman spectrum is located at longer wavelength, the laser wavelength of dispersive Raman lasers is limited to about 800 nm. One of the more important problems associated with Raman spectroscopy is interference by fluorescence. To minimize fluorescence a longer wavelength laser, such as a Nd:YAG laser emitting at 1,064 nm, could be used. Since the exiting laser source has a wavelength longer than 1 μm, the virtual state is of lower energy and it is less likely that it will overlap an upper electronic state which reduces fluorescence interferences. However, the Raman spectrum cannot be observed with a CCD detector in this case. Instead a FT-Raman-spectrometer equipped with a detector that responds at longer wavelength must be used. This fact is important when hydrogels with aromatic groups are investigated since the fluorescence spectrum can mask the Raman signals.

Like FT-IR spectrometers, the central component of FT-Raman spectrometers is an interferometer. The interferometer encodes the unique frequencies of the Raman scattering into a single signal known as an interferogram. The signal is measured very quickly, making signal averaging fast and accurate. Most modern dispersive Raman spectrometers are equipped with a single monochromator and an optical filter that eliminates the Rayleigh-scattered radiation. Common detectors in such configurations are cooled CCD line or CCD array detectors with up to 2,048 pixel in a row. Recent developments of high-power near-infrared diode lasers, of volume-phase transmission multiplex holographic gratings, notch filters and high-sensitivity CCD arrays enable very efficient multichannel spectrometers and even Raman imaging devices to be built. A micro-Raman spectroscopic system comprises an optical microscope for observing a field of view of few micrometers of the sample. In micro-Raman spectroscopy the laser beam is focused by means of a microscope objective. The scattered Raman light is collected through the same microscope and directed into the Raman spectrometer.

3.1.4 Sample Preparation

The appropriate sample preparation is essential and often has to be chosen as a compromise between the different requirements of sample, the vibrational technique and the aim of the investigation. Generally, each sample preparation technique is intended for use with specific types of hydrogels and has its own strengths and weaknesses. The first step is to select the vibrational spectroscopic method. Since FT-IR spectroscopy is based on direct absorption of light and Raman spectroscopy is based on scattering of light, the sample preparation is mainly determined by the spectroscopic technique chosen. Raman spectroscopy is to be preferred when a strong swollen or water-containing hydrogel sample is to be

analyzed. Since water exhibits very intense broad absorption bands in its IR spectrum the relatively weak absorption bands of the hydrogel are overlaid on the water absorption bands. Nevertheless, as discussed in the following sections, under certain conditions, FT-IR spectroscopy is also useful for the investigation of water-containing hydrogels. In case of dry hydrogel samples, on the other hand, FT-IR spectroscopy provides spectra with a high signal-to-noise ratio and a short acquisition time. Hence, a variety of different techniques can be applied according to the requirements of the sample.

Sampling Techniques for FT-IR Spectroscopy

The sampling techniques for spectroscopic investigations in the transmission mode can be divided into two main classes. Solid samples are usually ground with potassium bromide (KBr) and compressed into a transparent pellet. However, this common sample preparation technique has a number of disadvantages in the case of hydrogels. First, most hydrogels can not be ground to a fine powder, which is essential to obtain good spectra. Sample particles that have a size of larger than 2 μm lead to a scattering of the IR light. Another problem is that the hydrogel must be dry. Furthermore, after being compressed into a pellet, the hydrogel cannot be used for additional investigations. Finally, opaque pellets or such with too little hydrogel will give poor spectra.

Cast films are an alternative way of preparing hydrogels for transmission spectroscopy. Thin cast films are prepared by dissolving the hydrogel in a suitable solvent. Unfortunately, this method does not work with cross-linked hydrogels because of their low solubility. Only films of monomers or low cross-linked hydrogels can be cast. The use of sealed liquid cells is also possible for measurement of the transmission spectrum. Usually, the cell consists of two IR-transparent windows separated by a gasket of specific thickness. The fluid sample is introduced into cell through holes in one of the windows. Cells from 6 to 100 μm optical path length are typical. The advantages of liquid cells are the simple handling, prevention of the hydrogel from drying, and the known path length. Major disadvantages are the strong absorption of water and that it is difficult to fill the cells even when the polymer is not cross-linked. In addition, the most sealed liquid cells consist of KBr windows. KBr is water-soluble and hygroscopic so that ZnSe or CaF_2 windows have to be used (Garton 1992; Zerbi 1999).

Possibly the best way to obtain transmission spectra from hydrogels is to prepare a capillary thin film onto a water-insoluble and IR-transparent window. The preparation of capillary films is simple: a drop or smear of the hydrogel sample is placed onto the window and a second window is placed on the top of the first. The resulting sandwich is placed in the IR beam.

Attenuated total reflection is an optimal technique to study hydrogels under native conditions. Similar to Raman spectroscopy there is no special sample preparation required and even thick samples can be investigated, although it should be recognized that only the sample within about 1 μm of the surface of the ATR

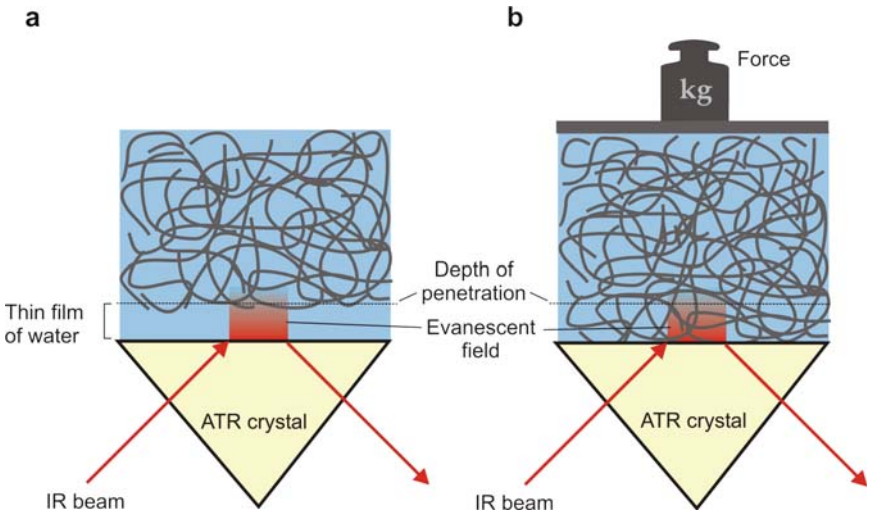

Fig. 13 ATR spectroscopy of a water-containing hydrogel network. (a) A thin film of water is formed between the ATR crystal surface and the hydrogel network. Interactions between the hydrogel network and the evanescent field are weak. (b) A pressure onto the hydrogel network causes a replacement of the water film. Molecular groups of the network come closer to the ATR crystal surface resulting in increased absorption bands of the hydrogel

crystal is interrogated by the evanescent field. When possible, the hydrogel sample should be pressed with a mild force onto the ATR crystal. Several studies have demonstrated that water-containing hydrogels can also be investigated (Guo et al. 2008). Since water bands are difficult to subtract from the sample spectra a very good signal-to-noise ratio is recommended. Often the spectral regions of the strong water absorption bands can not be used for the spectra evaluation. Another important aspect is the optical contact between the hydrogel and the ATR crystal. Usually, when the swollen hydrogel is placed onto the ATR crystal, a thin film of water is present between the surface and the hydrogel network (see Fig. 13). As consequence, water molecules initially occupy regions of high strength of the evanescent field. A pressure on the hydrogel may improve the optical contact between the hydrogel and the ATR crystal. Molecules that have direct contact to the ATR crystal surface experience a much higher strength of the evanescent field and absorb more IR light than molecules more than about 1 μm away from the surface. The replacement of water by the hydrogel leads to an increased intensity of the absorption bands of the hydrogel.

Deuterium Oxide Instead Water?

Two general problems in the FT-IR spectroscopy of hydrogels are that the water content of hydrogels is often high and that monomers may tend to aggregate. On the other hand, the chemical relevance of structural investigations on dry hydrogels

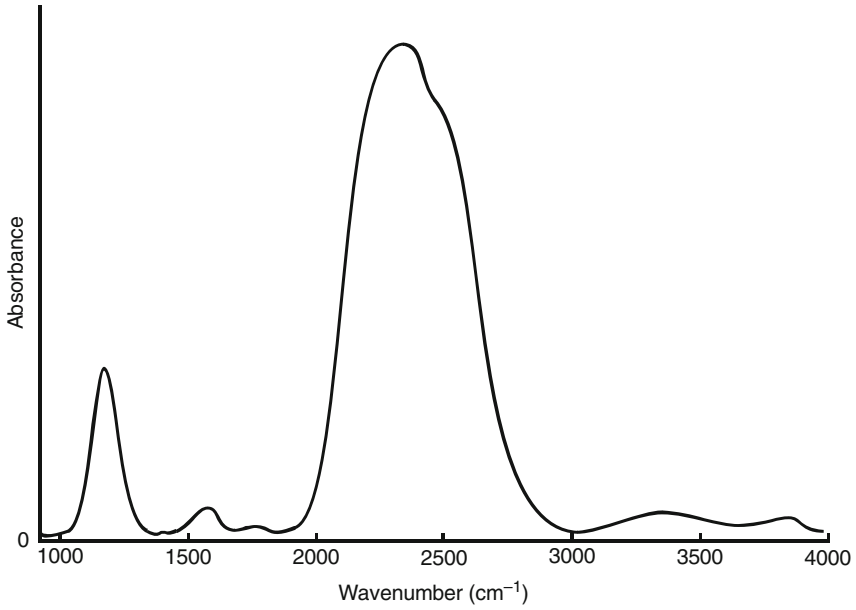

Fig. 14 IR spectrum of liquid deuterium oxide

would be questionable. A way out of this dilemma that leads to a significant improvement of the sensitivity of FT-IR spectroscopy when water bands overlay the important absorption bands of the sample can be achieved through the replacement of water by deuterium oxide (D_2O). Clearly, D_2O instead water could be an option for the IR spectroscopic analysis of hydrogels. The typical D_2O absorption spectrum is shown in Fig. 14. The absorption band at 1,210 cm^{-1} is the bending vibration of D_2O. A combination of the bending and the vibrational band of hydrogen-bonded water causes a weak band centered at 1,555 cm^{-1}. The broad and intense absorption band between 2,000 and 2,800 cm^{-1} arises from stretching modes. D_2O is to be preferred when the hydrogel absorption bands of interest lie between 1,700 and 1,500 cm^{-1} or between 3,200 and 3,600 cm^{-1}. It should be noted that D_2O is never 100% pure and usually includes HOD molecules and traces of H_2O. D_2O with high purity is expensive and it will adsorb water directly from the atmosphere. Nonetheless, the use of D_2O as an alternative to water is often beneficial when absorption bands of the hydrogel in the spectral regions where water absorbs.

Sampling Techniques for Raman Spectroscopy

Unlike most other techniques, Raman spectroscopy requires no special preparation of the sample. In fact, no contact with the sample is needed at all because Raman spectroscopy involves only illumination with a laser and collection of the scattered

light. Thus, Raman spectroscopy is a non-destructive analytical technique. In addition, since the Raman spectrum of water is weak and unobtrusive, good spectra of water-containing hydrogels can be acquired (da Costa and Amado 2001).

3.1.5 Qualitative Spectral Interpretation

General Approaches

Hydrogels as complex molecules have many bonds and show several intramolecular as well as intermolecular interactions leading to IR absorption bands at characteristic frequencies that may be related to chemical groups and/or to molecular interactions. A vibrational spectrum of a hydrogel network may have more than a hundred absorption bands, many of which are strongly overlapped. However, it is impossible to assign each band to a bond or to a type of interaction. From a practical point of view, there is also no need to assign the majority of bands. Often the most intense bands give rise to indicate the basic structure. Generally, there are six basic vibrations: symmetrical (ν_s) and antisymmetrical (ν_{as}) stretching, scissoring (s), rocking (r), wagging (ω) and twisting (t).

Although each vibration mode in an IR or Raman spectrum can be assigned to a molecular bond or to a movement of a group of atoms it is often difficult to identify the origin of the vibration. This is particular true for long molecules such as hydrogels which have so many atoms and hence so many possibilities for intermolecular interactions. For example, when a hydrogel chain consists of $N = 10{,}000$ atoms, about 30,000 vibrational modes are expected. Because many of these bands are overlaid it would be expected that the spectrum should consist of a relatively small number of very broad absorption bands. In practice, however, these vibration modes often occur in narrow ranges at certain spectral positions so that the spectra of most hydrogels exhibits a relatively small number of sharp bands that can be assigned to specific functional groups. The bands in a spectrum of a hydrogel network may be even sharper than the corresponding bands of the monomers because the vast majority of the functional groups are in a very similar environment and hence absorb at approximately the same frequency. However, there are also several clear spectral differences that occur when the hydrogel network contains water. Generally, crystalline substances exhibit sharp and narrow bands whereas non-crystalline substances have broader bands. When a hydrogel network is swollen, more different molecular interactions between functional groups and changes in the molecular structure may occur.

The majority of functional groups presented in hydrogels give rise to both Raman scattering and IR absorption. Although it is not absolutely necessary to identify vibrational modes on a basic level it is very helpful to have some understanding of the theoretical aspects. The spectra of most dry hydrogels usually consist of sharp bands that are often related to characteristic spectral patterns of monomers. Water-containing hydrogels exhibit a number of intermolecular interactions between polar groups of the hydrogel and water molecules (Maeda 2001).

Consequently, vibrational modes get broader and may shift towards lower frequencies. Although water gives only a very weak Raman spectrum, interactions between water and functional groups of the hydrogel affect the Raman spectrum as well (Kwak and Lafleur 2003).

IR and Raman spectra can be divided into three basic wavenumber regions, namely: 3,800–2,000 cm^{-1}, 2,000–900 cm^{-1} and below 900 cm^{-1}. The region between 3,800 and 2,700 cm^{-1} contains stretching vibrations of O–H, N–H_x and C–H_x groups. Vibrations of the corresponding deuterated groups are at an about 70% lower frequency. Many (but not all) of the bands between 2,000 and 900 cm^{-1} can be assigned to vibrations that are characteristic of certain functional groups. Bands in the region below 900 cm^{-1} are often due to vibrational modes in which more than three of four atoms are involved (often called skeletal vibrations.) The lower frequency region is also important for Raman spectra.

The Region 2,000–3,800 cm^{-1}

The stretching modes of light atoms absorb in this region. The O-H vibrations are generally very strong in IR spectra and weak or absent in Raman spectra. A shifting and broadening are indicative of increased strength of hydrogen bonding. In contrast to the O–H vibration modes, N–H vibrations can be observed in Raman spectra. Stretching vibrations of C–H groups are most clearly seen in the Raman spectra as strong and sharp bands. In IR spectra these bands are less prominent than N–H and O–H vibrations. Table 4 summarizes the most important vibration modes within this region (Smith 1999; Socrates 2006).

Bands in the spectral region between 2,000 and 2,700 cm^{-1} usually arise from C–D, O–D, N–D, C≡C, C≡N, N≡N or groups containing hydrogen and heavier atoms like S–H, Si–H or P–H. However, because these bonds are very rare in hydrogels this spectral region is of little importance in this field.

The Region 900–2,000 cm^{-1}

The stretching modes of many chemical groups with single or double bonds between atoms heavier than hydrogen, as well as several bending modes involving hydrogen atoms, absorb in this region. Below 1,500 cm^{-1}, not every band can be assigned to the vibration of a specific functional group; thus, this region is often called the fingerprint region. Since vibration modes from a wide variety of double-bonded chemical groups are important for the identification of hydrogels the fingerprint region is extended here to 2,000 cm^{-1}. The most intense vibrations in the IR spectrum are stretching and bending modes. Because many hydrogels are based on single bonds between carbon, nitrogen and oxygen and the strength of these bonds is similar, the vibrational modes are at similar wavenumbers in the fingerprint region (typically between 1,400 and 1,000 cm^{-1}). As more atoms are involved in the vibrational mode, the oscillations are shifted to lower wavenumbers.

Table 4 Assignment of vibration modes in the spectral range 2,000–3,800 cm^{-1}. The intensity is classified as very strong (vs), strong (s), medium (m) and weak (w). The symbol ν_s signifies a symmetric stretching mode and ν_{as} signifies an antisymmetric stretching mode, respectively.

Functional groups	Region cm^{-1}	Intensity		Vibration mode
		Infrared	Raman	
OH free	3,580–3,670	vs	w	ν
OH water	3,100–3,600	vs	w	ν usually broad
OH hydrogen bonded	3,200–3,560	vs	w	ν usually broad
OH of COOH (free)	3,500–3,580	m-vs	w	ν
OH of COOH (assoc.)	2,500–3,300	m-vs	w	ν
OH pri. alipatic alcohols	3,630–3,650	vs	w	ν
OH chelated	2,500–3,300	vs	w	ν usually broad
OH sec. alipatic alcohols	3,620–3,640	vs	w	ν
OH tert. alipatic alcohols	3,610–3,630	vs	w	ν
OD	2,100–2,700	vs	w	s usually broad
NH pri. amines	3,330–3,550	m	w	ν_{as}
NH sec. amines	3,310–3,500	m	w	ν_{as}
NH imined	3,300–3,400	m	w	ν_{as}
$-CH_3$ (aliphatic)	2,950–2,980	m-s	m	ν_{as}
$-CH_3$ (aliphatic)	2,860–2,890	m	m-s	ν_s
$-CH_2$ (acyclic)	2,910–2,940	m	m-s	ν_{as}
$-CH_2$ (acyclic)	2,840–2,870	m	m-s	ν_s
Ar-CH_3	2,930–3,000	m-s	m-s	ν_{as}
Ar-CH_3	2,920–2,940	m-s	m-s	ν_s
Ar-CH_3	2,740	w		overtones
CH vinyles	3,010–3,050	m	m	ν_s
S-H thiols, mercaptans	2,540–2,600	w	s	ν
P-H	2,200–2,500	m	w-m	ν
Si-H	2,100–2,560	m-s	m-s	ν

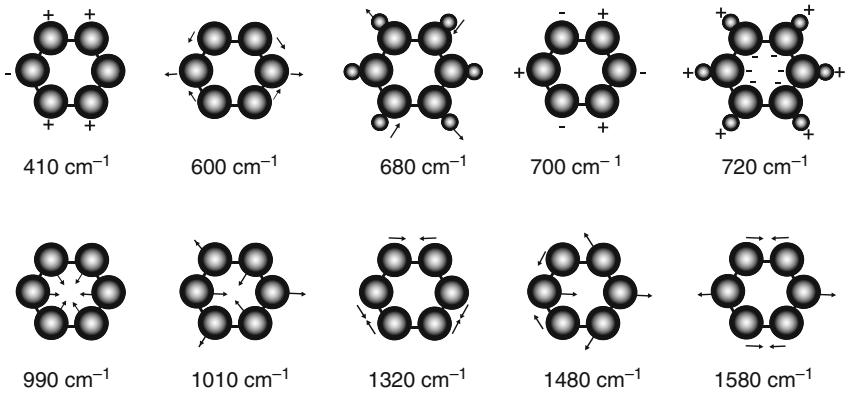

Fig. 15 Examples of ring vibration modes with respect to their wavenumber

Nonetheless, based on the group frequencies, many positions of vibration modes and their intensities can be clearly identified. Vibration modes for some important groups are given in Table 5. (Smith 1999; Socrates 2006).

Aromatic components exhibit several vibration modes of the ring system. Some basic vibrations are depicted in Fig. 15. Prominent bands occur between 1,400 and 1,600 cm^{-1} which are mainly ring modes involving C–C partial double bonds.

The Region 500–900 cm^{-1}

In this region many characteristic bands of aromatic compounds occur (see Fig. 15). In-plane bending modes are generally found above 1,000 cm^{-1} with out-of-plane modes at lower frequencies. The absence of strong and sharp bands indicates the lack of aromatic rings. Besides aromatic compounds, carbon-halogen stretching modes are also found in this region. Other relevant vibration modes of hydrogels are the strongly Raman-active C–S–C stretching vibrations between 600 cm^{-1} and 710 cm^{-1} and several combinations of amides, CH wagging vibrations and CH deformation of alkenes and alkynes. Finally, the C = S bound give a strong Raman signal around 730 cm^{-1} (Smith 1999; Socrates 2006).

3.1.6 FT-IR and Raman Spectra of Hydrogels

One of the best-studied hydrogels is poly(ethylene glycol) (PEG). PEG consists solely of C–C, C–O–C and C–H single bonds. Figure 16 shows the IR-ATR spectrum of a dry PEG film in the fingerprint region. The strongest band between 1,000 and 1,170 cm^{-1} arises from vibrations of the C–O–C groups. Other weaker bands indicate mainly C–H deformation and wagging vibrations (see Table 6). Ethers may have clusters of bands between 1,000 and 1,300 cm^{-1} in the spectra due to C–C vibrations. Since the C–O bond is very polar the dipole moment change of the C–C bond can be large as well resulting in relatively intense absorption bands.

The IR spectrum of poly(vinyl methyl ether) (PVME) in Fig. 17 is quite similar to the spectrum of PEG. PVME has also a strong C–O–C stretching band which is composed of the antisymmetric and symmetric vibration mode (Schmidt et al. 2003). The vibrations of the aliphatic chain between 1,250 and 1,350 cm^{-1} are very weak or even nonexistent.

The IR spectrum of poly(vinyl pyrrolidone) (PVP) in Fig. 18 is dominated by the strong C = O stretching mode that absorbs between 1,560 and 1,730 cm^{-1}. Due to molecular interactions the band is broad and asymmetric. The pyridine ring leads to a more complex spectrum. Ring vibrations occur mainly between 1,100 and 1,300 cm^{-1}. Vibrations of the C–N bond are generally weak for tertiary amines.

Water is dominant in the IR spectrum of swollen hydrogels. Figure 19a shows the ATR spectrum of water-containing PVP. The three strongest absorption bands are due to vibrational modes of water. The weak bands that are indicated by a star in Fig. 19a arise from PVP. The Raman spectrum of the same sample is represented in

Table 5 Assignment of some vibration modes in the spectral range 900-2,000 cm^{-1}. The symbol δ refers to a bending mode.

Functional groups	Region cm^{-1}	Intensity		Vibration mode
		Infrared	Raman	
		Infrared	Raman	
OH water	1,600–1,700	s	w	δ
OH alcohols	1,310–1,440	s	w	δ
OH carboxyl acids	890–970	s	m-s	δ out of plane
OH phenols	1,180–1,260	s	m	δ
CH_3 aliphatic	1,440–1,470	m	m	δ
CH_3 aliphatic	1,370–1,390	m-s	w	δ
CH_2 aliphatic	1,350–1,410	m	w	δ
CH_2 aliphatic	1,440–1,490	m	m	δ
CH ether groups	1,370–1,420	m-s	m	δ
CH acetate groups	1,340–1,390	m-s	m	δ
CH ester groups	1,370–1,400	m-s	m	δ
CH ketone groups	1,350–1,360	s	m	δ
CH ketone groups	1,400–1,450	s	m	δ
CH amide groups	1,400–1,420	s	m-w	δ
C–C skeletal $CH(CH_3)_2$	1,160–1,180	w	w	ν
C–C skeletal $C(CH_3)_3$	1,220–1,260	m	m	ν
C–C straight chain	1,120–1,180	m	m	doublet
C–C straight chain	1,040–1,100	w	s	
C–C straight chain	800–900	–	s	
C–C–O esters, aromatic	1,100–1,160	s	m	ν_s
C–C–O esters, aliphatic	1,160–1,210	s	m	ν_s
O–C–C esters, aromatic	1,100–1,300	s	m	ν_s
C = C vinyl	1,630–1,660	m	m	ν_s
C = N oxime, imine	1,620–1,690	s	s	ν
C–O primary alcohols	1,000–1,100	s	m-s	ν(CCO)
C–O secondary. alcohols	1,070–1,150	s	m-s	ν_s(COO)
C–O tertiary alcoholes	1,100–1,210	s	m-s	ν_s(COO)
C–O aryl	1,000–1,080	s	m-s	ν_s(CO)
C–O phenols	1,180–1,260	s	m	ν_s(CO) in combination with δ(OH)
C–O–C aliphatic ethers	1,060–1,150	vs	w	ν
C–O–C alkyl-aryl ethers	1,210–1,310	vs	w	ν
C–O–C diaryl ethers	1,170–1,250	s	m	ν
O–C–O sat. carbonates	1,240–1,280	s	m	ν
C = O carboxylic acids	1,680–1,760	vs	w-m	ν_{as}
C = O carboxylic acid salts	1,560–1,670	vs	w	ν_{as}
C = O carboxylic acid salts	1,340–1,460	m-s	w	ν_s
C = O anhydrides	1,850–1,800	vs	w-m	ν_{as}
C = O anhydrides	1,740–1,790	vs	w-m	ν_{as}
C = O aromatic	1,680–1,710	vs	m	ν_{as}
C = O aldehydes aliphatic	1,710–1,730	vs	m	ν_{as}
C = O aldehydes aryl	1,680–1,720	vs	m	ν_{as}
C = O esters	1,700–1,790	vs	m	ν_{as}
amide I (C = O vibr.)	1,630–1,720	vs	w-m	ν
amide II (C–N vibr.)	1,490–1,610	s	m	δ
amide III	1,200–1,300	w-m	w	δ (NH) + d(OCN)
$-NH_3^+$	1,580–1,670	s	m	ν_{as}

(*continued*)

Table 5 (continued)

Functional groups	Region cm^{-1}	Intensity		Vibration mode
		Infrared	Raman	
$-NH_3^+$	1,480–1,530	w-m	m	ν_s
C–N amines	1,030–1,240	m	m-s	ν
aromatic components	1,450–1,630	m	m-s	ring modes
aromatic components	1,000–1,300	m	m	ring modes

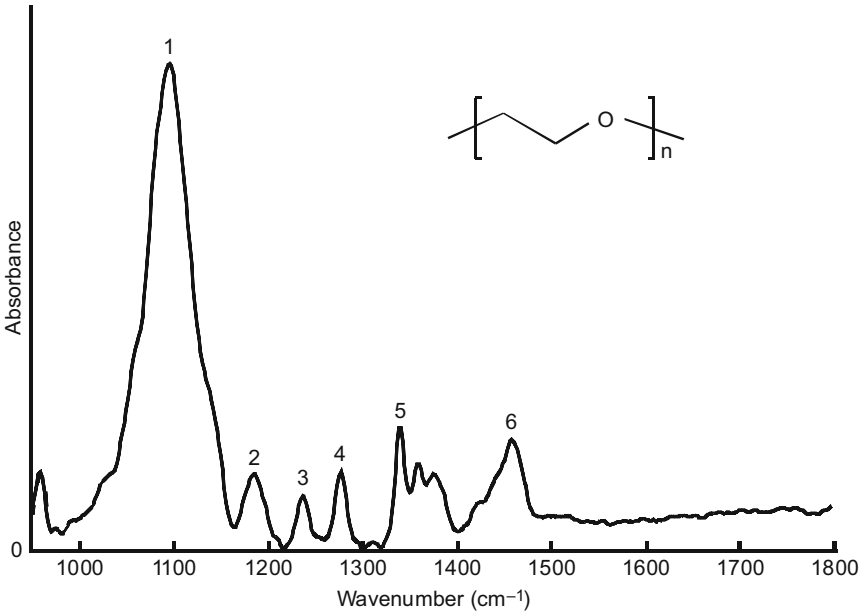

Fig. 16 ATR spectrum of a dry film of poly(ethylene glycol)

Table 6 Assignment of the absorption bands of the spectrum in Fig. 16. The symbol r refers to the rocking mode and the symbol t refers to the twisting mode

Band	Spectral position cm^{-1}	Vibration mode
1	1,000–1,170	ν_s(C–O–C), ν_{as}(C–O–C) and in combination with ν(C–C)
2	1,190	ν(C–C) mixed with ν(C–O–C) and r(CH_2)
3	1,240	$t_s(CH_2)$, $t_{as}(CH_2)$
4	1,278	$t_{as}(CH_2)$
5	1,340	ν (C–C) mixed with δ(CH_2)
6	1,460	δ(CH_2)

Fig. 19b. Although the hydrogel was maximally swollen the spectrum exhibits only a weak band of water between 3,300 and 3,500 cm^{-1}. This is a good example showing that Raman spectroscopy is more useful than IR spectroscopy when water-containing samples have to be investigated.

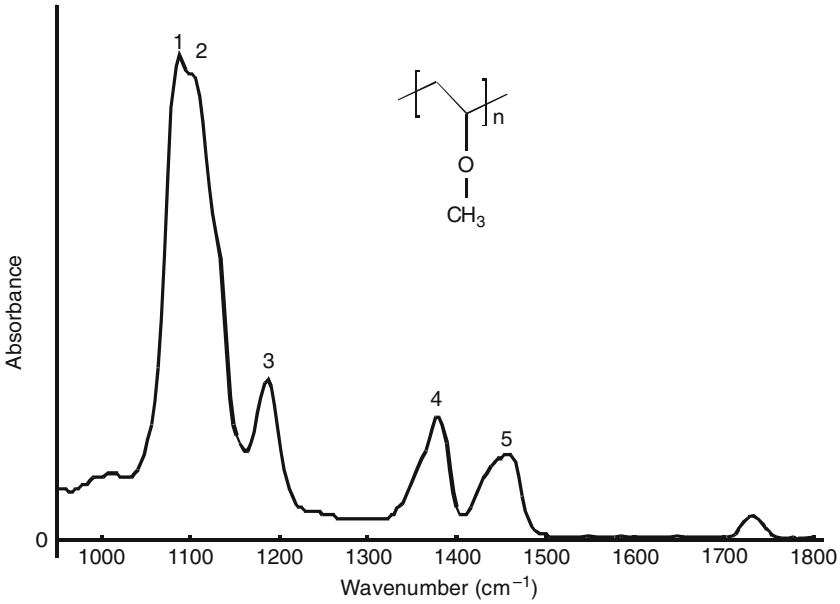

Fig. 17 ATR spectrum of a dry film of poly(vinyl methyl ether), assignment see Table 7

Table 7 Assignment of the absorption bands of the spectrum in Figure 17

Band	Spectral position cm^{-1}	Vibration mode
1, 2	1,050–1,150	ν_s(C–O–C), ν_{as}(C–O–C)
3	1,195	ν(C–C) in combination with ν(C–O–C) and r(CH_2)
4	1,380	δ(CH_3)
5	1,460	δ(CH_2), δ(CH_3)

When hydrogels swell then the molecular structure of the network may be changed. However, when the intermolecular interactions are weak and the driving force of the swelling is not related to changes of the molecular structure of the hydrogel, the spectral signatures of dry and water-containing hydrogels should be quite similar. Since the swelling process is mainly related to interactions between polar groups Raman spectroscopy is less sensitive to such changes than IR spectroscopy. For example, Fig. 20 shows the Raman spectra of dry and water-containing PVP.

There are only a few very small differences between the spectrum of the dry and water-containing hydrogel network. In contrast to the Raman spectra, the IR spectra of the same samples exhibit much more spectral changes between dry and water containing PVP (Fig. 21). The spectral window is limited to the region where no water bands occur and the interpretation of the changes are very difficult. The strongest changes occur in ring vibrations which are mainly based on a coupling between the polar carbonyl group and water.

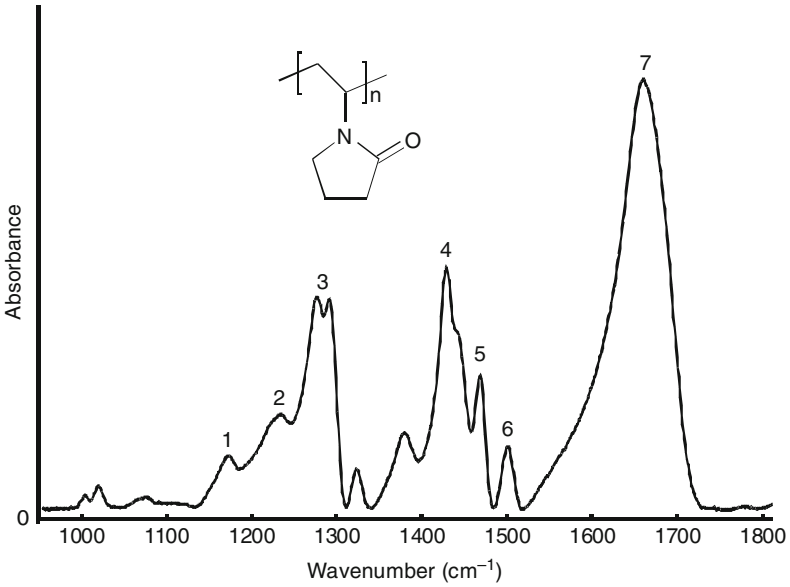

Fig. 18 ATR spectrum of a dry film of poly(vinyl pyrrolidone), assignment see Table 8

Table 8 Assignment of the absorption bands of the spectrum in Fig. 18. The symbol ω refers to the wagging mode

Band	Spectral positioncm^{-1}	Vibration mode
1	1,180	ω(CH_2)
2,3	1,200–1,350	ring vibrations
4	1,420	t(CH_2), r(CH_2)
5	1,480	ring vibration ν(C–N)
6	1,340	ring vibration ν(C–C)
7	1,560–1,720	ν(C = O)

Poly(acrylic acid)/poly(vinyl alcohol) (PAAc/PVA) hydrogels swell and shrink in response to a change in pH value of the surrounding solution (Sahoo et al. 2006). The basic condition for swelling is the dissociation of the carboxylic acid groups (COOH) of PAAc to the carboxylate ion (COO^-). The chain-bound, negatively charged carboxylate groups repel each other and the resulting electrostatic force causes a swelling. The dissociation of the carboxylic acid groups can be observed by FT-IR spectroscopy. Figure 22 shows the ATR spectra of the PAAc/PVA hydrogel network for different pH values of the solution.

The protonated carboxylic acid group has a strong absorption at 1,700 cm^{-1} that is assigned to the C = O stretching mode. The bond order of the C–O bond in carboxylate ions is less than that of the corresponding carboxylic acid. As a result, the position of the ν(C = O) mode of the carboxylic ion is shifted towards lower wavenumber and appears at 1,560 cm^{-1}. Both absorption bands are overlaid by the δ(OH) mode of water which is located at 1,630 cm^{-1}.

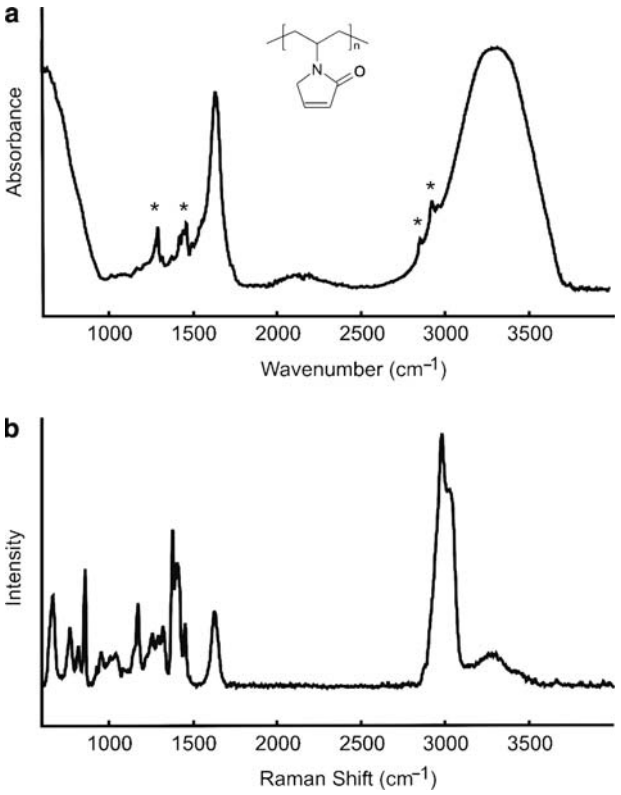

Fig. 19 a) IR-ATR spectrum of poly(vinyl pyrrolidone) in water and b) Raman spectrum of the same sample

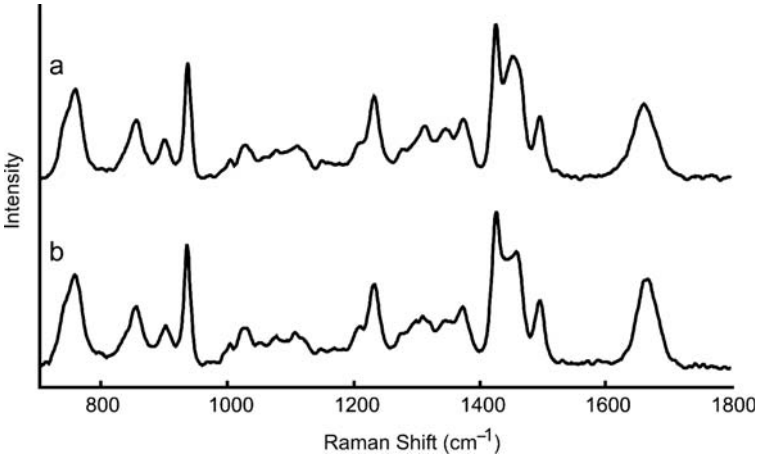

Fig. 20 Raman spectra of a) water containing poly(vinyl pyrrolidone) and b) dry poly (vinyl pyrrolidone)

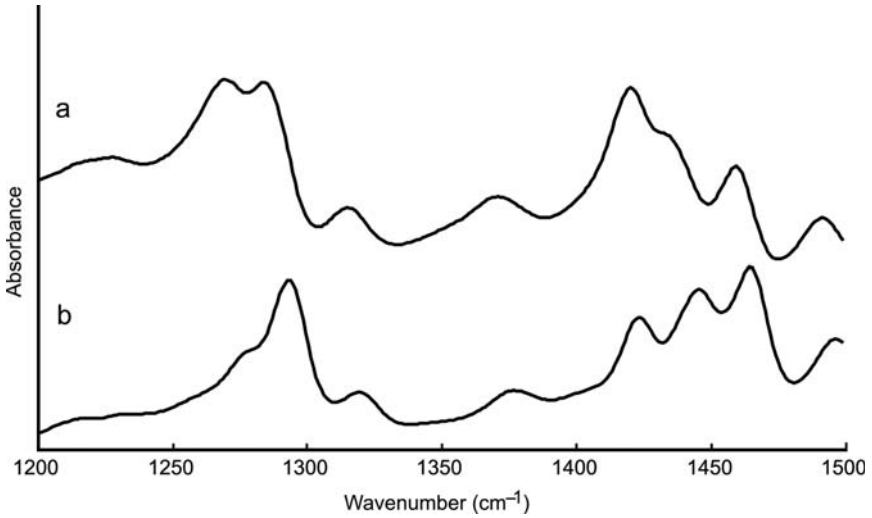

Fig. 21 ATR spectra of a) water containing poly(vinyl pyrrolidone) and b) dry poly(vinyl pyrrolidone)

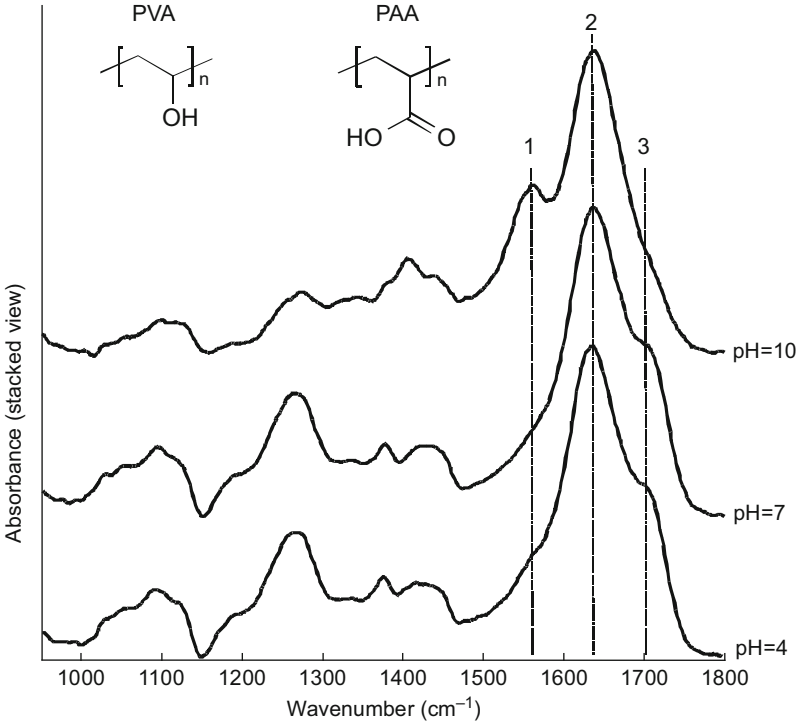

Fig. 22 ATR spectra of the poly(acrylic acid)/poly(vinyl alcohol) network at different pH values of the surrounding medium. 1: $\nu_{as}(C=O)$ mode of the COO^- group, 2: $\delta(OH)$ of water and 3: $\nu(C=O)$ of the COOH group

The ν(C = O) mode of the COOH group is to be seen as a shoulder on the H–O–H bending mode of water. As the pH value is increased the absorbance of this band gets smaller and at the same time the intensity of ν_{as}(C = O) mode of the COO^- group becomes stronger (Sorber et al. 2008).

3.1.7 FT-IR and Raman spectroscopic imaging

A recent milestone in vibrational spectroscopy was the development of high sensitive array detectors with a large number of small detector elements. Each detector element, also called as pixel, is capable of simultaneously collecting data and recording a two-dimensional spectroscopic image. Instruments of this type allow more complex hydrogel systems to be characterized and processes such as swelling and diffusion to be monitored. The spectroscopic images measured on such instruments show the spatial distribution of chemical information and increase the chances of identifying molecular process that have a high relevance to the behaviour of the hydrogel. Just as in conventional spectroscopy, FT-IR and Raman imaging spectroscopy are highly complementary. In addition, spectroscopic images can be available in few seconds and provide chemical information in real time.

FT-IR and Raman spectroscopic imaging techniques may employ three general approaches to obtain spatially resolved chemical information: mapping, imaging with a multi-element detector, and spatial encoding and decoding.

Mapping involves a point-by-point rastering across a sample and is, therefore, an inherently slow measurement. This single-detector-based technique uses an aperture to determine the spatial resolution. Since imaging is based on an array detector, spatially resolved spectra may be collected simultaneously. The imaging technique is not only faster than mapping but also produces spectroscopic images of superior quality with a spatial resolution close to the diffraction limit since the spatial resolution is determined by the size of the detector pixels rather than by an aperture. Spatial encoding divides a sample into a number of pixel regions. The spatial encoding is provided by a mask, which is often a digitally controlled mirror array. The mirror array masks the IR radiation that is passed to the sample. The signal reflected or transmitted from the sample is then focused onto a single-element detector. As the mask pattern provided by the mask changes, the output signal of the detector is monitored, and the spectroscopic signal of each of the pixel regions is resolved using a spatial decoding method.

In general, high-fidelity spectroscopic imaging can be performed most efficiently by array detectors. Raman spectroscopy is often used in the red and near-infrared spectral range so that highly sensitive silicon CCD detectors may be used. Multi-element IR detectors are fabricated from material that is sensitive in the spectral range from ca. 1 μm to over 10 μm (10,000-1,000 cm^{-1}). These IR-sensitive focal plane array (FPA) detectors, originally developed for military applications, became available for research and civil applications in the 90's (Bhargava and Levin 2005).

FT-IR and Raman Imaging Spectrometer

The coupling of a FPA detector to a common FT-IR spectrometer provides an imaging instrument. Microspectroscopic imaging needs an IR microscope attached to the spectrometer. In some instruments, visible light is used to allow the sample position to be observed visually or to choose a certain area for the spectroscopic imaging. In some contemporary instruments, the visible light is coupled into the IR beam path. Dichromatic mirrors ensure that exactly the same sample area that is observed in the visible light is imaged by the FPA detector. Samples which are not transparent in IR have to be investigated in the reflection mode. Using a typical Cassegrainian IR objective with a numerical aperture of 0.4, the image size captured with a 64x64 pixel IR detector is 270 x 270 μm. Larger sample areas can be investigated in the so-called macro chamber. The sample size for the same detector array is ca. 4 x 4 mm, giving a spatial resolution of 62 μm.

Like FT-IR spectroscopic imaging, Raman imaging is also based on conventional Raman spectroscopy. A laser is needed to excite the Raman scattering light. Three Raman imaging techniques are available. Point mapping is the sequential registration of a series of single Raman spectra measured from different positions on the sample, followed by the construction of the spectroscopic map. Point mapping requires the use of a computer-controlled motorized stage to move the sample and a microscope if high spatial resolution is needed. The second technique is line focus imaging. The sample is mapped by a series of lines. The Raman-scattered light is imaged through a slit system and captured by an array detector. Each spectrum corresponds to a particular position on the detector line. The line scan technique is faster than the point imaging and reduces the instantaneous power density of the laser on the sample. "True" Raman imaging technique is similar to the FT-IR imaging technique where spectroscopic image is captured with an array detector. The illumination of the sample determines the sample size and intensity of the Raman signals. The Raman scattered light from the sample is collected by an objective and passed through a Rayleigh-rejection filter before being detected by the CCD array. Each pixel of the array contains intensity data at a single wavelength.

The use of FT-IR spectroscopic imaging has been used in a number of different studies to characterize hydrogels. High contrast can be observed when the absorbance values of strong bands are plotted. Figure 23 shows FT-IR spectroscopic images of a PVME-PVP blend system. The images are composed of four individual FT-IR images. Each individual image was constructed from 64 x 64 (4,096) complete IR spectra. The upper image generated by the integrated absorbance of the $\nu(C=O)$ mode represents PVP. The contrast of the bottom image is based on the integrated absorbance of the ν(C–O–C) modes and indicates PVME (see Fig. 24). The images show the distribution of the two hydrogels and indicate domains in the blend.

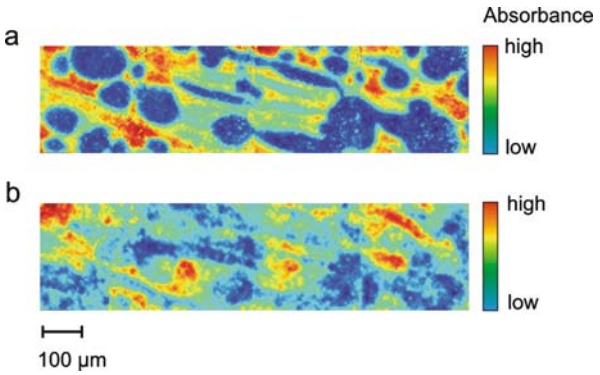

Fig. 23 FT-IR spectroscopic imaging of a poly(vinyl pyrrolidone) / poly(vinyl methyl ether) blend system. (a) Integrated absorbance in the spectral range between 1,500 and 1,720 cm^{-1}, (b) integrated absorbance in the spectral range between 1,050 and 1,150 cm^{-1}

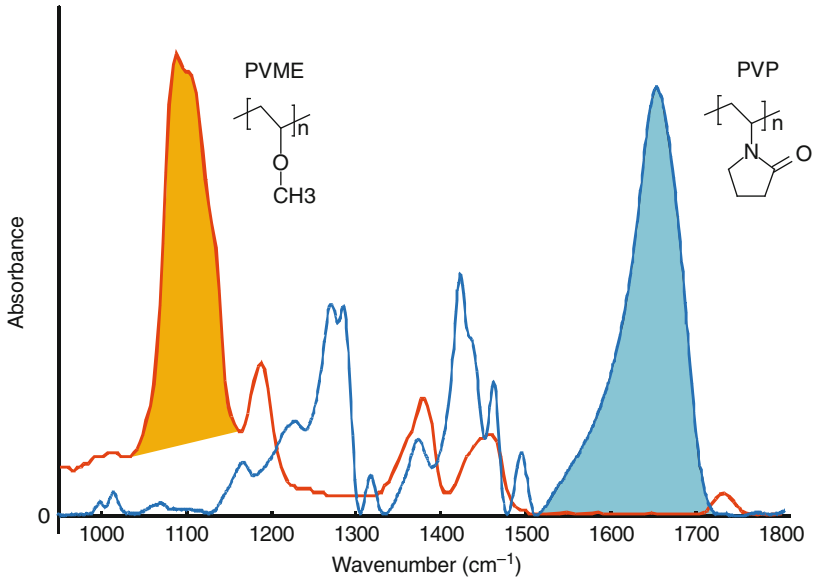

Fig. 24 IR spectra of poly(vinyl pyrrolidone) and poly(vinyl methyl ether). The gray areas indicate the spectral ranges which were used to calculate the contrast of the FT-IR spectroscopic images in Fig. 23

Enhanced Data Analysis and Imaging Evaluation

In order to transfer also small spectral variances into a molecular image that reflects the desired information, techniques for data and image evaluation have to be used. Chemometric imaging is the term that encompasses a wide range of mathematical

techniques for classifying data, pattern recognition and generating false color images. Most approaches for data and imaging evaluation involve multistage processes. A long list of different methods as well as combinations of different methods can be applied to spectroscopic imaging data sets. The best strategy for data and imaging evaluation is dependent on a variety of different factors, e.g., on the information that is wanted, the nature of the sample itself, and the experimental and environmental conditions. The path from the raw spectroscopic imaging data to a chemical image is divided in four main steps:

1. data preprocessing
2. selection of spectral features and classification
3. image processing including pattern recognition
4. highlighting the desired molecular information.

Preprocessing is crucial in order to obtain "correct" spectra. The aim of preprocessing is to remove artifacts and to reduce the large number of spectral features in order to make the available information more accessible.

Feature extraction is a general term for methods of constructing combinations of the variables to get around these problems while still describing the data with sufficient accuracy. The selection of spectral features is an important phase in chemometric imaging. The fundamental function of feature selection is to find a set of features that will represent the wanted molecular information in the optimal way at high specificity. Information that is either redundant or irrelevant to the following classification task is removed from the data set. The first goal of feature selection is to simplify the amount of resources required to describe a large set of data accurately. When performing analysis of complex data one of the major problems is based on the number of variables involved. Analysis with a large number of variables generally requires a large amount of memory and computation power. Therefore, the dimension of the selected spectral feature is usually much smaller than the dimension of the original data set so that the computation time and the memory requirements are greatly reduced. The second goal is to provide an indication about the discriminatory potential of the features. Thus, feature selection is also used as a tool to determine whether it is necessary to find after additional features that would allow the improvement of the performance of the classier. Finally, feature selection is also used as tool to reduce the noise level. Common approaches for feature selection involve principal components analysis (PCA), partial least squares regression (PLS), and the use of wavelets. Several other approaches such as partitioning the original spectra into smaller subspaces by using a recursive algorithm or an emerging of certain bands have also been used.

PCA is a mathematical transformation that transforms the spectral data to a new coordinate system such that the greatest variance by any projection of the data comes to lie on the first coordinate, which is called the first principal component, the second greatest variance on the second coordinate, and so on. Retaining those characteristics of the spectra that contribute most to its variance by keeping the

corresponding principal components reduces the dimension of the data set. Usually, higher-order principal components represent the basic characteristics while lower order ones contain more detailed information. PLS is similar to PCA, but instead of finding the maximum variance, PLS calculates a linear model describing some predicted variables in terms of other observable variables. It is often used to find the fundamental relations between two matrices. A PLS model will try to find the multidimensional direction in one spectral region that explains the maximum multidimensional variance direction in the other one, which leads to a reduction of the data set.

Wavelets and the wavelet transformation refer the representation of a spectral data set in terms of a finite spectral range or a rapidly decaying oscillating waveform. This waveform is scaled and translated to match the original spectrum. Wavelet transformation may be considered to calculate the time-frequency representation, related to the subject of harmonic analysis. The projection of a spectrum on a single wavelet or a series of wavelets reduces the dimensionality of the data set. Wavelet transforms are broadly divided into three classes, the continuous wavelet transform, the discrete wavelet transform and multiresolution-based wavelet transforms. Each class has advantages and disadvantages in terms of the wanted information.

Spectral classification is a procedure in which individual spectra are placed into groups based on spectral quantitative information. The algorithms can be divided into a supervised and unsupervised classification. Supervised classification is based on a training set of previously classified spectra. In unsupervised classification a spectral data set of input objects is gathered for which there is no a priori information about the spectra and typically treats with the input data as a set of random variables. While there are many methods for classification, they are all oriented towards solving the basic problem of partitioning the spectra or the pre-selected spectral features into classes and assigning a label to each class. There are a widespread set of classification algorithms. One group of classification algorithms do not yield confidence or class probabilities. In another group, unsupervised classifications are first applied, after which an attempt to label each of the classes is made. Several algorithms estimate the class-conditional probabilities and then compute the class probability. Examples of classification algorithms, which are often used in spectroscopic image analysis, are Linear Discriminant Analysis (LDA), Cluster Analysis (CA), Artificial Neural Network (ANN), and Factor Analysis (FA) (Bhargava and Levin 2005).

3.2 NMR Imaging

3.2.1 Application on Network Characterization

An important application of nuclear magnetic resonance (NMR) spectroscopy is its use in imaging the interior of solids. NMR imaging has proven to be the most

powerful technique for obtaining information on soft tissues. The similarity of soft tissues and hydrogels gives the motivation for an application of the technique to swollen polymer networks.

It can be distinguished between two groups of experiments which are used in polymer network characterization:

- NMR imaging can visualize the spatial distribution of a solvent in a polymer gel. For instance, information on the homogeneity of a gel is possible due to the strong correlation between the cross-linking density and the degree of swelling.
- The transport of a swelling agent during swelling/shrinking or the diffusion of substances into a swollen gel can be followed in real time by time-resolved measurements. The method provides information about the nature of diffusion processes into a polymer matrix on a spatially resolved level with a lateral resolution of about 50. . .100 μm.

In principle, we can measure a one- or more-dimensional image of the concentration and the mobility of the solvent molecules in a polymeric sample. On the other hand, NMR imaging monitors changes in properties of the polymeric chain, e.g., originated from the swelling/shrinking processes, time-resolved at different sample positions.

The aim of an investigation determines the method to obtain contrast[14] in NMR. Let us consider the case of evaluating the distribution of cross-linking density inside a network. By classical mechanical measurements, e.g., compression or stress-strain experiments, we can calculate a cross-linking density, which represents a mean value over the sample volume we used in measurements. NMR enables the characterization on a microscopic level if we can investigate the properties of network chains at different sample positions.

In network characterization, there are three origins for the contrast in NMR images:

- Contrast in the NMR measurement arises from the solvent concentration: In the equilibrium state of swelling, the degree of swelling depends on the cross-linking density, respectively the molecular weight of the network chains (power law $Q \sim M_c^a$ with $a = 3/5$ or 3/8 depending on solvent quality, see Sect. 1.4). This enables us to measure the distribution of cross-linking density inside the gel, at least in a qualitative manner.
- Contrast arises from polymer matrix: The mobility of the net-chains depends on the concentration of a solvent due to the softening influence of the solvent. It is possible to monitor the changes of mobility of the net-chains during a transport process. For responsive polymers, it is also possible to monitor the drastic change in mobility during the volume phase transition, e.g., induced by heating.

[14] Contrast means a difference in NMR signals which enables us to identify and to observe a defined species in an ensemble of other species.

- Contrast arises from an additional component (e.g., organic solvent): This enables us to monitor the transport of this species into a swollen gel or to determine diffusion coefficients of this component inside the gel.

Although NMR imaging gives a lot of information on a microscopic level, some experimental difficulties have prevented a routine application of the method until now. Nevertheless, the method of NMR imaging has achieved some considerably success in the last decades (Callaghan 1991; Blümich 2000; Blümlich and Casanova 2006).

3.2.2 Principle of NMR Imaging

The basic principle of NMR imaging was firstly introduced by Lauterbur in (Lauterbur 1973). The spatial resolution is obtained by a magnetic field gradient. A static magnetic field B_0 is superimposed by a magnetic field gradient G. The frequency ω is shifted and the spatial coordinate (voxel) corresponds to the resonance frequency of the signal:

$$\omega = \gamma (B_0 + G), \tag{67}$$

where ω is the resonance frequency of the signal and γ the gyro-magnetic ratio (e.g., of protons). In this way, the resonance frequency of a given spin (Larmor frequency), depends not only on the identity of the spin but also on the local magnetic field. The latter is determined by the location of the spin relatively to the poles of the magnet.

Typically, a NMR measurement consists of two steps. At first the contrast, in dependence on the effect under investigation, is prepared. In a second step, the frequency axis is converted into a space axis by applying of the gradient field in direction of the desired profile. For a three-dimensional image, this has to be done in each local direction x, y, and z (y and z analogous):

$$\omega_x = \gamma (B_0 + G_x), \tag{68}$$

where ω_x denotes the resonance frequency at place x.

The spatial resolution Δx depends on the power of the gradient field and on the width of the NMR resonance line $\Delta\omega$ (in polymer gels typically 0.1 . . . 2 kHz, for solvent molecules only a few Hz). For a gradient power of 500 mT/m it follows a spatial resolution in gels of about 50 µm.

To obtain information about the polymer, a material parameter imaging is used. Different properties can be utilized to provide image contrast without adding other substances. Such properties include the relaxation times T_1 (relaxation time of longitudinal magnetization decay, spin-lattice relaxation) and T_2 (relaxation time of transversal magnetization decay, spin-spin relaxation), as well as the chemical shift. Frequently, the decay of magnetization is measured. For liquids, a simple

exponential decay is observed and T_2 can be calculated. For more solid-like materials like polymers or gels, the decay is non-exponential. A multi-component fit is necessary, which gives more information on the polymer matrix than a one-exponential fit. The shorter values of T_2 reflect the solid-like, the longer T_2-values the liquid-like nature of the polymer networks. Often, a non-exponential part at the beginning of the relaxation curve can be observed. This provides information on the material, like anisotropy of molecular motion, which can measure the cross-linking density (Knörgen et al. 1999). For experimental details of the method see (Sotta et al. 1996).

3.2.3 Examples

NMR imaging can be applied for different problems of network characterization. The following experiments were done with a VARIAN unity 200 MHz (wide bore) equipped with a homemade imaging probe of following specifications: active-shielded design, maximum gradient 5 mT/cm; RF part: resonance frequency 67 MHz (deuterium), 200 MHz (protons); saddle coil or solenoid with different inner diameter (5 mm, 7 mm, and for deuterium coil: 26 mm); temperature control between 0 °C and 120 °C.

Monitoring of Transport Processes

Cylindrical samples of a water-swellable polymer were immersed in water for different times. The profile of the water front moving from the surface to the inner core of the sample is visualized (Ghi et al. 1997) and compared with model calculations of the water transport. The Fickian nature of the diffusion process is proved. As a result of stress formation during the diffusion processes, cracks were formed. From analysis of T_2 the presence of two types of water within the polymer follows: a less mobile phase of water that is interacting strongly with the polymer matrix and a more mobile phase within the cracks.

Proton NMR imaging was used to study the volume phase transition in a thermo-responsive hydrogel (Ganapathy et al. 2000). The thermally induced volume phase transition was clearly seen in the proton image. The shrinking of a polyelectrolyte gel under the application of an electrical DC field was observed in real time (Hotta and Ando 2002).

Transport Processes for Drug Release

The NMR imaging method is also applied on monitoring transport processes for drug release. Cellulose derivates are often used as polymer matrix in pharmaceutics. The concentration profile of polymer across a swollen tablet is measured with NMR imaging as a function of swelling time (Baumgartner et al. 2005). The

processes during swelling and the swell kinetics of a dry hydrogel with high glass transition temperature were briefly discussed in Sect. 2.1. Time- and spatially-resolved analysis of the water uptake of a polyelectrolyte gel at pH = 7 showed the existence of a rigid core which constrains and retards the swelling. The swelling was described as a two-stage process. In the first stage swelling takes place in the outer zone of the gel. The swelling front moves towards the inner core. In a second stage, the swelling accelerates. On macroscopic level, a sigmoidal swelling curve is observed (Prior-Cabanillas et al. 2007).

Volume Phase Transition of a Temperature Sensitive Hydrogel

For the example of PNIPAAm, we have demonstrated the two step process of volume phase transition induced by heating of the swollen gel. Figure 25 shows the cross-sections of cylindrical gel samples swollen in D_2O at different times. The contrast results of the mobility of the net-chains. If the temperature of the volume phase transition will be exceeded the signals diminish. The net-chains are almost immobile. On a macroscopic level, the modulus increases, but the degree of swelling is not altered. The network is not in equilibrium. It begins to shrink with a typical time constant as discussed in Sect. 2.3. These findings are in accordance with the two-step model in Sect. 2.4.

Diffusion of Small Molecules into a Swollen Hydrogel

The diffusion of a low-molecular- weight compound into a network is of great importance for the application of hydrogels, e.g., as drug release system or as sensor material. The volume phase transition can be induced by a change of the composition of the swelling agent at constant temperature. Figure 26 shows a

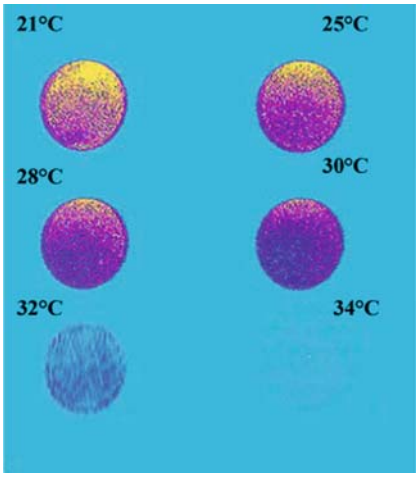

Fig. 25 2D-^{1}H-Fourier images of *T*-sensitive PNIPAAm-gel swollen in D_2O at different temperatures. The contrast arises from the protons of the polymer matrix (T_2-weighted). To seen are cross-sections of cylindrical samples. The signal density reflects the mobility of the net-chains. Reproduced from (Arndt et al. 2006), Fig. 4, p.186, with kind permission of Springer Science and Business Media

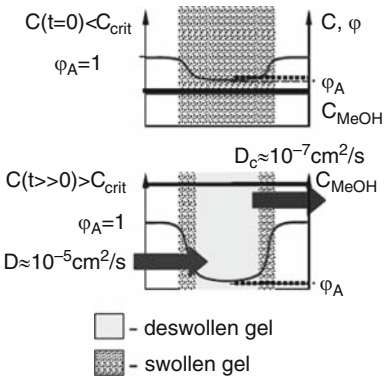

Fig. 26 Diffusion processes in hydrogels at volume phase transition. The phase transition is induced by diffusion of a low-molecular-weight compound (i.e., organic solvent into a water swollen gel); $D_c = D_{coop}$; φ_A volume fraction swelling agent; C_{MeOH} methanol concentration in the swelling agent

scheme of the diffusion processes at the volume phase transition. The diffusion coefficient of partially per-deuterated methanol (CH_3OD) into a water (D_2O)-swollen gel was determined by NMR measurements. The increase of magnetization inside the gel, here at a distance of $l = 4.8$ mm from the gel surface, is shown in Fig. 27. Assuming a Fickian diffusion of the methanol, the diffusion coefficient of methanol can be calculated from the measured time lag as 26 min by using (69).

$$D = l^2/(6t_{lag}) = \{23.04/(6 \times 60 \times 26)\}\text{mm}^2/\text{s} = 2.510^{-5}\text{cm}^2/\text{s}. \quad (69)$$

The self-diffusion coefficient of water was determined by the same method. The contrast arises from a small amount of H_2O added to D_2O. The self diffusion is not influenced by the swollen gel.

Figure 28 shows the transport of labelled water (D_2O) into a water-swollen gel. The swollen hydrogel is immersed into D_2O which diffuses into the gel. The pictures show the concentration of D_2O inside the gel in dependence on diffusion time. The intensity of the signals is proportional to their brightness (dark: no signal, what means only H_2O). With increasing time, the intensity changes due to the increase of D_2O concentration. Remarkable are the local differences of D_2O content. The network was synthesized with a high cross-linker concentration which yields to inhomogeneities which act as a kind of diffusion channels.

Distribution of Swelling Agent inside a Swollen Gel

NMR techniques enable us not only to understand transport processes, but also to visualize the distribution of components inside a gel. This is demonstrated for the two different gels in the collapsed state.

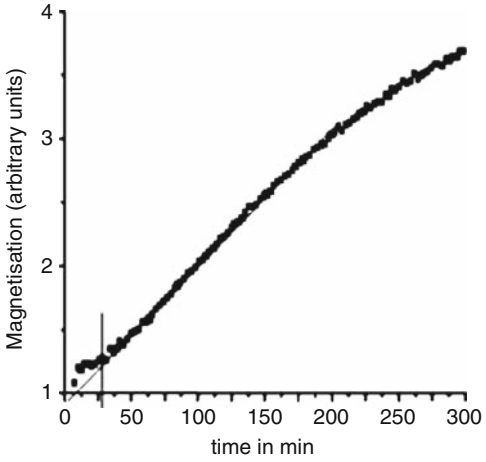

Fig. 27 Determination of the diffusion coefficient of partially per-deuterated methanol into a water (D_2O) swollen PNIPAAm gel at 21 °C. The increase of magnetisation of a thin sample layer (thickness about 100 µm) is measured. The layer is located at a distance of 4.8 mm from the sample surface

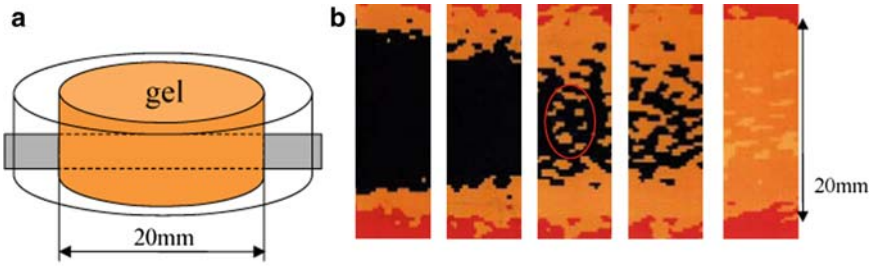

Fig. 28 D_2O diffusion into a water swollen PNIPAAm gel immersed into D_2O: (a) Geometry of the experimental set-up: The grey bar indicates the area investigated. (b) Deuterium flash imaging of the 5 mm thin vertical layer at 20 °C marked on a) (from left: time after immersion into D_2O: 2 min, 82 min, 162 min, 212 min, 24 h). The gel was cross-linked with a high cross-linker concentration and, therefore, inhomogeneous. The inhomogeneity in cross-linking density and in degree of swelling is visualized by differences in the D_2O-signals (black: no signal). Reproduced from (Arndt et al. 2006), Fig. 6, p.187, with kind permission of Springer Science and Business Media

The water (D_2O)-swollen gels were immersed into a mixture of D_2O and CH_3OD with a methanol content of 40 vol-%. The volume phase transition under isothermal conditions occurs at a content of about 20 vol-% methanol in the swelling agent. If the condition of volume phase transition is fulfilled, the network chains collapse. A dense layer is formed on the gel surface (skin effect) by the collapsed chains. As seen in Fig. 29a, in case of a homogeneous gel, this layer is very thin affecting the swelling/deswelling processes only very slightly.

In case of a porous gel, the collapsed network chains form a thicker layer. It acts as a barrier and prevents shrinking processes. The shrinkage barrier separates the inner swollen part of the gel from the outer part. The shown distribution of solvent inside the sponge-like gel was measured three days after immersion it into water/methanol.

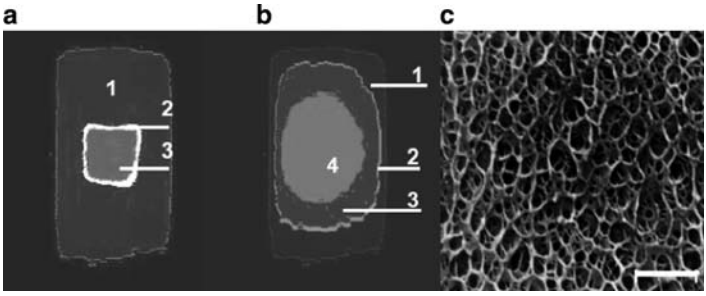

Fig. 29 Distribution of water inside a collapsed PNIPAAm gel. The volume phase transition was induced by per-deuterated methanol. The figures show Fourier images (slice selection, T_2-weighted) of a vertical plane of PNIPAAm swollen in D_2O. Distribution of water inside (a) a homogeneous gel and (b) a sponge-like gel. (c) Structure of the sponge-like gel (FESEM micrograph), scale bar: 250 nm. 1 D_2O/CH_3OD environment; 2 collapsed skin; 3 shrunken gel (shrinkage barrier); 4 swollen gel. Reproduced from (Arndt et al. 2006), Fig. 7, p.188, with kind permission of Springer Science and Business Media

The skin and shrinkage barrier formation is a time-distance problem of different diffusion processes taking place simultaneously. It can also be observed if the volume phase is induced by heating. The diffusion coefficient of a low molecular weight species is fast in comparison to the cooperative diffusion of the network; see Sect. 2.4. The time of the swelling/deswelling process depends on the square of the characteristic dimension of the gel. For a sponge-like gel, this dimension is small and, therefore, the response to a change in environmental condition is fast. Thus, the shrinking process is faster in comparison with the diffusion of the low-molecular-weight component.

The skin effect influences the behaviour of smart hydrogels. Inducing the volume phase transition by the high concentration of a hydrophobic component or high temperature strengthens the effect.

Acknowledgments The author thanks M. Knörgen (Martin-Luther-Universität Halle) for the fruitful cooperation on application of NMR imaging on smart hydrogels, and R. Reichelt (Westfälische Universität Münster) for the FESEM micrograph.

References

Alfrey T Jr, Gurnee EF, Lloyd WG (1966) Diffusion in glassy polymers. J Polym Sci C (Polymer Symp) 12:249–261

Arndt K-F, Richter A, Ludwig S, Zimmermann J, Kressler J, Kuckling D, Adler H-J (1999) Poly (vinyl alcohol)/poly(acrylic acid) hydrogels: FT-IR spectroscopic characterization of cross-linking reaction and work at transition point. Acta Polym 50:383–390

Arndt K-F, Schmidt T, Menge H (2001) Poly(vinyl methyl ether) hydrogel formed by high energy irradiation. Macromol Symp 164:313–322

Arndt K-F, Knoergen M, Richter S, Schmidt T (2006) NMR Imaging: monitoring of swelling of environmental sensitive hydrogels. In: Webb GA (ed) Modern Magnetic Resonance, Part 1. Springer, Dordrecht

Bajpai SK, Bajpai M, Sharma L (2007) Inverse suspension polymerization of poly(methacrylic acid-co-partially neutralized acrylic acid) superabsorbent hydrogels: synthesis and water uptake behavior. Desig Monom Polym 10:181–192

Baumgartner S, Lahajnar G, Sepe A, Kristl J (2005) Quantitative evaluation of polymer concentration profile during swelling of hydrophilic matrix tablets using ^{1}H NMR and MRI methods. Europ J of Pharmaceutics and Biopharmaceutics 59:299–306

Bhargava R, Levin IW (2005) Spectrochemical analysis using Infrared multichannel detectors. Blackwell, Oxford

Blümlich B (2000) NMR Imaging of Materials. Oxford University press, Oxford

Blümlich B, Casanova F (2006) Mobile NMR. In: Webb GA (ed) Modern Magnetic Resonance. Part 1. Springer, Dordrecht

Borchard W, Steinbrecht U (1991) Colloid Polym Sci 269:95

Callaghan PT (1991) Principles of Nuclear Magnetic Resonance microscopy. Oxford University Press, Oxford

Chiarelli P, Domenica C, Genuini G (1993) Crazing dynamics in the swelling of thermally cross-linked poly(vinyl alcohol)–poly(acrylic acid) films. J Material Sci: Materials in Medicine 4:5–11

da Costa A, Amado AM (2001) Cation hydration in hydrogel polyacrylamide-phosphoric acid network: a study by Raman spectroscopy. Solid State Ionics 145:79–84

Dong LC, Hoffman AS (1990) Synthesis and application of thermally-reversible heterogels for drug delivery. J Controlled Release 13:21–31

Dušek K, Patterson D (1968) Transition on swollen polymer networks induced by intramolecular condensation. J Polym Sci A-2(6):1209–1216

Eckert F (2003) Bestimmung der kooperativen Diffusionskoeffizienten von Poly (acrylsäure)-Netzwerken. Diploma thesis, TU Dresden.

Erman B, Flory PJ (1978) Theory of elasticity of polymer networks.II. The effect of geometric constraints on junctions. J Chem Phys 68:5363–5369

Ferraro JR, Nakamoto K (1994) Introductory Raman spectroscopy. Academic Press, San Diego

Flory PJ (1942) Thermodynamics of high-polymer solutions. J Chem Phys 10:51–61

Flory PJ (1944) Network structure and the elastic properties of vulcanized rubber. Chem Rev 35:51–75

Flory PJ (1953) Principles of Polymer Chemistry. Cornell University Press, Ithaca NY

Flory PJ (1976) Statistical thermodynamics of random networks. Proc Royal Soc London A 351 (1666):351–380

Flory PJ (1977a) Theory of elasticity of polymer networks. The effect of local constraints on junctions. J Chem Phys 66:5720–5729

Flory PJ (1977b) The molecular theory of rubber elasticity. Contemp Top Polym Sci 2:1–18

Flory PJ, Rehner J Jr (1943a) Statistical mechanics of cross-linked polymer networks. I. Rubber-like elasticity. J Chem Phys 11:512–520

Flory PJ, Rehner J Jr (1943b) Statistical mechanics of cross-linked polymer networks. II. Swelling. J Chem Phys 11:521–526

Freundlich H (1932) Kapillarchemie, Vol 2. Akad Verlagsges mbH, Leipzig, p 567

Ganapathy S, Rajamohanan PR, Badiger MV, Mandhare AB, Mashelkar RA (2000) Proton magnetic resonance imaging in hydrogels: volume phase transition in poly(*N*-isopropylacrylamid. Polymer 41:4543–4547

Garton A (1992) Infrared Spectroscopy of polymer blends, composites and surfaces. Hanser, Munich

Gehrke SH (1993) Synthesis, equilibrium swelling, kinetics, permeability and applications of environmentally responsive gels. Adv Polym Sci 110:81–144

George KA, Wentrop-Byrne E, Hill DJT, Whittaker AK (2004) Investigation into the diffusion of water into HEMA-co-MOEP hydrogels. Biomacromolecules 5:1194–1199

Ghi PY, Hill DJ, Maillet D, Whittaker AK (1997a) N.m.r. imaging of the diffusion of water into poly(tetrahydrofufuryl methacrylate-co-hydroxyethylmethacrylate). Polymer 38:3985–3989

Gotoh T, Nakatani Y, Sakohara S (1998) Novel synthesis of thermosensitive porous hydrogels. J Pol Sci 69:895–906
Griffiths PR, de Haseth JA (2007) Fourier Transform Infrared Spectroscopy. Wiley, Hoboken
Günzler H, Gremlich HU (2002) IR Spectroscopy. Wiley-VCH, Weinheim
Guo Y, Peng Y, Wu P (2008) A two-dimensional correlation ATR-FTIR study of poly(vinyl methyl ether) water solution. J Molec Structure 87:486–492
Hermans JJ (1947) Deformation and swelling of polymer networks containing comparatively long chains. Trans Faraday Soc 43:591–600
Hirotsu S (1991) Softening of bulk modulus and negative Poisson's ratio near the volume phase transition of polymer gels. J Chem Phys 94:3949–3957
Hirotsu S, Hirokawa Y, Tanaka T (1987) Volume-phase transitions of ionized N-isopropylacrylamide gels. J Chem Phys 87:1392–1395
Hotta Y, Ando I (2002) A study of shrinkage process of a polymer gel under electric field by ^{1}H NMR imaging method using an NMR cell with thin platinum electrodes. J Molec Structure 602–603:165–170
Huggins ML (1941) Solutions of long-chain compounds. J Chem Phys 9:440
Huggins ML (1943) Thermodynamic properties of solutions of high polymers. The empirical constant in the activity equation. Ann N Y Acad Sci. 44:431–443
James HM, Guth E (1943) Theory of the elastic properties of rubber. J Chem Soc 11:455–481
Knörgen M, Heuert U, Schneider H, Heinrich G (1999) NMR relaxation and NMR imaging of elastomers in the course of thermal aging. J Macromol Sci Phys B38:1009–1022
Knörgen M, Arndt K-F, Richter S, Kuckling D, Schneider H (2000) Investigation of swelling and diffusion in polymers by ^{1}H NMR imaging: LCP networks and hydrogels. J Molec Struc 554:69–79
Kuckling D, Adler H-J P, Arndt K-F (2003) Poly(N-isopropylacrylamide) copolymers: hydrogel formation via photocrosslinkling. In: Bohidar HB, Dubin P, Osada Y (eds) Polymer Gels: fundamentals and applications, ACS Symp Ser 833. ACS, Washington
Kwak S, Lafleur M (2003) Raman spectroscopy as a tool for measuring mutual-diffusion coefficients in hydrogels. Appl Spectroscopy 57:768–773
Lauterbur PC (1973) Image formation by induced local interactions. Examples employing nuclear magnetic resonance. Nature 242:190–191
Li Y, Tanaka T (1990) Kinetics of swelling and shrinking of gels. J Chem Phys 92:1365–1371
Maeda Y (2001) IR spectroscopic study on the hydration and the phase transition of poly(vinyl methyl ether) in water. Langmuir 17:1737–1742
Maeda Y, Mochiduki H, Yamamoto H, Nishimura Y, Ikeda I (2003) Effects of ions on two-step phase separation of poly(vinyl methyl ether) in water as studied by IR and Raman spectroscopy. Langmuir 19:10357–10360
Mark JE (1982) The use of model polymer networks to elucidate molecular aspects of rubberlike elasticity. Adv Polymer Sci 44:1–26
Onuki A (1993) Theory of phase transition in polymer gels. Adv Polymer Sci 109:63–121
Pelton R (2000) Temperature-sensitive aqueous microgels. Adv Colloid Interface Sci 85:1–33
Prior-Cabanillas A, Barrales-Rienda J, Frutos G, Quijada-Garrido I (2007) Swelling behaviour of hydrogels from methacrylic acid and poly(ethylene glycol) side chains by magnetic resonance imaging. Polym Int 56:506–511
Raasmark PJ, Andersson M, Lindgren J, Elvingson C (2005) Differences in binding of a cationic surfactant to cross-linked sodium poly(acrylate) and sodium poly(styrene sulfonate) studied by Raman spectroscopy. Langmuir 21:2761–2765
Richter S (2006) Contributions to the dynamical behavior of cross-linked and cross-linking systems: stimulus-sensitive microgels and hydrogels, reversible and irreversible gelation processes. Habilitation thesis, TU Dresden
Sahoo P, Rana P, Swain S (2006) Interpenetrating polymer network PVA/PAA hydrogels. Intern J of Polym Mater 55:65–78

Saiano F, Pitarresi G, Mandracchia D, Giammona G (2005) Bioadhesive properties of a polyaminoacidic hydrogel: Evaluation by ATR FT-IR spectroscopy. Macromol Bioscience 5: 653–661

Saito S, Konno M, Inomata H (1993) Volume phase transition of N-alkylacrylamide gels. Advanced Polymer Sci. 109:207–232

Schmidt T, Querner C, Arndt K-F (2003) Characterization methods for radiation cross-linked poly (vinyl methyl ether) hydrogels. Nucl Instr and Meth in Phys Res B 208:331–335

Shibayama M (1998) Spatial inhomogeneity and dynamic fluctuations of polymer gels. Macromol Chem Phys 199:1–30

Shibayama M (2006) Universality and specificity of polymer gels viewed by scattering methods. Bull Chem Soc Jpn 79:1799–1819

Shibayama M, Norisuye T (2002) Gel formation analyses by dynamic light scattering. Bull Chem Soc Jpn 75:641–659

Shibayama M, Morimoto M, Nomura S (1994) Phase separation induced mechanical transition of poly(N-isopropylacrylamide)/water isochore gels. Macromolecules 27:5060–5066

Smith AL (1979) Applied Infrared spectroscopy. Wiley, New York

Smith BC (1996) Fundamentals of Fourier Transform Infrared spectroscopy. CRC, New York

Smith BC (1999) Infrared Spectral Interpretation. CRC, London

Socrates G (2006) Infrared and Raman characteristic group frequencies. Wiley, West Sussex

Sorber J, Steiner G, Schulz V, Guenther M, Gerlach G, Salzer R, Arndt K-F (2008) Hydrogel-based piezoresistive pH sensors: investigations using FT- IR attenuated total reflection spectroscopic imaging. Anal Chem 80:2957–2962

Sotta P, Fülber C, Demco DE, Blümlich B, Spiess HW (1996) Effect of residual dipolar interactions on the NMR relaxation in cross-linked elastomers. Macromolecules 29:6222–6230

Suzuki M, Hirasa O (1993) An approach to artificial muscle using polymer gels formed by microphase separation. Adv Polym Sci 110:241–261

Tanaka T, Fillmore DJ (1979) Kinetics of swelling of gels. J Chem Phys 70:1214–1218

Tanaka T, Hocker LO, Benedek GB (1973) Spectrum of light scattered from a viscoelastic gel. J Chem Phys 59:5151–5159

Wall FT (1942) Statistical thermodynamics of rubber. J Chem Phys 10:132–134

Wall FT (1943) Statistical thermodynamics of rubber. III. J Chem Phys 11:527–530

Wall FT (1951) Statistical thermodynamics of rubber elasticity. J Chem Phys 19:1435–1439

Yan Q, Hoffman AS (1995) Synthesis of macroporous hydrogels with rapid swelling and deswelling properties for delivery of macromolecules. Polymer 36:887–889

Yoshida R, Uccida K, Kaneko Y, Sakai K, Kikuchi A, Sakurai Y, Okano T (1995) Comb-type grafted hydrogels with rapid deswelling response to temperature changes. Nature 374:240–242

Zerbi G (1999) Modern Polymer Spectroscopy. Wiley-VCH, Weinheim

Modelling and Simulation of the Chemo-Electro-Mechanical Behaviour

Thomas Wallmersperger

Abstract Ionic polymer gels are attractive actuation materials with a great similarity to biological contractile tissues. They consist of a polymer network with bound charged groups and a liquid phase with mobile ions. Absorption and delivery of the solvent lead to a large change of volume. This swelling mechanism results from the equilibrium between different forces such as osmotic pressure forces, electrostatic forces and visco-elastic restoring forces and can be triggered by chemical (change of salt concentration or pH in the solution), thermal or electrical stimulation. In this chapter, an overview over different modelling alternatives for chemically and electrically stimulated electrolyte polymer gels in a solution bath are investigated. The modelling can be conducted on different scales in order to describe the various phenomena occurring in the gels. If only the global macroscopic behaviour is of interest, the statistical theory which can describe the global swelling ratio is sufficient. By refining the scale, the Theory of Porous Media (TPM) may be applied. This is a macroscopic continuum theory which is based on the theory of mixtures extended by the concept of volume fractions. By further refining, the mesoscopic coupled multi-field theory can be applied. Here, the chemical field is described by a convection-diffusion equation for the different mobile species. The electric field is obtained directly by solving the Poisson equation in the gel and solution domain. The mechanical field is formulated by the momentum equation. By investigating the structure on the micro scale, the Discrete Element (DE) method is predestined. In this model, the material is represented by distributed particles comprising a certain amount of mass; the particles interact mechanically with each other by a truss or beam network of massless elements. The mechanical behaviour, i.e. the dynamics of the system, is examined by solving the Newton's equations of motion while the chemical field, i.e. the ion movement inside the gel and from the gel to the

T. Wallmersperger
Institut für Statik und Dynamik der Luft- und Raumfahrtkonstruktionen, Universität Stuttgart, Stuttgart, Germany
e-mail: wallmers@isd.uni-stuttgart.de

G. Gerlach and K.-F. Arndt (eds.), *Hydrogel Sensors and Actuators*,
Springer Series on Chemical Sensors and Biosensors 6,
DOI: 10.1007/978-3-540-75645-3_4, © Springer-Verlag Berlin Heidelberg 2009

solution, is described by diffusion equations for the different mobile particles. All four formulations can give chemical, possibly electrical and mechanical unknowns and all rely on the assumption of the concentration differences between the different regions of the gel and between gel and solution forming the osmotic pressure difference, which is a main cause for the mechanical deformation of the polyelectrolyte gel film.

Keywords Ionic polymer gels • Modelling • Numerical simulation • Chemical stimulation • Electrical stimulation • Multi-field formulation • Finite elements • Discrete elements

Contents

Abbreviations

DE	Discrete Element
FE	Finite Element
FEM	Finite Element Method
TPM	Theory of Porous Media

Symbols

$\mathbf{b}$	Body force vector
c	Concentration
c^{fc}	Concentration of the fixed charges
$\mathbf{C}$	Elasticity tensor
D	Diffusion constant
d	Material-dependent swelling coefficient
$\mathbf{D}$	Dielectric displacement tensor

e	Specific energy
E	Elastic modulus, stiffness
$\mathbf{E}$	Electric field tensor
f	Friction coefficient
F	Faraday constant; $F = 96487$ C^{-}mol
F	Free energy
i	Current density
$\mathbf{I}$	Identity matrix
J_s	Jacobian of the solid
$\mathbf{K}$	Jacobian (matrix)
l	Liquid
l	Length
l_{gel}	Length of the gel
$\mathbf{L}$	Tensor of the deformation velocities
m	Mass
$m^{P\alpha}$	Production term of the rotational momentum
M	Moment
N	Number
N_b	Number of bound species
N_f	Number of free species
n_1	Molar number of the solvent
$\mathbf{p}^{P\alpha}$	Momentum production term
q	Swelling (ratio)
$\mathbf{q}$	Heat flow
r	Source term; Energy Supply due to external heat sources
R	Gas constant; $R = 8.3143$ J/mol/K
$\mathbf{R}$	Residual, Jacobian (vector)
s	Solid
s	Structural factor
t	Time
T	Temperature
$\mathbf{T}$	Stress tensor
$\mathbf{u}$	Displacement vector
$\mathbf{v}$	Velocity vector (of the mixture)
V	Volume
x	Spatial coordinate
x_i	Spatial coordinate, spatial direction
z_α	Valence of the species α
Δ	Difference
Δ	Laplace operator
∇	Divergence operator
α	Species α
β	Species β
ε_0	Permittivity of free charge; $\varepsilon_0 = 8.854\ 10^{-12}$ As/(Vm)
$\boldsymbol{\varepsilon}_r$	Dielectric constant

$\boldsymbol{\varepsilon}$	Strain tensor
$\bar{\boldsymbol{\varepsilon}}$	Prescribed strain (tensor)
ϕ	Volume fraction
φ_β	Volume fraction of the component β
φ	(rotation) Angle
γ^α	Constituent
ν^*	Material parameter
χ	Flory-Huggins interaction parameter
v_1	Molar volume of the solvent
π	Osmotic pressure
$\Delta\pi$	Differential osmotic pressure
μ	Mobility
ρ	Mass density
ρ^α	Partial density of the constituents γ^α
$\rho^{P\alpha}$	Mass (density) production term of the constituents γ^α
ρ_{el}	Volume charge density
$\boldsymbol{\sigma}$	Stress tensor
Θ	Moment of inertia
Ψ	Electric potential

Indices

0	Initial
1	Solvent
I	Node I
II	Node II
+	Positive, cation
−	Negative, anion
A	Anionic bound charges
B	Bound
el	Elastic
f	Free, mobile
fc	Fixed charge
g	Gel
i	Iteration number
Ion	Ion
M	Mixture, mixing
p	Polymer
P	Production
r	Relative
s	Solution
s	Salt
α	Counting index
β	Counting index

β Index of the component
$,i$ Spatial derivative $,i = \partial/\partial x_i$

1 Modelling on Different Scales

Polyelectrolyte gels are ductile-elastic materials. They consist of a polymer network with bound charged groups and a liquid phase with mobile ions (Fig. 1). By inducing different kinds of stimuli, such as change of temperature, pH-value or salt concentration in the solution (chemical stimulation) or by an applied electric field (electrical stimulation), a considerably large change of volume – by absorption or delivery of solvent – can be triggered (Fig. 2). Due to this capability, electrolyte polymer gels are designated as actuators for technical applications where large swelling and shrinkage is desired, such as for artificial muscles or other chemo-electro-mechanical actuators (Gülch et al. 2000; Chiarelli et al. 1992; Bar-Cohen 2001) (Chap. 5 and 6).

The swelling and bending behaviour of hydrogels results from the equilibrium of different forces: osmotic pressure forces, electrostatic forces, visco-elastic restoring forces, etc. To describe the different phenomena occurring in the gels and between the gel and solution phase adequately, the modelling can be performed on different scales (Fig. 3):

- If only the global macroscopic behaviour is of interest, the statistical theory is sufficient.
- To gain a more precise insight into the phenomena occurring in gels, the Theory of Porous Media (TPM), or the coupled chemo-electro-mechanical formulation is a good choice. Normally, the TPM is applied for the gel only, while the coupled multi-field formulation incorporates the gel and the surrounding solution.
- If the micromechanical behaviour and large deformations should also be taken into account, the Discrete Element formulation is predestined.

Note that a refinement of the modelling from macroscopic to microscopic always involves an increase of computational effort.

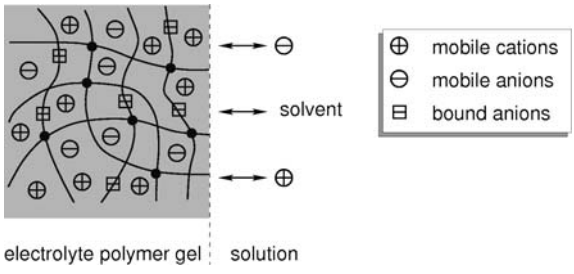

Fig. 1 Schematic of a polyelectrolyte gel in a solution bath

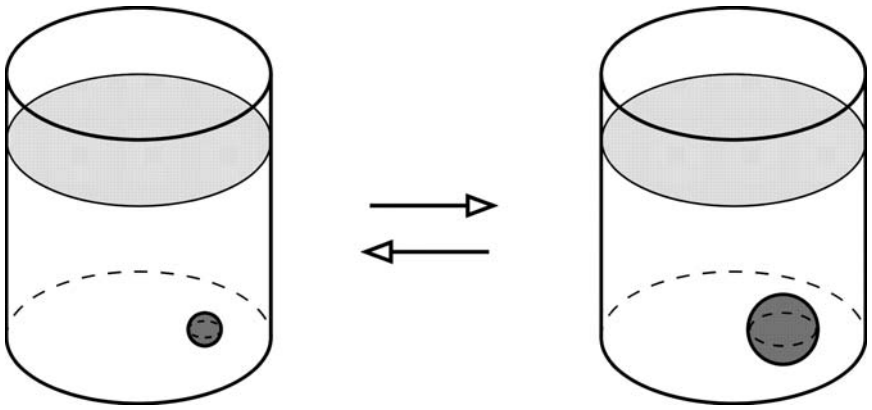

Fig. 2 Polymer gel in solution: (a) in collapsed and (b) in swollen state

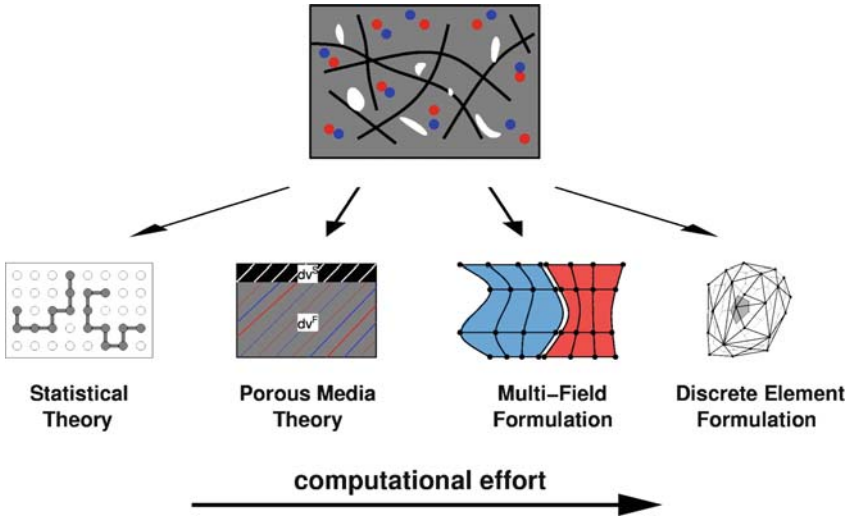

Fig. 3 Modelling on different scales

In the following sections the different formulations are introduced and compared.

1.1 Statistical Theory

In the 1940s, Flory and Rehner (Flory and Rehner 1943a, b; Flory 1953) were the first to formulate the theory of "swelling of network structures". Here the change of ambient conditions can be represented by a change of the Gibb's free energy ΔF (see also Chap. 3).

The total free energy is the sum of the:

- Free energy of mixing ΔF_M
- Free energy of elastic deformation ΔF_{el}
- Free energy of ion concentration differences ΔF_{ion} (see e.g. Rička and Tanaka (1984), Schröder and Oppermann (1996), etc.)

The equilibrium state is characterized by a minimum of the total free energy, i.e. the chemical potentials μ_1 of the solvent in the gel and in the solution phase are identical:

$$\Delta\mu_1 = \mu_1^{gel} - \mu_1^{sol} \stackrel{!}{=} 0$$

$$\begin{aligned}\Delta\mu_1 &= \left(\frac{\partial \Delta F_M}{\partial n_1}\right)_{p,T} + \left(\frac{\partial \Delta F_{el}}{\partial n_1}\right)_{p,T} + \left(\frac{\partial \Delta F_{ion}}{\partial n_1}\right)_{p,T} \\ &= \underbrace{\Delta\mu_{1,M}}_{\substack{\text{mixture}\\ \text{potential}}} + \underbrace{\Delta\mu_{1,el}}_{\substack{\text{elastic}\\ \text{potential}}} + \underbrace{\Delta\mu_{1,M}}_{\substack{\text{mobile ion}\\ \text{potential}}} = 0. \end{aligned} \tag{1}$$

Here n_1 is the molar number of the solvent. In the unswollen state of the gel, solvent and polymer matrix are completely separated. In the swollen state, the solvent has migrated into the gel phase, i.e. both polymer and solvent are in the gel part. The mixture potential $\Delta\mu_{1,M}$ reads

$$\Delta\mu_{1,M} = RT\left(\ln(1-\phi_p) + \phi_p + \chi\phi_p^2\right) \tag{2}$$

ϕ_p is the volume fraction of the polymer in the gel, χ is the Flory-Huggins gel-solution interaction parameter, R is the universal gas constant and T the temperature. The total swelling ratio q is given by the product of the initial swelling in the cross-linked (reference) state q_0 and the relative swelling according to the reference state q_r:

$$q = q_0\, q_r = \phi_p^{-1} \tag{3}$$

The (Gaussian) elastic potential may be given as

$$\Delta\mu_{1,el} = v^* RT\, v_1\, s\, q_0^{-1}\, q_r^{-1/3} \tag{4}$$

where v^* is the number (in mol) of elastically effective network chains per unit dry volume, s the structural factor and v_1 the molar volume of the solvent.

Note that the elastic potential can be formulated in different ways, see e.g. Flory and Rehner (1943b), or Treloar (1958) (see also Chap. 3).

The mobile ion potential depending on the concentration differences in both phases may be given as

$$\Delta\mu_{1,ion} = -RTv_1 \sum_{\alpha=1}^{N_f} \left(c_\alpha^{(g)} - c_\alpha^{(s)} \right) \tag{5}$$

$c_\alpha^{(g)}$ and $c_\alpha^{(s)}$ are the concentrations of the species α in gel (g) and solution (s), respectively, and N_f is the number of different the mobile species. Additionally, the ion distribution in both domains must satisfy the neutrality condition

$$\sum_{\alpha=1}^{N_f+N_b} \left(z_\alpha c_\alpha \right) = 0 \tag{6}$$

where z_α is the valence of the ions and N_b is the number of bound species.

In order to model also the dissociation effects, the concentrations of the bound groups and mobile ions are functions of space and time. For incorporating the hysteretic behaviour, refer to Günther et al. (2007) (see also Chap. 5).

The relationship between concentrations c_α and electric potential Ψ is given by the Donnan equation

$$\frac{c_\alpha^{(g)}}{c_\alpha^{(s)}} = \exp\left(- z_\alpha \frac{F}{RT} \left(\Psi^{(g)} - \Psi^{(s)} \right) \right) \tag{7}$$

where F is the Faraday constant. By eliminating the electric potential the relationship between different concentrations (of the species α and β) is obtained:

$$\left[\frac{c_\alpha^{(g)}}{c_\alpha^{(s)}} \right]^{-\frac{1}{z_\alpha}} = \left[\frac{c_\beta^{(g)}}{c_\beta^{(s)}} \right]^{-\frac{1}{z_\beta}} \tag{8}$$

Finally, the total swelling ratio is obtained by using (1) combined with (2)–(8). A typical plot of the swelling behaviour for different kinds of gels in a solution bath is depicted in Fig. 4 and schematically in Fig. 5. In Fig. 4, the equilibrium swelling ratio $q = V/V_0$ – where V is the actual volume of the gel immersed in solutions of different salt concentrations and V_0 represents the volume of the xerogel – of two gel cylinders of PAAm/PNa^+A^- and PAAm/PAA is plotted as a function of the outer KCl concentration.

This method only works for chemical stimulation where the ion concentration for each species α is independent of the local position in the gel.

If an electric field is applied, the concentrations are dependent on the local position in the gel. In this case, the gel has to be subdivided into various small

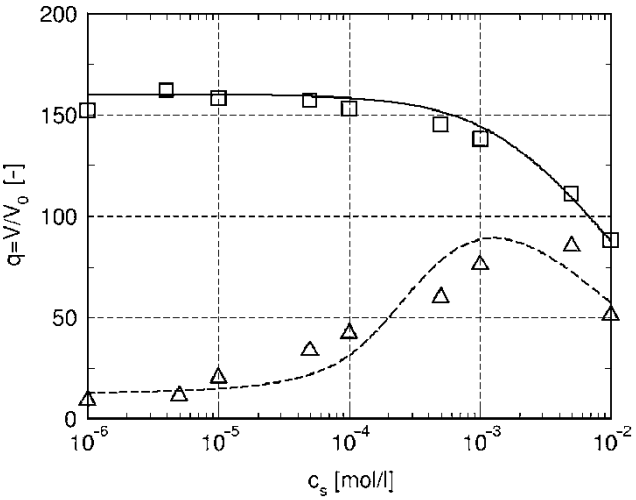

Fig. 4 Stationary swelling ratio $q=V/V_0$ of PAAm/PNa^+A^- gel (□) and of PAAm/PAA gel (Δ) as a function of the salt concentration c_s in the solution. The symbols represent measured values. The solid line shows the calculated values for completely dissociated fixed charges. The dashed line shows the curve for weak fixed charge groups

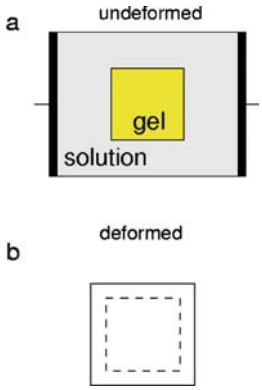

Fig. 5 Chemically stimulated polymer gel in a solution bath without electric field; (a) in undeformed state, (b) in deformed state

parts to realize different actual concentrations (Fig. 6c). By measuring the difference of the electric potential at variable positions in the gel by a microelectrode technique (Gülch et al. 2000), the concentrations required for the mobile ion potential can be determined by (7). Finally, locally different swelling ratios are obtained by using (1), see Fig. 6d. For more details please refer to Wallmersperger (2003).

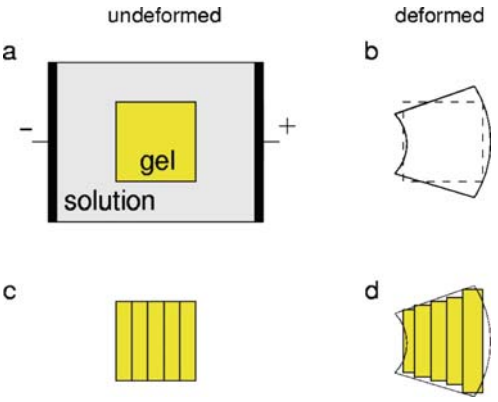

Fig. 6 Electrically stimulated polymer gel in a solution bath with applied electric field; (a) in undeformed state, (b) in deformed state, (c) sub-division of gel film in various portions for application of local statistical theory, (d) gel film portions with locally different swelling ratios

1.2 Porous Media Theory

The general Theory of Porous Media (TPM) is a macroscopic continuum theory which is based on the theory of mixtures extended by the concept of volume fractions. In this theory neither the local porous micro structure nor the actual geometrical distributions of all the constituents have to be known. The TPM is a homogenized model, i.e. all geometrical and physical quantities can be seen as statistical averages of the real quantities (Bowen 1980; Ehlers 2002).

In the two-phase theory only a mixture of the solid and the liquid phase exists. The (n+2)-phase theory comprises a system of n+2 constituents:

- The (solid) network (s)
- The electrolyte solution (f) consisting of
  - The liquid (l)
  - And n different species α

By assuming that the whole material is saturated, the saturation condition can be given as

$$\sum_{\beta = s, l, 1, \ldots, n} \varphi_\beta = 1 \tag{9}$$

where the volume fraction φ_β is given as

$$\varphi_\beta = \frac{V_\beta}{V} \tag{10}$$

V_β is the volume of the constituent and V the total volume.

If only one positive and one negative species are present, (9) simplifies to

$$\sum_{\beta = s, l, 1, \ldots, n} \varphi_\beta \;=\; \varphi_s \;+\; \underbrace{\varphi_l \;+\; \varphi^+ \;+\; \varphi^-}_{\varphi_f} \;=\; 1 \tag{11}$$

The governing equations for the extended porous media theory are the mechanical balance equations:

Mass balance for constituents:

$$\frac{\partial \rho^\alpha}{\partial t} \;+\; \operatorname{div}\left(\rho^\alpha \mathbf{v}^\alpha\right) \;=\; \rho^{P\alpha}; \quad \alpha \;=\; s,\; l,\; 1,\; \ldots,\; n \tag{12a}$$

Mass balance for mixture:

$$\frac{\partial \rho}{\partial t} \;+\; \operatorname{div}\left(\rho\, \mathbf{v}\right) \;=\; 0 \tag{12b}$$

Momentum balance:

$$\operatorname{div} \mathbf{T}^\alpha \;+\; \rho^\alpha \mathbf{b}^\alpha \;+\; \mathbf{p}^{P\alpha} \;=\; \mathbf{0}; \quad \alpha \;=\; s,\; l,\; 1,\; \ldots,\; n \tag{13a}$$

$$\operatorname{div} \mathbf{T} \;+\; \rho\, \mathbf{b} \;=\; \mathbf{0} \tag{13b}$$

Rotational momentum balance:

$$\mathbf{I} \times \mathbf{T}^\alpha \;+\; \mathbf{m}^{P\alpha} \;=\; \mathbf{0}; \quad \alpha \;=\; s,\; l,\; 1,\; \ldots,\; n \tag{14a}$$

$$\mathbf{I} \times \mathbf{T} \;=\; \mathbf{0} \tag{14b}$$

Energy balance:

$$\rho^\alpha \left(\frac{\partial e^\alpha}{\partial t} + \mathbf{v}^\alpha \operatorname{grad} e^\alpha\right) = \mathbf{T}^\alpha \mathbf{L}^\alpha - \operatorname{div} \mathbf{q}^\alpha + \rho^\alpha r^\alpha + e^{P\alpha}; \quad \alpha = s, l, 1, \ldots, n \tag{15a}$$

$$\rho \left(\frac{\partial e}{\partial t} \;+\; \mathbf{v} \operatorname{grad} e\right) \;=\; \mathbf{T}\,\mathbf{L} \;-\; \operatorname{div} \mathbf{q} \;+\; \rho\, r \tag{15b}$$

and the electro-chemical balance equations:

Electro-neutrality conditions:

$$\text{Gel: } z^{fc} c^{fc} + \sum_{\beta = 1, \ldots, n} z_\beta^{(g)} c_\beta^{(g)} = 0 \tag{16a}$$

$$\text{Solution: } \sum_{\beta = 1, \ldots, n} z_\beta^{(s)} c_\beta^{(s)} = 0 \tag{16b}$$

Continuity of bound charges:

$$c^{fc} = c_0^{fc} \frac{\varphi_0^l}{\varphi_0^l + J^s - 1} \tag{17}$$

Current flow:

$$\mathbf{i} = F \varphi^l \left(\sum_{\beta = 1, \ldots, n} z_\beta c_\beta \mathbf{v}_\beta + z^{fc} c^{fc} \mathbf{v}^{fc} \right) \tag{18}$$

ρ^α is the partial density for the constituents γ^α and ρ is the (mass) density of the mixture, i.e. of the whole system. $\rho^{P\alpha}$ is the mass production term of the constituents due to chemical reactions or phase changes. $\mathbf{v}^\alpha$ and $\mathbf{v}$ are the velocities of each constituent γ^α and of the whole mixture, respectively.

$\mathbf{T}$ is the stress tensor, $\mathbf{b}$ the vector of the body (volume) forces and $\mathbf{p}^{P\alpha}$ represents the exchange of the momentum as a kind of momentum production term.

$\mathbf{I}$ is the identity matrix and $m^{P\alpha}$ the production term of the rotational momentum.

$\mathbf{L}$ represents the tensor of the deformation velocities, $\mathbf{q}$ is the heat flow, r is the energy supply due to the external energy or heat sources, and e and $e^{P\alpha}$ are the specific internal energy and the specific internal energy production of the constituent γ^α, respectively.

c^{fc} is the concentration of the fixed charges, i.e. of the bound groups, z the valence of the ions, J the solid Jacobian, i is the current density and F the Faraday constant.

More details on these formulations can be found e.g. in Ehlers et al. (2002) and Kunz (2003).

The TPM is generally designated for the chemical stimulation and can provide local chemical as well as mechanical unknowns. In most cases, the gel phase only is investigated by prescribing the concentrations at the boundary of the gel (at the gel-solution interface) by using the Donnan Equation (7) together with the electro-neutrality condition of (6).

An actual research topic is to also capture the electrical stimulation. In this case the influence of the local change of the concentrations and the electric potential – in the solution phase – on the unknowns in the gel phase has to be considered. In Avci et al. (Avci 2008), the electro-neutrality condition is substituted by an equation for the electric potential. So the electric potential may be used as an additional degree of freedom.

1.3 Coupled Chemo-Electro-Mechanical Model

The coupled chemo-electro-mechanical multi-field formulation is a model on the micro-mesoscopic scale. It has been developed to gain a more precise insight into

the phenomena occurring in polyelectrolyte gels, i.e. ion movement, development of an inner electric field, etc. (Wallmersperger et al. 2001, 2004).

The ion concentrations and the electric potential inside these materials can be computed by the chemical and the electrical field equations. The local concentration differences form an osmotic pressure difference which results in a mechanical strain. Based on this, the swelling/bending of the polymer gel film may be obtained.

1.3.1 Chemical Field

The chemical field is described by the convection-diffusion equation for all the species α:

$$\dot{c}_\alpha = \nabla \cdot [D_\alpha \nabla c_\alpha + z_\alpha c_\alpha \mu_\alpha \nabla \Psi] - \nabla \cdot (c_\alpha \mathbf{v}) + r_\alpha \tag{19}$$

where c_α is the concentration of the species α, D_α the diffusion constant, $\mu_\alpha = \frac{F}{RT} D_\alpha$ the unsigned mobility, F the Faraday constant, Ψ the electric potential, and r_α the source term due to chemical conversion. i denotes the spatial direction x_i and the subscript ,i the spatial derivative $\partial/\partial x_i$.

Equation (19) consists of four contributing terms:

- The diffusive term resulting from concentration differences
- The migrative term due to differences in the electric potential
- The convective term due to an applied velocity of the solvent, and
- The source term due to chemical reactions

In the further research the last two terms stemming from the applied velocity of the solvent and from the chemical conversion have been neglected.

1.3.2 Electrical Field

The electrical field is described by the Poisson equation:

$$\Delta \Psi = -\frac{F}{\varepsilon_r \varepsilon_0} \sum_{\alpha}^{N_f + N_b} (z_\alpha c_\alpha) \tag{20}$$

where ε_0 is the permittivity of free space, ε_r the dielectric constant of the material, and N_b and N_f are the numbers of bound and mobile species.

The velocity of propagation of the electrical field is much higher than the one occurring in the chemo-electrical field, (19). Hence, the quasi-static form of the Poisson equation is adequate. Equation (20) results from the second and fourth Maxwell equations:

Gauss' Law for magnetism and Maxwell-Faraday equation:

$$\nabla \cdot \mathbf{B} = 0 \quad \text{and} \quad \nabla \times \mathbf{E} = -\frac{\partial \mathbf{B}}{\partial t} \tag{21a}$$

Helmholtz law:

$$\mathbf{E} \;=\; \nabla \Psi \tag{21b}$$

Gauss' law:

$$\nabla \cdot \mathbf{D} \;=\; \rho_{\mathrm{el}} \tag{21c}$$

where $\mathbf{D}$ is the tensor of the dielectric displacement, $\mathbf{E}$ the tensor of the electric field strength, and ρ_{el} the density of the volume charge.

Note that the whole domain (gel and solution) is solved together and thus no additional conditions prescribing the jump (e.g. obtained by the Donnan Eq. (7)) of the electric potential have to be given. In the regions outside the boundary layers, the neutrality condition of (6) is fulfilled, i.e. $\Delta\Psi \;\equiv\; 0$.

1.3.3 Mechanical Field

The mechanical field is formulated by the momentum equation. Due to the relatively slow swelling process, the influence of the inertia term is very small and the second order in time contribution can therefore be neglected. The momentum equation reads

$$f\,\dot{\mathbf{u}} \;=\; \nabla \cdot \boldsymbol{\sigma} \;+\; \rho\,\mathbf{b} \tag{22}$$

$\mathbf{u}$ is the displacement vector, $\boldsymbol{\sigma}$ the stress tensor, $\mathbf{C}$ the elasticity tensor, f the friction coefficient, $\mathbf{b}$ the body force vector, and ρ the mass density.

1.3.4 Coupling of the Involved Fields

The chemical field (19) and the electrical field (20) are directly coupled through the concentrations c_α and the electric potential Ψ.

The coupling of the mechanical field with the chemical field is realized as follows: As there are bound charges present in the gel, a jump in the concentrations of the mobile ions at the interface between the gel and the solution is obtained. This difference in the concentrations leads to an osmotic pressure difference $\Delta\pi$ between gel and solution. As a consequence of this pressure difference, the gel takes up solvent, which leads to a change of the swelling of the gel. This deformation is described by the prescribed strain $\bar{\boldsymbol{\varepsilon}}$. This means that the mechanical stress is obtained by the product of the elasticity tensor $\mathbf{C}$ and the difference of the total (geometrical) strain $\boldsymbol{\varepsilon}$ and the prescribed strain:

$$\boldsymbol{\sigma} = \mathbf{C}\,(\boldsymbol{\varepsilon} - \bar{\boldsymbol{\varepsilon}}) \tag{23}$$

where

$$\bar{\boldsymbol{\varepsilon}} = \mathbf{d}\,\Delta\pi = \mathbf{d}\,RT \sum_{\alpha=1}^{N_f} \left(c_\alpha^{(g)} - c_\alpha^{(s)} \right) \tag{24}$$

$\Delta\pi$ is the osmotic pressure difference, $\mathbf{d}$ is the material dependent swelling coefficient and $c_\alpha^{(g)}$ and $c_\alpha^{(s)}$ are the concentrations in the gel and in the solution, respectively.

This unidirectional chemo-electrical to mechanical coupling is given in Fig. 7.

The reverse coupling from the mechanical to the electrical field results from the conservation of the bound charges: As the number of moles of bound charges in the gel is constant, the change of the gel geometry leads to a change of the concentration of bound charges c_{A^-}. This can be formulated as

$$c_{A^-} = c_{A_0^-} \det(\mathbf{F})^{-1} = c_{A_0^-} \frac{V_0}{V} \tag{25}$$

$c_{A_0^-}$ is the initial concentration of bound charges, $\mathbf{F}$ the deformation gradient tensor – which characterizes the local deformation – and V and V_0 are the actual and the initial volume, respectively.

The complete coupling is depicted in Fig. 8.

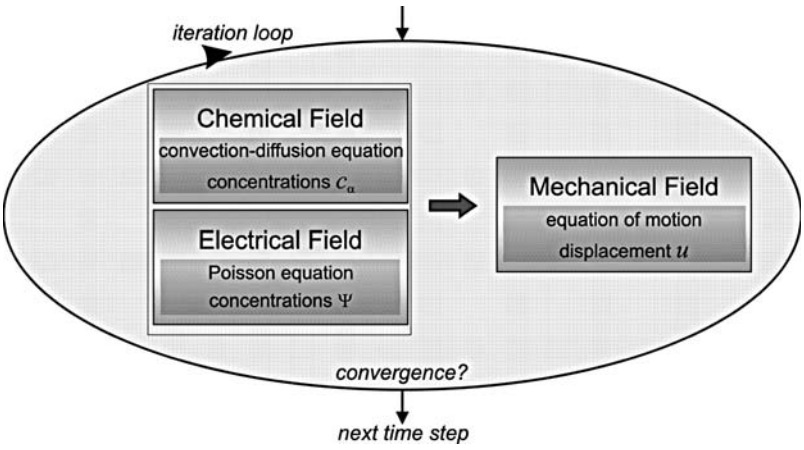

Fig. 7 Unidirectional chemo-electro-mechanical coupling scheme (chemical field, (19); electrical field, (20); mechanical field, (22))

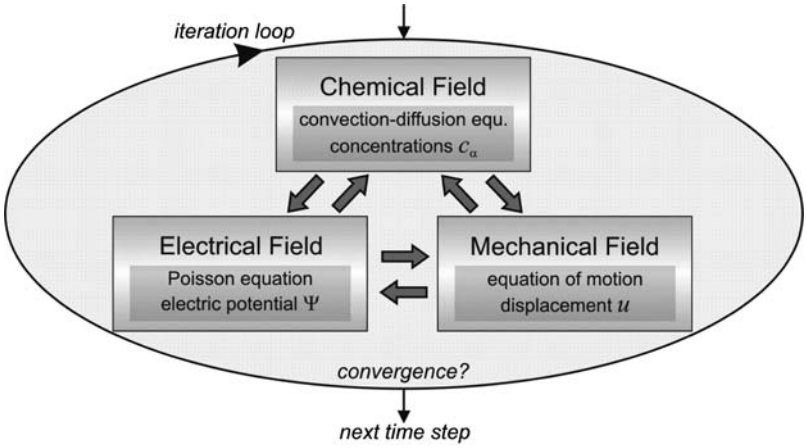

Fig. 8 Full chemo-electro-mechanical coupling scheme (chemical field, (19); electrical field, (20); mechanical field, (22))

1.4 Discrete Element Model

The Discrete Element Model (DEM) (Bicanic 2004) is a numerical method on the micro scale. It is an explicit dynamic numerical method for the solution of interacting particle systems. Continuum properties are obtained by the cumulative behaviour of a large number of particles with short range interactions (Bicanic 2004). The particles can interact mechanically by particle contact (Johnson 2001), by a superimposed truss or beam network of massless elements (Hrennikoff 1941) or both (Herrmann and Roux 1990).

In the general case the material is described by discrete point masses m_α and the interactions between them. The behaviour of the system is described by the Newton equations – the momentum equation and the rotational momentum equation – for each particle α by

$$m_\alpha \, \ddot{\mathbf{x}}_\alpha = \sum_\beta \mathbf{F}_{\alpha\beta} \tag{26}$$

$$\boldsymbol{\Theta}_\alpha \, \ddot{\boldsymbol{\varphi}}_\alpha = \sum_\beta \mathbf{M}_{\alpha\beta} \tag{27}$$

The forces $\mathbf{F}_{\alpha\beta}$ and the moments $\mathbf{M}_{\alpha\beta}$ stem from the interactions of particle α with its neighbouring particles β. The state vectors of the positions $\mathbf{x}_\alpha$ and rotations $\boldsymbol{\varphi}_\alpha$ are obtained by an explicit numerical integration technique.

Several of the problems can be investigated by the Discrete Element Method, as different kinds of interactions can be prescribed (Fig. 9). For example the interactions could be spring or damper elements, which leads to a specific force network.

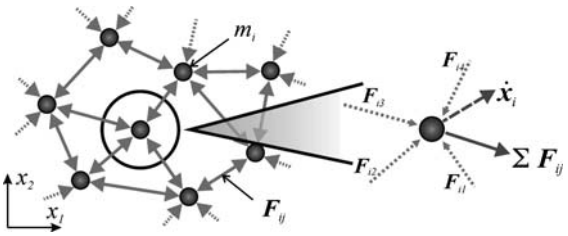

Fig. 9 Material representation as point masses and interactions in the framework of the Discrete Element Method. Reprinted from Wallmersperger et al. (2007). Reproduced with kind permission of Wiley-VCH Verlag GmbH & Co. KGaA.

To obtain particles which occupy a certain volume in space, contact laws could be defined between the nodes. In the system, linear or non-linear interactions could be considered. The meshless approach of the DEM allows to model problems including large deformations with geometrical and physical non-linearities, large displacements even with free motion and localisation phenomena like damage and fracture. Through the direct control over the applied interactions, the local state of the system is always accessible in a simulation.

In the Discrete Element simulation for chemically stimulated polymer gels in a solution bath, the gel only is investigated: This process is conducted by applying the mechanical field (26) and (27) and the chemical field (19) by considering the diffusive term only; i.e. the migrative, the convective and the source terms are neglected.

The boundary conditions, i.e. the gel-solution boundaries, are computed at each time step by solving the Donnan Eq. (7) together with the neutrality condition of (6). The concentration change in the gel creates a variation of the differential osmotic pressure $\Delta\pi$ and thus a change of the swelling ratio, resulting in a modification of the gel geometry (Wallmersperger 2006). Due to the number of moles of bound charges n_A in the gel remaining constant, the concentration of fixed charges c_A- is dependent on the actual volume V according to (25).

2 Coupled Chemo-Electro-Mechanical Model

2.1 Discretisation

For the spatial solution of the nonlinear coupled multi-field problem given in Sect 1.3, the Finite Element Method (FEM) is applied. The equations for the three fields are solved with a Newton-Raphson algorithm, and the time integration is performed with the implicit Euler backwards scheme.

The domain is discretised in 2D with bi-linear Finite Elements, while linear Finite Elements are applied for the 1D problem. The whole gel-solution domain is discretised with the same type of elements, while different material parameters are used to represent the different material (gel or solution). The coupled formulation

contains degrees of freedoms for the displacement u, the concentrations of mobile ions c^+ and c^-, the concentration of bound charges c_A-, the reference concentrations $\tilde{c}^+$and $\tilde{c}^-$, and the electric potential Ψ.

Note that the reference concentrations are only necessary for the electrical stimulation as the concentrations in the solution are dependent on the actual position in the domain. This means that, the vector of the generalised displacements for the electrical stimulation case reads

$$\hat{\mathbf{u}} = \begin{bmatrix} u & c^+ & c^- & c_{A^-} & \tilde{c}^+ & \tilde{c}^- & \Psi \end{bmatrix}^T \tag{28}$$

In the framework of the Newton-Raphson scheme, the generalised displacements $\mathbf{u}_{i+1}$ of the next iteration are obtained by

$$\mathbf{u}_{i+1} = \mathbf{u}_i + \Delta\mathbf{u}_{i+1} \tag{29}$$

The increment of the generalised displacements $\Delta\mathbf{u}_{i+1}$ is calculated from

$$\mathbf{K}\left(\mathbf{u}_i\right) \Delta\mathbf{u}_{i+1} = \mathbf{R}\left(\mathbf{u}_i\right) \tag{30}$$

The Jacobian $\mathbf{K}\left(\mathbf{u}_i\right)$ contains the contributions of the three fields and their couplings as well as the interrelation of the state of the reference concentrations. Note that the reference concentrations are only coupled with themselves and with the displacement $\mathbf{u}$ via the osmotic pressure. $\mathbf{R}\left(\mathbf{u}_i\right)$ is the residuum of the Jacobian at the current iteration. The resulting element matrices are non-linear and unsymmetric (for more details see Wallmersperger and Ballhause (2008)).

In the 1D case, the resulting two-node Finite Element with linear shape functions contains 14 degrees of freedom (Fig. 10).

2.2 Coupling Schemes

As discussed in Sect 1.3, there are different strategies for simulating the chemo-electro-mechanical field:

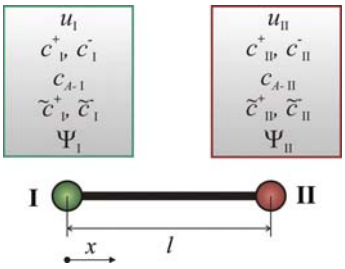

Fig. 10 One-dimensional chemo-electro-mechanical Finite Element with linear shape functions

- The first possibility is to solve all three fields independently and update the values of the different unknowns in the same or the following iteration. This is a kind of weak coupling and can either lead to a large amount of iterations for one time step or does not converge at all.
- The second possibility is to solve the chemo-electrical field simultaneously. The mechanical field is solved afterwards, considering the differential osmotic pressure – stemming from the concentration differences – as an external force, (Fig. 7). In this case the mechanical field is often solved for the gel only, without considering the surrounding solution.
- The third possibility is to solve all three fields at once in the sense of a strong coupling. In this case, gel and solution are modelled chemo-electro-mechanically; i.e. in the mechanical simulation, gel and solution are also solved together, but they own different material properties.

In Fig. 8, the chemo-electro-mechanical coupling scheme is shown. For one time step, all the involved fields are used in iteration loops until a converged solution is obtained. Then, the same procedure for the next time step will be applied.

2.3 Numerical Simulation of the Chemo-Electrical Field

In this section, the gel film in a solution bath is investigated for chemical as well as electrical stimulation by applying the coupled chemo-electrical formulation. The swelling effect due to concentration differences between the gel and solution phase is neglected. To capture the jumps in the concentration and in the electric potential, the domain of this test case contains both, gel and solution, and the distribution of the related variables is obtained in the whole integration domain. The distinction between the gel and the solution phase is realised by using different material parameters for each domain.

In the considered test case, a gel ($l_{\text{gel}} = 5$ mm) is immersed in a solution bath (total length $l = 15$ mm). The applied discretisation of the gel-solution domain is depicted in Fig. 11. In order to resolve the large gradients/jumps, an adaptive mesh refinement is applied.

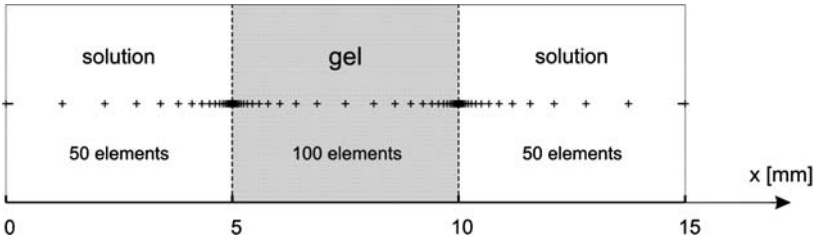

Fig. 11 Gel-solution domain for the test case considered here

2.3.1 Chemical Stimulation

In the first test case, the chemo-electrical behaviour of the polymer gel film under chemical stimulation, i.e. change of salt concentration in the solution, is investigated. The material parameters and initial conditions applied in all the test cases are given in Table 1. The concentration of the bound charges in the gel is prescribed to $c_{A^-} = 1$ mM and the concentrations of the mobile ions in the solution are set to $c^{+(s)}(t=0) = c^{-(s)}(t=0) = c_{s,0} = 1$ mM. This results in a concentration of the mobile ions in the gel (outside the boundary layer) of $c^{+(g)}(t=0) = 1.62$ mM and $c^{-(g)}(t=0) = 0.62$ mM, leading to a difference of the electric potential between gel and solution of $\Delta\Psi = -12$ mV (Fig. 12).

For $t > 0$, the concentration in the solution has been reduced to $c^{+(s)} = c^{-(s)} = c_s = 0.5$ mM. In the steady-state mobile concentrations of $c^{+(g)} = 1.21$ mM and $c^{-(g)} = 0.21$ mM in the gel are obtained (Fig. 13a). Although the mobile cationic concentration in the gel is reduced, the differential osmotic pressure is increased

Table 1 Simulation parameters and constants for the test case

Parameter / constant	Symbol	Value	Dimension
Initial ion concentrations in the solution	$c_{s,0}$	1.0	mM
Valence of the anions	z^+	1	–
Valence of the cations	z^-	−1	–
Initial concentration of the bound charges	$c_{A_0^-}$	1.0	mM
Valence of the bound charges	z_{A^-}	−1.0	–
Temperature	T	293	K
Gas constant	R	8.3143	J mol^{-1} K^{-1}
Faraday constant	F	96487	C mol^{-1}
Vacuum permittivity	ε_0	8.854 10^{-12}	A s V^{-1} m^{-1}
Relative permittivity	ε_r	100.0	–
(One-dimensional) swelling coefficient	d	10.0	mN^{-1}
(Normalized) stiffness	E_{gel}	1.0	N m^{-2}

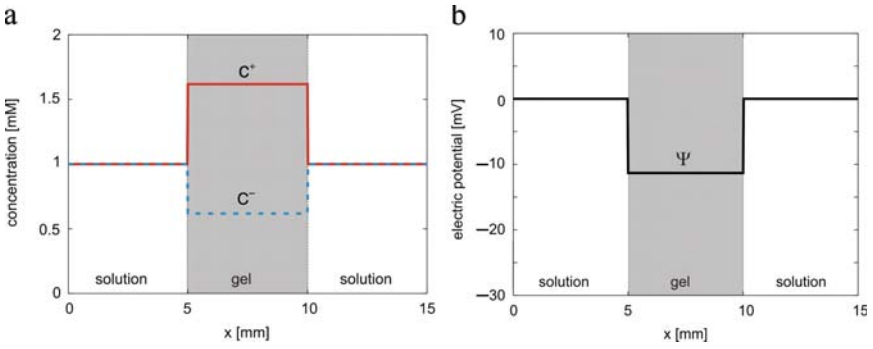

Fig. 12 Initial conditions a) of the mobile concentrations c^+ and c^- and b) of the electric potential at $t = 0$

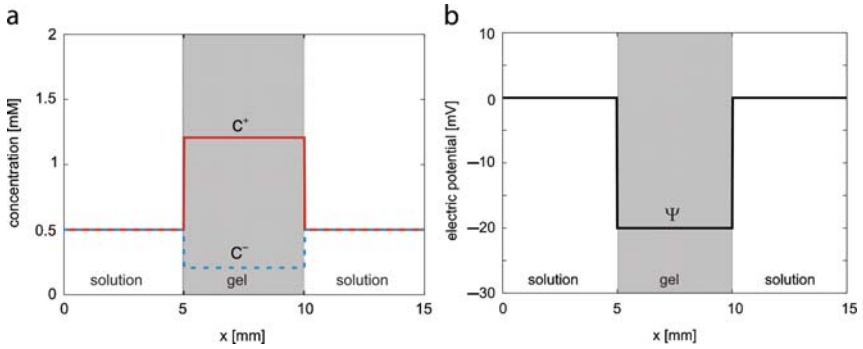

Fig. 13 Steady-state results (a) of the mobile concentrations c^+ and c^- and (b) of the electric potential after chemical stimulation

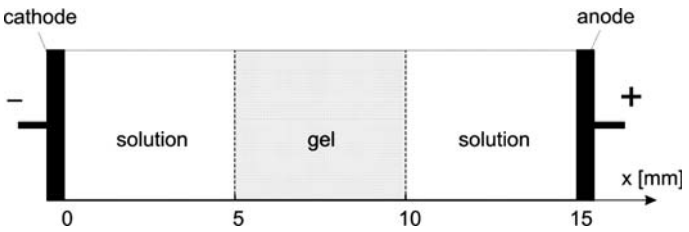

Fig. 14 Gel-solution domain for electrical stimulation

compared to the initial state. This means that the increase of the differential osmotic pressure between the two states would lead to an increase of the gel domain, if the fully coupled chemo-electro-mechanical formulation is applied without fixing the gel mechanically.

2.3.2 Electrical Stimulation

In this test case, the electrical stimulation of the polymer gel film is investigated. The same initial conditions as for the chemical stimulation are applied.

For $t > 0$, an electric potential $\Delta\Psi_{\text{cathode}} = -50\,\text{mV}$ at the cathode side and $\Delta\Psi_{\text{anode}} = +50\,\text{mV}$ at the anode side of the solution bath have been applied (Fig. 14).

The steady-state results of the concentrations and of the electric potential are depicted in Fig. 15. For the electrical stimulation there is a variation of both, the concentrations and the electric potential versus x. It can be seen that there is an increase of the concentrations over x in the solution, but a decrease over x in the gel (Fig. 15a). In Fig. 15b an increase of the electric potential over x can be noticed. This can be explained by the higher conductivity of the gel phase compared to the solution phase, i.e. there is a smaller increase over x of the electric potential in the

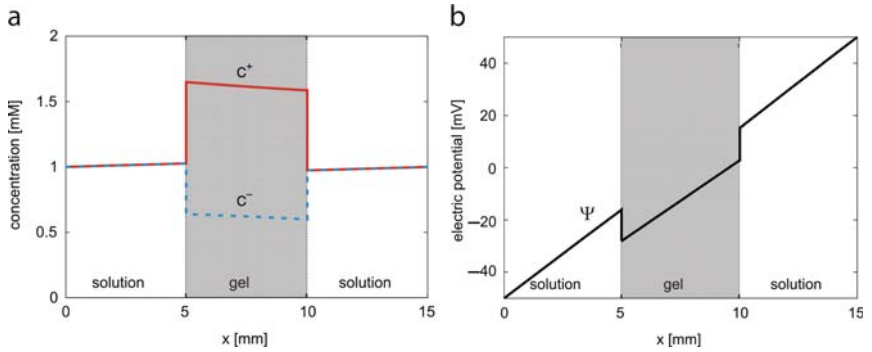

Fig. 15 Steady-state results (a) of the mobile concentrations c^+ and c^- and (b) of the electric potential after electrical stimulation

gel than in the solution. These differences in the spatial gradient of the electric potential are compensated by a smaller jump on the cathode side and a larger one on the anode side. Note that this can be also seen when computing the differential osmotic pressure at both gel-solution interfaces.

This means that, if the full coupling between the chemo-electrical and the mechanical field is introduced, a locally different swelling is obtained: a reduced swelling on the cathode and an increased swelling on the anode side.

2.4 Numerical Simulation of the Chemo-Electro-Mechanical Field

2.4.1 Chemical Stimulation

In this test case, the chemical stimulation of the gel film placed in the solution bath is investigated by the fully coupled chemo-electro-mechanical formulation. That is additionally, the mechanical deformation of the gel domain is considered and the chemo-electro-mechanical field is directly solved on the deformed domain.

In this test case, the same material parameters as in Sect 2.3.1 are used, see Table 1. As in the first test case, the concentration in the solution has been reduced to $c^{+(s)} = c^{-(s)} = c_s = 0.5$ mM. The increase of the concentration differences between gel and solution leads to an increase of the osmotic pressure. This provokes an increase of the gel domain and therefore a decrease of the concentration of bound charges according to (25). Due to the change of the bound charges, the mobile charges are also modified. The whole nonlinear process is iteratively solved – according to the coupling scheme given in Fig. 8 – until a steady-state solution is obtained.

The steady-state results of the concentrations and of the electric potential are depicted in Fig. 16. If we compare the stationary concentrations of the gel in this

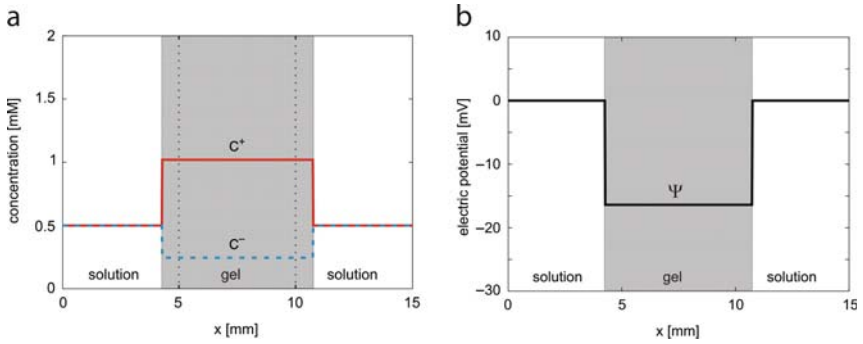

Fig. 16 Coupled chemo-electro-mechanical simulation: Steady-state results (a) of the mobile concentrations c^+ and c^- and (b) of the electric potential after chemical stimulation

test case with the one in Sect 2.3, we can ascertain that the cationic ones are smaller and the anionic ones are slightly larger. This means that the osmotic pressure is smaller than in the test case discussed in Sect 2.3.1, but it is still larger than the differential osmotic pressure in the initial state.

In Fig. 16b it can be seen, that the jump in the electric potential is also smaller than in the steady-state solution of the chemo-electrical test case.

Summarizing, a change of the concentration in the solution by a chemical stimulation provokes a change of the concentration, of the electric potential, and of the gel domain. This fully chemo-electro-mechanical coupling is quite robust and works as a kind of limiter for the change of the chemical, electrical and mechanical unknowns compared to the unidirectional chemo-electrical to mechanical coupling.

2.4.2 Electrical Stimulation

In this section, the electrical stimulation is investigated with the fully coupled chemo-electro-mechanical formulation. As in test case of Sect 2.3.2, for $t > 0$, an electric potential $\Delta\Psi_{\text{cathode}} = -50\,\text{mV}$ at the cathode side and $\Delta\Psi_{\text{anode}} = +50\,\text{mV}$ at the anode side of the solution bath have been applied. As the change of the concentrations is quite small and only present at the interface boundaries, the global (volume) change of the gel geometry is negligible. However, the osmotic pressure difference on the cathode side of the gel is smaller and on the anode side larger than in the initial state, a locally different swelling is obtained: a deswelling on the cathode side and an additional swelling on the anode side. In a 2D or 3D simulation, this results in a bending of the polymer gel film towards the cathode.

2.4.3 Mechanical Stimulation

By introducing a (mechanical) change of the gel geometry without applying any other kind of stimulation, the concentration of the bound charges is changed

according to (25). As the concentrations in the solution remain constant, the chemo-electrical field can be solved directly on the new geometry. As the change of the geometry is prescribed and the change of the concentrations and of the differential osmotic pressure does not lead to any further domain deformations, no additional iterations of the mechanical field have to be performed. This means that, the whole process can be captured directly and can be seen as a numerical simulation towards a new equilibrium of the chemo-electrical field.

3 Comparison with Experimental Results

The coupled chemo-electro-mechanical formulation is a quite powerful tool for capturing the behaviour of the chemical, electrical and mechanical unknowns. In order to compare numerical results with experimental results, the numerically obtained relative swelling ratio q versus the prescribed concentration c_s in the solution is depicted in Fig. 17. The initial state of the test cases discussed in Sect 2 has been taken as reference value.

It can be seen that an increase of the prescribed concentration leads to a decrease of the swelling ratio, while a decrease of the concentration in the solution leads to an increase of the swelling ratio. For both cases, a limited swelling value is obtained for very high or low prescribed concentrations. These results are in good qualitative accordance with the experimentally obtained behaviour of hydrogels under chemical stimulation, see e.g. Fig. 3, or examples given in Gülch et al. (2000) or Rička and Tanaka (1984).

The mechanical deformation under electrical stimulation is much smaller than under chemical stimulation. Under electrical stimulation, an unsymmetrical distribution of the concentrations and thus of the osmotic pressure difference leads to an unsymmetrical deformation. It can be seen that the chemical stimulation triggers a homogeneous swelling of the gel film, while the electrical stimulation leads to an

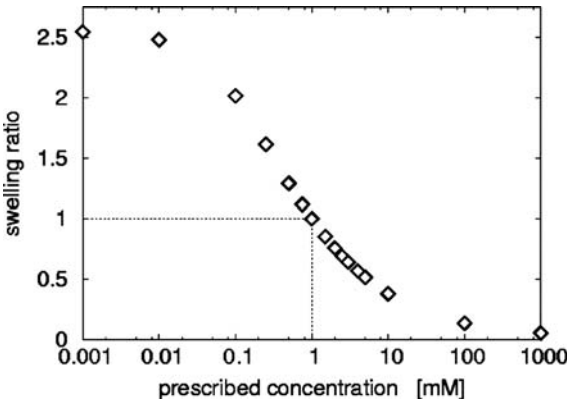

Fig. 17 Relative swelling ratio q_r versus the prescribed salt concentration c_s in the solution. In this case, the reference value $q_r = 1$ is set for a prescribed salt concentration of 1 mM.

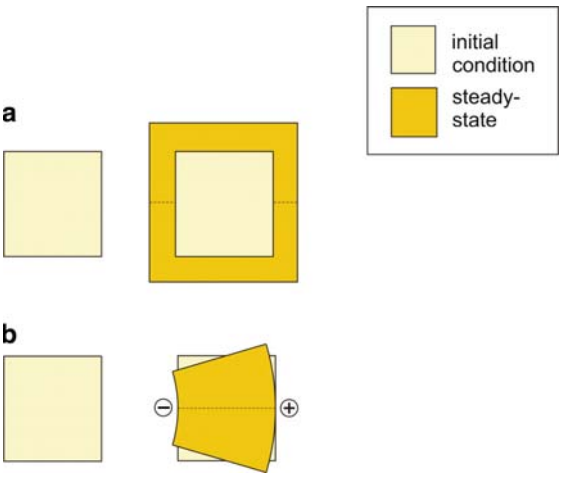

Fig. 18 Swelling and bending for (a) chemical and (b) electrical stimulation

inhomogeneous swelling. If the unsymmetrical deformation of the 1D numerical simulation is extrapolated into a 2D deformation, a bending shape of the gel will be obtained (Fig. 18) for chemical and electrical stimulation. It can be seen that for the electrical stimulation we obtain a decrease of the gel film on the cathode side and an increase on the anode side, which results in a bending towards the cathode. This observation is in accordance with experimental results, e.g. performed by Gülch et al. (2001), and shows the major difference between chemical and electrical stimulation.

4 Conclusions and Outlook

In this chapter an overview over different modelling alternatives for chemically and electrically stimulated electrolyte polymer gels in a solution bath has been investigated. The modelling on different scales allows to describe the various phenomena occurring in the gels. If only the global macroscopic behaviour has to be considered, the statistical theory will be sufficient. For investigating the local mechanical and chemical unknowns, the macroscopic Theory of Porous Media can be applied. By refining the scale, the mesoscopic coupled multi-field theory can be applied. Here, the chemical field is described by a convection-diffusion equation for the different mobile species. The electric field is directly obtained by solving the Poisson equation in the gel and solution domain. The mechanical field is formulated by the momentum equation. By further refining the scale, the whole structure can be investigated on the microscale by the Discrete Element (DE) method. In this model, the material is represented by distributed particles comprising a certain amount of mass; the particles interact with each other mechanically by a truss or beam network

of massless elements. The mechanical behaviour, i.e. the dynamics of the system, is examined by solving the Newton equations of motion while the chemical field, i.e. the ion movement inside the gel and from the gel to the solution, is described by diffusion equations for the different mobile particles. All four formulations can give chemical, possibly electrical and mechanical unknowns, and all rely on the assumption that the concentration differences between the different regions of the gel and between gel and solution form the osmotic pressure difference, which is a main cause for the mechanical deformation of the polyelectrolyte gel film.

In this chapter numerical simulations by applying the coupled chemo-electro-mechanical multi-field formulation on a deforming mesh have been performed. It has been shown that this formulation is an excellent method for describing the coupled behaviour of polymer gels in a solution. This method is capable to explain the mechanisms of the behaviour of polyelectrolyte gels under chemical and electrical stimulation, the ion distributions as well as the swelling and bending behaviour.

Acknowledgements Parts of this research have been financially sponsored by the Deutsche Forschungsgemeinschaft (DFG) in the frame of the Priority Programme 1259 "Intelligente Hydrogele". The author wants to thank Dr. Dirk Ballhause for his contributions to this research work.

References

Avci A (2008) Modellierung und Simulation elektroaktiver Polymere im Rahmen der Theorie poröser Medien. Master's Thesis, Universität Stuttgart

Bar-Cohen Y (2001) Electroactive Polymer (EAP) Actuators as Artificial Muscles - Reality, Potential, and Challenges, PM 98, ch. EAP History, Current Status, and Infrastructure, pp. 4-44, SPIE Press, Bellingham, WA, USA

Bicanic B (2004) Discrete element methods. In: Stein E, de Borst R, Hughes TJR (eds) Encyclopedia of Computational Mechanics: Fundamentals. Wiley, New York, pp 311–337

Bowen RM (1980) Incompressible porous media models by use of the theory of mixtures. Int J Engg Sci 18(9):1129–1148

Chiarelli P, Basser PJ, De Rossi D, Goldstein S (1992) The dynamics of a hydrogel strip. Biorheology 29(4):383–398

Ehlers W (2002) Foundations of multiphasic and porous materials. In: Ehlers W, Bluhm J (eds) Porous media: theory. experiments and numerical applications, Springer, Berlin, pp 3–86

Ehlers W, Markert B, Acartürk A (2002) A continuum approach for 3-d finite viscoelastic swelling of charged tissues and gels. In: Mang A, Rammerstorfer FG, Eberhardsteiner J (eds) Proceedings of Fifth World Congress on Computational Mechanics, Vienna University of Technology 2002; International Association for Computational Mechanics

Flory PJ, Rehner J Jr (1943a) Statistical mechanics of cross-linked polymers I. rubberlike elasticity. J Chem Phys 11:512–520

Flory PJ, Rehner J Jr (1943b) Statistical mechanics of cross-linked polymers II. swelling. J Chem Phys 11:521–526

Flory PJ (1953) Principles of polymer chemistry. Cornell University Press, Ithaca, NY

Günther M, Gerlach G, Wallmersperger T (2007) Modeling of nonlinear effects in pH-sensors based on polyelectrolytic hydrogels. In: Bar-Cohen Y (ed) Proceedings of the SPIE Electroactive Polymer Actuators and Devices, vol. 6524. p 652416f

Gülch RW, Holdenried J, Weible A, Wallmersperger T, Kröplin B (2000) Polyelectrolyte gels in an electric fields: a theoretical and experimental approach. In: Bar-Cohen Y (ed) Proceedings of the SPIE Electroactive Polymer Actuators and Devices, vol. 3987:193–202

Gülch R W, Holdenried J, Weible A, Wallmersperger T, Kröplin B (2001) Electrochemical stimulation and control of electroactive polymer gels. In: Bar-Cohen Y (ed) Proceedings of the SPIE Electroactive Polymer Actuators and Devices, vol. 4329:328–334

Herrmann HJ, Roux S (1990) Statistical models for the fracture of disordered media. Elsevier Science Publishers B.V, Amsterdam, The Netherlands

Hrennikoff A (1941) Solution of problems of elasticity by the framework method. J Appl Mech 8(4):A169–A175

Johnson KL (2001) Contact mechanics. Cambridge University Press, UK

Kunz W (2003) Mehrpasenmodell zur Beschreibung ionischer Gele im Rahmen der Theorie poröser Medien. Master's thesis, Universität Stuttgart

Rička J, Tanaka T (1984) Swelling of ionic gels: quantitative performance of the Donnan theory. Macromolecules 7:2917–2921

Schröder UP, Oppermann W (1996) Properties of polyelectrolyte gels. In: Cohen Addad J P (ed.). Physical properties of polymeric gels, Wiley, pp 19–38

Treloar LRG (1958) The physics of rubber elasticity. Oxford University Press, Oxford

Wallmersperger T (2003) Modellierung und Simulation stimulierbarer polyelektrolytischer Gele, Forschritt-Berichte VDI, Reihe 5: Grund- und Werkstoffe, Kunststoffe, VDI Verlag Düsseldorf

Wallmersperger T, Kröplin B, Gülch RW (2004) Coupled chemo-electro-mechanical formulation for ionic polymer gels–numerical and experimental investigations. Mech Mater 36(5–6): 411–420

Wallmersperger T, Kröplin B, Holdenried J, Gülch RW (2001) Coupled multifield formulation for ionic polymer gels in electric fields. In: Bar-Cohen Y (ed) Proceedings of the SPIE Electroactive Polymer Actuators and Devices, vol 4329. SPIE, Newport Beach, USA, pp 264–275

Wallmersperger T, Wittel F, Kröplin B (2006) Multiscale modeling of polyelectrolyte gels. In: Bar-Cohen Y (ed) Proceedings of the SPIE Electroactive Polymer Actuators and Devices, vol. 6168. p 61681H

Wallmersperger T, Ballhause D, Kröplin B (2007) On the modeling of polyelectrolyte gels. Macromol Symp 254:306–313

Wallmersperger T, Ballhause D (2008) Coupled chemo-electro-mechanical FE-simulation of hydrogels–part II: electrical stimulation. Smart Mater Struct 17:045012

Hydrogels for Chemical Sensors

M. Guenther and G. Gerlach

Abstract A rapidly expanding field of on-line process monitoring and on-line control in biotechnology, food industry, pharmaceutical industry, process chemistry, environmental measuring technology, water treatment and sewage processing requires the development of new micro fabricated reliable chemical and biosensors that are specific for particular species and can attain the analytic information in a faster, simpler and cheaper manner. Using a functionalised hydrogel coating in sensors provides the possibility to detect, transmit and record the information regarding the concentration change or the presence of a specific analyte (a chemical or biological substance that needs to be measured) by producing a signal proportional to the concentration of the target analyte. In this chapter, we describe piezoresistive chemical microsensors for a comprehensive characterization of solutions, which could be embedded inside fluidic systems for real time monitoring of organic and inorganic contaminants.

Keywords Piezoresistive sensor • Biochemical sensor • Polyelectrolytic hydrogel • pH-sensitive • Temperature sensitive • Swelling behaviour

Contents

M. Guenther (✉)
Solid-State Electronics Laboratory, Technische Universität Dresden, Germany
e-mail: mguenthe@mail.zih.tu-dresden.de

G. Gerlach and K.-F. Arndt (eds.), *Hydrogel Sensors and Actuators*,
Springer Series on Chemical Sensors and Biosensors 6,
DOI: 10.1007/978-3-540-75645-3_5, © Springer-Verlag Berlin Heidelberg 2009

Abbreviations

MBAAm	*N*,*N*′-methylene-bisacrylamide
DMAAm	Dimethylacrylamide
DMAEMA	*N,N*-dimethylaminoethyl methacrylate
DMIAAm	2- (dimethyl maleinimido)acrylamide
DMIMA	2-(dimethyl maleinimido)ethyl methacrylate
EDTA	Ethylene diamine tetra-acetic acid
NIPAAm	*N*-Isopropylacrylamide
NMRP	Nitroxide mediated radical polymerization
PAAc	Poly(acrylic acid)
PBS	Phosphate buffer saline
PECVD	Plasma enhanced chemical vapour deposition
PVA	Poly (vinyl alcohol)
P2VP	Poly (2-vinylpyridine)
P4VP	Poly (4-vinylpyridine)

Symbols

B	Viscosity coefficient in Jones-Dole expression
c_g	Concentration of ionizable groups on the polymer backbone
c_{gi}	Concentration of ionized groups on the polymer backbone
c_α	Additive concentration in the gel
c_α^0	Additive concentration in the surrounding solution
D_α	Effective diffusion coefficient of the additive
d	Thickness of the swollen gel layer
d_d	Thickness of the dry gel layer
F	Faraday constant

f	function
I	Ionic strength
k	Equilibrium constant of the reaction: $k = k_f/k_b$
k_b	Backward reaction rate constant
k_f	Forward reaction rate constant
M_n	Molecular weight
p	Pressure
pK_a	Acid exponent
R	Universal gas constant
r	Resistance
S	Sensitivity
T	Absolute temperature
T_{cr}	Volume phase transition temperature (critical temperature)
t	Time
U_{out}	Output voltage
V	Volume of the hydrogel
$V_{M,\alpha}$	Molar volume of the additive
v	Initial slope of the swelling curve
w	Deflection
x	Coordinate
z_i	Valence of i-th ionic species
Δ	Difference
ε	Strain
ε_0	Permittivity of vacuum
ε_1	Relative dielectric constant of the solvent
η	Viscosity
μ_i	Chemical potential of component i
ν_c	Cross-linking degree
π	Osmotic pressure
Ψ	Electrical potential
σ	Stress
τ	Time constant

Indices

a	Acid
b	Backward
c	Cross-linking
cr	Critical
d	Dry
eq	Equilibrium
f	Forward
g	Gel
α	Additive, species

1 Hydrogel-Based Piezoresistive Chemical Sensors

"Stimuli-responsive" or "smart" gels have attracted particular attention in the novel and most intensively developing field of polymers with sensor-actuator functions. The sensitivity of hydrogels to a large number of physical factors like temperature (Kuckling et al. 2003a; Richter et al. 2004a), electrical voltage (Richter et al. 2003; Wallmersperger 2003, Wallmersperger et al. 2004), pH (Kuckling et al. 2003a; Wohlrab and Kuckling 2001; Oktar et al. 2005), concentration of organic compounds in water (Arndt et al. 2000; Saito et al. 1993; Kumar et al. 2006; Orakdogen and Okay 2006), and salt concentration (Saito et al. 1993; Panayiotou and Freitag 2005; Liu et al. 2003; Cong et al. 2002) make them promising materials for a broad range of applications as microsensors (Liu et al. 2003; Cong et al. 2002; Richter et al. 2004b; Bashir et al. 2002; Lei et al. 2006; Herber et al. 2004; Gerlach et al. 2004; Gerlach et al. 2005; Guenther et al. 2005, 2006, 2007a, 2007b, 2007c, 2008) and microactuators (Kuckling et al. 2003a; Richter et al. 2004a; Richter et al. 2003; Arndt et al. 2000) in MEMS devices.

Stimuli-responsive hydrogels are capable of reversibly converting chemical energy into mechanical energy. That makes them very useful as sensitive material for chemical and biosensors. The following principles for the detection of environmental parameters are used in sensors based on the swelling behavior of hydrogels:

- Changes of the holographic diffraction wavelength in optical Bragg-grating sensors (Liu et al. 2003; Cong et al. 2002)
- Shifts of the resonance frequency of a quartz crystal microbalance in microgravimetric sensors (Richter et al. 2004b)
- Bending of micromechanical bilayer cantilevers (Bashir et al. 2002)
- Deflection of a membrane, or bending plate[1] in capacitor/inductor micromachined resonator (Lei et al. 2006) and in piezoresistive pressure sensors (Herber et al. 2004; Gerlach et al. 2004; Gerlach et al. 2005; Guenther et al. 2005, 2006, 2007a, 2007b, 2007c, 2008)

In the following, we describe a chemical sensor combining a smart hydrogel and a micro fabricated pressure sensor chip for continuously monitoring the analyte-dependent swelling of a hydrogel in aqueous solutions.

1.1 Operational Principle

Figure 1 illustrates the operational principle of hydrogel-based sensors. Pressure sensor chips with a flexible thin silicon bending plate and with an integrated piezoresistive Wheatstone bridge inside this plate have been employed as

[1] Bending plates are characterized by bending deformations, whereas in membranes tensile stress dominates instead of bending stresses. Nevertheless, bending plates are often called membranes.

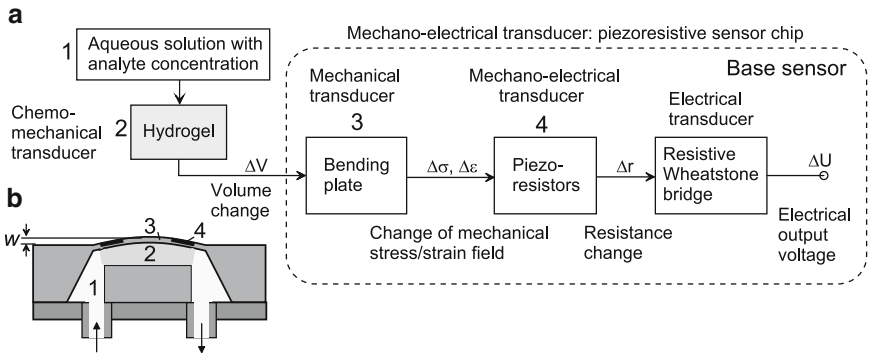

Fig. 1 Operational principle (a) and cross-section (b) of hydrogel-based chemical sensor: 1 measuring solution; 2 hydrogel; 3 Si bending plate; 4 piezoresistors

mechano-electrical transducer for the transformation of the plate deflection w into an appropriate electrical output signal U_{out}.

The aqueous solution to be measured is pumped through the inlet channels into the chip cavity and induces swelling or shrinking processes of the hydrogel inside the chip cavity. These processes were monitored by corresponding changes in the piezoresistance of an integrated Wheatstone bridge inside a rectangular silicon plate. The plate deflection causes a stress state change inside the plate and therefore a resistivity change of the resistors affecting proportionally the output voltage U_{out} of the sensor (German Patents DE 101 29 985C2, DE 101 29 986C2, DE 101 29 987C2, June 12 2001). An increase of U_{out} corresponds to the hydrogel swelling whereas a reduction of the electric output voltage corresponds to the shrinkage of the gel.

1.2 Sensor Design

For the design of the chemical sensor, commercially available pressure sensor chips (AktivSensor GmbH, Stahnsdorf, Germany) were used. The hydrogel itself was brought into a cavity at the backside of the silicon chip and was closed with a cover. This cavity on the backside of the chip was wet etched with a silicon nitride mask as etch resist. Therefore, only the backside of the chip came in contact with the measuring species, whereas the front side carrying the electronic components was strictly protected from it. Since the sensor chips show excellent stable properties, the long-term stability of the sensor is solely determined by the stability of the hydrogel characteristics.

The sensor chip was bonded to a socket with inlet and outlet flow channels. The aqueous solution to be measured was pumped through the inlet tubes into the silicon chip cavity coated with a 220 nm thick PECVD silicon nitride film to provide chemical protection. In the present work, three sensor designs have been used:

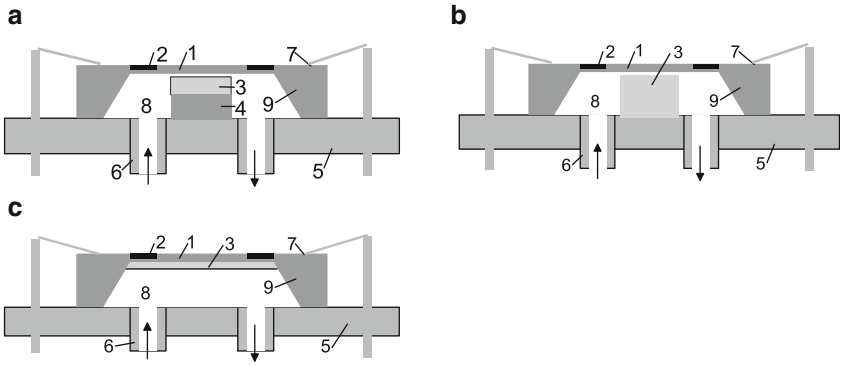

Fig. 2 Design variants of hydrogel-based sensors: 1 bending plate; 2 mechano-electrical transducer (piezoresistive bridge); 3 swellable hydrogel; 4 Si substrate (5 mm x 5 mm x 0.3 mm); 5 socket ; 6 tube ; 7 interconnect; 8 solution; 9 Si chip (5 mm x 5 mm x 0.4 mm). Reprinted from (Gerlach et al. 2004; Gerlach et al. 2005; Guenther et al. 2005, 2006, 2007b) with kind permission from Elsevier, Wiley-VCH and SPIE

- In order to obtain a sufficient measuring signal, a 50...100 µm thick hydrogel layer is located on a silicon platform to achieve a small enough gap between dry (absolutely unswollen) hydrogel and the silicon bending plate (Fig. 2a). The hydrogel layer was spin-coated on the Si wafer, which was covered with a 550 nm thick silicon oxide layer and with a 17 nm thick adhesion promoter layer, dried and then cross-linked.
- A 250 µm thick cross-linked and dried hydrogel foil was cut into pieces of 1 mm x 1 mm. A piece of foil was glued to a socket inside the chip cavity (Fig. 2b).
- In order to improve the sensor response time, a thin hydrogel layer was directly deposited onto the backside of the bending plate covered with a 220 nm thick PECVD silicon nitride film and with a 17 nm thick adhesion promoter layer (Fig. 2c). The final thickness of the dried and then cross-linked hydrogel layer was 4...50 µm.

1.3 Sensor Calibration

The calibration curves $w=f(p)$, $w=f(U_{\text{out}})$, and $p=f(U_{\text{out}})$ of the sensor have been obtained by using the controller of the pressure p to deflect a 20 µm thick silicon plate (Fig. 3). The silicon plate deflection w has been measured by means of a two-beam laser interferometer (Guenther et al. 2007a, 2008). The regression equations w (µm) vs. U_{out} (mV) and p (kPa) vs. U_{out} (mV) were obtained by fitting with the experimental curves as

$$w = 3.4 + 0.1U_{out} + 7.7 \times 10^{-4}U_{out}^2, \tag{1}$$

$$p = -0.8 + 4.14\exp(U_{out}/52.7). \tag{2}$$

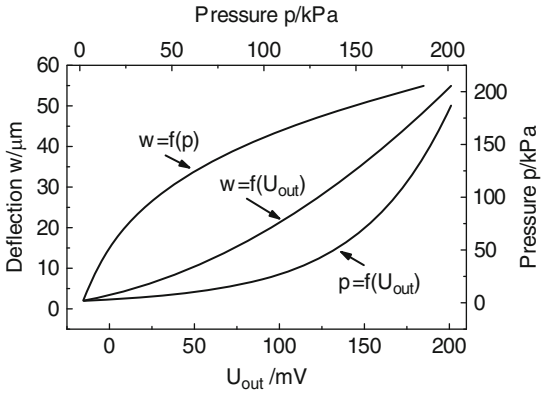

Fig. 3 The calibration curves $w=f(p)$, $w=f(U_{out})$, and $p=f(U_{out})$ of the chemical sensor. Reprinted from (Guenther et al. 2008) with kind permission from Elsevier

2 Hydrogel Material Preparation and Characterization

The following cross-linked hydrogel systems were used in the present work (Table 1):

- *Poly(vinyl alcohol)/poly(acrylic acid) (PVA/PAAc) blends*: The swelling degree of these polyanionic hydrogels changes steeply with the change of the pH value of the measuring species: it is at minimum in acids and takes its maximum in bases (Arndt et al. 1999).
- *N-Isopropylacrylamides (NIPAAm)*: PolyNIPAAm (PNIPAAm) is one of the best-studied thermo-responsive materials. PNIPAAm gel contains hydrophilic amino and carbonyl groups as well as hydrophobic isopropyl groups and exhibits large and sharp changes in its swellability in water upon raising the temperature above its volume phase transition temperature $T_{cr}=33$ °C. The thermally induced reversible collapse of PNIPAAm can be controlled by the use of mixed solvents (Arndt et al. 2000; Saito et al. 1993; Kumar et al. 2006; Orakdogen and Okay 2006; Guenther et al. 2006, 2008), addition of salts (Saito et al.7 1993; Panayiotou and Freitag 2005; Guenther et al. 2006, 2007b, 2008), addition of metal ions (Oktar et al. 2005; Guenther et al. 2007b, 2007c, 2008; Kuckling and Pareek 2003), or addition of surfactants (Caykara et al. 2006) that results in a T_{cr}–shift. Practical applications of PNIPAAm usually involve its chemical modification which has been achieved by its co-polymerization with anionic (Oktar et al. 2005; Harmon et al. 2003), neutral (Harmon et al. 2003; Kuckling et al. 2002), and cationic (Wohlrab and Kuckling 2001; Harmon et al. 2003) monomers. Changes in the polymer composition have allowed to vary the gel volume phase transition temperature (T_{cr}) from 25° to 58°C (Wohlrab and Kuckling 2001; Kuckling et al. 2002; Kuckling et al. 2000). The micro-fabricated thermo-responsive hydrogels have been prepared using a photolithographic patterning of photo cross-linkable PNIPAAm polymers (Kuckling et al. 2003b; Hoffmann et al. 1999). Scaling to microdimensions is very effective

Table 1 Chemical structure of the used hydrogels

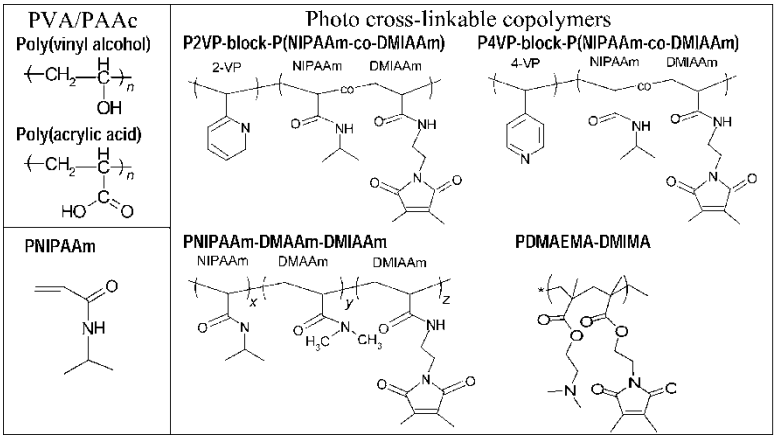

in decreasing the response time. The possibility for an enhancement of the gel's time response is particularly relevant for applications of smart hydrogels in microsystems.

- *Copolymer of N,N-dimethylaminoethyl methacrylate (DMAEMA)*: This polycationic pH- and temperature-sensitive gel possesses specific coordination binding sites for transition-metal ions.

2.1 *Thermally Cross-Linked Poly(vinyl Alcohol)/ Poly(Acrylic Acid) Blend*

PVA and PAAc polymers obtained from Aldrich Chemical Co. were dissolved separately in distilled water under stirring at 80°C (PVA 15 wt% and PAAc 7.5 wt%). For hydrogel formation, the solutions are then mixed in such a manner that 80 wt% were PVA and 20 wt% PAAc. This mixture is stirred for 1 h at 60°C to manufacture a homogeneous solution (Arndt et al. 1999). The films of PVA/PAAc blends were deposited onto the Si wafer (Fig. 2a) or onto the backside of the silicon bending plate (Fig. 2c). A solution of α-amino propyltriethoxysilane was used as adhesion promoter. Finally, the dried hydrogel films were isothermally annealed in an oven at 130°C for 20 min.

2.2 *Chemically Cross-Linked* N*-Isopropylacrylamide*

The cross-linked PNIPAAm hydrogels were prepared according to (Arndt et al. 2000) by free radical polymerization of NIPAAm in water with *N*,*N*′-methylene-bisacrylamide (MBAAm; MBAAm content: 4 mol%) as the cross-linking agent. A solution of

NIPAAm, MBAAm (overall monomer concentration 0.53 mol/l) and potassium peroxodisulfate as initiator (3×10^{-3} mol/mol monomer) were cooled to 0 °C and purged with nitrogen for 15 min. *N*,*N*,*N*',*N*'-tetramethylethylenediamine as accelerator (3×10^{-3} mol/mol monomer) was added and the solution was immediately transferred into a Petri dish to get hydrogel foils. After 17 h reaction time at 20°C, the gels were separated and washed with water for 1 week. For PNIPAAm chemical sensors, 250 µm thick hydrogel foil pieces were used (Fig. 2b). The dried PNIPAAm foils were prepared by evaporation of water at room temperature and then cut into pieces of 1 mm × 1 mm. The hydrogel was glued to a socket as a piece of foil.

2.3 Photo Cross-Linkable Copolymers

In order to prepare thin hydrogel layers, photo cross-linkable copolymers were used.

2.3.1 Materials

N-isopropylacrylamide (NIPAAm, ACROS) was purified by recrystallisation from hexane and afterwards dried in vacuum. 2-vinylpyridine 98 % (2VP, Merck) was stirred over calcium hydride for 24 h and distilled over calcium hydride. Diethyl ether, ethyl acetate, dioxane, and tetrahydrofuran (THF) were distilled over potassium hydroxide. Dimethylformamide (DMF), cyclohexanone were purified by distillation over calcium hydride. 2,2´-Azobis(isobutyronitrile) (AIBN) was recrystallized from methanol. All other reagents were of analytical grade. The 2-(dimethylmaleinimido)acrylamide (DMIAAm) monomer was synthesized according to (Vo et al. 2002). 1-[3-(chloro-dimethyl-silanyl)-propyl]-3,4-dimethylmaleimide was prepared according to (Kuckling et al. 2003b). The synthesis of *N*-tert-butyl-*N*-(2-methyl-1-phenyl-propyl)-*O*-(1-phenyl-ethyl)-hydroxylamine and the corresponding nitroxide 2,2,5-trimethyl-4-phenyl-3-azahexane-3-oxyl (TIPNO) is described in (Krause et al. 2004; Benoit et al. 1999).

2.3.2 P2VP-block-P(NIPAAm-co-DMIAAm) block copolymer

This polymer was synthesized via NMRP (Nitroxide Mediated Radical Polymerization) (Benoit et al. 1999) by sequential polymerization of 2VP and a mixture of NIPAAm and DMIAAm. Using the macroinitiator method, the preparation of well-defined linear block copolymers consisting of a homo polymer block P2VP (pH-sensitive) and a random copolymer block of PNIPAAm (temperature sensitive) with DMIAAm (photo crosslinker) was possible.

A mixture of 3.5 ml (0.032 mol) 2VP, 100 µl acetic anhydride, and 0.125 g (0.38 mmol) of the alkoxyamine was degassed by three freeze/thaw cycles, sealed under

argon, and heated at 110 °C for 6 h. After that the polymerization was stopped by freezing with liquid nitrogen. The reaction mixture was then diluted with THF and precipitated in n-pentane. The powder was dried in vacuum to give the desired alkoxyamine-terminated P2VP.

A mixture of 0.25 g (1.1 mmol) alkoxyamine-terminated P2VP macroinitiator, 3.5g (0.33 mol) NIPAAm, DMIAAm (5 mol%/mol monomer), TIPNO (0.5 mol%/mol macroinitiator) dissolved in 3.5 ml DMF was degassed by three freeze/thaw cycles, sealed under argon and heated at 135°C for 48 h. The reaction was stopped by liquid nitrogen. The solvent was evaporated under reduced pressure. The concentrated mixture was redissolved in chloroform and precipitated in cold diethylether. The resulting brownish powder was dried in vacuum. To remove the unreacted P2VP, the polymer was purified by dialysis in THF using a Spectra/Por membrane.

2.3.3 PNIPAAm-DMAAm-DMIAAm terpolymer

This PNIPAAm copolymer was obtained by free radical polymerization of NIPAAm, dimethylacrylamide (DMAAm) and DMIAAm initiated with AIBN at 70 °C in dioxane with a total monomer concentration of 0.55 mol/l under nitrogen for 7 h. The polymer was precipitated in diethylether and purified by reprecipitation from THF into diethylether (1:3).

2.3.4 PDMAEMA-DMIMA copolymer

This copolymer was obtained by free radical polymerization of *N*,*N*-dimethylaminoethyl methacrylate (DMAEMA) and 2-(dimethyl maleinimido)ethyl methacrylate (DMIMA) as the chromophore initiated with AIBN at 70 °C in ethylmethylketone for 7 h. The polymer was precipitated in *n*-pentane and purified by reprecipitation from ethylmethylketone into *n*-pentane (1:8).

2.3.5 Polymer characterization

The molecular weight (M_n) of the copolymers was determined by gel permeation chromatography (GPC) with a PL120 instrument equipped with RI detector using PSS "GRAM" columns. The samples were measured at 50 °C in dimethylacetamide (DMAc) containing 0.42 g/l lithium bromide as mobile phase with a flow rate of 1 ml/min. The molecular weight of the copolymers was about 44.6 kg/mol for P2VP-block-P(NIPAAm-co-DMIAAm) and 29.0 kg/mol for PNIPAAm-DMAAm-DMIAAm (Table 2). The molecular weight $M_n = 26$ kg/mol of the PDMAEMA-DMIMA copolymer was determined by GPC with a JASCO instrument equipped with UV and RI detector using Waters "Ultrastyragel" columns. The samples were measured against 3,5-di-*tert*-4butylhydroxytoluene (BHT) standard at 30 °C in chloroform containing 0.1 vol% triethylamine as the mobile phase with a flow rate of 1 ml/min.

Table 2 Chemical composition, molecular weight M_n, and phase transition temperature T_{cr} of the used photo cross-linkable hydrogels. Reprinted from (Guenther et al. 2007b, 2007c, 2008) with kind permission from Elsevier, Wiley-VCH and SPIE

Gel	Chemical composition, mol%							M_n, kg/mol	T_{cr}, °C
	P2VP	NIPAAm	DMIAAm	P4VP	DMAAm	DMAEMA	DMIMA		
1a	18.9	73.1	8.0					44.6	25
1b	21.9	72.9	5.2					41.5	
2a		79.9	5.6	14.5				45.0	22
2b		62.6	8.6	21.0				28.8	
3		66.3	3.0		30.7			29.0	43
4						90.2	9.8	25.6	33.5

The chemical composition of the copolymers was determined by ^{1}H NMR (Table 2). The ^{1}H NMR spectra were recorded on a BRUKER DRX 500 spectrometer (500 MHz). The solvent was used as an internal reference.

The phase transition temperature of the 5 wt% aqueous polymer solution was determined by DSC with a TA Instruments DSC 2920. The P2VP-block-P (NIPAAm-co-DMIAAm) block copolymer has a lower value of T_{cr} (T_{cr}=25 °C) than PNIPAAm (T_{cr}=33 °C) due to the additional hydrophobic P2VP and DMIAAm components whereas the PNIPAAm-DMAAm-DMIAAm terpolymer has a higher value of T_{cr} (T_{cr}=43 °C) than PNIPAAm due to the additional hydrophilic DMAAm component (Table 2).

2.3.6 UV Cross-Linking

The DMI-chromophore was selected for cross-linking because it is known to form stable dimers. The DMI-chromophore reacts via a [2+2]-cycloaddition under irradiation. By using thioxanthone as photo sensitizer, a complete conversion of the chromophores could be achieved within a few minutes (Kuckling et al. 2003b).

The adhesion promoter layer was prepared by absorbing 1-[3-(chloro-dimethyl-silanyl)-propyl]-3,4-dimethylmaleimide from 0.3 vol% solution in dicyclohexyl on Si/Si_3N_4 surface of the chip bending plate for 24 h. The substrates were rinsed with chloroform. Photo cross-linkable polymer films were deposited by pipetting of 3 µl cyclohexanone solution containing 10 wt% polymer and 2 wt% (with respect to the polymer) thioxanthone sensitizer (Guenther et al. 2007b). The PDMAEMA-DMIMA copolymer was dissolved in ethylmethylketone. The films were dried at 60 °C for 15 min and then under vacuum at 20 °C for 5 min. The dry films were cross-linked by UV irradiation, using a mercury lamp producing an irradiance at the substrate plane of 1.7 mW/cm^2. The resulting dry film thicknesses ranged from 4 to 6 µm.

2.4 Hydrogel Conditioning

After the sensor preparation, an initial gel conditioning procedure was performed. A corresponding initial gel swelling in de-ionized water at low temperature ($T < T_{cr}$)

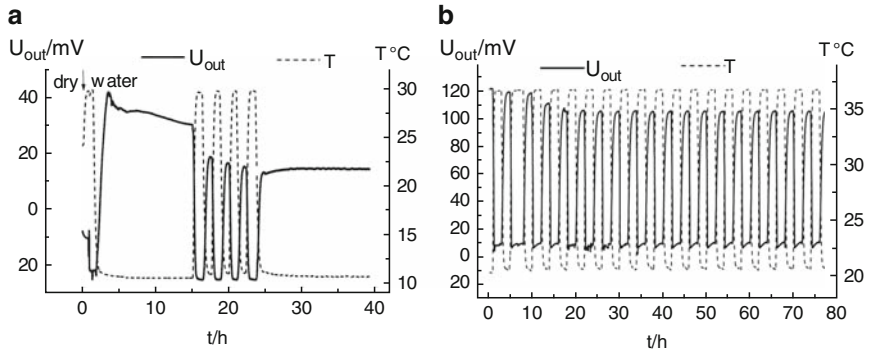

Fig. 4 Initial gel conditioning procedure in de-ionized water for (a) P2VP-block-P(NIPAAm-co-DMIAAm) (Gel 1a in Table 2) (Guenther et al. 2007c) and (b) PNIPAAm (MBAAm 4 mol%) (Guenther et al. 2006). Reprinted with kind permission from Wiley-VCH and SPIE

for 24 h preceded the deswelling/swelling cycling at increasing/decreasing temperature. During the first operation the hydrogel sensor often shows a poor repeatability and a drift of the sensor parameters. This phenomenon is caused by changes in the microscopic structure of the polymer network. It was found that the stability of the sensitivity (Fig. 4a) and the repeatability (Fig. 4b) can be significantly increased by performing a number of conditioning cycles. The conditioning process was accomplished after 5. . .7 swelling cycles. The sensor's output voltage was measured during the swelling/deswelling of the hydrogel layer under variable, tightly controlled ambient conditions. The temperature was controlled with a Vaisala HMP 230 humidity and temperature sensor with an uncertainty $\Delta T = \pm 0.1\,K$. An uncertainty of the temperature setting was $\Delta T = \pm 0.5\,K$. The solution was pumped with a flow rate of 0.8 ml/min.

2.5 *Temperature Sensitivity of PNIPAAm Gels*

The thermo-shrinking cross-linked copolymers of PNIPAAm were investigated as a functionalised polymer coating in chemical sensors using an appropriate measuring setup. The gel, initially swollen in water at room temperature, shrinks with increasing temperature. The volume phase transition of PNIPAAm occurs at 33 °C (Fig. 5a, 1). Changes in the polymer composition have allowed to vary the gel volume phase transition temperature (T_{cr}) from 22 °C to 25 °C for P4VP-block-P(NIPAAm-co-DMIAAm) and P2VP-block-P(NIPAAm-co-DMIAAm), respectively to 43 °C for PNIPAAm-DMIAAm-DMAAm terpolymer (Fig. 5a and Table 2). Fig. 5b demonstrates that a sufficiently high long-term stable sensitivity of the PNIPAAm gel in chemical sensors is maintained during the several years under the specific measurement and storage conditions (see Sect. 3.3).

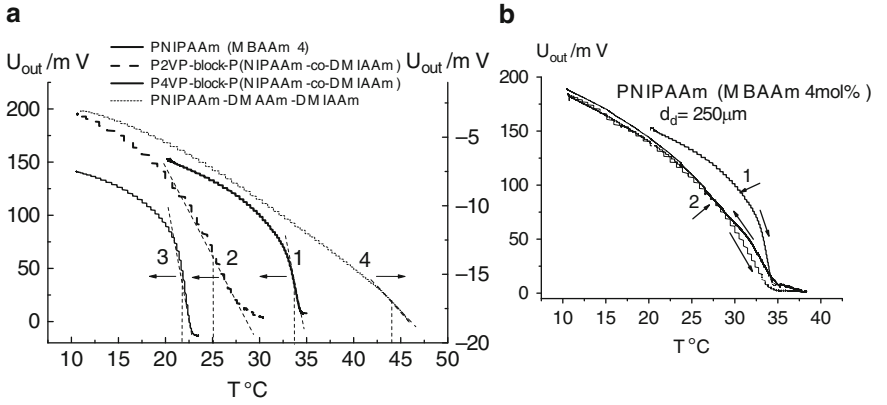

Fig. 5 Sensor output voltage in dependence on temperature: (a) for PNIPAAm (MBAAm 4) (1), P2VP-block-P(NIPAAm-co-DMIAAm) (2), P4VP-block-P(NIPAAm-co-DMIAAm) (3), and PNIPAAm-DMAAm-DMIAAm (4) in water; (b) for PNIPAAm (MBAAm 4) after sensor preparation (1) and after 2.8 working years of the sensor (2)

3 pH Sensors

The swelling ability of pH-sensitive polyelectrolyte hydrogels depends on the functional acidic or basic groups at the polymer backbone. Due to the dissociation of these groups and the influx of counterions, the concentration of ions in the hydrogel is higher than in the surrounding solution. This causes a difference in osmotic pressure and results in a solution flux into the hydrogel and, consequently, a swelling. The interaction and repulsion of charges along the polymer chain also lead to an increased swelling. Quasi-equilibrium of ionic gels occurs when the elastic restoring force of the polymer network balances the osmotic forces. During the swelling process of PVA/PAAc at pH values near and above the acid exponent of acrylic acid ($pK_a = 4.7$), hydroxide ions are transported into the neutral gel, while during the shrinkage protons diffuse into the gel and neutralize the negatively charged acidic carboxylate groups. This ion diffusional flux induces an electrical potential difference that drives the electromigration of the ions in the direction opposite to that of the diffusion. After the time t_{eq}, the quasi-equilibrium between the gel and the solution is reached. In the so called Donnan quasi-equilibrium state, the diffusional flux of the ions in one direction is equal to the electromigrational flux in the opposite direction, resulting in a net nearly zero mass transport and a net nearly zero charge transport.

The concentration $c_{\alpha,eq}$ of the ionic additive in the gel after the time t_{eq} differs from that one in the surrounding solution $c_\alpha{}^0$ and is determined by a Donnan quasi-equilibrium condition as

$$c_{\alpha,eq} = c_\alpha^o \exp\left[-(z_\alpha F\Delta\Psi + \pi V_{M,\alpha} + \Delta\mu_\alpha^0)/RT\right]. \quad (3)$$

Here, $\Delta\Psi$ is the electrical Donnan potential at the gel-solution interface, π the osmotic pressure, $V_{M,\alpha}$ and $\Delta\mu_\alpha{}^0$ denote the additive molar volume and the difference between the additive standard chemical potentials in the gel and in the solution, respectively, and z_α the charge on the additive ion. The other notations are: R the universal gas constant, T the absolute temperature, and F the Faraday constant.

The electrical potential Ψ is described by the Poisson-Boltzmann equation

$$\Psi_{,xx} = -\frac{\mathrm{F}}{\varepsilon_1\varepsilon_0}\left[z_g c_{gi} + \sum_{\mathrm{i}} z_{\alpha_i} c^0_{\alpha_i} \exp\left(-\frac{z_{\alpha_i} e\Psi}{kT}\right)\right] \tag{4}$$

and by the charge neutrality condition inside the gel

$$z_g c_{gi} + \sum_i z_{\alpha_i} c_{\alpha_i} = 0. \tag{5}$$

Here, z_g is the charge on the ionized groups with the concentration c_{gi}, ε_0 the permittivity of vacuum, and ε_1 the relative dielectric constant of the solvent.

In order to realize pH sensors, the weak polyelectrolyte anionic PVA/PAAc as well as cationic P2VP-block-P(NIPAAm-co-DMIAAm) and P4VP-block-P (NIPAAm-co-DMIAAm) gels with a pH-value dependent swelling behaviour were used as chemo-mechanical transducers. Since P2VP and P4VP are weak polycations, their backbone charge increases as the solution pH is lowered. At pH < 6.7, P2VP is protonated (Houbenov et al. 2003) and a further decreasing of pH results in an increasing density of positive charges on the P2VP chains. For the sensor signal calibration, buffered solutions of 0.2 M ionic strength were used which varied between pH values of 1 and 11.

3.1 Sensitivity

Beside response time, stability and selectivity, the sensitivity is one of the most crucial parameters for a successful sensor implementation. The sensitivity $S = \Delta U_{\mathrm{out}}/\Delta pH$ of a pH sensor is determined by the polymer composition (the concentration c_g of the ionizable groups in the gel) as well as by its cross-linking degree ν_c. The latter depends on the content of the cross-linking agent in the polymer as well as on the UV irradiation conditions for the photo cross-linkable hydrogel. Fig. 6 (curves 1 and 2) shows the output characteristics obtained for sensors with P2VP-block-P(NIPAAm-co-DMIAAm) hydrogel layers of the same polymer composition, but with different cross-linking degrees $\nu_{\mathrm{c}1}$ and $\nu_{\mathrm{c}2}$ ($\nu_{\mathrm{c}1} < \nu_{\mathrm{c}2}$) due to different irradiation conditions (different irradiation times t_1 and t_2, $t_1 < t_2$). As consequence, $S_1 = 12.5$ mV/pH is higher than $S_2 = 8$ mV/pH. All measurements were performed with a signal resolution of 0.08 mV. For 4 μm thick photo-cross-linked hydrogel layers as well as for thermally cross-linked PVA/PAAc layers with a thickness of

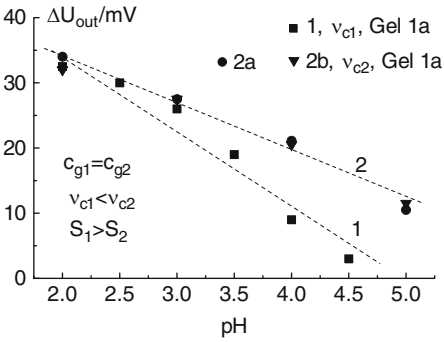

Fig. 6 Output characteristics of the pH-sensors with P2VP-block-P(NIPAAm-co-DMIAAm) gel

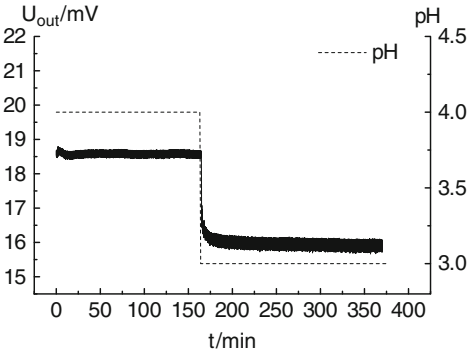

Fig. 7 Sensor output voltage during the deswelling process of PVA/PAAc from pH4 to pH3. Reprinted from (Guenther et al. 2005) with kind permission from SPIE

Table 3 Parameters of pH sensors with voltage, frequency, pressure or deflection output, respectively. Reprinted from (Guenther et al. 2007b) with kind permission from Elsevier

Hydrogel	Sensitivity, per pH unit	Signal resolution	Response time, s	Thickness of gel layer, μm	pH range	References
P2VP-block-P (NIPAAm-co-DMIAAm)	12.5 mV	0.08 mV	70	4	2–5	(Guenther et al. 2007b)
PVA/PAAc	2.5 mV	0.16 mV	90	6	3–4	(Guenther et al. 2005)
PVA/PAAc	13.2 kHz	0.62 kHz	0.5	0.39	2.55–3.45	(Richter et al. 2004b)
DMAEMA-co-HEMA	60 kPa	2 kPa	600	10	6–7.5	(Herber et al. 2004)
PMAA-PEGDMA-DMPA	18.3 μm	0.01 μm	70	2.5	5.9–6.7	(Bashir et al. 2002)

6 µm (Fig. 7) (which were directly deposited on the backside of the bending plate), a sufficient sensitivity has been obtained. For a comparison, the parameters achieved for hydrogel-based pH sensors are listed in Table 3.

3.2 Response Time

Because the gel response is typically diffusion-driven, the time response of the volume change approximately follows the square of the sample dimension. Scaling to micro-dimensions enhances the time response. Consequently, a reduction of the sample size improves the sensor performance. Time constants down to a few ten seconds have been found for thin hydrogel layers deposited directly on the backside of the bending plate (Table 3 and Fig. 8). However, a reduction of the gel thickness is limited by the necessity to obtain a sufficiently high sensor signal and consequently, a sufficient sensitivity. In order to achieve an optimum between the sensor signal amplitude and the sensor response time, the swelling/deswelling kinetics of the polyelectrolyte hydrogel was investigated (Gerlach et al. 2005; Guenther et al. 2005, 2007a, 2007b).

The several processes occur simultaneously during the hydrogel swelling in the solution with the additive concentration $c_\alpha{}^0$:

- Diffusion of the additive into the gel. The concentration c_α of the additive in the gel depends on the distance x from the gel surface and increases with the time as (Crank 1970)

$$c_\alpha = c_{\alpha 0} + (c_\alpha^0 - c_{\alpha 0})\left[1 - \mathrm{erf}(x/2\sqrt{D_\alpha t})\right], \tag{6}$$

  where $c_{\alpha 0}$ is the initial additive concentration in the gel, D_α the effective diffusion coefficient of the additive, and erf(δ) the error or probability function, given by

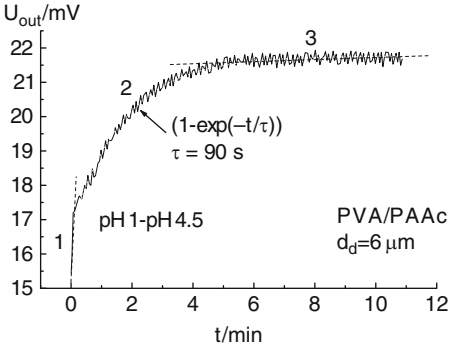

Fig. 8 Sensor output voltage during the swelling process of PVA/PAAc from pH1 to pH4.5. Reprinted from (Gerlach et al. 2005; Guenther et al. 2005) with kind permission from Elsevier and SPIE

$$\mathrm{erf}(\delta) = \frac{2}{\sqrt{\pi}} \int_0^{\delta} e^{-\varsigma^2} d\varsigma. \tag{7}$$

- This additive concentration sparks off the ionization process in the gel with a rate

$$\dot{c}_{gi} = k_f c_\alpha (c_g - c_{gi}) - k_b c_{gi}, \tag{8}$$

  where c_{gi} and c_g are the concentrations of the ionized and ionizable groups on the polymer backbone, respectively, k_f and k_b the forward and backward reaction rate constants, respectively. The backbone charge increases because of the ionization and leads to an increase of the gel hydrophilicity and consequently to additional water uptake.

- Additional water uptake. The amount of the absorbed water steadily increases due to the steadily increasing amount of ionized polymer groups induced by the additive (Gerlach et al. 2005; Guenther et al. 2007a).

The polymer chain relaxation rate is much slower than the diffusion rates of the additive and water. This leads to the retarded gel swelling which is limited by a relaxation process with the time constant τ (Fig. 8). It was found that the total amount of the additionally absorbed water as well as the rate of the initial rapid swelling (Fig. 8,1) and the rate of the slow long-time drift (Fig. 8,3) depends on the initial concentration gradient ($c_\alpha{}^0$- $c_{\alpha 0}$) of the additive between the solution and the gel (Gerlach et al. 2005; Guenther et al. 2007a). In order to shorten the sensor response time, the dependence of the rate v of the initial solution sorption on the initial concentration gradient can be used (Guenther et al. 2008). With the help of the values v_1 and v_2 for two solutions with a known concentration $c_{\alpha,1}{}^0$ and with an unknown one $c_{\alpha,2}{}^0$, the value of $c_{\alpha,2}{}^0$ can be estimated as

$$\lg(c^0_{\alpha,2} - c_{\alpha 0,2}) = \lg(c^0_{\alpha,1} - c_{\alpha 0,1}) + \lg(v_2/v_1). \tag{9}$$

Fig. 9a demonstrates the swelling curves for a thick PVA/PAAc layer ($d_d = 50$ μm) in buffer solutions with different pH values. The values of U_{out} were recalculated in terms of the change Δd of the gel layer thickness using Eq. (1) and taking into account that $\Delta d \approx w$ (Fig. 9b). The values of the initial slope obtained from Fig. 9b and the values of the hydroxide ions concentration estimated using Eq. (9) are listed in Table 4. One sees that the estimated values of $c_{OH^-}{}^0$ are in good agreement with the concentration values used in the experiment. By applying this method, the measuring time which is necessary to determine the additive concentration in a solution is essentially shortened from the time t_{eq} (to reach a full saturation of the solution uptake) to the time t_m which is necessary for the initial slope determination (Table 5).

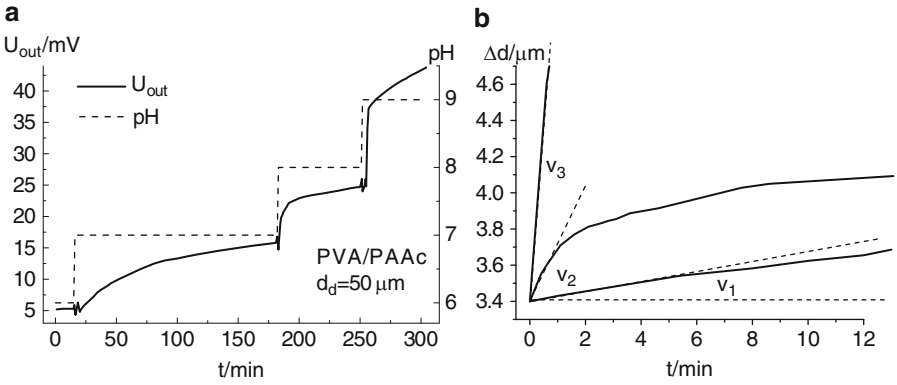

Fig. 9 Output voltage U_{out} of a pH sensor (a) and corresponding change Δd of the PVA/PAAc layer thickness (b) during the gel swelling in solutions with different pH values.

Table 4 Values of the initial slope v of the hydrogel swelling curves and corresponding calculated values of the OH^- concentration

pH	v, µm/min	lg $c_{OH^-}{}^0$
6		-8
7	0.02	-7
8	0.32	-6
9	1.75	-5

Table 5 Values of the equilibrium and measuring times t_{eq} and t_m for the kinetics curves of the 50 µm thick PVA/PAAc layer in the investigated solutions

pH	t_{eq}, min	t_m, min
7...11	>180	6
6...7	>150	6
7...8	>70	1
8...9	>50	0.5

3.3 Signal Reproducibility

Of particular interest is the reproducibility of repeated pH measurements under a specific set of conditions. It was found that a hysteresis in the output characteristic of a pH sensor is observed complicating the calibration procedure and affecting the signal reproducibility (Gerlach et al. 2004; Guenther et al. 2007a, 2007b). It was concluded, that a hysteresis in the output characteristic of a pH sensor is caused by a hysteresis in the deprotonation-protonation process of ionizable groups in the gel as well as by a rather complicated hydrogel swelling and deswelling kinetics. It should be noted, that

- The previous states of both the gel ionization and the swelling influence the shape of the titration curve $c_{gi}=f(\text{pH})$. This means that high signal reproducibility can be ensured only by performing a conditioning procedure before every measurement in order to achieve a certain reference sensor signal.
- Even if the pH measurements are performed in buffered solutions of constant ionic strength, the formation of low molecular salt occurs in the gel at adjusting the pH value by adding acid or base for cycling from basic to acidic conditions and vice versa. As a result, the change of the ionic strength affects the value of the osmotic pressure and consequently the sign (positive or negative) of the resulting water flux.
- The dependence of the concentration of ionized groups (and consequently the water uptake) on the duration t_{ex} of the immersion in the solution leads to an additional dynamical hysteresis in the sensor output characteristic which can be minimized by setting constant t_{ex} for all pH measurements.

Fig. 6 (curves 2a and 2b) shows the sensor output characteristics obtained for repeated measurements at the same pH change direction and at the same value $U_{out,ref}$ of the reference sensor signal as well as at $t_{ex}=const$ for all pH measurements. In order to provide the required high signal reproducibility as well as in order to maintain a sufficient long-term stable sensitivity, three procedures have been carried out for the temperature sensitive gel:

- Initial gel conditioning procedure consisting of a gel swelling in de-ionized water and a subsequent deswelling/swelling cycling (see Sect. 2.4)
- Regenerating procedure before every measurement in order to achieve a certain reference sensor signal. This signal was gained by the gel deswelling at high temperature $T>T_{cr}$ (Fig. 10). The gel shrinking allowed to press out the previous measuring solution and to completely rinse the gel layer using a special rinsing solution (German Patent 2006). An additional rinsing cycle at $T<T_{cr}$ was carried out for those analytes which are particularly difficult to rinse out (Fig. 11). This complete cycle provides the full rinsing out of the previous solution from the gel and prevents its influence on the following measurement results. It should be

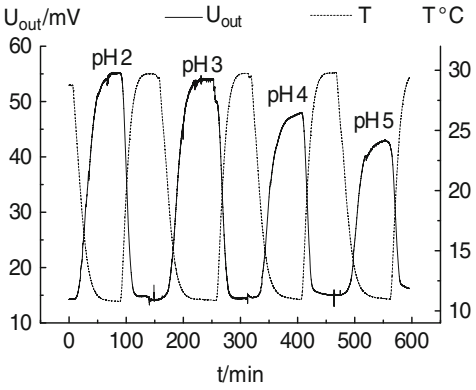

Fig. 10 Measuring and rinsing cycles for the temperature-sensitive P2VP-block-P(NIPAAm-co-DMIAAm) gel. Reprinted from (Guenther et al. 2007b) with kind permission from Elsevier

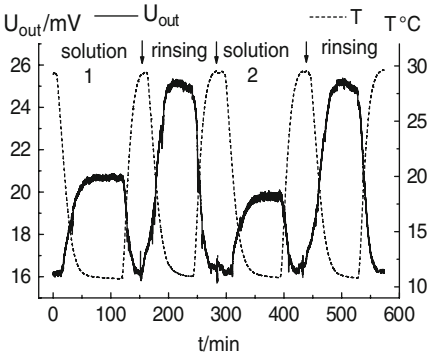

Fig. 11 Measuring cycle with additional gel swelling in rinsing solution at $T < T_{cr}$

noted that an appropriately chosen rinsing solution should be used for a certain analyte and for a certain polymer

- Rinsing in de-ionized water during sensor storage between measurements

A sufficiently long-term stable sensitivity during several working years of the pH sensors has been provided by performing these procedures as well as by avoiding large pH changes and measurements in solutions with pH < 2.

4 Sensors for Concentration Measurements in Aqueous Solutions

The swelling state of thermo-shrinking cross-linked polymers containing hydrophilic and hydrophobic groups depends on the balance of hydrophilic and hydrophobic interactions in the three-component system of polymer-water-analyte, which determine the polymer swelling/shrinking with changing temperature (Saito et al. 1993).The addition of a small amount of analyte to the water-swollen gel can perturb the water-polymer hydrogen bonding and therefore it can lead to a T_{cr}-shift.

Generally, the additives change the structure of water and thus the free energy of the interaction between polymer and water. The additives influence the solution viscosity and are classified into structure making (cosmotropes) and structure breaking (chaotropes). The viscosity η of an aqueous solution (up to about 0.1 M), relative to the viscosity η_0 of water at the same temperature, varies with the additive concentration c_α according to the Jones-Dole expression

$$\eta/\eta_0 = 1 + A\sqrt{c_\alpha} + Bc_\alpha, \tag{10}$$

where the coefficient A is related to the mobilities and interactions between the additives. The coefficient B reflects the interactions between the additive and the water molecules and results from the degree of water structuring. At higher

concentrations, a further term (Dc_α^2) may be added to the right hand side of Eq. (10) (Nickolov and Miller 2005). It has been accepted that the sign of the coefficient B determines whether a certain additive is a water structure breaker (negative B) or a water structure maker (positive B). Adding an analyte-cosmotrope as well as increasing the temperature leads to an enhancement of the polymer chain stiffness, which affects the chain mobility. In contrast, adding an analyte-chaotrope leads to the opposite effect.

A complex information containing the value of the swelling degree of the functionalised polymer in the presence of the additive, the value and direction of the induced T_{cr}-shift, and the value of the solution viscosity might allow to exactly detect the analyte as well as its concentration range. A portable biocompatible rheochemical microsystem for a comprehensive characterization of solutions, which combines a chemical sensor with a viscosity sensor and which could be embedded inside water systems for real time monitoring of organic and inorganic contaminants, is presented in (Guenther et al. 2008).

4.1 Sensors for Organic Solvents

In order to realize an organic solvent concentration sensor, we have used the ability of PNIPAAm to change its degree of swelling in water-organic solvent mixtures (Guenther et al. 2006, 2008). Fig. 12 demonstrates the output characteristic of such a sensor. The sensor's output voltage was measured during the swelling/shrinking of the hydrogel under the influence of water solutions with different ethanol contents at $T=20$ °C. Fig. 12 also shows the dependence of the relative viscosity η_{rel} of the ethanol-water mixture on the ethanol content c_α at $T=20$ °C. This dependence exhibits two flanks as well as the characteristic of the sensor with the PNIPAAm layer. The viscosity maximum is observed at about 40 vol.% of ethanol. The dependence $U_{out}=f(c_\alpha)$ demonstrates the broad asymmetric minimum corresponding to the shrunken state of the PNIPAAm hydrogel in the concentration range from 20 to 50 vol.% of ethanol. The shape of this characteristic is influenced

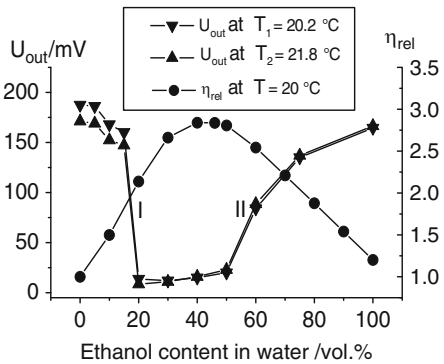

Fig. 12 Dependence of the output voltage U_{out} of a PNIPAAm (MBAAm 4)-based sensor and of the relative viscosity η_{rel} in aqueous ethanol mixtures on the ethanol content. Reprinted from (Guenther et al. 2006, 2008) with kind permission from SPIE and Elsevier

by the dependence of the partial molar volume of ethanol in aqueous solutions on the ethanol content, which runs through a sharp minimum at $c_\alpha < 30$ vol.% of ethanol (Hüther et al. 2004; Atkins 1990). The gel volume phase transition occurs at about 20 vol.% of ethanol. The first flank is induced by the shrinking of the hydrogel when the ethanol content is increased up to 40 vol.%. The second flank describes the hydrogel reswelling when the ethanol content is further increased from 50 to 100 vol.%. In order to exactly detect the ethanol concentration range, a small temperature rise was used. We have observed a gel shrinking at a small ethanol content (flank I) and a gel swelling at a high ethanol content (flank II) when we increased the temperature from $T = 20.2$ °C to $T = 21.8$ °C. With increasing temperature, the hydrophilic interactions dominating in the PNIPAAm-water-alcohol system at low alcohol content decrease leading to a hydrogel shrinking whereas the hydrophobic interactions dominating at high alcohol content increase and stimulate the gel swelling.

The polar organic additives of normal alcohols have a positive viscosity coefficient B and tend to enhance the hydrophobic interaction (for ethanol, $B = 0.170$ l/mol) (Saito et al. 1993). The addition of a small amount of alcohol to the water-swollen gel perturbs the water-polymer hydrogen bonding and leads to strong polymer-polymer interactions. These are reflected as desorption of water by the gel, and shift the gel volume phase transition temperature T_{cr} to lower values. The T_{cr}-shift is stronger when the carbon number of alcohol is increased (Arndt et al. 2000; Saito et al. 1993; Kumar et al. 2006; Orakdogen and Okay 2006). At high alcohol concentration, when alcohol-polymer interactions overtake polymer-polymer interactions, the gel reswells. The competing weak interactions between organic solvent-water and organic solvent-polymer results in a complex "reentrant" swelling behavior of the hydrogel in mixed co-solvents.

A reswelling dynamics of PNIPAAm gel in mixed co-solvents was investigated at $T = 20$ °C (Fig. 13). The water-swollen gel exhibits two successive states during reswelling in the solutions with an ethanol concentration higher than $c_\alpha^* = 50$ vol.%. Initially, the additive incoming into the gel has a lower concentration $c_{\alpha s1}$ in the gel subsurface layer than that one in the surrounding solution ($c_{\alpha s1} < c_\alpha^0$).

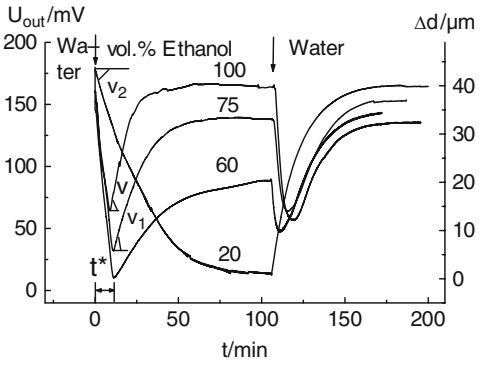

Fig. 13 Sensor output voltage U_{out} and change Δd of the gel layer thickness during the reswelling process of an initially water-swollen PNIPAAm (MBAAm 4) gel in solutions with different ethanol contents. Reprinted from (Guenther et al. 2008) with kind permission from Elsevier

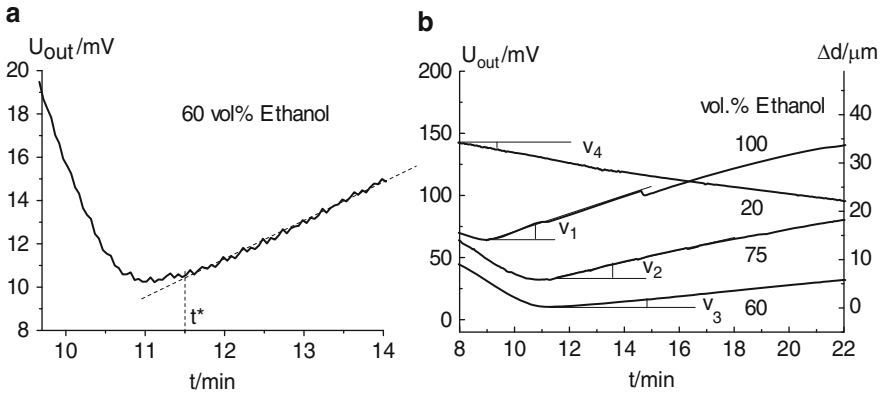

Fig. 14 Sensor output voltage U_{out} and change Δd of the gel layer thickness during the reswelling process of an initially water-swollen PNIPAAm (MBAAm 4) gel in solutions with different ethanol contents

This low additive concentration $c_{\alpha s1} < c_\alpha^*$ sparks off the gel collapse due to the suddenly decreasing polymer-solution affinity. The interface between the outer collapsed and the inner swollen regions (shrinking front) proceeds from the outside towards the inside of the gel within the time $0 < t < t^*$. The change Δd of the gel layer thickness at small times $t \ll t^*$ is proportional to $t^{1/2}$. The concentration $c_{\alpha 1}$ increases with the time according to Eq. (6).

When the additive concentration $c_{\alpha 1}$ reaches the critical value of 50 vol.% at a depth $x = d$ (d is the thickness of the swollen gel layer), the gel begins to reswell (Fig. 14). At $t = t^*$ the boundary starts to move in the opposite direction. With the help of the values $t^* = 11.5$ min (see Fig. 14a), $c_\alpha^0 = 0.6$, $c_\alpha^* = 0.5$, and $d = 284$ μm the ethanol diffusion coefficient D_α in the swollen gel has been calculated using Eq. (6). The estimated value $D_\alpha = 1.3 \times 10^{-9}$ m^2 s^{-1} is in good agreement with the value $D_{MeOD} = 1.8 \times 10^{-9}$ m^2 s^{-1} obtained in (Arndt et al. 2006) for partially deuterated methanol in a D_2O-swollen PNIPAAm (MBAAm 4) hydrogel.

At $t > t^*$, the reswelling curve has an initial slope $v = \delta(\Delta d)/\delta t$ (Figs. 13 and 14b), which is determined by the rate of the ethanol sorption process and thereby is proportional to $(c_\alpha^0 - c_\alpha^*)$ as

$$v = k(c_\alpha^0 - c_\alpha^*). \tag{11}$$

Here, k is the rate constant. For an ethanol solution with a concentration $c_{\alpha,1}{}^0$, one obtains using Eq. (11)

$$v_1 = k(c_{\alpha,1}^0 - c_\alpha^*) = v(c_{\alpha,1}^0 - c_\alpha^*)/(c_\alpha^0 - c_\alpha^*). \tag{12}$$

Table 6 Values of the initial slope v of the hydrogel reswelling/shrinking curves and corresponding calculated values of the ethanol concentration $c_\alpha{}^0$ of the investigated solutions. Reprinted from (Guenther et al. 2008) with kind permission from Elsevier

Solution	v, μm/min	$c_\alpha{}^0$, vol.%
1	1.6	100
2	0.84	76
3	0.31	60
4	0.62	19.5

With the help of the values v and v_1 for two ethanol solutions with a known concentration $c_\alpha{}^0 > c_\alpha{}^*$ and with an unknown one $c_{\alpha,1}{}^0 > c_\alpha{}^*$, the value of $c_{\alpha,1}{}^0$ can be estimated as

$$c^0_{\alpha,1} = c^*_\alpha + (c^0_\alpha - c^*_\alpha)v_1/v. \tag{13}$$

For an ethanol solution with a small concentration $c_{\alpha,2}{}^0 < c_\alpha{}^*$, one uses

$$c^0_{\alpha,2} = -(c^0_\alpha - c^*_\alpha)v_2/v, \tag{14}$$

where $v_2 < 0$ is the initial slope at $t > 0$ for the second solution. Table 6 summarizes the values of the solution concentrations obtained from the slopes of the kinetic curves using the known value $c_\alpha{}^0 = 100$ vol.%. The calculated values of $c_\alpha{}^0$ are in good agreement with the experimental values given in Figs. 13 and 14b. The same two-step reswelling kinetics is observed for an ethanol-swollen gel in water.

4.2 Sensors for Salt Concentrations

The chemical sensors based on cationic P2VP-block-P(NIPAAm-co-DMIAAm) gel as well as those based on neutral PNIPAAm and PNIPAAm-DMAAm-DMIAAm gels have demonstrated a clear dependence of the gel swelling degree on the salt concentration in aqueous solutions. Fig. 15a shows the value of the sensor signal at different concentrations of NaCl and NaI salts at $T = 20$ °C. The sensor characteristics demonstrate a "salting out" effect of NaCl salt in a PNIPAAm gel over the whole range of the salt concentration. In contrast, NaI shows a "salting in" effect at low concentrations in accordance with the hydration degree of Cl^- and I^- anions and their position in the Hoffmeister series. The strongly hydrated Cl^- ions exhibit strong interactions with water molecules, destroy the water-polymer hydrogen bonding and lead in this way to an enhancement of the gel hydrophobicity. Additionally, they shift the gel volume phase transition temperature T_{cr} to lower values proportionally to the increasing salt concentration (Figs. 15b and 16). The values of T_{cr} were determined as inflection points of the resulting sensor signal curves which are depicted versus the temperature. On the other hand, the I^- ions

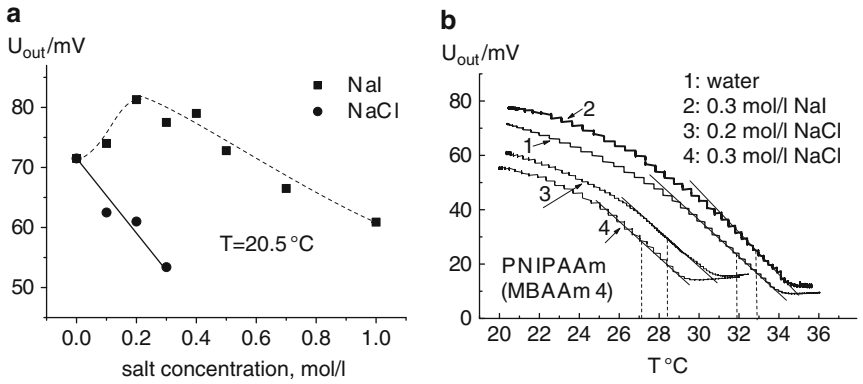

Fig. 15 Sensor signal (a) and its temperature dependence (b) for PNIPAAm (MBAAm 4) at different concentrations of NaCl and NaI salts. Reprinted from (Guenther et al. 2006, 2007b) with kind permission from SPIE and Elsevier

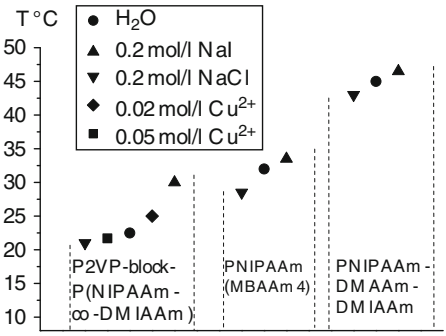

Fig.16 Gel volume phase transition temperature T_{cr} in solutions with different content of salts and metal ions. Reprinted from (Guenther et al. 2007b) with kind permission from Elsevier

exhibit a weak hydration ability in water, tend to disperse the polymer chains, preventing them from intramolecular interactions, and as a result, increase the gel solubility at low NaI concentrations below 0.5 mol/l. The "salting in" effect of NaI salt in the PNIPAAm gel leads to a T_{cr}-shift to higher values (Figs. 15b and 16).

It should be noted that strongly hydrated salts increase the solution viscosity due to their tightly bound high-density ordered water and are known as water structure makers. The Cl^- ions have a viscosity coefficient $B = -0.007$ l/mol whereas I^- ions have a more negative $B = -0.069$ l/mol (Saito et al. 1993). They are known as water structure breakers and decrease the solution viscosity. Fig. 17 demonstrates the change of the sensor output voltage which corresponds to a change in the gel swelling degree in dependence on the relative viscosity of the 0.2 mol/l NaI and NaCl solutions for P2VP-block-P(NIPAAm-co-DMIAAm), PNIPAAm (MBAAm 4), and PNIPAAm-DMAAm-DMIAAm based sensors. The value of ΔU_{out} was calculated as the difference between the sensor signals obtained from a salt solution and from pure water. Adding NaCl salt as well as increasing the temperature leads to an enhancement of the polymer chain stiffness, which affects the chain mobility,

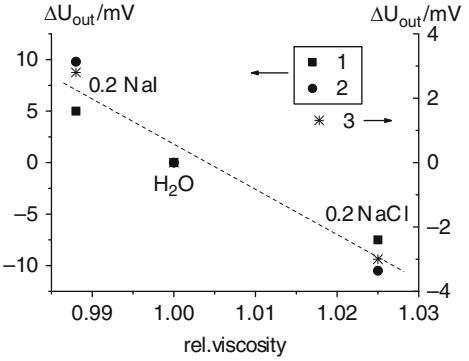

Fig. 17 Change of the sensor output voltage ΔU_{out} in dependence on the relative viscosity of the 0.2 mol/l NaI and NaCl solutions for P2VP-block-P(NIPAAm-co-DMIAAm) (1), PNIPAAm (MBAAm 4) (2), and PNIPAAm-DMAAm-DMIAAm (3) based sensors. Reprinted from (Guenther et al. 2007b) with kind permission from Elsevier

whereas adding NaI salt leads to the opposite effect. Finally, we note that multiresponsive hydrogels are very useful as sensitive material for measuring the rheochemical characteristics of solutions.

4.3 Sensors for Metal Ions Concentrations

The swelling behaviour of the P2VP-block-P(NIPAAm-co-DMIAAm) and PDMAEMA-DMIMA gels was analyzed as a function of the concentration C_{Me2+} of transition-metal ions in aqueous solutions. The dependence demonstrates a non-monotonic behaviour (Fig. 18). Since both P2VP-block-P(NIPAAm-co-DMIAAm) and PDMAEMA-DMIMA are weak polyelectrolytes (due to the amino groups), their uncompensated backbone charge increases at small ion concentrations. This leads to an increase of the gel hydrophilicity and consequently to a gel swelling at $c_{Me2+} < 0.03$ mol/l. A small change in the affinity of the comonomer with regard to the solvent has a large effect on swelling by shifting the phase transition temperature T_{cr} to higher values (Fig. 16).

With further increase of c_{Me2+}, more and more metal ions become trapped within the P2VP-block-P(NIPAAm-co-DMIAAm) and PDMAEMA-DMIMA gels which possess specific coordination binding sites for metal ions. The transition-metal cations form complexes with N atoms which have a pair of unshared electrons and are capable to satisfy the coordination number of the metal (Kuckling and Pareek 2003). As a result, the electrostatic repulsion between the charged units decreases, and the gel starts to contract. In this case, the metal ions might act as crosslinkers by coordination binding to nitrogen atoms of different chains. It was found that the complexation of the polymer units by divalent metal ions (due to the formation of chelate rings with metal ions) affects the T_{cr}-shifting toward lower values (Fig. 16) and increases in accordance with a series: $Ca^{2+} < Fe^{2+} < Cu^{2+} < Zn^{2+} < Mn^{2+} < Ni^{2+}$ (Fig. 18a).

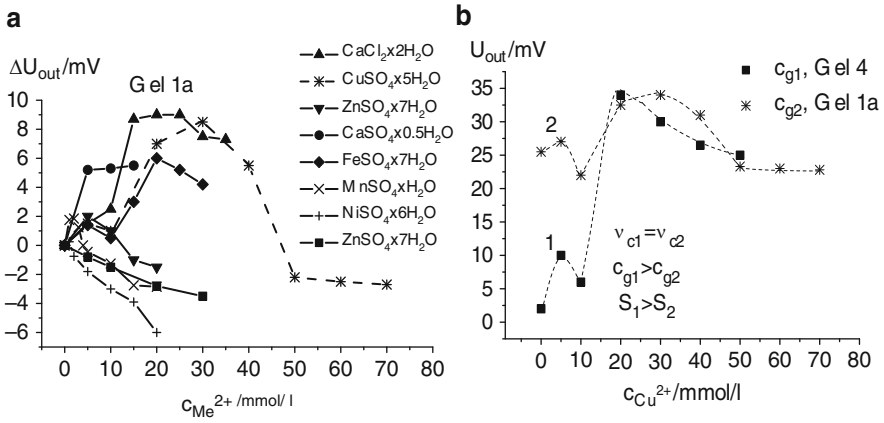

Fig. 18 Sensor output characteristics in solutions with transition-metal ions for (a) P2VP-block-P (NIPAAm-co-DMIAAm) (Gel 1a) and for (b) PDMAEMA-DMIMA (Gel 4) based sensors. Reprinted from (Guenther et al. 2007b, 2007c) with kind permission from Elsevier and Wiley-VCH

An increasing ionic strength I of the solution at $c_\alpha > 0.03$ mol/l is an additional reason for a decreasing equilibrium swelling. It results from the screening effect of the counter ions, i.e. SO_4^{2-}, which shield the charges on the polymer chains and prevent their efficient repulsion. Fig. 18b (curves 1 and 2) shows the sensor output characteristics obtained for two sensors with hydrogel layers of nearly the same cross-linking degree (i.e. nearly the same content of the cross-linking agent in the polymer and the same irradiation time) but with different concentrations c_g of ionizable groups ($c_{g1} > c_{g2}$) in the gels 4 and 1a (Table 2). One observes that the sensitivity S_1 is higher than S_2.

In order to provide the required high signal reproducibility of the sensors, a regenerating procedure before every measurement was carried out in order to achieve a certain reference sensor signal. An appropriate rinsing solution was chosen for a certain combination of analyte and polymer. A mixture of the phosphate buffer saline (PBS, 10 mg/ml) yielding pH = 7.3 and 0.01 mol/l EDTA was found as a suitable rinsing solution for the P2VP-block-P(NIPAAm-co-DMIAAm) gel after measurements in solutions with metal ions.

Additionally, it should be noted that the pH value of the solution has a significant influence on the binding capacity of metal ions to amino groups. At low pH values, the metal ions cannot strongly affect the phase transition temperature of the gel. This is due to the protonation of the amino groups, which disrupts the interaction with metal ions (Oktar et al. 2005; Kuckling and Pareek 2003; Wang and Wang 2006; Chang et al. 2006). The absorption capacity of the hydrogels is important for the detection of metal ions in biological systems and for environmental monitoring of heavy metal ions. The functionalised hydrogels are widely used as chelating agents, as sorbents in such technical processes as electroplating, removal of toxic metal ions from waste-water, purification of sewage and drinking water.

5 Summary

We have demonstrated the operational principle of hydrogel-based piezoresistive chemical sensors. In order to realize chemical sensors, the polyelectrolyte as well as neutral gels were used as chemo-mechanical transducers. The hydrogel swelling leads to a bending of a thin silicon plate and, by this, to an electrical output voltage of the sensor chip. Combining a hydrogel and a micro fabricated pressure sensor chip allowed to continuously monitor the analyte-dependent swelling of a hydrogel in aqueous solutions. The sensitivity of hydrogels with regard to the concentration of such additives as H^+-ions (pH sensor), transition-metal ions, salts and organic compounds in water was investigated. It has been demonstrated that the sensitivity depends on the polymer composition as well as on the polymer cross-linking degree. A higher sensitivity was observed for polyelectrolyte hydrogels with higher concentrations of ionizable groups.

Changes in the composition of thermo-shrinking *N*-isopropylacrylamide (NIPAAm) copolymer gels have allowed to vary the gel *volume phase transition temperature* (T_{cr}) from 22 °C for P4VP-block-P (NIPAAm-co-DMIAAm) to 43 °C for PNIPAAm-DMIAAm-DMAAm terpolymer. This possibility for variations of the working temperature range is particularly relevant with respect to possible applications of the chemical sensors. It was shown that the phase transition of the gel is influenced by the ion concentration in aqueous solutions as well as by the viscosity of the solution. By this, we have demonstrated that multiresponsive smart hydrogels are promising materials for a rheochemical characterization of solutions.

Because the gel response is typically diffusion-driven, the time response of the volume change approximately follows the square of the sample dimension. Scaling to micro-dimensions enhances the time response. Consequently, a reduction of the sample size improves the sensor performance. Time constants down to a few ten seconds have been found for thin hydrogel films deposited directly on the backside of the silicon bending plate. In order to achieve an optimum between sensor signal amplitude and sensor response time, the gel swelling/deswelling kinetics was investigated. It was found that the sensor response time and signal reproducibility is limited by the visco-elastic and hysteresis behaviour of the polymer material. Some methods improving the properties of the chemical sensors have been proposed. An analysis of the measured swelling/deswelling kinetic curves by means of appropriate models allowed to essentially shorten the measuring time which is necessary to determine the additive concentration in a solution.

Beside sensitivity and response time, signal reproducibility and long-term stability are the most crucial aspects for a successful sensor implementation. Since the sensor chips show excellent stable properties, the long-term stability of the sensor is solely determined by the stability of the hydrogel characteristics. The polymer film preparation conditions and measurement conditions, which are necessary for high signal reproducibility and high long-term stable sensor sensitivity, were determined. In order to provide the required high signal reproducibility of the sensors, two

procedures were carried out: (1) an initial gel conditioning procedure consisting of a gel swelling in de-ionized water and a subsequent deswelling/swelling cycling, and (2) a regenerating procedure before every measurement in order to achieve a certain reference sensor signal. The long-term measurements have shown that the life time of piezoresistive chemical sensors can be prolonged up to several years provided that specific operation and storage conditions are fulfilled.

Acknowledgments The authors gratefully acknowledge the support for this work from the Deutsche Forschungsgemeinschaft (Collaborative Research Center (SFB) 287).

References

Arndt K-F, Richter A, Ludwig S, Zimmermann J, Kressler J, Kuckling D, Adler H-J (1999) Poly (vinyl alcohol)/poly(acrylic acid) hydrogels: FT-IR spectroscopic characterization of cross-linking reaction and work at transition point. Acta Polym 50:383–390

Arndt K-F, Kuckling D, Richter A (2000) Application of sensitive hydrogels in flow control. Polym Adv Technol 11:496–505

Arndt K-F, Knörgen M, Richter S, Schmidt T (2006) NMR Imaging: monitoring of swelling of environmental sensitive hydrogels. In: Webb GA (ed) Modern magnetic resonance: Applications in chemistry, vol.1 Springer, Berlin

Atkins PW (1990) Physical Chemistry. Oxford Press, Oxford

Bashir R, Hilt JZ, Elibol O, Gupta A, Peppas NA (2002) Micromechanical cantilever as an ultrasensitive pH microsensor. Appl Phys Lett 81(16):3091–3093

Benoit D, Chaplinski V, Braslau R, Hawker CJ (1999) Development of a universal alkoxyamine for "living" free radical polymerizations. J Am Chem Soc 121:3904–3920

Caykara T, Kiper S, Demirel G (2006) Thermosensitive poly(N-isopropylacrylamide-co-acrylamide) hydrogels: synthesis, swelling and interaction with ionic surfactants. Eur Polymer J 42:348–355

Chang Y-C, Chang S-W, Chen D-H (2006) Magnetic chitosan nanoparticles: Studies on chitosan binding and adsorption of Co(II) ions. React Funct Polym 66:335–341

Cong J, Zhang X, Chen K, Xu J (2002) Fiber optic Bragg grating sensor based on hydrogels for measuring salinity. Sens Actuat B 87:487–490

Crank J (1970) The Mathematics of Diffusion. Oxford Univ Press, London

Gerlach G, Guenther M, Suchaneck G, Sorber J, Arndt K-F, Richter A (2004) Application of sensitive hydrogels in chemical and pH sensors. Macromol Symp 210:403–410

Gerlach G, Guenther M, Sorber J, Suchaneck G, Arndt K-F, Richter A (2005) Chemical and pH sensors based on the swelling behavior of hydrogels. Sens Actuat B 111–112:555–561

German Patent DE 10 2006 027 051.7 A1, 10.06.2006

German Patents DE 101 29 985C2, DE 101 29 986C2, DE 101 29 987C2, June 12, 2001

Guenther M, Gerlach G, Sorber J, Suchaneck G, Arndt K-F, Richter A (2005) pH sensors based on polyelectrolytic hydrogels. In: Bar-Cohen Y (ed) Proceedings of the SPIE, Smart structures and materials: electroactive polymer actuators and devices, San Diego, 5759: 540–548

Guenther M, Gerlach G, Kuckling D, Kretschmer K, Corten C, Weber J, Sorber J, Suchaneck G, Arndt K-F (2006) Chemical sensors based on temperature-responsive hydrogels. In: Inaudi D, Ecke W, Culshaw B, Peters K J, Udd E (eds) Proceedings of the SPIE, Smart structures and materials 2006: smart sensor monitoring systems and applications, San Diego, 6167: 61670T1–61670T11

Guenther M, Gerlach G, Wallmersperger T (2007a) Modeling of nonliniar effects in pH sensors based on polyelectrolytic hydrogels. In: Bar-Cohen Y (ed) Proceedings of the SPIE, Electroactive polymer actuators and devices. SPIE Press, San Diego, CA, 6524: 6524171–65241711

Guenther M, Kuckling D, Corten C, Gerlach G, Sorber J, Suchaneck G, Arndt K-F (2007b) Chemical sensors based on multiresponsive block copolymer hydrogels. Sens Actuat B 126:97–106

Guenther M, Gerlach G, Corten C, Kuckling D, Müller M, Shi Z, Sorber J, Arndt K-F (2007c) Application of polyelectrolytic temperature-responsive hydrogels in chemical sensors. Macromol Symp 254:314–321

Guenther M, Gerlach G, Corten C, Kuckling D, Sorber J, Arndt K-F (2008) Hydrogel-based sensor for a rheochemical characterization of solutions. Sens Actuat B 132(2):471–476

Harmon ME, Kuckling D, Frank CW (2003) Photo-cross-linkable PNIPAAm copolymers. 5. Mechanical properties of hydrogel layers. Langmuir 19:10660–10665

Herber S, Eijkel J, Olthuis W, Bergveld P, van den Berg A (2004) Study of chemically induced pressure generation of hydrogels under isochoric conditions using a microfabricated device. J Chem Phys 121:2746–2751

Hoffmann J, Plötner M, Kuckling D, Fischer W-J (1999) Photopatterning of thermally sensitive hydrogels useful for microactuators. Sens Actuat 77:139–144

Houbenov N, Minko S, Stamm M (2003) Mixed polyelectrolyte brush from oppositely charged polymers for switching of surface charge and composition in aqueous environment. Macromolecules 36:5897–5901

Hüther A, Xu X, Maurer G (2004) Swelling of *n*-isopropyl acrylamide hydrogels in water and aqueous solutions of ethanol and acetone. Fluid Phase Equilib 219:231–244

Krause T, Habicher WD, Messerschmidt M, Voit BI (2004) A novel method for the synthesis of alkoxyamine initiators for nitroxide-mediated radical polymerization using $Mn(OAc)_3$ as electron-transfer reagent. Design Monom Polym 7(4):391–397

Kuckling D, Pareek P (2003) Synthesis of transition-metal-ion-selective poly(N-isopropylacrylamide) hydrogels by the incorporation of an aza crown ether. J Polym Sci A 41:1594–1602

Kuckling D, Adler H-J P, Ling L, Habicher WD, Arndt K-F (2000) Temperature sensitive polymers based on 2-dimethylmaleinimido)-N-ethyl-acrylamide: copolymers with N-isopropylacrylamide. Polym Bull 44:269–276

Kuckling D, Harmon ME, Frank CW (2002) Photo-cross-linkable PNIPAAm copolymers. 1. Synthesis and characterization of constrained temperature-responsive hydrogel layers. Macromolecules 35:6377–6383

Kuckling D, Richter A, Arndt K-F (2003a) Temperature and pH dependent swelling behavior of poly(*N*-isopropyl-acrylamide)-copolymer hydrogels and their use in flow control. Macromol Mater Eng 288:144–151

Kuckling D, Hoffmann J, Plötner M, Ferse D, Kretschmer K, Adler H-J P, Arndt K-F, Reichelt R (2003b) Photo cross-linkable poly(N-isopropylacrylamide) copolymers III: micro-fabricated temperature responsive hydrogels. Polymer 44:4455–4462

Kumar V, Chaudhari CV, Bhardwaj YK, Goel NK, Sabharwal S (2006) Radiation induced synthesis and swelling characterization of thermo-responsive N-isopropylacrylamide-co-ionic hydrogels. Europ Polym J 42:235–246

Lei M, Baldi A, Nuxoll E, Siegel RA, Ziaie B (2006) A hydrogel-based implantable micromachined transponder for wireless glucose measurement. Diabetes Techn Therap 8(1):112–122

Liu X, Zhang X, Cong J, Xu J, Chen K (2003) Demonstration of etched cladding fiber Bragg-grating-based sensors with hydrogel coating. Sens Actuat B 96:468–472

Nickolov ZS, Miller JD (2005) Water structure in aqueous solutions of alkali halide salts: FTIR spectroscopy of the OD stretching band. J Colloid Interface Sci 287:572–580

Oktar O, Caglar P, Seitz WR (2005) Chemical modulation of thermosensitive poly(N-isopropylacrylamide) microsphere swelling: a new strategy for chemical sensing. Sens Actuat B 104:179–185

Orakdogen N, Okay O (2006) Reentrant conformation transition in poly(N, N-dimethylacrylamide) hydrogels in water-organic solvent mixtures. Polymer 47:561–568

Panayiotou M, Freitag R (2005) Influence of the synthesis conditions and ionic additives on the swelling behaviour of thermo-responsive polyalkylacrylamide hydrogels. Polymer 46:6777–6785

Richter A, Kuckling D, Arndt K-F, Gehring T, Howitz S (2003) Electronically controllable microvalves based on smart hydrogels: magnitudes and potential applications. J Microelectromech Syst 12(5):748–753

Richter A, Howitz S, Kuckling D, Arndt K-F (2004a) Influence of volume phase transition phenomena on the behavior of hydrogel-based valves. Sens Actuat B 99:451–458

Richter A, Bund A, Keller M, Arndt K-F (2004b) Characterization of a microgravimetric sensor based on pH sensitive hydrogels. Sens Actuat B 99(2–3):579–585

Saito S, Konno M, Inomata H (1993) Volume phase transition of N-alkylacrylamide gels. In: Dusek K (ed) Responsive gels: volume transitions I. Springer, Berlin

Vo CD, Kuckling D, Adler H-J P, Schönhoff M (2002) Preparation of thermosensitive nanogels by photo-cross-linking. Colloid Polym Sci 280:400–409

Wallmersperger T (2003) Modellierung und Simulation stimulierbarer polyelektrolytischer Gele. Fortschritt-Berichte VDI, Reihe 5, Nr. 688, VDI-Verlag, Düsseldorf

Wallmersperger T, Kröplin B, Gülch RW (2004) Coupled chemo-electro-mechanical formulation for ionic polymer gels - numerical and experimental investigations. Mech Mater 36(5–6):411–420

Wang C-C, Wang C-C (2006) Adsorption characteristics of metal complexes by chelated copolymers with amino group. React Funct Polym 66:343–356

Wohlrab S, Kuckling D (2001) Multisensitive polymers based on 2-vinylpyridine and N-isopropylacrylamide. J Polym Sci A 39:3797–3804

Hydrogels for Biosensors

G.A. Urban and T. Weiss

Abstract Hydrogels are valuable materials for use in biosensors. They can be used for immobilization as well as for creating protecting layers controlling diffusion and enhancing biocompatibility. Highly stable biosensors use hydrogels for entrapment of enzymes on microelectrodes. The stability of enzymes in hydrogel membranes for biosensors can be enhanced by choosing the right microenvironment using micro-hydrogels. The thermodynamic stability of the entrapped enzymes in micro-gels can be characterized via differential scanning calorimetry (nano-DSC). Hydrogel-based biosensors were characterized by nano-DSC showing that hydrogel membranes are excellent for creating long-term stable enzyme biosensors. Additionally, smart hydrogels can be used as stimuli responsive materials enabling sensing as well as actuating performance.

Keywords Multi-analyte biosensor • Microelectrode-array • Enzyme immobilization • Enzyme stability • Differential scanning calorimetry (DSC) • Chip-calorimeter

Contents

G.A. Urban (✉)
Institute for Microsystems Technology (IMTEK), Freiburg Institute for Advanced Studies, University of Freiburg (FRIAS), Germany
e-mail: urban@imtek.de

T. Weiss
Institute for Bioprocessing and Analytical Measurement Techniques, Bad Heiligenstadt, Germany

G. Gerlach and K.-F. Arndt (eds.), *Hydrogel Sensors and Actuators*,
Springer Series on Chemical Sensors and Biosensors 6,
DOI: 10.1007/978-3-540-75645-3_6, © Springer-Verlag Berlin Heidelberg 2009

Abbreviations

3D	Three dimensional
AA	Acrylamid
BIS	N,N´-methylene bisacrylamide
bipy	2,2´-Bipyridine
CaM	Calmoduline
Co	Cobalt
CPZ	Chlorpromazine
DSC	Dynamic scanning calorimetry
FAD	Flavine adenine dinucleotide
GndHCl	Guanidinium hydrochloride
GOx	Glucose oxidase
HEMA	Hydroxyethyl methacrylate
LC	Liquid crystal
Med_{ox}	Electrochemical active mediator (oxidized form)
MEMS	Micro electro mechanical systems
N	Number of electrons
Os	Osmium
PAAm	Poly(acrylamide)
PBS	Phosphate buffered saline
PCB	Printed circuit board
PDMS	Poly(dimethylsiloxan)
PECVD	Plasma enhanced chemical vapour deposition
PEG-3000	Poly(ethylene glycol) of molecular weight 3000 g/mol
pHEMA	Poly(hydroxyethyl methacrylate)
PVA	Poly(vinyl alcohol)
Ru	Ruthenium
TEGDMA	triethylene glycol dimethacrylate
TEMED	N,N,N′,N′-tetramethyl ethylenediamine
vinpy	4-Vinylpyridine

Symbols

A	Electrode area
c^{s}	Analyte concentration
D_{S}	Diffusion coefficient of analyte s
δ_{N}	Nernst layer thickness
$\Delta^{\mathrm{D}}{}_{\mathrm{N}}G$	Free energy of denatutration
$\Delta^{\mathrm{D}}{}_{\mathrm{N}}H$	Enthalpy of denatutration
$\Delta^{\mathrm{D}}{}_{\mathrm{N}}S$	Entropy of denatutration
$\Delta^{\mathrm{D}}{}_{\mathrm{N}}C$	Heat capacity of denatutration
F	Faraday constant
I_{d}	Diffusional current
N	Number of electrons
T	Temperature
T_{m}	Denaturation temperature

1 Introduction

Progress in medical science has led to tremendous enhancement of quality of life. This is mainly attributed to improved pharmaceutical and biomedical engineering technologies in hospital as well as for home care monitoring. All of these innovations become possible with the development of high-tech instrumentation. Among such instrumentation two different strategies were the development of large-sized high-tech imaging and therapeutic instruments and the introduction of miniaturized smart systems for analytical and therapeutic treatments. Such smart devices are called biomicrosystems with the prominent example of microbiosensors (Urban 2006; Bashir 2004). One example is the miniaturized glucose biosensors for home care, which enables a tailored therapy for diabetic patients. Such metabolic sensors combine biological sensing elements with microtransducers. The increasing demand for monitoring of environmental conditions in the field of biosecurity, especially of pollutants and biohazardous substances, can certainly be met only with networks of distributed miniaturized and highly selective biosensors (Ligler 2006). The combination of biological substances such as enzymes, whole cells or antibodies on a microsystem poses the problem of immobilization of such biomolecules in a microsystem. One important example of an immobilization matrix of biomolecules and whole cells are hydrogels. Hydrogels are hydrophilic polymeric networks that are able to absorb a large quantity of water and were originally developed for biomedical applications (Wichterle and Lim 1960). Hydrogels possess a high degree of flexibility as a function of the water content similar to that of natural tissues. Common ingredients of hydrogels are e.g. polyvinyl alcohol, sodium polyacrylate, methacrylate polymers and copolymers with an abundance of

hydrophilic groups. Also natural hydrogel materials have been investigated as polymeric immobilization matrices including agar, gelatine, agarose, methylcellulose, hyaluronic acid and other naturally derived polymers.

Hydrogels act in biosensors not only passively as immobilization matrix but also as responsive (smart) material. Current uses for smart hydrogels in the bioanalytical and biomedical field are

- Hydrogels as scaffold material in tissue engineering which contain human cells in order to repair tissue (Tsang and Bhatia 2004; Cushing and Anseth 2007)
- Hydrogels sensitive to environmental changes (pH, temperature, metabolite concentration) responding with swelling and eventually release of their payload drug (Guiseppi-Elie et al. 2002)
- Bio-smart hydrogels that are responsive to specific molecules (e.g. glucose, antigens) can be used as biosensors as well as in smart drug release (Brahim et al. 2002; Ulijn et al. 2007)
- Hydrogels as antifouling coatings that prevent protein absorption (Tirrell et al. 2002)
- Diffusion barriers: analytes and the reaction products are transported while diffusion of interferents to the microtransducer is prevented (Jobst et al. 1996a)

In this chapter, the focus is laid on biosensor principles and a short introduction into hydrogels as immobilization matrix for enzymes is given. Measurement methods for investigating the long-term stability of used enzymes will be presented and finally smart applications of hydrogels combining sensor and therapeutic attributes will be discussed.

2 Biosensor Devices

Biosensors measure selectively and reversibly the concentration of a biochemical substance without any other instrument or additional reagents. A definition of biosensors is given by IUPAC: “A biosensor is a self-contained reversible integrated device using a biological recognition element which is retained in direct spatial contact with a transduction element” (Thevenot et al. 2001). This definition shows the double (twin) aspect of biosensors: on one hand the world of biorecognition and on the other hand the field of technical transducers. As biological recognition elements are used:

- Enzymes
- Antibodies
- Nucleic acids
- Whole cells

with enzymes as most prominent biocomponents. These biological entities are combined with the following transduction principles:

- Electrochemical
- Optical
- Thermometric or
- Gravimetric transducers
- Mechanical.

The most important ones are electrochemical and optical methods.

Therefore, a variety of different biosensors for each adequate application can be realized. In the year 1962 the first biosensor was introduced by Clarke and since that biosensor research made considerable progress (Clark et al. 1962; Clark et al. 1984; Turner et al. 1987; Nakamura and Karube 2003; Wilson and Gifford 2005). Chiefly miniaturized glucose sensors faced an immense boom due to monitoring of diabetics at home with an inexpensive diagnostics instrument allowing a more precise adjustment of insulin.

3 Enzyme Biosensors

The most important biosensors use enzymes as biological sensor elements. An enzyme is a protein that accelerates or catalyses a biochemical reaction. It can be used in biosensors when the enzyme catalyses the conversion of an analyte to a molecule which can be measured by a microtransducer. Enzymes are usually very selective to their substrate molecules. The catalytic reaction is set off by binding of the substrate to the enzymes active site. Enzymes can speed up chemical reactions by up to a million times, but function only within a narrow temperature and pH range, outside of which they will be destabilized, lose their structure and become denatured. The binding lowers the activation energy of the chemical transformation by bringing together the reactants in a favourable orientation. Thus, the extreme selectivity to a given substrate and the high effectiveness in increasing the rate of a biochemical reaction enable enzymes to combine recognition with amplification necessary for precise sensors. The most important enzymes for biosensors are redox enzymes (oxidases, dehydrogenases, etc.) because they catalyse electron transfer reactions, which can be coupled with microelectronic transducers.

The most commonly employed enzyme used for glucose biosensors is glucose oxidase (GOx). GOx catalyses the oxidation of glucose to gluconolacton and hydrogen peroxide. Oxygen is needed as a co-substrate for transferring the enzyme back to the initial state. The produced hydrogen peroxide is electrochemically measured at the electrode (Eq. 1).

$$\text{Glucose} + O_2 \rightarrow \text{enzyme(GOx)} \rightarrow \text{gluconolactone} + H_2O_2 \qquad (1)$$

The prosthetic group of Glucose oxidase (GOx) for accepting electrons from glucose is flavine adenosine di-nucleotide (FAD) (Eq. 2). The reduced flavine is reoxidized in a subsequent step by ambient oxygen (Eq. 3).

$$\text{Glucose} + \text{FAD} \rightarrow \text{gluconolactone} + \text{FADH}_2 \quad (2)$$

$$\text{FADH}_2 + \text{O}_2 \rightarrow \text{FAD} + \text{H}_2\text{O}_2 \quad (3)$$

Besides electrochemical methods, the hydrogen peroxide can also be measured with optical methods. Recently, glucose estimation was done according the Saifer-Gerstenfield method using optical readout and the enzyme peroxidase:

$$\begin{aligned} \text{H}_2\text{O}_2 + o\text{-dianisidine} &\rightarrow \text{peroxidase oxidation} \\ &\rightarrow \text{H}_2\text{O} + \text{oxidized chromogen} \end{aligned} \quad (4)$$

Optical readout needs sophisticated optical elements, which are cost-intensive and not easy to miniaturize. Due to this fact, the recent revolution of the home care market was achieved with miniaturized disposable electrochemical sensors.

4 Immobilization of Enzymes and Whole Cells Via Hydrogel Encapsulation

For any enzymatic biosensor application, the right immobilization is the crucial point to get reliable sensor readouts. There are different immobilization procedures available. The simplest one is the adsorption of enzymes on electrodes which yield high efficient catalyzation of glucose but is only applicable for single-use devices. Yet, such devices were commercially very successful (Pollmann et al. 1994; Ek 2004).

Covalent attachment of enzymes to solid supports exhibit highly stable enzyme immobilizations, with reduced activity however. The sensitivity of such sensors is limited because only monolayers of enzyme molecules can be produced.

Cross-linking enzymes with e.g. glutardialdehyd and co-immobilization with bovine serum albumin yield thick and stable enzyme layer, with mediocre reproducibility however. The principal obstacle to immobilize proteins is that the conformational state of many proteins is very labile and unable to withstand the conditions used for deposition and patterning on solid surfaces.

One approach to develop more biologically compatible surfaces for immobilizing proteins is to incorporate a matrix, such as a hydrogel, as an interface between the protein and the solid surface (Burnham et al. 2006). The entrapment of enzymes in a hydrogel layer provides excellent long-term stability and the possibility to adjust the polymer matrix to the specific needs of a certain enzyme. Hydrogels are useful for linking proteins to solid surfaces because their hydrophilic nature and porous structure can help to keep these labile molecules in the native functional state.

Three-dimensional hydrogels provide a suitable matrix for biomolecule immobilization because they

- Have an increased capacity for the immobilization of proteins by enlarging the surface matrix
- Have a network conducive to ligand diffusion and binding to occur
- Show minimum auto-fluorescence and in general no electrochemical activity
- Are photo-cross-linkable and photo-patternable

In particular, 3D hydrogels provide free range of motion for the immobilized biomolecule, potentially promoting increased interaction with the target ligands, if these ligands are able to diffuse to the site of interaction. It also creates an environment that is stable, biocompatible and simulates a solution-phase system. It became evident that the binding kinetics between protein–ligand pairs and the diffusion of biomolecules in a 3D hydrogel matrix can be affected by the hydrogel porosity and hydrogen bonding between the network and the biomolecules.

Especially for the production of microbiosensors, the spatial control of the enzyme immobilization is very important. Hydrogels can be structured using a photochemical approach. Polymerisation of suitable monomers with UV-light can be used to cover microelectrodes with hydrogel layers. Precursors of the monomers together with a photoinitiator can be polymerised in the presence of enzymes. In an alternative approach a prepolymerised polymer is functionalised with methacrylic side-chains to yield a polymer that is cross-linkable with UV-light (Yu et al. 1995). This approach is very interesting for the immobilization of whole cells as well. Here the biocompatibility of the used polymers is very important. Biopolymers like hyaluronic acid, gelatine and alginate are interesting candidates for immobilization matrices and they have been modified with methacrylic or cinnamyl side groups to become photo-cross-linkable (23). Important parameters for the proper choice of polymer are the hydrophilicity and water-solubility to be compatible with enzyme solutions or cell suspensions. This is also important for additives used in the precursors for adjusting their viscosity to the needs of photolithography. Suitable additives are poly (vinyl alcohol) (PVA), polymeric sugars like Ficoll^{TM} or dextran and poly (ethylene glycol) (PEG) and pHEMA (Angenendt et al. 2003; Barsky et al. 2003). In summary, it was shown that low-water-content hydrogels exhibit excellent properties for spatial controlled enzyme immobilization in microsystems.

5 Whole-Cell-Based Hydrogel Biosensors

In tissue- or cell-based biosensors, changes in the physiology of the cells are monitored making it possible to detect a broad range of known and unknown agents (Bousse 1996; Lei et al. 2006).

There are a lot of advantages of whole cells over isolated enzymes and antibodies: whole cells and tissues are a source of a large quantity of enzymes in their natural environment where enzymatic pathways are already optimised and all cofactors, substrates and reactants are available. Also the stability of the enzyme is not compromised by purification steps, which can be expensive and decrease the

biological activity of the protein. The use of whole-cell biosensors permits the detection of various groups of substances via the overall metabolism of the cell.

Whole-cell biosensors use either prokaryotic cells (e.g. bacteria) or simple eucaryotic cells (yeasts) (Elad et al. 2008). Bacterial and cell biosensors rely on the ability of cells to produce a detectable signal that can serve as a reporter of a particular environmental condition. Constitutive reporter cells produce a constant measurable signal and the toxicity of a sample is estimated from the inhibition of this signal. Inducible reporter microorganisms are usually more specific in their performance as they are based on a reporter gene fused to an inducible promoter that is activated by a target compound or stress response. They use genetically engineered strains with luminescence reporter genes (*luxAB, luc*) for detection of organic contaminants such as benzene, toluene, naphthalene and metal ions (e.g. copper, lead) (Applegate et al. 1998; Fine et al. 2006).

Bioluminescent protein expression requires cofactor or substrate addition. This is disadvantageous. An alternative to bioluminescence is the use of green fluorescent proteins (GFP) without addition of cofactor. GFPs can be used in combination with multiphenotypic biosensors to measure up-regulation of gene expression (Chalfie et al. 1994). However, as with the *lux* system, the use of GFP relies on the ability to know which specific gene or protein to monitor and then to generate the relevant transfected cell line. This can be advantageous for screening drug candidates, but is not necessarily applicable for cell viability determination.

Therefore, a time- and cost-efficient approach is the use of small fluorescent molecules. For example, calcein AM can be used for optical whole-cell biosensors for the detection of toxins and drug candidates. Loading cells with the fluorescent dyes occurs under an hour. Calcein AM is a cell-permeant dye fluorescent active in the presence of esterases in viable cells. Upon cell death calcein ceases to fluorescence (Itle and Pishko 2005).

Hydrogels like poly (ethylene glycol) gels are an optically transparent in vivo-like environment. The transparent nature of hydrogels makes them suitable for optical signal transduction and readout and also for array technology used in HTS-screening (High-Throughput Screening).

The largely unresolved concern of the shelf-life of such whole-cell sensors is not addressed in many reports. It is still a challenge to storage a reporter cell at ambient temperatures for prolonged periods with maintained response characteristics and without the need for re-growing the cells. An immobilization matrix for cells must allow the cells to keep alive and active. Hydrogels can do this by mimicking the natural cellular environment. The attractiveness of hydrogels is a function of their ability to provide a stable fluid environment and that they can be formulated with a wide range of physical and chemical properties. A high porosity of the matrix is necessary to allow for the rapid diffusion transport of nutrients, cell wastes and analyte molecules. In flow sensor systems a stable material with a high mechanical integrity is required to provide protection to the cells from shear forces, external stresses and environment conditions. Cell-compatibility refers to a non-cytotoxic material that is able to support cell attachment and adhesion. Although PAAm gels has been used for cell encapsulation (Fesenko et al. 2005), in principle biopolymer

gels are more apt because acrylic monomers are cytotoxic. Some of the strategies developed for the stabilization of enzymes are also suitable for whole cells. Normally, each cell type has its own formulation requirements (Bjerketorp et al. 2006). Commonly used is agar. Immobilization in nutrient agar enabled the preservation in microtiter plates of different strains of toxicity-sensing *E. coli* for 2 weeks (Kim and Gu 2003) and one strain of *Salmonella typhimurium* for up to 6 weeks (Park et al. 2005). Another frequently used hydrogel matrix for whole-cell encapsulation matrix is alginate, which can be cross-linked with divalent cations into a highly porous meshwork. Polyiak et al. used modified alginate for encapsulation of a recombinant, bioluminescent genotoxicity-responsive *E. coli* strain, which remained responsive for several weeks (Polyak et al. 2004). Macroporous PVA hydrogels produced by cryogelation at −20°C are used as well for stabilizing immobilization of cells for biosensor applications (Philp et al. 2003).

6 Amperometric Biosensors

Most of the biosensor devices use an electrochemical transducer method and almost all commercially available biosensors are amperometric enzyme biosensors (Heller 1996). The standard biosensor is an enzyme biosensor with an amperometric transduction principle. This enzyme catalyses the conversion of an analyte to an electrochemically active product which can be oxidized or reduced at a working electrode. By applying a specific potential between counter and working electrode a reaction on the working electrode is induced and yields a current which is proportional to the concentration of such species. There are two possibilities of amperometric measurement: The first one is the cathodic reduction which is applied in, e.g., oxygen detection, the second method is the anodic oxidation which is the underlying principle of, e.g., H_2O_2 determination. The overall current is the sum of all currents caused by all electro-active species for an applied potential. In order to achieve selectivity, it is important to prevent interfering responses. Different strategies can be applied:

- Selection of an appropriate redox potential or using redox soluble mediators or redox polymers (see Sect. 7)
- Selective transduction of the desired signal by using the selectivity of a biologically selective moiety
- Selective mass transport through permselective hydrogel membranes

The electrochemical electrode reaction oxidizing H_2O_2 is an anodic reaction on platinum (+ 0.6V vs. Ag /AgCl): The signal is represented by current I_d and is directly proportional to the concentration c^S of the analyte in the sample following the first Fick´s law:

$$I_d = n \cdot A \cdot \mathrm{F} \cdot D_S \cdot \frac{c^S}{\delta_N} \tag{5}$$

with A the area of the electrode, D_S the diffusion coefficient of the analyte S, c^S the concentration of the analyte in solution, δ_N the thickness of the stagnant (Nernst) layer, F the Faraday constant, and n the number of exchanged electrons.

As can be seen from Eqs. (5), (2) and (3), the reaction of electrochemical enzyme-based biosensors relies on different mechanisms: the right transport of substrate, co-substrate and products. For venous blood measurements or in vivo applications the proper transport of oxygen is not maintained. Therefore, new microgel formulation has to be used based on functionalised polymers.

7 Redox Polymers

For home care monitoring discrete measurements of blood glucose concentrations up to five times per day are required (Group TDCaCTR 1993). Therefore, reliable and easy-to-use disposable sensor devices were developed using adsorption procedures and screen-printing technologies. Historically, the first devices were based on optical principles but the easy-to-use electrochemical one-shot devices entered the market very quickly. However, one of the problems is related to the oxygen supply for the GOx reaction (Eq. (1)) which can be cumbersome for venous blood sampling. Also the catalytic behaviour of the electrochemical transduction element can be limiting. This can be overcome by using electrochemically active mediators for replacing oxygen which is now state of the art for disposables (Abruna 1988; Chen et al. 2001; Kaneko and Wöhrle 1988; Murray 1984):

$$\mathrm{FADH_2} + \mathrm{Med_{ox}} \rightarrow \text{electrode} \rightarrow \mathrm{FAD} + \mathrm{Med_{red}}. \tag{6}$$

As mediators different molecules can be applied, e.g. ferrocene, ruthenium (III) hexamine or tetrathiafulvalene, which are reoxidized on an electrochemical electrode, preferably carbon (Cass et al. 1984). Such electrochemical working principle allows the miniaturization of a biosensor using screen-printed or thin-film electrodes with adsorbed or immobilized enzymes also facilitating mass production for creating disposable glucose sensors with revenues of several million euros per anno.

In contrast to mediators, also redox polymers can be used. These polymers are mainly characterized by the presence of specific electrochemically active sites. There are different possibilities to facilitate redox transfer: by shuttling electrons via redoxactive groups in non-conductive or conductive polymers. In general, a redox polymer consists of a system where a redoxactive molecule is covalently bound to a polymer backbone which may or may not be electroactive. Frequently, electroactive polymers are formed by the electropolymerization of suitable monomer complexes. A few representative examples of electron shuttle molecules are shown in Fig. 1.

The interest in these polymers has been accelerated by their applicability in the area of chemically modified electrodes (Abruna 1988; Kaneko and Wöhrle 1988). Especially biosensor applications are very interesting applications for redox polymers

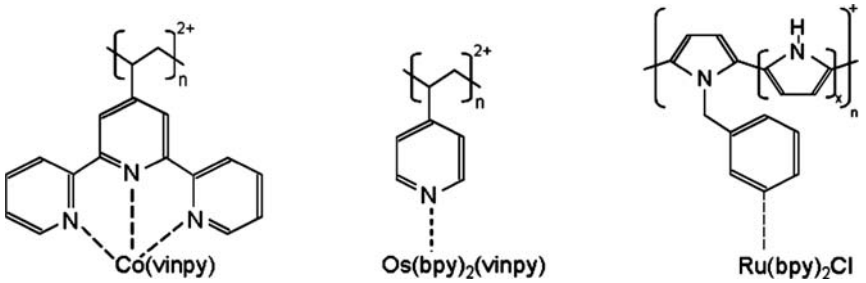

Fig. 1 Redox polymers

because of high sensitivities and the minor influence of co-substrate availability (Heller 2006). One goal of coating electrodes with electro-active polymers is the development of new materials with catalytic properties. The majority of the work deals with systems where the polymer itself is inert and serves only as a support for the electro-catalytic metal sites. The electrocatalytic molecule functions as a mediator, facilitating the transfer of electrons between the electrode and the enzyme substrate. For amperometric electrodes electrocatalysis is of outstanding importance because the electrochemical reactions can be driven selectively and at lower potentials. One possibility is to use modified electrodes by embedding electrocatalytic transition metal species in a polymermodified electrode matrix which is a proper method of facilitating electron transfer and to endow the electrode with the immobilized molecule (Murray 1984). A number of additional advantages include:

- Better control of the reaction rate by the applied potential
- Close proximity of the polymerembedded electrocatalytic sites to the electrode,
- High 3D concentration of active centres
- Possible cooperative effects stemming from the proximity of other catalyst sites

Unlike the electronically conducting polymers, redox polymers characteristically exhibit conductivity only over a very narrow potential range, with maximum conductivity occurring when the concentrations of the oxidized and reduced forms are equal in the film, i.e. at the formal potential of the redox centres.

The details of charge transport between the electrode and the supported redox sites are fundamental considerations. It is commonly held that redox conduction in polymers occurs by the electron hopping process proposed by Kaufman and co-workers (Kaufman et al. 1980) whereby electron transfer proceeds as a process of sequential self-exchange steps between adjacent redox groups. Since electroneutrality in the film must be maintained, the generation of charge at the electrode and the motion of the charge throughout the polymer must be balanced by counterions. Full characterization should consider both electronic and ionic conductivities of the material. Similar consideration can be assumed for electric conductive polymers where also a phonon hopping process with neutralizing counterions occurs. The increasing interest in redox polymers was induced by using such polymers for in vivo applications.

8 Multi-Analyte Monitoring Devices

Despite that a considerable amount of research has been attributed to the development of a microminiaturized implantable glucose sensor, to date there is no clinically applicable concept for monitoring glucose to get information for a closedloop insulin therapy – such devices are not feasible to perform long-term measurements till now. Stability of sensors as well as biocompatibility issues have not been solved in the last decades. Short-term monitoring applications are possible, but with only retrospective analysis of glucose values and no direct link to therapy. Accuracy and precision of such short-term implantable sensors exhibit not the standard used in clinical chemistry. Nevertheless, the use of short-term monitoring devices for investigating metabolic states of the body remains useful for diagnostics beyond glucose monitoring.

In all cases such biosensor devices have to be further miniaturized and optionally implemented within a microfluidics. For functional monitoring of multi-metabolic parameters, for system biology and much more pronounced for clinical applications biosensor arrays (Urban et al. 1990; Urban et al. 1998) with integrated microfluidics have to be used (Jobst and Moser 2006). In such a way analyte volumes in the nanoliter range can be analysed fast, reliable and with excellent long-term stability. Such task can be achieved using advanced immobilization techniques as enzyme entrapment in photo-patterned multistack hydrogel membranes (Fig. 2). The immobilization of the biocomponents can be done in a photolithography process or by nano-dispensing and subsequent exposure to UV-light. The thin-film device consists of platinum working electrodes of a diameter of 400 µm and an Ag/AgCl reference electrode (Jobst et al. 1996a; Jobst et al. 1997).

A Pt layer was deposited by means of high vacuum evaporation, patterned via a lift-off process and insulated with PECVD silicon nitride. The working electrodes

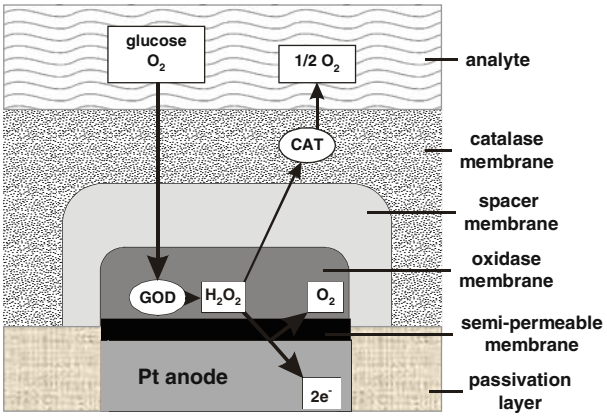

Fig. 2 Scheme of biosensor multiple-membrane setup. Main transport and reaction pathways indicated for a glucose sensor

are covered with a semi-permeable membrane deposited by electro-polymerisation (53). The respective oxidases like glucose oxidase, lactate oxidase, glutamate oxidase, and glutamate oxidase together with glutaminase were immobilized onto the working electrodes in a photo-cross-linked pHEMA membrane and additionally covered by a diffusion-limiting layer and a catalase-containing top layer to prevent crosstalk between different biosensors in the array (Moser et al. 1995; Moser et al. 2002; Jobst et al. 1996b). The use of appropriate miniaturization technology leads to mass-producible devices for in vivo and ex vivo applications in whole blood or in fermentation broth (Urban et al. 1994).

The lifetime of a biosensor array is always limited by the enzyme which loses its activity first. Compared with the stable enzymes glucose oxidase and glutamate oxidase, lactate oxidase is very brittle and unstable. However, owing to the overloading of enzyme activity in the membranes and especially by the stabilizing effect of pHEMA, even the lactate biosensor can be operated continuously in bovine serum for 1 month at 37°C.

For patient monitoring as well as for extracellular microphysiometry low volume fluid handling systems with integrated microbiosensor arrays have to be developed (Trajanoski et al. 1996). A very versatile and reliable technology is the use of polymer laminate film. The laminate is based on a PCB material and provides mixed fluidic-electric platform for the assembly of a biosensor array and microfluidic channels. Subsequent lamination of dry film resist layers over previously patterned layers allows the creation of closed channels without the use of any sacrificial layer (Fig. 3).

In this way, a printed circuit board (PCB) with a sensor flow chamber also comprising a large counter-electrode, a mixing coil, and electrical leads and pads is created.

Assembling the PCB microfluidic with the biosensor array results in the bioanalytical microsystem with a flow cell volume of 150 nl and a mixing coil volume

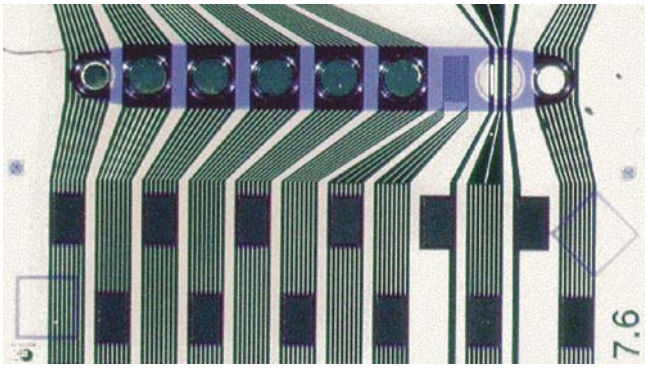

Fig. 3 Metabolomic chip for measurement of glucose, lactate, glutamate, glutamine and pyruvate concentrations in undiluted biological fluids

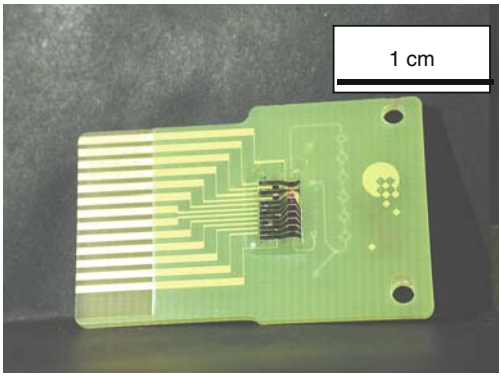

Fig. 4 Photograph of an integrated biosensor with laminated microfluidic. At top of the glucose–lactate–glutamate biosensor chip the mixing structure can be seen

of 1 µl (Fig. 4). Similar devices are already commercially available (Jobst Technologies).

Additionally, these microfluidic biosensor devices can be combined with microdialysis to have access to interstitial fluids for monitoring purposes and for control of diabetic patients (Petrou et al. 2002; Petrou et al. 2003).

In any case the stabilization of the biosensor specification is of outstanding importance. Not only enzyme stability but also the reaction products of enzymatic processes have to be taken into account because they will be enriched at the location of enzymes, can change pH and also attack the microenvironment of the enzymes chemically. Therefore, diffusion and permeation of these products are very important to deal with (Bakker 2004; Asberg and Inganas 2003). First priority is given in any way to stabilize enzymes in an appropriate matrix. Here the thermodynamic stability of enzymes in a hydrogel has to be taken into consideration.

9 Characterization of the Stability of Entrapped Enzymes

The balance between the native folded and denatured state of the enzyme structure is highly affected by the solvent or microenvironment composition. The cell interior is rather hydrogel-like than a dilute solution due to the high content of charged biopolymers like proteins and nucleic acids and carbohydrates. It is well known that this microenvironment stabilizes the compact folded structure of enzymes and enforces aggregation of (bio)polymers into complex structures (metabolons) by a mechanism called macromolecular crowding (Ellis 2001). Synthetic hydrogels mimic this crowded microenvironment and can provide stable enzyme formulations for long-term stable biosensors.

Thermodynamically, the stability of the three-dimensional fold of an enzyme can be described as the equilibrium between the folded native state (N) and the denatured random coil configuration (D). The temperature function of the free

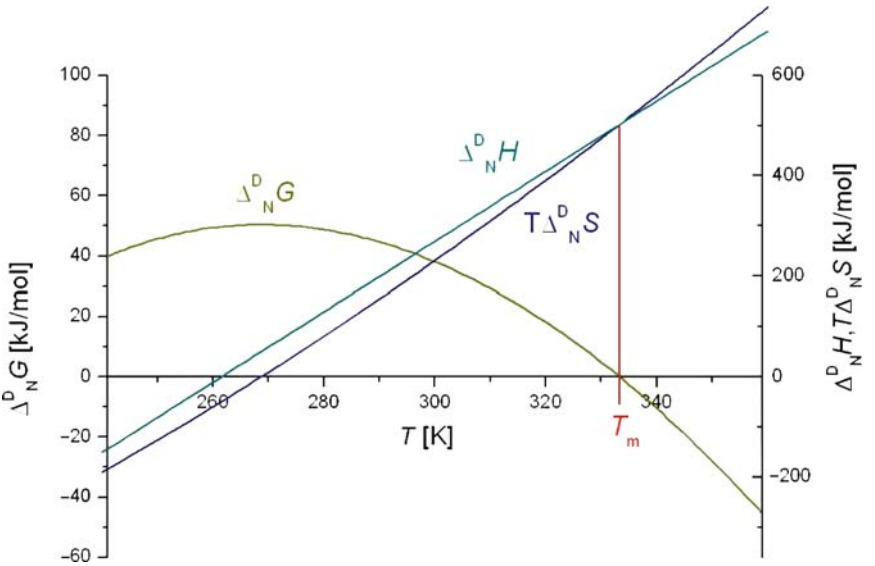

Fig. 5 Stability curve of a model enzyme, which denatures according a two-state model. The parameters for the transition are $T_m = 333$ K, $\Delta^D{}_N H(T_m) = 500$ kJ/mol, $\Delta^D{}_N C = 7$ kJ/mol and $\Delta^D{}_N S = 1{,}5$ kJ/mol/K

denaturation energy $\Delta^D{}_N G$, expressed in terms of the transition temperature T_m, the transition enthalpy $\Delta^D{}_N H$ and heat capacity $\Delta^D{}_N C$ between the two states is called enzyme stability curve (Fig. 5, Eq. (7)).

$$\Delta^D_N G(T) = \Delta^D_N H(T_m)\left(1 - \frac{T}{T_m}\right) - \Delta^D_N C\left[T_m - T + T \cdot \ln\left(\frac{T}{T_m}\right)\right]. \qquad (7)$$

Interestingly, the curved nature of the stability function implies that for any protein in a specific formulation a temperature of maximum stability exists and that besides the denaturation at higher temperature cold denaturation can happen at lower temperature as well (Becktel and Schellman 1987).

To characterize the stabilizing effect of a hydrogel microenvironment, a differential scanning calorimetry was used to get thermodynamic information of the unfolding phase transition. In scanning calorimetry the heat uptake accompanied by a phase change process is measured while the sample is heated up. The transition can be characterized by the temperature T_m of the midpoint of the heat uptake peak. The complete thermodynamic analysis of dilute protein solution needs ultrasensitive calorimeters that are able to measure heat flows in the low nW range and which have highly stable baselines (e.g. VP-DSC, MicroCal™, Nano DSC, TA Instruments™). These modern calorimeters use capillary cells of approximately 0,5 ml

sample volume tightly connected to thermocouples. Gel-like samples cannot be measured using this kind of instrument.

For stability investigation a conventional scanning calorimeter (Perkin-Elmer DSC 7) was used with aluminium pans having 40 µl volume and comparably high protein concentrations (typically 5%). The stabilizing effect of additives was measured which were added to the enzyme solutions and were indicated by an upward shift of the transition temperature. Glucose oxidase (GOx) was found to be stabilized by itself. The phase transition temperature rose from 344 K for a 1% solution and 349 K for a 10% solution to 352 K for a 20% solution. On the contrary, a typical denaturant of proteins, guanidinium hydrochlorid, lowered the T_m of GOx concentration-dependent from 341 K in 2M GdnHCl and 393 K in 3M GndHCl to 332 K in a 5M concentration. With sodium chloride as stabilizer the transition temperature shifted to 356 K in 2M concentration. Another stabilizer for the GOx was PEG-3000. In 20% PEG-3000 solution the T_m was 358 K and in 40% dextran concentration the transition temperature was 366 K. While the denaturing temperature of GOx solutions in the presence of monomers like acrylamid (AAm) and hydroxyethyl methacrylate (HEMA) was lowered, indicating a destabilizing effect, the T_m shifted to higher temperatures after radical polymerization of the precursor with ammoniumperoxodisulfate/TEMED as initiator to 350 K in a 10% pHEMA hydrogel and to 348 K in a 20% PAAm hydrogel. The stabilization effect due to addition of soluble stabilizers and due to the hydrogel-encapsulation was shown to be additive. The T_m in a 20% PAAm hydrogel together with 30% PEG-3000 was shifted to 358 K and together with additional polymeric sucrose the T_m was shifted to 355 K. The same T_m was measured for a pHEMA hydrogel with 2 M NaCl (Table 1).

The T_m shift is indicating a higher thermodynamic stability of the folded structure of the enzyme. It is suggested that the stabilization of enzymes by solvent engineering is achieved by raising the stability curve (Fig. 6) (Becktel and Schellman 1987; Rees and Robertson 2001).

Table 1 Transition temperatures T_m of GOx in different formulations

Stabilizer[1]	Concentration	T_m / K
GOx	1, 10, 20, % (w/v)	345, 349, 352
NaCl	0,5, 1, 2 M	354, 355, 356
GndHCl	1 M, 2 M, 3 M, 5 M	348, 341, 339, 332
Dextran	1, 5, 10, 20, 30, 40 % (w/v)	348, 348, 349, 363, 363, 366
PAAm	10, 20, 40, 50 % (w/v)	350, 348, 353, 349, 350
pHEMA	10, 15, 20, 25 %[2]	350, 348, 345, 342
pHEMA (25%) + NaCl	0,5, 1, 2 M	352, 356, 355
PAAm (20%[2]) + PEG-3000	300 mg/ml	358
PAAm (20 %[2]) + Ficoll™	250 mg/ml	355

[1]All enzyme formulations were prepared with KH_2PO_4 buffer, pH 7,0 as solvent; [2]monomer concentration (w/v), cross-linker (bis-acrylamid) concentration 1,2 %(w/v); [3]monomer concentration, cross-linker TEGDMA 1,2 % (w/v).

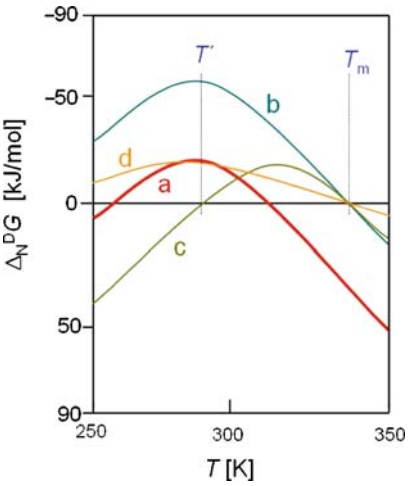

Fig. 6 Formally, the thermodynamic stability of a protein can be enhanced by raising (b), shifting (c) or increasing the breadth (d) of the stability curve (a)

10 Nanocalorimetry

Recently, a new generation of miniaturized calorimeters has been developed with highly reduced dimensions compared to the state-of-the-art microcalorimeters and capable of being highly parallelised and accessible to non-liquid media. Chip calorimeters made with microsystem technologies equipment based on thin membranes down to 1 μm thickness have improved the time resolution of thermal analysis because of highly reduced thermal mass (Höhne 2003; Wang L and Lin 2005; Jägle 2003; Johannessen et al. 2002; Olson et al. 2000; Chancellor et al. 2004; Garden et al. 2004; Chateau et al. 2005) and are used e.g. to measure size-dependent phase transitions of metal nanoparticles. A nanocalorimeter was used which is made of a cavity in an anisotropically etched silicon chip with a volume of about 200 nl to take in the liquid or gel-like sample (Ernst 2001). A membrane of silicon nitride of 1 μm thickness forms the bottom closure of the cavity (Fig. 7).

Amorphous germanium thermistors with temperature resolution of < 100 μK are placed in the membrane and on the chip body. In differential scanning calorimetry both the temperature of the sample and the temperature difference between the sample and a reference is measured while they are heated up in an external temperature field. Conventionally, a twin-type design is used with identical sample and reference cells. It was demonstrated that the thermistor on the silicon body with a defined distance to the heatproducing sample can serve as a pseudo reference to make the measured difference signal almost independent of the global temperature rise (Weiß 2007). Therefore, the two thermistors are connected in one half of a Wheatstone bridge, so that temperature changes affecting both the membrane and the bulk thermistor compensate one for each other. The other side of the measuring bridge can be filled with another two thermistors on the other side of the membrane for doubling the sensitivity. Calibration of the differential scanning calorimeter was

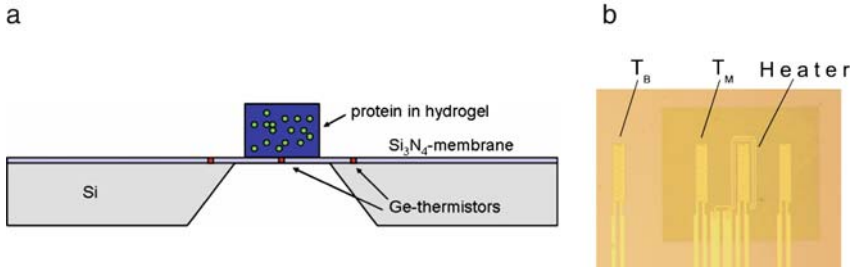

Fig. 7 Scheme a) and detail b) of the chip with thermistors T_M on the membrane and T_B on the chip body. The central thermistor is surrounded by an electrical heater for calibration

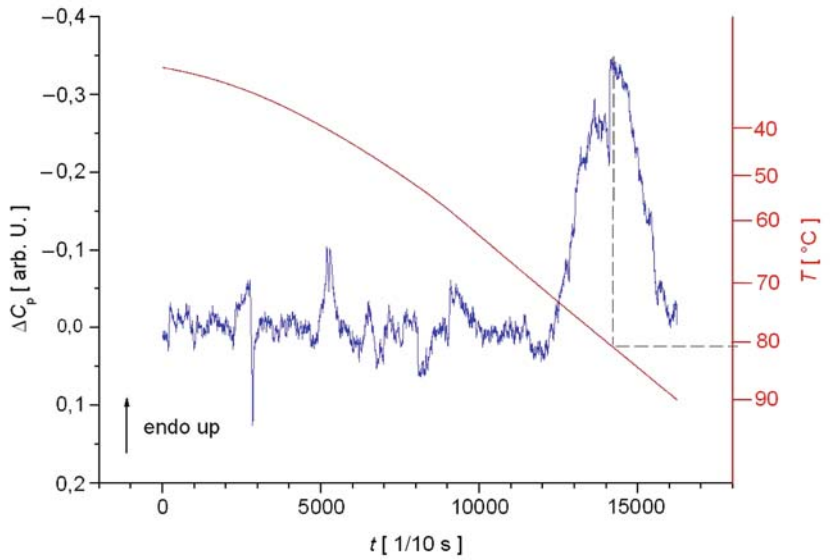

Fig. 8 Melting of GOx (5 µg/100 nl) entrapped in 20% PAAm hydrogel showing the denaturation phase transition peak at about 80°C

done with an internal electrical heater made of chromium that is also placed on the membrane, and by measuring the phase transitions of liquid crystalline reference materials (MH24 and HP53 received from Merck KGaA, Darmstadt) (Weiß et al. 2004). For measurements of the denaturation of the enzyme glucose oxidase (GOx) the water-containing sample must be heated up to 100°C without evaporation. Therefore, the sample cavity was sealed with an adhesive tape which was perforated with a fine needle for allowing the pressure to equilibrate and preventing disturbances of the measurement. For the measurements of GOx phase transition a

hydrogel precursor containing 5 % (w/w) was polymerised in the chip cavity by initiation with ammonium peroxydisulfate and tetramethyl ethylenediamine (Weiß et al. 2007).

Fig. 8 shows the denaturation of an enzyme in a hydrogel. This example shows the possibility to investigate the thermodynamic stability of immobilized enzymes in microgels.

11 Smart Hydrogels for Biosensors

Advantages of hydrogels in smart devices are their inherent actuating properties: stimuli-responsive hydrogels are changing their volume or diffusion properties by external physical or chemical variations (see Chap. 5). The change in volume due to molecular recognition or chemical reactions leads to a completely new class of biosensors using micromechanical and microoptical instead of electrochemical transducing principles.

One example is coupling of pH sensitive hydrogels with proton generating enzymatic reactions. One of the products of the enzymatic reaction of glucose oxidase is gluconic acid ($pk_a = 3{,}4$). Thus, the pH value is lowered in the environment of the enzyme in response to glucose concentration. Hydrogels with basic amine side groups become protonated leading to increased electrostatic repulsion between polymer chains and a resulting volume increase of the hydrogel. Various principles are established in transducing volume changes of hydrogels in measurable signals or in usable motion. Thus, imparting pH-sensitive hydrogels with glucose-sensitivity by loading with e.g. glucose oxidase can be used to produce glucose biosensors. The bending principle of transducing the volume change in responsive hydrogels was reviewed in detail in Chap. 5 along with other mechanical transducing principles.

A different new type of transducer combines capacitive pressure sensing techniques with bioresponsive hydrogels, using an adaptable MEMS fabrication platform. Hydrogel swelling in response to analyte concentration exerts contact pressure on a deformable conducting diaphragm, producing a capacitance change; in this particular case pHEMA was used with excellent sensitivity. The device was incorporated into a passive LC resonant circuit and the resonance frequency was measured as a function of diaphragm deflection as a function of hydrogel swelling (Strong et al. 2002).

A different microoptical technique for transducing volume changes in optical signals are responsive hydrogel photonic crystals. Holtz and Asher have developed a hydrogel-based photonic crystal that acts as glucose sensor. Glucose oxidase, attached to polystyrene nanospheres, is polymerised within a pH sensitive hydrogel. Swelling of the hydrogel increases the separation between the nanospheres leading to a shift of the diffracted light wavelength which can be observed by a colour change of the material (Holtz and Asher 1997). This sensor can be implanted into contact lenses to detect changes in the tear fluid glucose level, which is known to be

well correlated to the blood glucose level. In a similar approach the sensitivity to glucose is incorporated into a polyacrylamide hydrogel with pendent boronic acid groups fixed on a crystalline colloidal array (Alexeev et al. 2004).

Reversible antibody-antigen cross-links at the surface of a hydrogel microlens allow focal tuning of the microlens in response to soluble antigens to form the basis of a label-free biosensor/bioassay technique, whose sensitivity can be tuned by controlling the number of cross-links required to effect a specific swelling response (Kim et al. 2006). While these lenses present substantial improvement from previous technologies, there is still a need for a new generation of chemically responsive microlenses that exhibit reversible three-dimensional changes within the bulk of the polymer networks as a response to a biochemical stimulus. A new approach therefore incorporates a biological recognition element within the bulk of a hydrogel matrix. The genetically engineered protein calmodulin (CaM) was used as a model protein for the development of chemically tunable microlenses. CaM was covalently immobilized within the bulk of a PAAm hydrogel together with its ligand phenothiazine. The affinity of CaM for phenothiazine resulted in the formation of reversible chemically controlled cross-links. In the presence of a high-affinity CaM ligand, like the drug chlorpromazine (CPZ), the protein binds to CPZ releasing the hydrogel-bound phenothiazine. The result is the breaking of the cross-link and relaxation of the hydrogel network with concomitant swelling of the hydrogel microdome and a decrease in its refractive index (Ehrick et al. 2007). Such adaptive microlenses activated by stimuli-responsive hydrogels are readily integrated into arrays for high-throughput diagnostic applications (Dong et al. 2006).

Additionally, stimuli-responsive hydrogels can be used in smart drug delivery devices. Moreover, feedbacked systems with integrated glucose sensing and insulin delivery microdevice can be designed: using a biodegradable glucose-sensitive in situ gelling system based on chitosan for pulsatile delivery of insulin was realized. The developed glucose-sensitive sol/gel system responded to varied glucose concentrations in vitro indicating their ability to function as environment-sensitive systems. Insulin load in the gels was optimised and was found to affect the rheological behaviour of these gels. These gels released the entrapped insulin in a pulsatile manner in response to the glucose concentration in vitro. Furthermore, the formulations demonstrated their ability to release insulin in response to glucose concentration (Guiseppi-Elie et al. 2002; Kashyap et al. 2007).

When biosensor implants are placed into a biological system issues of biocompatibility have to be taken into account. Protein-resistant surfaces are prerequisites for medical devices and biosensor implants in contact with blood to avoid or reduce non-specific protein absorption that occurs at the surface of a foreign material whenever it is inserted into a biological environment. This protein absorption is the initial step of cell adhesion and subsequent biofouling leading to sensor failure and undesirable responses of the living system to the device. Antifouling coatings of biosensor implant materials can impart biocompatibility due to prevention of non-specific protein absorption. Hydrogel-like materials are generally considered to favour biocompatibility, particularly due to their high water content (Kudela 1987).

Hydrogel coatings mask the underlying surface and produce a hydrophilic interface between the solid surface and the aqueous bulk. Water-soluble analytes can readily diffuse through the water-swollen hydrogel layer. Especially polyethyleneglycol is very effective in preventing protein absorption. The underlying mechanism is normally ascribed to its hydrophilic water-like character, high mobility as well as the fact, that it is uncharged. The similarity to water results in very low interfacial free energy with water (Bozukova et al. 2008). The absence of hydrogen bond donors is also reported to correlate to protein resistance (Larsson 2007).

12 Summary

Biosensors attracted great interest in the past because it was expected that continuous blood glucose monitoring would further increase patient comfort enabling an exact control of insulin delivery. Unfortunately, it turned out in the last decades that onlinemonitoring is very complicated, cumbersome and not reliable enough for closed-loop therapeutic insulin treatments. One drawback is the proper immobilization technology to get long-term stable enzyme biosensors. Single-use glucose sensor only reveals adsorbed enzymes which cannot be used for implant. To get stable biosensors covalent immobilizations or enzyme entrapments in gels are appropriate. One excellent example to immobilize enzymes in a thermodynamic stable phase is the use of hydrogels as immobilization agent on microsensors which also enable the integration of multibiosensor arrays.

References

Abruna HD (1988) Coordination chemistry in two dimensions: chemically modified electrode. Coord Chem Rev 86:135–189

Alexeev VL, Das S, Finegold DN, Asher SA (2004) Photonic crystal glucose-sensing material for noninvasive monitoring of glucose in tear fluid. Clin Chem 50(12):2353–2360

Allcock HR, Phelps MVB, Barrett EW, Pishko MV, Koh WG (2006) Ultraviolet photolithographic development of polyphosphazene hydrogel microstructures for potential use in microarray biosensors. Chem Mater 18(3):609–613

Angenendt P, Glokler J, Konthur Z, Lehrach H, Cahill DJ (2003) 3D protein microarrays: performing multiplex immunoassays on a single chip. Anal Chem 75(17):4368–4372

Applegate BM, Kehrmeyer SR, Sayler GS (1998) A chromosomally based tod-luxCDABE whole-cell reporter for benzene, toluene, ethybenzene, and xylene (BTEX) Sensing. Appl Environmental Microbiol 64(7):2730–2735

Asberg P, Inganas O (2003) Hydrogels of a conducting conjugated polymer as 3-D enzyme electrode. Biosens Bioelectron 19(3):199–207

Bakker E (2004) Electrochemical sensors. Anal Chem 76(12):3285–3298

Barsky VE, Glokler J, Konthur Z, Lehrach H, Cahill DJ (2003) Biological microchips with hydrogel – immobilized nucleic acids, proteins, and other compounds: properties and applications in genomics. Mol Biol 36:437–455

Bashir R (2004) BioMEMS: state-of-the-art in detection, opportunities and prospects. Adv Drug Deliv Rev. 56(11):1565–1586

Becktel WJ, Schellman JA (1987) Protein stability curves. Biopolymers 26(11):1859–1877

Bjerketorp J, Håkansson S, Belkin S, Jansson J (2006) Advances in preservation methods: keeping biosensor microorganisms alive and active. Curr Opin Biotechnol 17(1):43–49

Bousse L (1996) Whole cell biosensors. Sens Act B 34:270–275

Bozukova D, Pagnoulle C, De Pauw-Gillet MC, Ruth N, Jérôme R, Jérôme C (2008) Imparting antifouling properties of poly (2-hydroxyethyl methacrylate) hydrogels by grafting poly (oligoethylene glycol methyl ether acrylate). Langmuir 24(13):6649–6658

Brahim S, Narinesingh D, Guiseppi-Elie A (2002) Bio-smart hydrogels: co-joined molecular recognition and signal transduction in biosensor fabrication and drug delivery. Biosens Bioelectron 17(11–12):973–981

Burnham MR, Turner JN, Szarowski D, Martin DL (2006) Biological functionalization and surface micropatterning of polyacrylamide hydrogels. Biomaterials 27(35):5883–5891

Cass AGE et al (1984) Ferrocene-mediated enzyme electrode for amperometric determination of glucose. Anal Chem 56(4):667–671

Chalfie M, Tu Y, Euskirchen G, Ward WW, Prasher DC (1994) Green fluorescent protein as a marker for gene expression. Science 263(5148):802–805

Chancellor EB, Wikswo JP, Baudenbacher F (2004) Heat conduction calorimeter for massively parallel high throughput measurements wit picoliter sample volumes. Appl Phys Let 85: 2408–2410

Chateau E, Garden JL, Bourgeois O, Chaussy J (2005) Physical kinetics and thermodynamics of phase transitions probed by dynamic nanocalorimetry. Appl Phys Let 86:151913

Chen T, Binyami G, Schmittke K, Friedman K, Heller A (2001) In vivo glucose monitoring with miniature "wired" glucose oxidase electrodes. Anal Sci 17:i297–i300

Clark LC, Leland C, Lyons P, Champ P (1962) Electrode systems for continuous monitoring in cardiovascular surgery. Ann N Y Acad Sci 102(1):29–45

Clark C, Moves T, Grooms P, Moore P (1984) Direct rapid electroenzymatic sensor for measuring alcohol in whole blood and fermentation products. Ann N Y Acad Sci 434(1):515–519

Cushing MS, Anseth KS (2007) Hydrogel cell cultures. Science 316:1133–1134

Dong L, Agarwal AK, Bebee DJ, Jiang H (2006) Adaptive liquid microlenses activated by stimuli-responsive hydrogels. Nature 442:551–554

Ehrick JD, Stokes S, Bacgas-Daunert S, Moshou EA, Deo SK, Bachas LG, Daunert S (2007) Chemically tunable lensing of stimuli-responsive hydrogel microdomes. Adv mat 19:4024–4027

Ek S (2004) Diabetes care: beyond meters and strips. Roche R&D Day http://www.roche.com/pages/downloads/investor/pdf/praesentations/irp050504rdd4.pdf

Elad T, Lee J, Belkin S, Gu M (2008) Microbial whole-cell arrays. Microbial Biotechnology 1 (2):137–148

Ellis RJ (2001) Macromolecular crowding: obvious but underappreciated. Trends Biochem Sci 26 (10):597–604

Ernst H (2001) Dissertation, Universität Freiburg.

Fesenko DO, Nasedkina TV, Prokopenko DV, Mirzabekov AD (2005) Biosensing and monitoring of cell populations using the hydrogel bacterial microchip. Biosens Bioelectron 20(9):1860–1865

Fine T, Leskinen P, Isobe T, Shiraishi H, Morita M, Marks RS, Virta M (2006) Luminescent yeast cells entrapped in hydrogels for estrogenic endocrine disrupting chemical biodetection. Biosens Bioelectron 21(12):2263–2269

Garden JL, Chateau E, Chaussy J (2004) Highly sensitive ac nanocalorimeter for mcroliter-scale liquids or biological samples. Appl Phys Let 84:3597–3599

Group TDCaCTR (1993) The effect of intensive treatment of diabetes on the development and progression of long-term complications in insulin-dependent diabetes mellitus. N Engl J Med 329(14):977–986

Guiseppi-Elie A, Brahim S I, Narinesingh D (2002) A chemically synthesized artificial pancreas: release of insulin from glucose-responsive hydrogels. Adv. Materials 14(10):743–746
Heller A (1996) Amperometric biosensors. Curr Opin Biotechnol 7(1):50–54
Heller A (2006) Electron-conducting redox hydrogels: design, characteristics and synthesis. Curr Opin Chem Biol 10(6):664–672
Höhne GWH (2003) Cip-kalorimeter for small samples. Thermochimica Acta 403:43–53
Holtz JH, Asher SA (1997) Polymerized colloidal crystal hydrogel films as intelligent chemical sensing materials. Nature 389(6653):829–831
Itle L, Pishko M (2005) Multiphenotypic whole-cell sensor for viability screening. Anal Chem 77(24):7887–7893
Jägle M (2003) A fast and highly sensitive nano-calorimeter. Techn Mes 12:557–560
Jobst G, Moser I (2006) Smallest volume metabolic monitoring. In: Proceedings of the ninth congress of biosensors, Toronto, p 558
Jobst G et al (1996a) Thin-film microbiosensors for glucose-lactate monitoring. Analy Chem 68(18):3173–3179
Jobst G, Moser I, Urban G (1996b) Numerical simulation of multi-layered enzymatic sensors. Biosensors and Bioelectronics 11(1–2):111–117
Jobst G, Svasek P, Moser I, Varahram M, Trajanoski P, Wach P, Kotanko P, Skrabal F, Urban G (1997) Mass producible miniaturized flow through device with biosensor array. Sens Act B 43:121–125
Johannessen EA, Weaver JMR, Cobbold PH, Cooper A (2002) A suspended membrane nanocalorimeter for ultralow volume bioanalysis. IEEE Trans Nanobiosci 1(1):29–36
Kaneko M, Wöhrle D (1988) Polymer coated electrodes: new materials for science and industry. Advances in Polymer Science, vol 84. Springer, Berlin, pp 141–228
Kashyap N, Viswanad B, Sharma G, Bhardwaj V, Ramarao P, Ravi Kumar MNV (2007) Design and evaluation of biodegradable, biosensitive in situ gelling system for pulsatile delivery of insulin. Biomat 28(11):2051–2060
Kaufman FB, Schroeder AH, Engler EM, Kramer SR, Chambers JQ (1980) Ion and electron transport in stable, electroactive tetrathiafulvalene polymer coated electrodes. J Am Chem Soc 102(2):483–488
Kim BC, Gu MB (2003) A bioluminescent sensor for high throughput toxicity classification. Biosens Bioelectron 18(8):1015–1021
Kim J, Singh N, Lyon AL (2006) Label-free biosensing with hydrogel microlenses. Angew Chem Int Ed 45(9):1446–1449
Kudela V (1987) Hydrogels in encyclopedia of polymer science and engineering, vol. 7. Wiley, NY, p 783
Larsson A (2007) Photografted poly(ethylene glycol) matrix for affinity interaction studies. Biomacromolecules 8(1):287–295
Lei Y, Chen W, Mulchandani A (2006) Microbial biosensors. Anal Chim Acta 568(1–2):200–220
Ligler FS (2006) Biosensors for detection of bioterrorist threats. In: Baldini F et al (eds) Optical chemical sensors NATO science series II, vol 224. Springer, Berlin, pp 437–455
Moser I et al (1995) Miniaturized thin film glutamate and glutamine biosensors. Biosens Bioelectron 10(6–7):527–532
Moser I, Jobst G, Urban GA (2002) Biosensor arrays for simultaneous measurement of glucose, lactate, glutamate, and glutamine. Biosens Bioelectron 17(4):297–302
Murray RW (1984) Electroanalytical Chemistry. In: Bard AJ (ed) vol. 13. Dekker, New York, p 191
Nakamura H, Karube I (2003) Current research activity in biosensors. Anal Bioanal Chem 377 (3):446–468
Olson EA, Efremov MY, Kwan AT, Lai S, Petrova V, Schiettekatte F, Warren JT, Zhang M, Allen LH (2000) Scanning calorimeter for nanoliter-scale liquid samples. Appl Phys Let 77:2671–2673
Park KS, Baumstark-Khan C, Rettberg P, Horneck G, Rabbow E, Gu MB (2005) Immobilization as a technical possibility for long-term storage of bacterial biosensors. Rad Environ Biophys 44(1):69–71

Petrou PS, Moser I, Jobst G (2002) BioMEMS device with integrated microdialysis probe and biosensor array. Biosens Bioelectron 17(10):859–865
Petrou PS, Moser I, Jobst G (2003) Microdevice with integrated dialysis probe and biosensor array for continuous multi-analyte monitoring. Biosens Bioelectron 18(5–6):613–619
Philp JC, Balmand S, Hajto E, Bailey MJ, Wiles S, Whiteley AS, Lilley AK, Hajto J, Dunbar SA (2003) Whole cell immobilised biosensors for toxicity assessment of a wastewater treatment plant treating phenolics-containing waste. Anal Chim Acta 487(1):61–74
Pollmann K H, Gerber M, Kost K M, Ochs M L, Walljing J, Bateson J, Kuhn L S, Han C A (1994) US Patent 5,288,636
Polyak B, Geresh S, Marks RS (2004) Synthesis and characterization of a biotin-alginate conjugate and its application in a biosensor construction. Biomacromol 5(2):389–396
Rees DC, Robertson AD (2001) Some thermodynamic implications for the thermostability of proteins. Protein Sci 10(6):1187–1194
Strong ZA, Wang AW, McConaghy CF (2002) Hydrogel-actuated capacitive transducer for wireless biosensors. Biomed Microdevices 4(2):97–103
Thevenot DR, Toth K, Durst RA, Wilson GS (2001) Electrochemical biosensors: recommended definitions and classification. Biosens Bioelectron 16(1–2):121–131
Tirrell M, Kokkoli E, Biesalski M (2002) The role of surface science in bioengineered materials. Surf Sci 500:61–83
Trajanoski Z, Wach P, Gfrerer R, Jobst G, Urban G, Kotanko P, Skrabal F (1996) Portable device for continuous fractionated blood sampling and continuous ex vivo blood glucose monitoring. Biosens Bioelectron 11(5):479–487
Tsang VL, Bhatia SN (2004) Three-dimensional tissue fabrication. Adv Drug Deliv Rev 56(11):1635–1647
Turner APF, Karube I, Wilson GS (1987) Biosensors: fundamentals and application. Oxford University Press, Oxford, p 770
Ulijn RE, Bibi N, Jayawarna V, Thornton PD, Todd SJ, Mart RJ, Smith AM, Gough JE (2007) Bioresponsive hydrogels. Mater Today 10(4):40–48
Urban GA (2006) BioMEMS. In: Senturia SD (ed) Microsystems, vol.16. Springer, Dordrecht, NL
Urban GA, Jobst G (1997) Biosensors with modified electrodes for in vivo and ex vivo applications. In: Scheller FW (ed) Frontiers in Biosensorics, vol II. Birkhäuser, Basel, pp 161–173
Urban G et al (1990) Thin-film electrodes for medical diagnosis. Biomed Tech 35 Suppl. 2: 100–111
Urban G, Jobst G, Aschauer E, Tilado O, Svasek P, Varahram M (1994) Performance of integrated glucose and lactate thin film microbiosensors for clinical analyzers. Sens Act B 19(1–3): 592–596
Urban G, Moser I, Jobst G (1998) Technical microsystem monitoring for determination of metabolic parameters. Biomed Tech 43 Suppl.:184
Wang L, Lin Q (2005) A polymer-based MEMS sensor for biocalorimetric measurements. In: Ninth international conference on miniaturized systems for chemistry and life sciences (micro-TAS 2005), Boston, MA
Weiß T (2007) Dissertation, Universität Freiburg.
Weiß T, Moser I, Igel G, Urban G A (2004) Scanning nano-calorimeter. Sensors Proceedings of IEEE, Wien, AT
Weiß T, Igel G, and Urban G (2007) Chip-based scanning nano-calorimeter for protein stability analysis in biosensor membranes 1761-1764. In: Transducers: Solid-State Sensors, Actuators and Microsystems, Lyon, FR
Wichterle O, Lim D (1960) Hydrophilic gels for biological use. Nature 185:117–118
Wilson GS, Gifford R (2005) Biosensors for real-time in vivo measurements. Biosens Bioelectron 20(12):2388–2403
Yu L, Urban G, Moser I, Jobst G, Gruber H (1995) Photolithographically patternable modified poly(HEMA) hydrogel membrane. Polymer Bull 35(6):759–765

Hydrogels for Actuators

Andreas Richter

Abstract In microsystem technology research a material with such a diversity and significance like silicon in microelectronics has not been established for the last 20 years. Recently in microfluidics and in special imaging systems hydrogels get ready to take this place. Here we present a review on hydrogel based microsystems with actuator or sensor-actuator functionalities. Automatic microfluidic systems based on the sensor-actuator properties of hydrogels offer functionalities which have not been yet realised with other systems or actuators. The functional principles of the basic elements are described on the example of hydrodynamic transistors, pumps and tunable microlenses. In the field of microelectromechanical microfluidic systems hydrogels provide a unique multi-functionality. We describe the basic principles applied on an electronic control for hydrogel actuators and also on the basic components for microfluidics: microvalve, micropump and hydrodynamic transistors. Furthermore, the first hydrogel-based highly integrated microsystem, a high-resolution tactile display containing 4,225 individually controllable actuator pixels, is reviewed. In the last two Sections we discuss essential physical phenomena und design rules, which have to be considered to avoid malfunctions of the designed devices.

Keywords Hydrogel • Actuator • Hydrodynamic transistor • Pump • Valve • LSI microsystems • Tactile display

Contents

A. Richter
Laboratory of Polymeric Microsystems, Technische Universität Dresden, 01062 Dresden, Germany
e-mail: andreas.richter7@tu-dresden.de

G. Gerlach and K.-F. Arndt (eds.), *Hydrogel Sensors and Actuators*,
Springer Series on Chemical Sensors and Biosensors 6,
DOI: 10.1007/978-3-540-75645-3_7, © Springer-Verlag Berlin Heidelberg 2009

Abbreviations

LCST	Lower critical solution temperature
MBAAm	*N*,*N*´-methylenebis(acrylamide)
NC	Normally closed
NO	Normally open
n.s.	Not specified
PCR	Polymerase chain reaction
PNIPAAm	Poly(*N*-isopropylacrylamide)

Symbols

A_C	Cross-section area of channel
$c_{Alcohol}$	Content of alcohol in aqueous solution
c_{EtOH}	Content of ethanol in aqueous solution
$c_{Glucose}$	Content of glucose in aqueous solution
c_{HxOH}	Content of hexanol in aqueous solution
c_{MeOH}	Content of methanol in aqueous solution
c_{NaCl}	Content of sodium chloride in aqueous solution
c_{PrOH}	Content of 1-propanol in aqueous solution
d	Valve chamber length
d_A	Effective diffusion way of a bulk actuator
pH	pH value
pk_a	pk value of acid
r_P	Particle radius

T	Temperature
T_g	Glass transition temperature
T_t	Volume phase transition temperature
$T_{Control}$	Control temperature of hydrodynamic transistor
t	Time
V	Swollen volume of hydrogel
V_0,V_{dry}	dry volume of hydrogel
V_C	Valve chamber volume
V_{Gel}	Bulk volume of dry hydrogel particles
x	Distance
Δd	Difference of valve chamber length
ΔpH	Difference of pH value
ΔT	Temperature difference
Δx	Displacement
Δd	Difference of valve chamber length
ΔpH	Difference of pH value
ΔT	Temperature difference
Δx	Displacement
λ	Wavelength of light

1 Introduction

Originally there was the expectation that stimuli-responsive hydrogels would provide a new type of actuator, the so called "artificial muscle" (Kuhn et al. 1948; Kuhn and Hargitay 1951). Hydrogels show properties similar to the natural muscle (Table 1). Therefore, they were intended as propulsion for robotic applications. Research groups developed spectacular applications such as "gel fish" (Osada and Gong 1998a; Kurauchi et al. 1991), "artificial elbow" (Suzuki 1991), "gel hand" (Kurauchi et al. 1991), and rotatory "gel motor" (Mitsumata et al. 1998; Mitsumata et al. 2000). However, due to the time-consuming swelling process of centimetre-sized gel components (Table 1, Sect. 3.2) and to the limited electronic controllability the present generation of hydrogels is not yet ready for the robotic "artificial muscle" or other macroscopic actuator applications. Nevertheless, to realise low dynamic applications such as medical pumps (Richter et al. 2004a) or automatic decubitus mattresses (Richter et al. 2005), hydrogels offer interesting properties.

Here, we report about the high potential of stimuli-responsive hydrogels as active materials for a platform technology of monolithic integrated microsystems. Similar to the computer science and to the electronics which are commonly using microprocessors consisting of integrated circuits in future medicine, biotechnology and chemistry could benefit from highly integrated fluidic circuits, such as the so-called microfluidic processors or lab-on-a-chip devices, which can significantly reduce the operating time,

Table 1 Properties of different actuator types

Actuator	Energy density [J cm^{-3}]	Elongation [%]	Pressure [MPa]	Reaction time [ms]
Solenoids	0.025	50	0.1	5
Piezo actuators	0.05	0.2	110	0.5
Magnetostrictive	0.025	0.2	70	0.4
Electrostrictive	0.17	32	2	1
Shape memory alloy	10	8	900	300 [1]
Hydrogels	0.35	90	4	300 [2]...h [3]
Electrochemical	0.14	50	25	16
Electrostatic	0.0015	50	0.03	0.003
Muscle	0.59	70	1.18	0.03

[1]depending on the applied heating power; [2]actuator size in the micrometre and sub-millimetre range; [3]actuator size in the centimetre range

the reagent volume and the required sample volume (Janasek et al. 2006; Dittrich and Manz 2006). In few commercial applications the advantages of large-scale integrated devices containing hundreds or thousands of valves are impressively demonstrated by micro-pneumatic multilayer soft-lithographic systems (Unger et al. 2000; Thorsen et al. 2002; http://www.fluidigm.com/products/biomark-chips.html, date: 25.06. 2008) based on the elastomer polydimethylsiloxane (PDMS). Due to the complex pneumatic control and to the limitation to only one basic functionality, which is a pneumatic displacement valve, the micro-pneumatics is not generally applicable.

Unlike the pure PDMS, stimuli-responsive hydrogels are active materials capable to change their properties, such as the volume. Hydrogels show excellent micro fabrication capability that allows a monolithic chip design as well as the largest known actuator effect of solid state actuators and within the sub-millimetre size a response time in the range from milliseconds to few seconds. As shown on the example of poly(*N*-isopropylacrylamide) (PNIPAAm) gels provide the realisation of all active components in microfluidics including valves (Richter et al. 2003; Yu et al. 2003a; Wang J et al. 2005), adjustable hydrodynamic transistors (Richter et al. 2007a), pumps (Richter et al. 2009a) and liquid sensors with only one required type of hydrogel material [19, Chap.5]. The only known material with a comparable multi-functionality is silicon in the field of microelectronics. An integration technology providing the fabrication and the individual addressing of thousands of active hydrogel components on a single chip is demonstrated on the example of an artificial skin (Richter and Paschew 2009). Here, we report about the fundamentals of two general applications of hydrogel-based microfluidic systems, automatic (Sect. 2) and micro-electromechanical systems (Sect. 3) and as a third application, high-resolution tactile display devices (Sect. 4).

2 Automatic Microfluidic Systems

The control of the concentration of certain chemical substances in mixtures is a key problem of fluidic processes. Current systems, which automatically regulate a chemical or physical condition of a liquid, are expensive and consist of sensors,

data processing and actuator units. However, stimuli-responsive polymers combine the properties of a chemical sensor and of an actuator by a reversible and reproducible change of their volume in response to small alterations of certain chemical (Tanaka 1978; Li et al. 2002; Arndt et al. 1999; Kataoka et al. 1998; Miyata et al. 1999) or energy-based (Arndt et al. 2001; Suzuki and Tanaka 1990; Tanaka et al. 1982; Osada and Gong 1998b) conditions of the liquids. They provide the probably simplest automatic closed-loop control systems. Besides the chemical control systems devices are of particular relevance, which are able to regulate biochemical substances, because systems substituting body functions like that of the pancreas, could be realised. In the future the sensor-actuator functionality of hydrogel could be the base of integrated automatic microfluidic systems performing event-sensitive microfluidic processing.

2.1 Hydrodynamic Transistors

The simplest functionality to regulate a liquid flow is provided by a throttle valve. To the best of my knowledge, the idea to use hydrogels in chemomechanical valves was presented in 1981 by Y. Osada for the first time (Osada and Takeuchi 1981). To realise this device the hydrogel-based sensor-actuator[1] controls the size of the channel cross-section by swelling or shrinking. Due to its automatic flow control depending on the ion and solvent concentrations this apparatus is, ultimately, a chemostat valve (greek: *chem*(*o*) = chemistry; *-stat* = regulating) or due to its equivalency to the electronic model a hydrodynamic transistor. Table 2 gives an overview of such devices described in the literature.

2.1.1 Directly Acting Hydrogel Component

The hydrodynamic transistors shown in Table 2 can be classified in two types distinguished by the function of the gel actuator. The actuator of type B acts as servo drive actuating the valve seat. The actuator of type B is directly placed within the flow channel. Therefore, the stimulant, which is typically a component of the process medium, directly controls the sensor-actuator element. The hydrogel swells or shrinks by absorption or release of the process medium and regulates the channel cross-section. Figure 1 shows two examples of such hydrodynamic transistors.

[1] In this chapter the sensor-actuator functionality is sometimes described as actuator according to terms used in the literature. Please note that a sensor-actuator transforms non-mechanical energy into mechanical energy, whereas an actuator is typically controlled by electrics or electronics.

Table 2 Comparison of hydrodynamic transistors

Authors	Type [1]	Control value	Pressure resistance	Response time	
				Opening	Closing
Peters (Peters et al. 1997)	A [1]	T	18 MPa	6 min	2 min
Arndt (Arndt et al. 2000)	A	T, pH, c_{MeOH}, c_{EtOH}, c_{PrOH}, c_{HxOH} [2]	900 kPa	25 s	35 s
Beebe (Beebe et al. 2000)	A,B	pH	184 kPa	n.s.	19 s
Beebe (Liu et al. 2002)	A	pH	300 kPa	8 s	12 s
Harmon (Harmon et al. 2003)	B	T	n.s.	s . . . min	
Kuckling (Kuckling et al. 2003)	A	T, pH	300 kPa	30 s	30 s
Baldi (Baldi et al. 2003)	B	pH, $c_{Glucose}$	5.4 kPa	7 min	13 min
Beebe (Sershen et al. 2005)	A	Light (λ)	n.s.	5 s	n.s.
Park (Park et al. 2006)	B	pH	11.8 kPa	6 min	3 min
Richter (Richter et al. 2007b)	A, B	T, c_{MeOH},c_{EtOH}, c_{PrOH}	20 kPa	n.s.	n.s.
Richter (Richter et al. 2007a)	A	c_{MeOH}, c_{EtOH}, c_{PrOH}, c_{NaCl}	600 kPa	n.s.	n.s.
Liu (Liu et al. 2007)	B	pH	n.s.	50 s	45 s
D. Kim (Kim & Beebe 2007)	A	pH	100 kPa [3]	0.51 s	0.47 s
Zhang (Zhang et al. 2008)	Flap	T	n.s.	10–20 s	

[1]type A: hydrodynamic transistor with directly acting hydrogel element, type B: hydrodynamic transistors with hydrogel acting as servo drive; [2]MeOH – methanol, EtOH – ethanol, PrOH – 1-propanol, HxOH – hexanol, NaCl – sodium chloride; [3]leakage flow is observed with increasing time

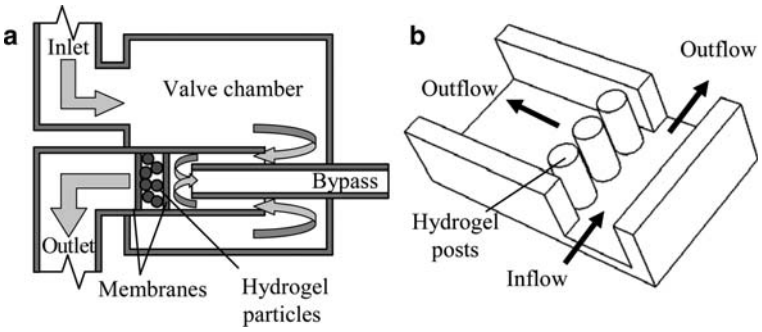

Fig. 1 Hydrodynamic transistors with direct acting hydrogel elements (a) with hydrogel particles according to (Arndt et al. 2000; Kuckling et al. 2003) and (b) with photopolymerised hydrogel posts according to (Beebe et al. 2000)

2.1.2 Hydrogel as Servo Drive

By swelling or shrinking the actuator of the "type B" valve moves a flexible membrane (Fig. 2a) or a boss (Fig. 2b) closing or opening the valve seat. At the valve seat the hydrogel has no direct contact with the medium. It is possible to use

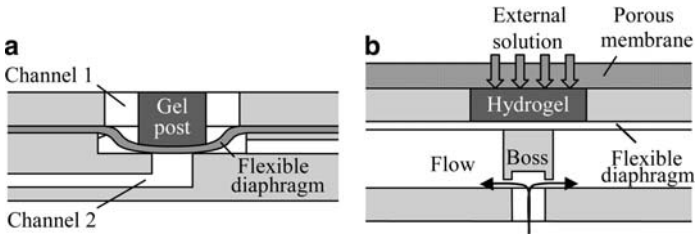

Fig. 2 Hydrodynamic transistors with hydrogel acting as servo drive (a) with a flexible diaphragm as valve seat according to (Beebe et al. 2000) and (b) with a boss as valve seat according to (Baldi et al. 2003)

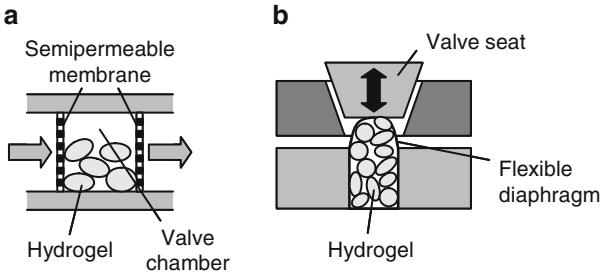

Fig. 3 Antagonistic hydrodynamic transistor types. The fully swollen state is assumed as normal state of the hydrogel component (a) Normally closed hydrodynamic transistors. (b) Normally open hydrodynamic transistors. The hydrogel acts as servo drive

one process circuit (channel 1) containing the hydrogel element regulating a second process circuit (channel 2, Fig. 2a).

2.1.3 Normally Closed and Normally Open Valves

It is essential that the swelling behaviour of the hydrogel can be alternatively used for both normally closed and open valves, respectively (Richter et al. 2007b). This valve function can be defined by the way the hydrogel moves the valve seat. To realise a normally closed (NC) valve the hydrogel is directly placed inside the flow channel. (Fig. 3a). After the hydrogel swelling the valve chamber is completely filled and thereby the valve is closed. Shrinking of the gel opens the valve.

As shown in Fig. 3b a normally open (NO) valve can be designed to keep the conic valve seat open by the swollen hydrogel. The valve seat is closed after shrinking of the gel.

Zhang et al. (Zhang et al. 2008) describe an antagonism for bimorph hydrogel-based flap valves. Depending on the layer arrangement by hydrogel swelling the

flap valve closes if the gel layer is on the top of the supporting strip or opens if it is below.

2.1.4 Mechanical Adjustability of the Regulation Point

The fixed regulation point, predefined by the type of the used hydrogel and by the valve design, is an essential problem of the hydrodynamic transistors. It is practically impossible to adapt the hydrogel element to each application. However, the adaption for applications is much easier if the device is designed adjustable (Richter et al. 2007b).

The actuation point of the NO valve (Fig. 4b) is designed to be adjustable by the possibility to vary the distance x. It is possible to assign a regulation point to each swelling state of the hydrogel by a variable displacement of the complete servo drive unit.

The regulation point of the NC valve (Fig. 4a) can be adjusted by a varying the size of the valve chamber, *e.g.* by using a thread. Thereby the regulation point condition is adjustable, at which the valve chamber volume equals the hydrogel volume (at a defined pressure resistance of the valve). In Fig. 5 a thermostat function of a NC valve based on the thermo-sensitive hydrogel PNIPAAm is presented. PNIPAAm shows lower critical solution temperature behaviour (LCST) (Fig. 5a). The hydrogel shrinks and opens the valve at higher temperatures or swells and closes the valve at lower temperatures. Adjusting the chamber size to a volume equal to the swelling degree of the hydrogel material at a defined temperature, the precise valve-opening or -closing temperature point can be predefined.

The standard deviation or control accuracy of the thermostat is 0.75 K. The range of regulation point adjustment is restricted to the volume phase transition range of the hydrogel (Fig. 5b). Above and below that range the volume change is too small.

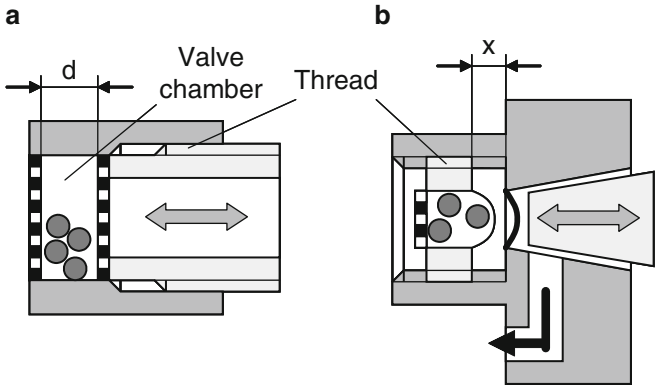

Fig. 4 Mechanically adjustable hydrodynamic transistors. (a) Normally closed and (b) normally open hydrodynamic transistors according to (Richter et al. 2007b)

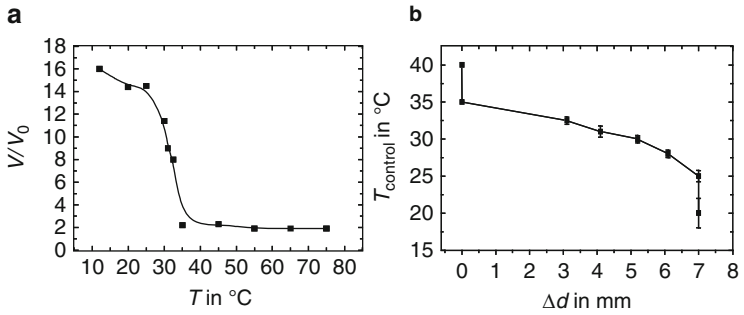

Fig. 5 Regulation point adjustment of a normally closed hydrodynamic transistor. (a) Swelling characteristics of PNIPAAm in aqueous solution depending on the temperature. (b) Temperature control point of the hydrodynamic transistor as function of the valve chamber length *d* (according to (Richter et al. 2007b))

In the meantime hydrodynamic transistors are ready for practical use. Their regulation precision (temperature ± 0.75 K, contents of alcohol ± 1 wt.-% (Richter et al. 2007b)) already has the required accuracy for many applications. The valve performance comprises an adjustable pressure resistance up to 18 MPa (Peters et al. 1997). The reported response time of the valves varies within the range of seconds or minutes which should be sufficient for most applications, because changes of liquid concentrations are typically processes with low dynamics. The possibility to adjust the hydrodynamic transistor control point is implemented which was a missing key feature required for the diversity of practical applications.

Devices that are able to regulate biochemical substances are of particular relevance for the implementation of systems substituting body functions, like that of the pancreas (Baldi et al. 2003).

2.2 Fluidic Propulsion

The sensor-actuator properties of hydrogels can also be used to generate a liquid flow or a pressure. Adapting the fundamental principle of the "osmotic pump" of Theeuwes and Yum (Theeuwes and Yum 1976) so far two types of pumps are described.

2.2.1 Chemostat Pumps

These pumps use the volume phase transition behaviour of gels to move small amounts of liquid. The characteristic feature of stimuli-sensitive hydrogels to change their volume absorbing or releasing aqueous solution has been used to realise displacement free valves. However, this gel property is inappropriate for the direct hydrogel actuator use in pumps. Therefore, the hydrogel swelling moves

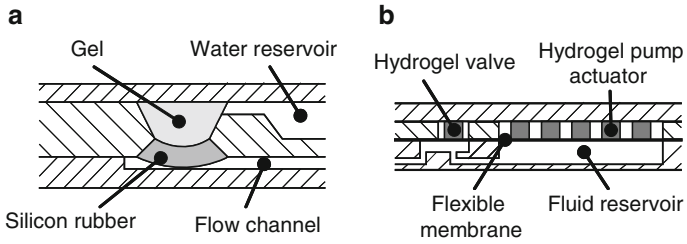

Fig. 6 Chemostat pumps. (a) Temperature-sensitive displacement pump according to (Suzuki et al. 2002). (b) pH-sensitive displacement pump according to (Eddington and Beebe 2004)

an elastic membrane into a fluid reservoir (pump chamber) and displaces the liquid (Fig. 6). Displacement pumps controlled by energetic quantities such as temperature require a special swelling agent reservoir (e.g. the water reservoir in Fig. 6a) (Suzuki et al. 2002). The hydrogel elements of pumps, which can be stimulated by special substances, need a direct contact to the process medium (Fig. 6b).

The pumps can be additionally equipped with a separate chemostat valve (Eddington and Beebe 2004). Compared to other pumps hydrogel-based chemostat pumps provide a medium performance (Nguyen et al. 2002; Laser and Santiago 2004). Beebe et al. report a flow rate of 2 µl min^{-1} generated by the pump and a maximal back pressure of 35 kPa (Eddington and Beebe 2004). For a fast bolus release the valve has to be opened after the swelling of the pump actuator. After valve opening the generated pressure releases the content of the pump chamber within a few seconds at an average flow rate of 540 µl min^{-1}. However, these investigations are of limited informational value, because these were performed by a practically not relevant switching condition from strong acidic liquids (pH 2) towards strong basic pH 12. Investigations of the chemostat pump performance at application-relevant pH variation in the order of 1 or 2 pH units or a few mass percent should be subjects of future investigations.

2.2.2 Autonomous Pumps

These pumps are intended as disposable, portable and inexpensive devices performing the pumping completely autonomously. Here, the hydrogel component does not act as a control element but as fluidic propulsion which does not need an external power supply. Autonomous hydrogel-based pumps can perform complete task sequences. The insulin pump described in (Richter et al. 2004a) (Fig. 7a) was developed for the treatment of the Dawn phenomenon of *diabetes mellitus* patients. Using the special possibilities to influence the swelling kinetics and the actuator dynamics, respectively, such as the variation of the swelling distance, defined counter-forces and limitations of the swelling agent supply (see Section 6), the pump realises a four task sequence.

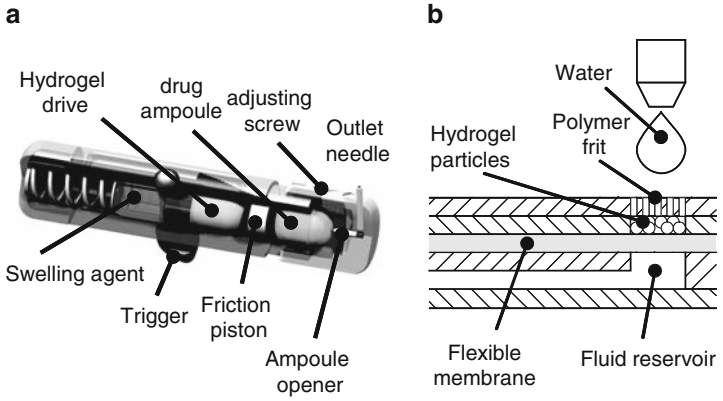

Fig. 7 Autonomous pumps. a) Medical pump with time-delay and ampoule opener functions according to (Richter et al. 2004a). (b) Portable water-activated pump according to (Good et al. 2007)

The pump is activated by switching on f the swelling agent supply (Fig. 7a). The trigger can open the supply unit or the swelling agent reservoir, respectively. A spring generates a permanent hydrostatic pressure within the swelling agent reservoir and provides a position independent swelling agent supply. The hydrogel swells and stretches a foil. At first, the actuator has to displace a friction piston. The length of the displacement is adjustable by the adjusting screw providing the adjustability of the time between the pump initialisation and the start of the drug release. After a time-delay the gel actuator presses the drug ampoule to the opener to open the sterile ampoule. In the last step the hydrogel actuator displaces the ampoule content and the pump releases the drug.

The pump shown in Fig. 7b can be initialised by a droplet of water (Good et al. 2007).

Disposable autonomous pumps do not require hydrogels with volume phase transition behaviour. Here, the strong swelling superabsorbers can be used, which are mostly more powerful than stimuli-responsive gels.

The performance of the autonomous pumps can be defined by the size of the actuator and the material. The actuator used in (Richter et al. 2004a) provides a maximal pressure of 200 kPa and is designed to release 500 µl insulin within 2 h.

2.3 Tunable Micro-Lenses

Due to the rapid development of optical imaging systems, optical communications, optical analytics and optical monitoring, the necessity to realise very compact and miniaturised micro-optical systems drastically increases. The adaptive lens is a key element of the micro-optics.

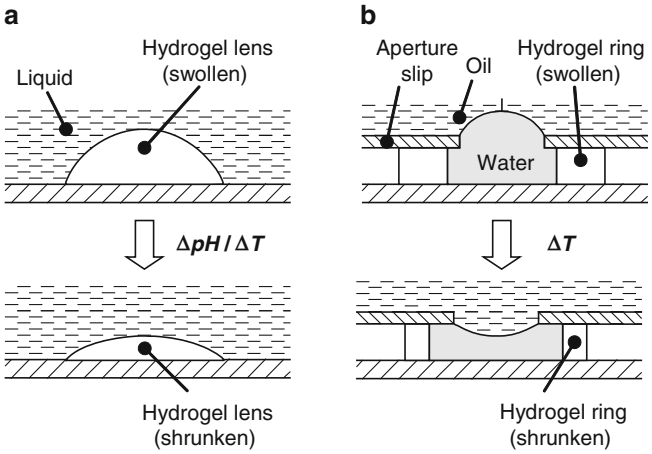

Fig. 8 Tunable micro-lenses. (a) Hydrogel-based micro-lens according to (Kim et al. 2004), (b) Liquid lens controlled by a hydrogel ring according to (Dong et al. 2007)

The outstanding transparency of hydrogels inspired the group of Lyon to develop tunable microlenses based on stimuli-responsive hydrogels (Kim et al. 2004, 2005a, b; Ehrick et al. 2007). By swelling or shrinking a planoconvex hydrogel structure bonded on the substrate deforms and changes its curvature (Fig. 8a). This leads to a tunability of the focal length of the lens.

The groups of Jiang and Beebe developed a liquid micro-lens consisting of a ring made of stimuli-responsive hydrogel which is filled with water (Fig. 8b). When the hydrogel is stimulated to change its volume the expansion or contraction of the ring regulates the shape of the oil-water interface and tunes the focal length of the micro-lens (Dong et al. 2006, 2007). The focal length is adjustable by thermal stimulation in a range between 3.3 mm and + ∞ at a response time of about 18 s.

3 Microelectromechanical Microfluidic Systems

For the last 20 years scientists have been vainly searching for a material which is able to fulfil a task in the microsystem technology comparable to the one of silicon in microelectronics. At the beginning of the 1990s stimuli-responsive hydrogels were discussed as such candidates, because these materials can be stimulated to perform the volume phase transition by light (Suzuki and Tanaka 1990) and electric field quantities (Tanaka et al. 1982). However, these effects are not really suitable for practical use in actuator devices. Therefore, in topical reviews on microfluidics or microsystem technology hydrogels are not considered at all (Stone et al. 2004; Whitesides 2006; Dittrich et al. 2006; Haeberle and Zengerle 2007).

For the last 10 years the fundamentals of a MEMS technique based on temperature-sensitive polymers have been developed by our group at the Technische Universität Dresden. In 2008 the first highly integrated hydrogel-based MEMS named "artificial skin" was presented (Richter and Paschew 2009).

In the following we introduce two key solutions of our platform technology, a concept able to control highly integrated systems containing hundreds or thousands of active polymeric elements and active microfluidic basic components.

3.1 Electrothermic and Optoelectrothermic Interface

Temperature-sensitive hydrogels with actuator properties show a LCST behaviour. They are swollen at low temperatures and shrink by exceeding of the volume phase transition temperature T_t. The best known hydrogel with LCST behaviour is PNIPAAm (Fig. 9).

The probably simplest controllable basic functionality consists of a thermosensitve hydrogel and a directly attached resistive heater (Fig. 10a) (Richter et al. 2003; Arndt et al. 2000). As a function of the electrical power per Joule heat the hydrogel can be heated above its volume phase transition temperature.

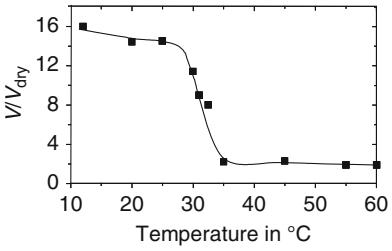

Fig. 9 Swelling behaviour of the temperature-sensitive hydrogel PNIPAAm

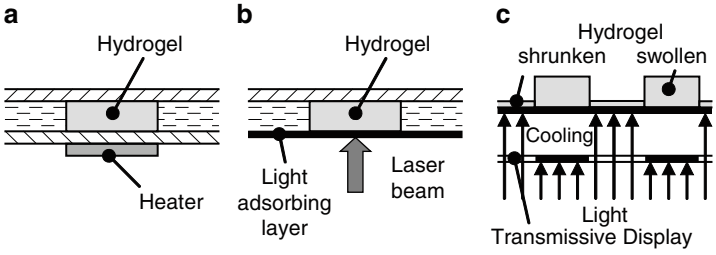

Fig. 10 (a) Electrothermic and (b,c) optoelectrothermic interfaces for the control of temperature-sensitive hydrogels based (a) on resistive heaters according to (Richter et al. 2003; Arndt et al. 2000), (b) on a laser beam according to (Wünschmann et al. 2002) and (c) on controlled light projection according to (Richter and Paschew 2009)

As resistive heating elements of this electrothermic interface thin film platinum resistors and surface mount technology (SMT) resistors are used (Richter et al. 2003, 2009a). The hydrogel components can be heated and cooled also by Peltier elements (Yu et al. 2003b; Luo et al. 2003a).

A similar effect can be obtained with an optoelectrothermic interface. Here, the hydrogel component is illuminated with high-energetic light, e.g., light of a laser source or a halogen lamp (Fig. 10b) (Wünschmann et al. 2002; Chen et al. 2008). It is recommendable to incorporate light-absorbing materials inside the gel matrix or to realise a light-absorbing interface of the hydrogel, which can be the supporting substrate (Wünschmann et al. 2002).

In the past it was expected that the electrothermic interface only allows a limited potential, because the physical and technological restrictions limit actuator density and large scale integration (Sugiura et al. 2007). This was proved to be a wrong estimation. In (Richter and Paschew 2009) an optoelectrothermic control of large-scale-integrated hydrogel-based MEMS is described. This control principle is possible since the temperature difference necessary to switch a PNIPAAm actuator from the fully swollen to the completely shrunken state is only 6 K. Furthermore, exceeding heat can be dissipated by an active cooling. The principle of the optoelectrothermic control is illustrated in Fig. 10c. The hydrogel actuators are placed onto a light absorbing black substrate. They are controlled by a commercial business video projection system. The illuminated areas are heated above the volume phase transition temperature of the gel. An active tempering keeps a constant temperature below the T_t on the bottom side of the substrate and in areas which are not illuminated. This system is suitable for individual addressing of each single actuator up to an actuator density of 566 elements per cm. A common video projector with additional optics could control approximately 100 actuators per cm (Richter and Paschew 2009).

3.2 Microvalves

Microvalves are the simplest hydrogel-based components. The gel actuator is directly placed within a valve chamber (Fig. 11a). The thermo-sensitive PNIPAAm is swollen at room temperature and closes the valve. For opening the attached resistive heater has to be activated. Exceeding the volume phase transition temperature of approximately 34 °C the gel shrinks and opens the valve seat.

As pointed up in Table 3 hydrogel-based microvalves show several excellent properties. They are miniaturisable, very pressure resistant, extremely particle permissive and show no leakage.

Wang et al. (Wang J et al. 2005) use microvalves in a polymerase chain reaction (PCR) chip, and the valves of Richter et al. are commercialised as single component or within microscopy chips (Gast et al. 2006).

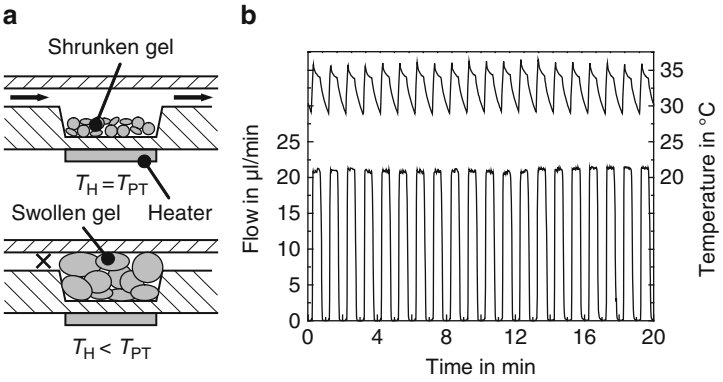

Fig. 11 Microvalve. (a) Principle according to (Richter et al. 2003; Arndt et al. 2000). (b) Behaviour according to (Richter et al. 2003)

Table 3 Hydrogel-based microvalves

Authors	Valve volume in mm^3	Pressure resistance in kPa	Time in s	
			Opening	Closing
Richter 2001, 2003 (Richter et al. 2003;	0.05	840	0.3	1
Richter et al. 2001)	0.0005	350	4	10
Yu 2003 (Yu et al. 2003a)	16	350	3–4	3–4
Luo 2003 (Luo et al. 2003b)	20	18,000	1	2
Wang 2005 (17. Wang J et al. 2005)	0.35	200	5	4.5
Sugiura 2007 (Sugiura et al. 2007)[1]	0.02	0.3	18–30	n.s.
Chen 2008 (Chen et al. 2008)[2]	n.s.	9,300	4	6.2

[1]optically controlled by using a photo-responsive hydrogel; [2]optoelectrothermic controlled by a halogen lamp

3.3 Micropumps

Integrable micropumps which act as fluidic propulsions or pressure sources are key elements of integrated microfluidic processors. Two types are described in the literature:

3.3.1 Diffusion Pumps

The characteristic feature of stimuli-sensitive hydrogels to change their volume absorbing or releasing aqueous solution has been used as advantage to realise displacement-free valves. However, this gel property is inappropriate for their use as direct-acting actuators of pumps. Therefore, the hydrogel actuator of the diffusion pump uses its swelling pressure to deform an elastic membrane which acts as pressure accumulator (Fig. 12a) (Richter et al. 2009a). If the swollen actuator is

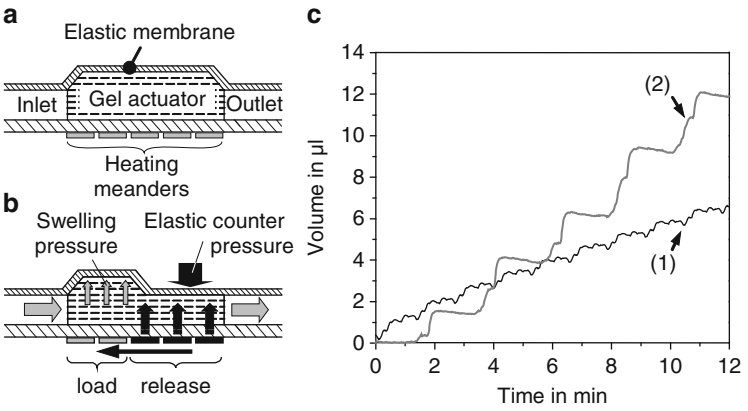

Fig. 12 Diffusion micropump. (a) Schematic set-up. (b) Operating principle. (c) Pump characteristics; (1) peristaltic mode, (2) pulsatile mode. Reproduced from (Richter et al. 2009a) by permission of The Royal Society of Chemistry

sequentially heated above its phase transition temperature by the heating meanders beginning outlet-sided then the actuator shrinks releasing the swelling agent. The released solution is immediately pushed to the outlet by the pressure of the elastic membrane because the inlet is sealed by a swollen actuator segment. To re-load the pump the heating meander has to be switched-off incipient inlet-sided. The gel cools down below the phase transition temperature and swells by absorbing liquid.

The pump can operate in two different modi (Fig. 12b). A peristaltic operation provides a continuous and relatively homogeneous pumping while a pulsatile operation of the pump is realised by a complete emptying of the pump chamber.

The pump provides a flow rate in the peristaltic mode of (0.54 ± 0.016) µl min^{-1} and in the pulsatile mode of (2.80 ± 0.350) µl within one minute. The maximum pressure is 1.28 kPa.

3.3.2 Displacement Micropumps

This pump type adapts the principle of the osmotic pump similar to chemostat pumps (Theeuwes and Yum 1976). The hydrogel actuator is placed in the actuator chamber which is located within a separate layer (Fig. 13a). This layer contains a swelling agent supply and is placed above the channel structure involving the pump chamber.

Unlike diffusion devices the displacement micropump pumps at increasing actuator volume (Fig. 13b) and fills the pump chamber at hydrogel shrinkage. The flow direction of the pump is defined by the valves placed inlet- and outlet-sided.

The pumping pressure of the displacement pump is generated by the swelling force of the hydrogel actuator. Besides the elastic membrane the back pressure of

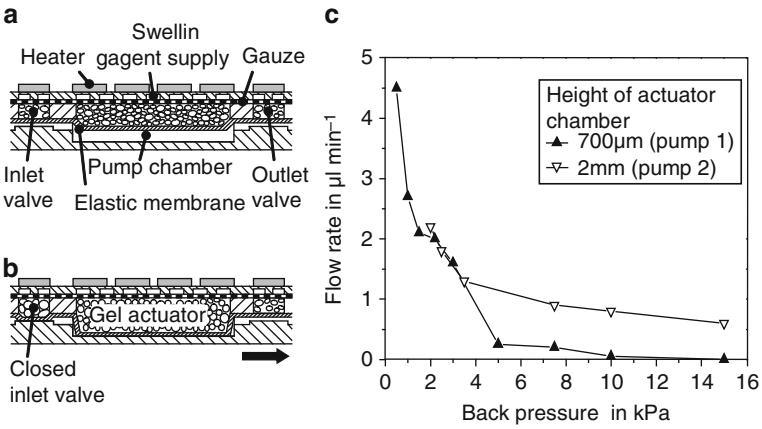

Fig. 13 Displacement micropump. (a) Schematic set-up. (b) Operating principle. (c) Pump characteristics. Reproduced from (Richter et al. 2009a) by permission of The Royal Society of Chemistry

the system counteracts the swelling pressure. Increasing back pressure decreases the flow rate of the device (Fig. 13c, pump 1). Maximal values of the pumping parameters are 4.5 µl min^{-1} at 0.5 kPa back pressure and 5 kPa at 0.2 µl min^{-1}. The pumping pressure can be increased by an increase of the actuator's thickness (Fig. 13c, pump 2). Generally, the correlation between the pumping pressure and the actuator thickness is a linear scaling law. The threefold thicker actuator of pump 2 pumps 0.6 µl min^{-1} at a back pressure of 15 kPa.

Compared to other micropumps hydrogel-based devices can be classified as pumps with small dead volume suitable for low- (diffusion micropump) and medium-performance (displacement micropump) applications (Nguyen et al. 2002; Laser and Santiago 2004).

3.4 Hydrodynamic Microtransistors

In presence of certain substances, the phase transition temperature of thermosensitive hydrogels is altered. This phenomenon is used to design electrothermically adjustable hydrodynamic microtransistors, which are also called chemostat microvalves (Richter et al. 2007a). The valve seat of the device (Fig. 14a) is tempered by a heater and an integrated temperature sensor is used for a closed-loop control. The volume phase transition temperature of PNIPAAm decreases with increasing alcohol content in water (Fig. 14b, solid symbols). Therefore, each critical alcohol concentration or volume phase transition correlates with one characteristic isotherm. Tempered at a particular isotherm the valve switches at a certain concentration (Fig. 14b, open symbols).

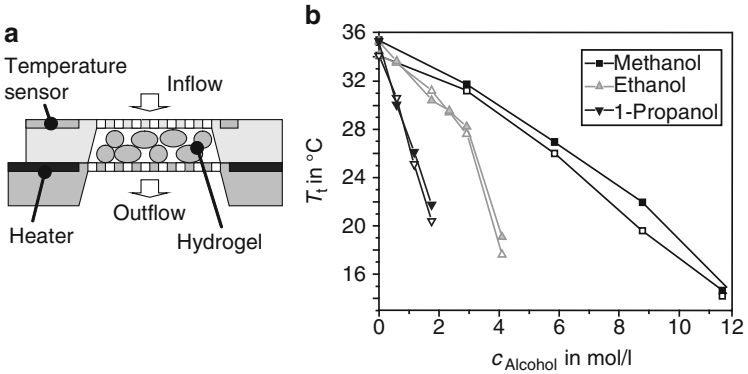

Fig. 14 Electronically controllable hydrodynamic microtransistor. (a) Schematic set-up. (b) Volume phase transition temperature of microgel determined by DSC measurements (solid symbols) as well as operating point of the transistor device (open symbols) for different alcohol concentrations in water. Reproduced with permission from (Richter et al. 2007a) p. 1109-1110, copyright Wiley-VCH Verlag GmbH & Co. KGaA.

At a certain alcohol concentration the PNIPAAm actuator loses its temperature-sensitivity due to the good solubility of the polymer chains in the solvent alcohol. This critical alcohol concentration is 11.7 mol l^{-1} for methanol, 4.1 mol l^{-1} for ethanol and 1.75 mol l^{-1} for 1-propanol. This device can be precisely adjusted to 60 mmol l^{-1} (methanol), 25 mmol l^{-1} (ethanol) and 15 mmol l^{-1} (1-propanol) concentration steps by a temperature alteration of 0.1 K.

In presence of other substances PNIPAAm does not lose its LCST behaviour. Here, the adjustability and the control range are only restricted by the solubility or by the miscibility of the substances.

4 High Resolution Tactile Displays

Besides microfluidics the human-machine interaction, especially the imaging systems, could enormously benefit from the availability of large-scale integrated actuator systems. Such systems could provide an additional mechanical data channel intended for the sense of touch of the human, which is a very sensitive aesthesia. A first impression about the performance of a high-resolution tactile display gives the “artificial skin” (Fig. 15a).

This system contains an actuator array consisting of 4,225 PNIPAAm actuators at a pitch of 580 μm (Richter and Paschew 2009). Each actuator pixel is individually switchable using the optoelectrothermic control based on a commercial business video projection system.

The artificial skin displays different types of information. Immediately after heating above the phase transition temperature of about 34 °C the PNIPAAm actuators change their colour from transparent to opaque. The artificial skin

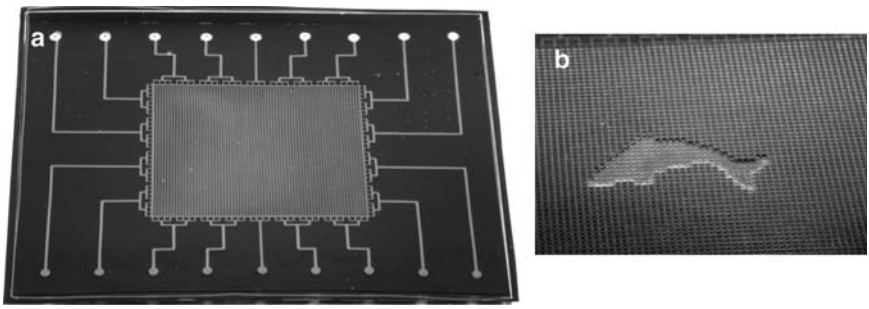

Fig. 15 Artificial skin consisting of 4,225 actuators at an area of (37 x 37) mm^2. (a) Photograph. (b) The skin maps the sharp outlines of a dolphin. The length of the dolphin from mouth to tail is 14.5 mm. Reproduced with permission from (Richter and Paschew 2009), copyright Wiley-VCH Verlag GmbH and Co. KGaA.

displays monochrome visual information. After the end of the shrinking process the artificial skin maps the dolphin with single pixel accuracy (Fig. 15b). The palpable information is based on changes in the actuator height from 500 μm at the swollen state to about 250 μm at the shrunken state and on the variation of the softness. A smooth surface of the skin's cover displays preferably differences in softness. Transferable impressions reach from the softness of fatty tissue at the swollen PNIPAAm state to the wood-like surfaces displayed by shrunken gel.

Because differences in height are hardly palpable on the soft hydrogel surface, the display is covered with a foil equipped with knobs which enhance the palpable edges.

The artificial skin would allow physical–auditory interaction with the virtual world of simulators and game engines by mapping of the computer-generated data. If the device is combined with image-based diagnostics such as computer tomography or ultrasonography then the artificial skin would provide new features in teleoperations and in diagnostics due to the virtual tactile access to inaccessible regions. The palpable recognition of objects inside the human body without the necessity to open it would improve diagnoses and allow preliminary simulation of surgical operations.

5 Influence of Material and Phase Transition Phenomena on the Operational Characteristics of Hydrogel Elements

5.1 Effects at the Initialisation of Gel Elements

After the synthesis of the active hydrogel components these are often not immediately ready to operate and show an unsatisfying behaviour. During the design process the causes of malfunctions have to be considered to avoid inoperative devices.

5.1.1 Conditioning Effect

During the first operation hydrogel elements often shows a poor repeatability and a drift of the parameters. This is caused by changes in the microscopic structure of the polymer network. By swelling and shrinking the too short polymer chains have to be cracked and the chains in general have to find their optimal moving way and position.

By performing a number of conditioning cycles the polymer network is "warmed up" and the repeat accuracy significantly increases. The conditioning process typically requires between six and thirty swelling cycles (Richter et al. 2004b). A detailed description of an initial gel conditioning procedure of a sensor is provided in Sect. 5.2.4.

5.1.2 Softening Effect

This effect is important if the hydrogel component operates between the dry state and the swollen state. The beginning of the swelling process of polymer networks with a high glass transition temperature T_g (higher than the operating temperature) can be delayed. Because of the high T_g the polymer network is glassy and the movement of the polymer chains, which is necessary for the swelling process, is disabled. Due to the self-diffusion the swelling agent penetrates the network and decreases T_g of the polymer. Now, the polymer chains are much more elastic and the polymer network begins to swell. The softening effect could be avoided using a hydrogel with a low T_g (Richter et al. 2004b).

5.1.3 Volume Change After Polymerisation

After the synthesis hydrogels significantly reswell. By adequate investigation this effect can be regarded during the design of the device. If neglected then this can lead to an irreversible malfunction or to a damage of the device, especially in components synthesised using *in-situ* polymerisation.

5.2 Phenomena at the Volume Phase Transition of Gels

5.2.1 Intrinsic Shrinkage Barrier Effect

The shrinkage process of hydrogels during the volume phase transition is sometimes affected by irregularities. A fast change of the stimulus leads to a rapid formation of a collapsed outer layer, while the rest of the hydrogel is still in the swollen state. This phenomenon is the so-called shrinkage barrier effect. After the additional collapsing of a substantial thicker layer, which is surrounding the

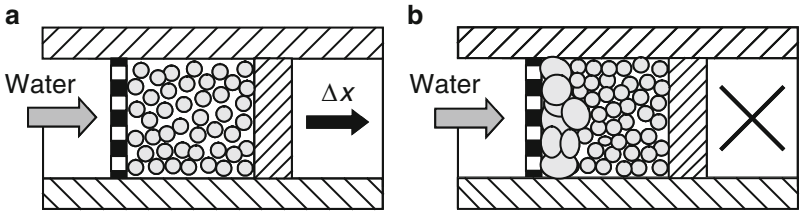

Fig. 16 Extrinsic shrinkage barrier effect. (a) After supplying the hydrogel actuator with water as swelling agent it should swell and perform a stroke. (b) The first layer of hydrogel particles swells and acts as a closing valve. Now, the further dry particles can not be supplied with water

hydrogel body beneath the thin already collapsed skin, this layer acts as shrinkage barrier preventing the swelling agent release. Therefore, the hydrogel core remains swollen. (see also Sect. 3.3.2). This effect leads to a malfunction of the device.

The shrinkage barrier effect was observed on hydrogels with porous structure stimulated by solvents and on homogeneous gels by temperature stimulation. However, this phenomenon depends on the dimensions of hydrogel. For structures with less than 200 m in size no shrinkage barrier effect is observable. The shrinkage barrier effect is avoidable using optimised hydrogels (size and homogeneity) (Richter et al. 2004b).

5.2.2 Extrinsic Shrinkage Barrier Effect

An effect similar to the shrinkage barrier effect can be observed at particle- or microgel-based actuators. This effect occurs more frequently than the intrinsic shrinkage barrier effect. It appears in packed particle actuators, when the first particle layer swells too fast and significantly decreases the swelling agent supply of the further layers similar to a valve (Fig. 16). The extrinsic shrinkage barrier effect depends on the used type of hydrogel but also on the load (particle-compressing counterforce). This can be avoided by a hydrogel material with optimised particle size which can be above or below the critical particle size.

5.2.3 Two-Step Mechanism of the Volume Phase Transition

As already described in Sect. 3.2.4 and 3.3.2, the volume phase transition takes place in two steps. At first, a fast phase separation of polymer chains occurs towards polymer-rich and polymer-poor zones. This effect can be observed in experiments as a prompt change of the Young´s modulus of the hydrogel. Following, the hydrogel shrinking process starts. The hydrogel shrinking is slower and takes

place in a second step after the phase separation. This mechanism influences the behaviour of the hydrogel elements during the operations.

For example, the prompt increase of the Young's modulus at the beginning of the shrinking process of hydrogel actuators leads to a small pressure peak. After initiation of the swelling process the Young's modulus of the hydrogel actuator abruptly decreases with a decrease of the actuator's pressure. Both phenomena are observable as discontinuities of the flow rate of valves and pumps (Richter et al. 2004b).

5.2.4 Screening Effect

Especially pH-sensitive hydrogels show a distinctive hysteretic swelling behaviour (Fig. 17) (Arndt et al. 1999). The transition from basic to acidic conditions is quite different from the acidic-to-basic curve. This is reflected in mechanical and optical hydrogel properties (Richter et al. 2008b). Suzuki explains that phenomenon with both a replacement of the H^+ counterion by an adequate ion such as Na^+ and with an excess of these ions inside the gel causing a shielding or screening of the ionised gel groups (Suzuki and Suzuki 1995).

As shown in the inset of Fig. 17, the hysteresis can be significantly lowered by a restriction to a very small operation range within the phase transition range.

5.2.5 Material Enrichment Inside the Hydrogel

In solutions with high ionic strength hardly soluble complexes or salts can be accumulated inside the hydrogels resulting in an irreversible malfunction of the sensor. Such agglomerates can appear within a few hours. This can be avoided if the hydrogel element is regularly purged and stored in deionised water. Only very thin hydrogel films do not tend to such effects. A correctly maintained hydrogel-based device can be used for several years.

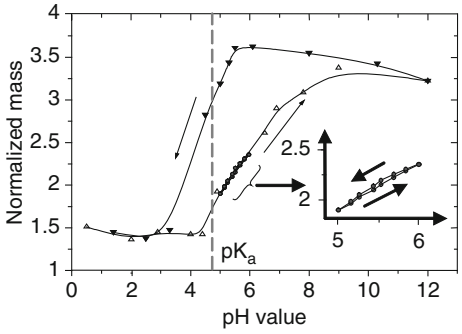

Fig. 17 pH sensitivity of a poly(vinyl alcohol) – poly (acrylic acid) hydrogel

6 Design and Performance

6.1 Response Time

6.1.1 Effective Diffusion Length

The swelling kinetics of stimuli-responsive hydrogels is described by the theory of cooperative diffusion (Sect. 3.2.2 and 3.2.3, (Tanaka and Fillmore 1979)). Besides the cooperative diffusion constant, which is specific for each solvent–polymer network combination (see Eq. (3.2.9)), the time behaviour of active hydrogel components can be as well influenced by further design-dependent aspects (Richter 2006, 2008b).

Due to the diffusion process hydrogel components with dimensions in the millimetre range or larger are very slow. To obtain fast hydrogel components different approaches are investigated. First, synthesis of porous hydrogels o minimises the effective diffusion length of the swelling agent inside the hydrogel (see Chap. 2 and Sect. 3.2.5). Unfortunately, the usability of this method is restricted because an increasing porosity of the gel significantly decreases the mechanical stability.

Furthermore, short effective diffusion lengths can be achieved by fragmentation of a large hydrogel component into many small particles (Fig. 18). Using microgels and hydrogel particles, respectively, the effective diffusion length is reduced from d_A to approximately r_P. A similar effect can be obtained with photolithographically patterned hydrogel posts (Beebe et al. 2000). Using the fragmentation method a time reduction of one or two orders of magnitude can be realised.

6.1.2 Swelling Agent Supply

Limitations of the swelling agent supply have a strong impact on the swelling kinetics. A decrease of the channel area A_C can increase the flow resistance to a value at which the hydrogel is restricted and can get only a fractional amount of the swelling agent volume flow which it would take in the case of free swelling. Therefore, the hydrogel swells remarkably slower than possible (Fig. 19a).

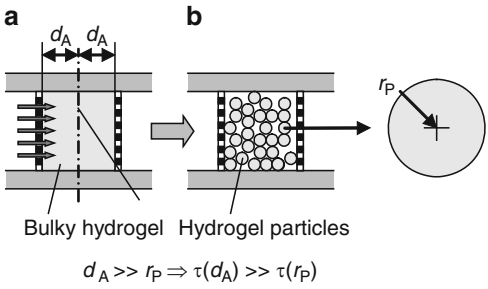

Fig. 18 Influence of the effective diffusion length on the response time of a hydrogel component. (a) Bulk hydrogel component. The effective diffusion length is d_A. (b) Component with hydrogel particles. The component volume equals with that of the bulk component. The effective diffusion length is approximately r_P

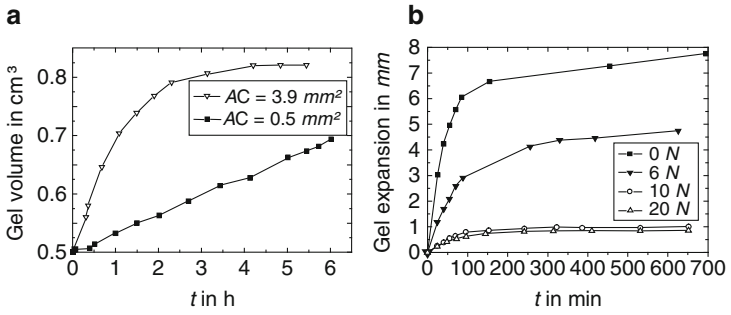

Fig. 19 Swelling characteristics of hydrogel components at (a) different channel cross-sections A_C and (b) various counterforces. As hydrogel a poly(vinyl alcohol) / polyacrylic acid network is used (Arndt et al. 1999)

6.1.3 Counterforces

The theory of Tanaka and Fillmore (Tanaka and Fillmore 1979) describes only the unloaded case. For actuator applications this case is almost impossible.

Practical investigations show that the time behaviour of the hydrogel components is strongly influenced by the counteracting forces during the swelling process of the gel. Increasing the counter-force significantly increases the response time and decrease the amplitude of the swelling degree (Fig. 19b). The shrinking process can be accelerated by counterforces.

6.1.4 Recirculation of Process Media

Inside microfluidic channels the flow is laminar. Due to the absence of turbulences different media do not mix or mix only spontaneously and very slowly. Automatic elements can only operate correct in the presence of sufficient process medium. Otherwise, in the absence of stimulation, the control functionality can not be performed. Therefore, inside microfluidic channel networks the realisation of a recirculation is recommended which can provide an independency from the state (open or closed) of the active hydrogel components.

6.2 Pressure Resistance and Particle Tolerance

Hydrogel is a soft material. However, hydrogel-based valves are outstandingly pressure-resistant (Richter et al. 2004b). The pressure resistance correlates with a maximal closing pressure which is mainly depending on the mechanical properties of the hydrogel and on the design parameters of the device. The pressure resistance of particle-based valves can be predefined by a variation of the filling degree of the

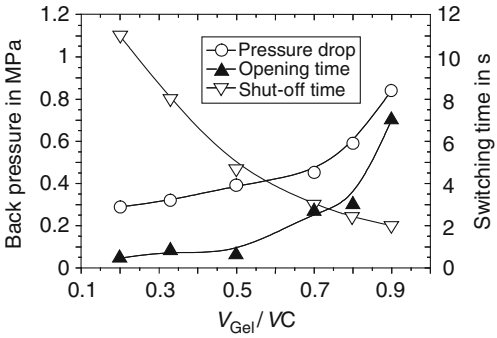

Fig. 20 Maximal back pressure without leakage flow and switching time of a microvalve in dependence on the filling degree V_{Gel}/V_C of the valve chamber. The valve chamber (800 μm × 800 μm × 200 μm) is filled with dry PNIPAAm MBAAm 4 particles; particle size 82.5 ± 5 μm (according to (Richter et al. 2004b)). V_{Gel} bulk volume of dry hydrogel particles, V_C valve chamber volume

actuator chamber with hydrogel. The back pressure of the valve increases with increasing filling degree. However, the filling degree also influences the switching time of the valve. Small filling degrees provide a fast opening but a slow closing time. A high filling degree leads to a fast closing and a slow opening time (Fig. 20). The pressure resistance of monolithic valves can be defined by the length of the valve (Yu et al. 2003b).

Due to its softness hydrogel elements are extremely particle permissive. This feature is important especially for valves. If a particle is present inside the valve seat during the closing process then the swelling hydrogel encloses it without any disturbance of the valve function.

Acknowledgments The author gratefully acknowledges the support for this work from the Deutsche Forschungsgemeinschaft (Collaborative Research Centre SFB 287 "Reactive Polymers", Heisenberg fellowship). G. Paschew is thanked for carefully proof-reading the manuscript.

References

Arndt KF, Richter A, Ludwig S, Zimmermann J, Kressler J, Kuckling D, Adler HJ (1999) Poly (vinyl alcohol)/poly(acrylic acid) hydrogels: FT-IR spectroscopic characterization of cross-linking reaction and work and transition point. Acta Polym 50:383–390

Arndt KF, Kuckling D, Richter A (2000) Application of sensitive hydrogels in flow control. Polym Adv Technol 11:496–505

Arndt KF, Schmidt T, Reichelt R (2001) Thermo-sensitive poly(methyl vinyl ether) micro-gel formed by high energy irradiation. Polymer 42:6785–6791

Baldi A, Gu Y, Loftness PE, Siegel RA, Ziaie B (2003) A hydrogel-actuated environmentally sensitive microvalve for active flow control. J Microelectromech Syst 12:613–621

Beebe DJ, Moore JS, Bauer JM, Yu Q, Liu RH, Devadoss C, Jo BH (2000) Functional hydrogel structures for autonomous flow control inside microfluidic channels. Nature 404:588–590

Chen G, Svec F, Knapp DR (2008) Light-actuated high pressure-resisting microvalve for on-chip flow control based on thermo-responsive nanostructured polymer. Lab Chip 8:1198–1204

Dittrich PS, Manz A (2006) Lab on a chip: microfluidics in drug discovery. Nature Rev Drug Disc 5:210–218

Dittrich PS, Tachikawa K, Manz A (2006) Micro total analysis systems. Latest advancements and trends. Anal Chem 78:3887–3907

Dong L, Agarwal AK, Beebe DJ, Jiang H (2006) Adaptive liquid microlenses activated by stimuli-responsive hydrogels. Nature 442:551–554

Dong L, Agarwal AK, Beebe DJ, Jiang H (2007) Variable-focus liquid microlenses and microlens arrays actuated by thermoresponsive hydrogels. Adv Mater 19:401–405

Eddington DT, Beebe DJ (2004) A valved responsive hydrogel microdispensing device with integrated pressure source. J Microelectromech Syst 13:586–593

Ehrick JD, Stokes S, Bachas-Daunert S, Moschou EA, Deo SK, Bachas LG, Daunert S (2007) Chemically tunable lensing of stimuli-responsive hydrogel microdomes. Adv Mater 19:4024–4027

Gast FU, Dittrich PS, Schwille P, Weigel M, Mertig M, Opitz J, Queitsch U, Diez S, Lincoln B, Wottawah F, Schinkinger S, Guck J, Käs J, Smolinski J, Salchert K, Werner C, Duschl C, Jäger MS, Uhlig K, Geggier P, Howitz S (2006) The microscopy cell (MicCell), a versatile modular flowthrough system for cell biology, biomaterial research, and nanotechnology. Microfluid Nanofluid 2:21–36

Gerlach G, Günther M, Sorber J, Suchaneck G, Arndt KF, Richter A (2005) Chemical and pH sensors based on the swelling behavior of hydrogels. Sens Actuat B 111–112:555–561

Good BT, Bowman CN, Davis RH (2007) A water-activated pump for portable microfluidic applications. J Colloid Interface Sci 305:239–249

Haeberle S, Zengerle R (2007) Microfluidic platforms for lab-on-a-chip applications. Lab Chip 7:1094–1110

Harmon ME, Tang M, Frank CW (2003) A microfluidic actuator based on thermoresponsive hydrogels. Polymer 44:4547–4556

http://www.fluidigm.com/products/biomark-chips.html, date: 25.06.2008

Janasek D, Franzke J, Manz A (2006) Scaling and the design of miniaturized chemical-analysis systems. Nature 442:374–380

Kataoka K, Miyazaki H, Bunya M, Okano T, Sakurai Y (1998) Totally synthetic polymer gels responding to external glucose concentration: their preparation and application to on-off regulation of insulin release. J Am Chem Soc 120:12694–12695

Kim D, Beebe DJ (2007) A bi-polymer micro one-way valve. Sens Actuat A 136:426–433

Kim J, Serpe MJ, Lyon LA (2004) Hydrogel microparticles as dynamically tunable microlenses. J Am Chem Soc 126:9512–9513

Kim J, Nayak S, Lyon LA (2005a) Bioresponsive hydrogel microlenses. J Am Chem Soc 127:9588–9592

Kim J, Serpe MJ, Lyon LA (2005b) Photoswitchable microlens arrays. Angew Chem Int Ed 44:1333–1336

Kuckling D, Arndt KF, Richter A (2003) Temperature and pH dependent swelling behavior of poly (N-isopropylacrylamide)-copolymer hydrogels and their use in flow control. Macromol Mater Eng 288:144–151

Kuhn W, Hargitay B (1951) Muskelähnliche Arbeitsleistung künstlicher hochpolymerer Stoffe. Z f Elektrochemie 55:490–502

Kuhn W, Künzle O, Katchalsky A (1948) Denouement de molecules en chaines polyvalentes par des charges electriques en solution. Bull Soc Chim Belg 57:421–431

Kurauchi T, Shiga T, Hirose Y, Okada A (1991) Deformation behaviors of polymer gels in electric field. In: D. DeRossi, K. Kajiwara, Y. Osada, A. Yamauchi (ed): Polymer gels: Fundamentals and biomedical applications. Plenum Press New York, 2

Laser DJ, Santiago JG (2004) A review of micropumps. J Micromech Microeng 14:R35–R64

Li W, Zhao H, Teasdale PR, John R, Zhang S (2002) Synthesis and characterisation of a polyacrylamide-polyacrylic acid copolymer hydrogel for environmental analysis of Cu and Cd. React Funct Polym 52:31–41

Liu RH, Yu Q, Beebe DJ (2002) Fabrication and characterization of hydrogel-based microvalves. J Microelectromech Syst 11:45–53

Liu C, Park JY, Xu Y, Lee SH (2007) Arrayed pH-responsive microvalves controlled by multi-phase laminar flow. J Micromech Microeng 17:1985–1991
Luo Q, Mutlu S, Gianchandani YB, Svec F, Fréchet JMJ (2003a) Monolithic valves for microfluidic chips based on thermoresponsive polymer gels. Electrophoresis 24:3694–3702
Luo Q, Mutlu S, Gianchandani YB, Svec F, Fréchet JMJ (2003b) Monolithic valves for microfluidic chips based on thermoresponsive polymer gels. Electrophoresis 24:3694–3702
Mitsumata T, Ikeda K, Gong JP, Osada Y (1998) Solvent-driven chemical motor. Appl Phys Lett 73:2366–2368
Mitsumata T, Ikeda K, Gong JP, Osada Y (2000) Controlled motion of solvent-driven gel motor and its application as a generator. Langmuir 16:307–312
Miyata T, Asami N, Uragami T (1999) A reversibly antigen-responsive hydrogel. Nature 399:766–769
Nguyen NT, Huang X, Chuan TK (2002) MEMS-micropumps: a review. Transact ASME 124:384–392
Osada Y, Gong JP (1998a) Soft and wet materials: Polymer gels. Adv Mater 10:827–837
Osada Y, Gong JP (1998b) Soft and wet materials: Polymer gels. Adv. Mater. 10:827–837
Osada Y, Takeuchi Y (1981) Water and protein permeation through polymeric membrane having mechanochemically expanding and contracting pores - Function of chemical valve-. J Polym Sci, Polym Lett Ed 19:303–308
Park JY, Oh HJ, Kim DJ, Baek JY, Lee SH (2006) A polymeric microfluidic valve employing a pH-responsive hydrogel microsphere as an actuating source. J Micromech Microeng 16:656–663
Peters EC, Svec F, Frechét JMJ (1997) Thermally responsive rigid polymer monoliths. Adv Mater 9:630–633
Richter A (2006) Hydrogel-based TAS. In C.T. Leondes: MEMS/NEMS Handbook: Techniques and Applications. Vol. 2: Fabrication Techniques, Chapter 5, Springer, New York
Richter A, Paschew G (2009) Optoelectrothermic control of polymer-based highly integrated MEMS applied in an artificial skin. Adv Mater 21:979–983
Richter A, Arndt KF, Krause W, Kuckling D, Howitz S (2001) Devices for flow control based on smart hydrogels. 7th Pacific polymer Conference, Oaxaca, Dec 3–7, 2001, p. 312
Richter A, Kuckling D, Howitz S, Gehring T, Arndt KF (2003) Electronically controllable microvalves based on smart hydrogels: magnitudes and potential applications. J Microelectromech Syst 12:748–753
Richter A, Klenke C, Arndt KF (2004a) Adjustable low dynamic pumps based on hydrogels. Macromol Symp 210:377–384
Richter A, Howitz S, Kuckling D, Arndt KF (2004b) Influence of volume phase transition phenomena on the behaviour of hydrogel-based valves. Sens Actuat B 99:451–458
Richter A, Krause W, Lienig J, Arndt KF (2005) Polymer networks as actuator and sensor systems to be used for automation of biomedical devices. Biomed Technik 50:66–68
Richter A, Türke A, Pich A (2007a) Controlled double-sensitivity of microgels applied to electronically adjustable chemostats. Adv Mater 19:1109–1112
Richter A, Wenzel J, Kretschmer K (2007b) Mechanically adjustable chemostats based on stimuli-responsive polymers. Sens Actuat B 125:569–573
Richter A, Klatt S, Paschew G, Klenke C (2009a) Micropumps operated by swelling and shrinking of temperature-sensitive hydrogels. Lab Chip 9:613–618
Richter A, Paschew G, Klatt S, Lienig J, Arndt KF, Adler HJ (2008b) Review on hydrogel-based pH sensors and microsensors. Sensors 8:561–581
Sershen SR, Mensing GA, Ng M, Halas NJ, Beebe DJ, West JL (2005) Independent optical control of microfluidic valves formed from optomechanically responsive nanocomposite hydrogels. Adv Mater 17:1366–1368
Stone HA, Stroock AD, Ajdari A (2004) Engineering flows in small devices: microfluidics towards a lab-on-a-chip. Annu Rev Fluid Mech 36:381–411
Sugiura S, Sumaru K, Ohi K, Hiroki K, Takagi T, Kanamori T (2007) Photoresponsive polymer gel microvalves controlled by local light irradiation. Sens Actuat A 140:176–184

Suzuki M (1991) Amphoteric poly(vinyl alcohol) hydrogel and electrodynamic control method for artificial muscles. In: D. DeRossi, K. Kajiwara, Y. Osada, A. Yamauchi (ed): Polymer gels: Fundamentals and biomedical applications. Plenum Press New York, 221-236

Suzuki A, Suzuki H (1995) Hysteretic behavior and irreversibility of polymer gels by pH change. J Chem Phys 103:4706–4710

Suzuki A, Tanaka T (1990) Phase-transition in polymer gels induced by visible-light. Nature 346:345–347

Suzuki H, Tokuda T, Kobajashi K (2002) A disposable "intelligent mosquito" with a reversible sampling mechanism using the volume-phase transition of a gel. Sens Actuat B 83:53–59

Tanaka T (1978) Collapse of gels and critical endpoint. Phys Rev Lett 40:820–823

Tanaka T, Fillmore DJ (1979) Kinetics of swelling of gels. J Chem Phys 70:1214–1218

Tanaka T, Nishio I, Sun ST, Ueno-Nishio S (1982) Collapse of gels in an electric field. Science 218:467–469

Theeuwes F, Yum SI (1976) Principles of the design and operation of generic osmotic pumps for the delivery of semisolid or liquid drug formulations. Annals Biomed Eng 4:343–353

Thorsen T, Maerkl SJ, Quake SR (2002) Microfluidic large-scale integration. Science 298: 580–584

Unger MA, Chou HP, Thorsen T, Scherer A, Quake SR (2000) Monolithic microfabricated valves and pumps by multilayer soft lithography. Science 288:113–116

Wang J, Chen Z, Mauk M, Hong KS, Li M, Yang S, Bau1 HH (2005) Self-actuated, thermo-responsive hydrogel valves for lab on a chip. Biomed Microdev 7: 313–322

Whitesides GM (2006) The origins and the future of microfluidics. Nature 442:368–373

Wünschmann W, Richter A, Dierigen HJ, Howitz, S, Kuckling D, Keller, M, Arndt KF, Taktile Anzeigeeinheit. German Patent Application DE 102 26 746.4, filing date 14/06/2002

Yu C, Mutlu S, Selvaganapathy P, Mastrangelo CH, Svec F, Fréchet JMJ (2003a) Flow control valves for analytical microfluidic chips without mechanical parts based on thermally responsive monolithic polymers. Anal Chem 75:1958–1961

Yu C, Mutlu S, Selvaganapathy P, Mastrangelo CH, Svec F, Fréchet JMJ (2003b) Flow control valves for analytical microfluidic chips without mechanical parts based on thermally responsive monolithic polymers. Anal Chem 75:1958–1961

Zhang Y, Kato S, Anazawa T (2008) A microchannel concentrator controlled by integral thermo-responsive valves. Sens Actuat B 129:481–486

Polymer Hydrogels to Enable New Medical Therapies

P. Welzel, M. Nitschke, U. Freudenberg, A. Zieris, T. Götze, M. Valtink, K. Engelmann, and C. Werner

Abstract Hydrogels are well-established materials in various biomedical technologies. This chapter highlights current trends in the research on hydrophilic polymer systems motivated by the demand of advanced, cell-based medical therapies. Two major aspects of the use of polymeric materials in regenerative medicine are discussed: Functional coatings for cell culture carriers and polymer scaffolds for *in vivo* tissue engineering. With respect to cell culture carriers emphasis is put on stimuli-responsive polymers used for the gentle harvest of cell sheets; the example given concerns the processing of corneal endothelial cell layers supporting new approaches for cornea repair. A second subsection is dedicated to polymer scaffolds for *in vivo* tissue engineering and refers to recent developments of biohybrid polymers containing heparin as the biomolecular component. The example reports on ongoing own research on star-poly(ethylene glycol)-heparin-hydrogels currently explored as injectable matrices to support angiogenesis, a key process in the regeneration of almost all tissues and organs.

Keywords Tissue engineering • Cell culture • Poly(*N*-isopropyl acrylamide) • Biohybrid material • Heparin • Star-poly(ethylene glycol) • Angiogenesis

P. Welzel, M. Nitschke, U. Freudenberg, A. Zieris, T. Götze, and C. Werner (✉)
Leibniz Institute of Polymer Research Dresden, Max Bergmann Center of Biomaterials, Germany
e-mail: werner@ipfdd.de

M. Valtink
Technische Universität Dresden, Medical Faculty, Germany

K. Engelmann
Klinikum Chemnitz, Department of Ophthalmology, Germany

K. Engelmann and C. Werner
Center for Regenerative Therapies Dresden, Germany

G. Gerlach and K.-F. Arndt (eds.), *Hydrogel Sensors and Actuators*,
Springer Series on Chemical Sensors and Biosensors 6,
DOI: 10.1007/978-3-540-75645-3_8, © Springer-Verlag Berlin Heidelberg 2009

Contents

Abbreviations

DEGMA	Diethyleneglycol methacrylate
ECM	*Extracellular matrix*
EDC	1-ethyl-3-(3-dimethylaminopropyl) carbodiimid
FGF-2	Basic fibroblast *growth factor*
FN	Fibronectin
FTIR-ATR	Fourier transform infrared attenuated total reflection
HUVECs	Human endothelial cells isolated from umbilical cord
MMP	Matrix metalloproteinase
PBS	Phosphate buffered saline
PEG	Poly(ethylene glycol)
PNIPAAm	Poly(*N*-isopropyl acrylamide)
RGD	Amino acid code for arginine-glycine-aspartic acid
SRP	Stimuli responsive polymer
sulfo-NHS	N-hydroxysulfosuccinimid
TCP	Tissue culture polystyrene
TGF-β	Transforming growth factor beta
VEGF	Vascular endothelial *growth factor*
XPS	X-ray photoelectron spectroscopy

1 Hydrogels in Biomedical Applications

Polymer hydrogels are used for the fabrication of medical devices already through several decades. Early examples include the work of Kolff to treat patients suffering from kidney failure by means of cellulose-based membranes (Kolff et al. 1997) and the pioneering studies of Wichterle and Lim to produce contact lenses from poly (hydroxyethyl methacrylate) (Wichterle and Lim 1960). Catheters used in cardiology for balloon dilatation or implantation of vascular stents are very often coated, nowadays with polymer hydrogels to reduce the friction at the vessel surface. Many diagnostic assays utilise surface-bound hydrophilic polymer coatings to limit the

non-specific adsorption from biofluids. These applications, as well as several others, draw benefit from the high affinity of hydrogels towards water, resulting in advantageous mechanical properties as well as weak interactions with the molecular and cellular components of biofluids, tissues and organs.

However, with the advent of regenerative therapies a number of additional options make polymer hydrogels even more attractive. Based on the progress of molecular cell biology a wealth of entirely new therapeutic concepts is now explored to cure various severe and fatal diseases such as myocardial infarction or neurodegenerative diseases. These strategies rely on the potential of stem/progenitor cells and ask for a re-invention of medical devices. Key feature of the novel therapeutic systems is the generation of spatio-temporally orchestrated signals acting exogenously on cells in order to induce and support regeneration were it is missing or incomplete in natural settings. To meet this challenge, hydrogels in regenerative therapies refer to the characteristics of the cellular microenvironment, the extracellular matrix (ECM). It consists of a variety of complex supramolecular assemblies of various proteins, proteoglycans and glycosaminoglycans. Importantly, ECM is a highly dynamic, feedback controlled structure of multiple biopolymers which modulates physical as well as molecular signalling events and various types of ECM are known to occur in living tissues to support such dedicated functions. To mimic and vary the characteristics of ECM, man-made hydrogels for regenerative therapies need to be adaptive with respect to structural features and have to undergo specific interactions with various biomolecular components of their local environments. The implementation of these characteristics requires the application of advanced design concepts as well as a very comprehensive analytical verification of the obtained gel structures, including the detailed investigation of interactions between the polymer materials and biosystems.

Addressing these challenges, various synthetic and biohybrid polymer materials have been developed and evaluated in the recent past (Peppas et al. 2006). A wealth of novel design concepts is currently explored to implement peptides, DNA and modified glycosaminoglycans enabling even more advanced, bio-mimetic as well as bio-responsive materials (Jia and Kiick 2009; Kopecek and Yang 2009). In this chapter, we refer to two rather distinct technologies to illustrate the wide range of demanding applications currently addressed by the related research: stimuli-responsive polymer films to harvest functional cell sheets and biohybrid polymer matrices to stimulate angiogenesis.

Stimuli-responsive polymers (SRP) with a thermally stimulated volume phase transition like poly(*N*-isopropylacrylamide) (PNIPAAm) (Schild 1992) or *N*-isopropylacrylamide (NIPAAm) containing copolymers (Rzaev et al. 2007) can be used to fabricate switchable cell culture carriers that allow to detach adherent cells or cell sheets without enzymatic treatment (Da Silva et al. 2007). Pioneering reports on this technique appeared in the early nineties. Takezawa et al. (Takezawa et al. 1990) applied soluble PNIPAAm-containing coatings on cell culture carriers and achieved a controlled cell detachment by thermally stimulated disintegration of the coating. In contrast, Yamada et al. (Yamada et al. 1990) demonstrated stimulated cell detachment from carriers covalently grafted with PNIPAAm. The strength of the

latter approach – permanent immobilisation of SRP coatings on solid surfaces – was shown by many authors since that time. The obtained coatings respond with reversible swelling and collapsing to small changes of the environmental temperature. Above the transition temperature, the collapsed layer allows cell attachment, growth and proliferation similar to tissue culture polystyrene (TCP), while decreasing the temperature causes an expansion of the SRP layer and, finally, a gentle detachment of the cultivated cells as an intact cell layer. Okano et al. systematically developed this technique mainly using electron beam irradiation to prepare PNIPAAm grafted TCP (Matsuda et al. 2007). To this day, the cell sheet engineering technique was proven by this group for a wide variety of cell types and tissues (Matsuda et al. 2007; Yamato et al. 2007). Furthermore, PNIPAAm grafted TCP dishes were commercialised for research purposes. Beyond that, there is a number of activities to fully exploit the potential of thermo-responsive cell culture carriers. Canavan et al. studied in detail the mechanism of cell detachment and the release of the extracellular matrix (Canavan et al. 2005). Bioactive molecules were bound to (Hatakeyama et al. 2006) or released (von Recum et al. 1998) from SRP coatings to locally control cell adhesion and proliferation. Towards ambitious tissue engineering concepts various types of lateral stuctured SRP coatings were applied (Chen et al. 1998; Tsuda et al. 2005; Schmaljohann et al. 2005).

Biohybrid gel materials containing synthetic and biomolecular components aim at the defined and systematic variation of the biomolecular complexity *and* the mechanical characteristics of biofunctional matrices to open new options for cell replacement therapies (Werner 2006; Lutolf and Hubbell 2005). While the previously used materials were often based on one main structural component (Drury and Mooney 2003; Van Tomme and Hennink 2007; Tessmar and Gopferich 2007; Hutmacher and Garcia 2005), recent studies aimed at implementing multiple sets of ECM components (Liu et al. 2007; Nillesen et al. 2007; Stamov et al. 2008), combined ECM motifs in self-assembling peptide-amphiphile nanofibres (Silva et al. 2004) and employed advanced materials for sequential release of signalling molecules (Fischbach and Mooney 2006; Pridgen et al. 2007). In particular, the incorporation of polysaccharidic ECM molecules into synthetic scaffolds is of raising interest (Seal and Panitch 2003; Pratt et al. 2004; Nie et al. 2007; Yamaguchi and Kiick 2005; Tae et al. 2006; Benoit and Anseth 2005; Benoit et al. 2007) to capitalise on their affinity to signalling molecules (e.g. growth factors) (Capila and Linhardt 2002). Beyond that, the mechanical properties of ECM-mimicking materials recently received attention as Discher et al. impressively confirmed the impact of the elasticity of culture substrates on stem cell differentiation (Discher et al. 2005).

2 Thermo-Responsive Cell Culture Carriers

For thermo-responsive cell culture carriers the transition temperature of the SRP coating should be slightly below 37°C to allow cell adhesion under standard culture conditions and cell detachment with a rather small temperature decrease. Pure

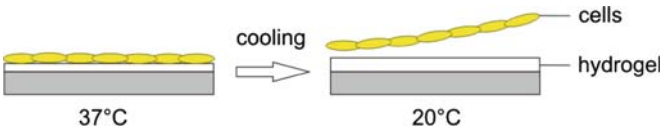

Fig. 1 Stimulated cell detachment from a thermo-responsive carrier

PNIPAAm with its transition in water at 32°C meets this criterion quite well. Cell detachment typically requires a temperature drop to 20°C (Fig. 1).

Since SRP materials relevant to this application are water-soluble in the swollen state, polymer molecules have to be immobilised on a substrate that ideally allows microscopic control of cell culture and cell detachment. Possible options are standard TCP dishes, other optically transparent polymeric carriers or glass slides. To permanently affix SRP thin films on these materials, a multitude of techniques can be applied.

In the "grafting from" approach, a surface, that was previously activated e.g. by plasma treatment, is exposed to a monomer solution (Huang et al. 2003). A more simple, one-step procedure is to irradiate a polymeric surface like TCP, which is covered with the monomer solution, by an electron beam (Yamada et al. 1990). Alternatively, ultraviolet light and a photosensitiser can be utilised to initiate polymerisation and cross-linking (Curti et al. 2005). A completely different route to prepare thin SRP coatings with good adhesion to solid substrates is plasma polymerisation (Biederman and Osada 1992). In this case, NIPAAm is used as a precursor in a plasmachemical thin film deposition process (Cheng et al. 2005; Pan et al. 2001).

Contrary to the monomer-based techniques described so far, low-pressure plasma immobilisation allows to permanently attach stimuli-responsive polymer films with a thickness of a few nanometers on polymeric substrates using an argon discharge. At appropriate treatment parameters, covalent fixation is achieved while important properties of the immobilised polymer like the thermo-responsive behaviour are preserved (Schmaljohann et al. 2004; Nitschke et al. 2004).

The successful immobilisation of the SRP material can be verified, e.g. by X-ray photoelectron spectroscopy (XPS) (Tsuda et al. 2005) or Fourier transform infrared attenuated total reflection spectroscopy (FTIR-ATR) (Hatakeyama et al. 2007). As a simple proof for the thermo-responsive behaviour of the coating, temperature-dependent water contact angle measurements are applied (Tsuda et al. 2004). Since the thickness of the immobilised SRP layer was found to be a crucial parameter for stimulated cell detachment (Da Silva et al. 2007), a reliable measurement technique for this value is of particular importance. While angle-resolved XPS or FTIR-ATR spectroscopy give a rather rough estimation, ellipsometry provides precise thickness data. Furthermore, ellipsometry can be performed under liquid media of a predefined temperature. This allows to monitor *in situ* the dynamic response of a SRP layer. A number of important physicochemical properties like the temperature dependent degree of swelling can be determined. In the example shown in Fig. 2, a value of about 5 was found for an expanded PNIPAAm layer prepared by the plasma immobilisation technique. Obviously, the transition range for PNIPAAm

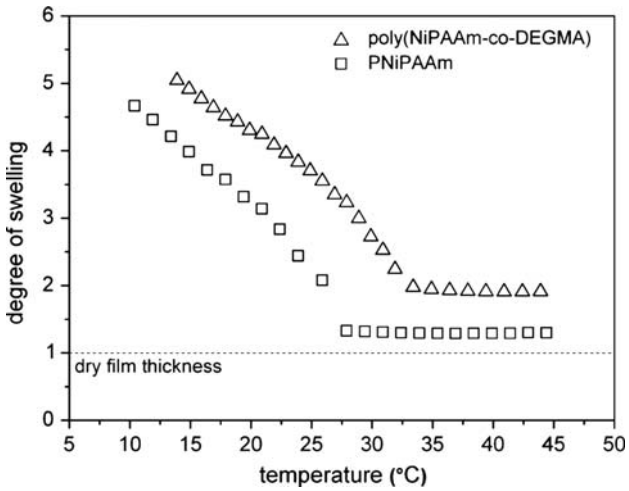

Fig. 2 Temperature-dependent swelling behaviour of PNIPAAm and poly(NiPAAm-co-DEGMA) thin films immobilised by low-pressure argon plasma treatment (reproduced from (Nitschke et al. 2007a) with permission)

immobilised on a solid surface is much broader compared to PNIPAAm in aqueous solution (Schmaljohann et al. 2004) and further broadens when pure water is replaced by phosphate buffered saline solution (PBS) or cell culture medium (Schmaljohann et al. 2003a). However, when correlating ellipsometry results with cell culture observations it was found, that cell detachment can appear clearly before the maximum degree of swelling is reached (Schmaljohann et al. 2003b).

Beyond the side effects discussed so far, the switching behaviour of the SRP coating can be tuned systematically to meet specific requirements of thermo-reversible cell culture carriers to be used in a particular application. Instead of pure PNIPAAm, appropriate copolymers allow to decrease or increase the transition temperature (Tsuda et al. 2004; Gramm et al. 2005). Shifting the transition further towards 37°C by means of a statistical copolymer of N-isopropylacrylamide and diethyleneglycol methacrylate (poly(NIPAAm-co-DEGMA), Fig. 2) minimises the temperature drop required for cell detachment (Nitschke et al. 2007a). Furthermore, copolymerisation can also provide functional groups on PNIPAAm-based coatings. Covalent binding of bioactive molecules to these sites is a versatile approach to control cell proliferation on these surfaces (Hatakeyama et al. 2006). The initial strength of cell adhesion and the ease of subsequent stimulated detachment can be adjusted by a certain roughness of the SRP-grafted substrate (Kwon et al. 2000), co-grafting of NIPAAm and poly(ethylene glycol) (PEG) (Kwon et al. 2003) or using PEG-containing copolymers (Nitschke et al. 2007b). Thermo-responsive cell culture carriers were successfully used for a wide variety of cell types. This includes tracheal epithelial cells (Kanzaki et al. 2006), aortic endothelial cells (Canavan et al. 2005), cardiomyocytes (Shimizu et al. 2002), corneal epithelial cells (Nishida et al. 2004) and corneal endothelial cells (Ide et al. 2006; Lai et al. 2006).

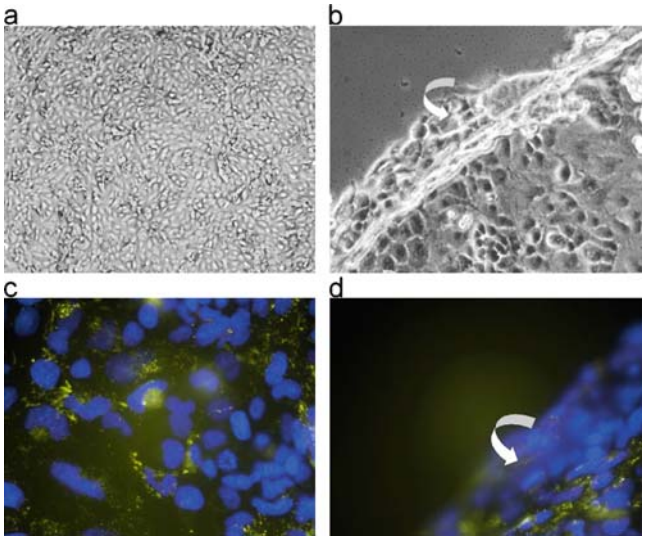

Fig. 3 (a,b) Cell detachment from a poly(NiPAAm-co-DEGMA) substrate: microscopy images of corneal endothelial cells after (a) standard cultivation at 37°C (1747 µm x 1385 µm) and after (b) cooling to 30°C (436 µm x 346 µm); (c,d) fluorescence microscopy images (213 µm x 162 µm, oval objects: nuclei, scattered material in between: fibronectin) of corneal endothelial cells on poly (NIPAAm-co-DEGMA) after (c) standard cultivation at 37°C and after (d) cooling to 30°C (reproduced from (Nitschke et al. 2007a) with permission)

Figures 3a, b illustrate the stimulated detachment of a confluent layer of human corneal endothelial cells (Nitschke et al. 2007a). *In vivo*, these cells form a delicate monolayer that regulates corneal hydration and transparency. Cell loss caused by accidental or surgical trauma, dystrophy, or corneal disease may result in impaired vision or even blindness because these cells lack a regenerative capacity. Corneal transplantation has achieved great success to restore vision, but the availability of donor corneas with a functional endothelium is limited. Therefore, constructing corneal endothelial cell sheets as transplants from cell cultures could help to overcome the shortage in corneal grafts. Here, the use of thermo-responsive cell culture carriers greatly facilitates the production of transplantable corneal endothelial cell sheets. Immunostaining of fibronectin (Figs. 3c, d) gives a first evidence for the detachment of the intact extracellular matrix together with the cell sheet. This important prerequisite for functional tissue generation is another significant advantage of thermally stimulated cell detachment compared to other methods. It could also be shown that the influence of these substrates does not exceed those of other cultivation parameters such as the culture medium. Thus, cultivation of these cells on thermo-responsive cell culture carriers does not interfere with the expression of typical and functional proteins (Götze et al. 2008).

Most of the preparation techniques mentioned above allow lateral patterning of thermo-responsive cell culture carriers by simple masking techniques. This includes ultraviolet (Chen et al. 1998) and electron beam irradiation (Tsuda et al. 2005) as

well as plasma immobilisation (Schmaljohann et al. 2005). Patterned co-cultures of different cells are promising tools for growing defined lateral structures that are more complex than a homogeneous layer of one particular cell type. Moreover, structured cell sheet generation by means of thermo-responsive carriers is the initial step in layer-by-layer approaches to produce complex 3D tissue constructs (Tsuda et al. 2007).

3 Biohybrid Cell Scaffolds for *In Vivo* Tissue Engineering

Cell replacement strategies comprise various approaches to locally deliver tissue-specific or undifferentiated cells or cellular assemblies in order to restore or replace the function of injured or damaged tissues or organs. To enable these strategies, carrier materials need to scaffold the cells of interest for transfer and deposition. Beyond that, such scaffolds are expected to mimic the natural extracellular matrix in providing support for cell adhesion, migration, and proliferation inducing differentiated function, tissue (re-)generation, and its 3D organisation. In view of the polymeric nature of ECM, the use of processed (ECM-derived) biopolymers and the adaptation of synthetic polymeric materials received a lot of attention in almost any variant of tissue engineering.

Since both the biopolymer-based (biomimetic, ECM-like) structures (such as Matrigel®[1]) and fully synthetic polymer materials are limited with respect to the control over well-evolved biological mechanisms with tailorable physical properties, biohybrid polymer networks containing both synthetic and natural or synthetic and bioanalogous components are considered promising to develop morphogenetic or tissue-specific matrices.

Several systems employ the synthetic polymer poly(ethylene glycol) as the main component which is decorated with biomimetic peptides and/or proteins. PEG-based materials are distinguished by relatively weak non-specific protein adsorption, and thus, can be used to introduce systematically selected cell signalling epitopes to explore their influence on cellular attachment and functions.

To enhance cell adhesion PEG-based (Hern and Hubbell 1998; Burdick and Anseth 2002; Burdick et al. 2004) and other hydrogels have been modified with amino acid sequences derived from natural proteins, e.g. integrin-binding domains as RGD[2].

In addition, the degradation properties of hydrogels were adjusted by incorporation of degradable linkers. By using enzyme-sensitive peptide sequences, cell-responsive biomaterials that mimic the proteolytic recognition of natural ECMs

[1] Matrigel is the trade name (BD Biosciences) for a solubilised basement membrane preparation extracted from the Engelbreth-Holm-Swarm mouse sarcoma, a tumor rich in extracellular matrix proteins. This mixture resembles the complex extracellular environment found in many tissues and is used as a substrate for cell culture.

[2] RGD is the one-letter amino acid code abbreviation for arginine-glycine-aspartic acid. Peptide sequences containing a RGD motif are used as specific ligands to mediate cell adhesion.

are available (Lutolf and Hubbell 2005; West and Hubbell 1999). Cross-linking of PEG vinyl sulfone macromers with enzymatically cleavable peptides (linear oligopeptide substrates for matrix metalloproteinases, MMPs) resulted in hydrogels that are susceptible to cell-mediated proteolytic breakdown (Lutolf et al. 2003) and remodelling. The cell invasion rate of human fibroblasts into these gels was found to be dependent on RGD ligand density, the sensitivity to MMPs, and the cross-linking density of the network. Recently, Hubbell and coworkers have shown that these cell-responsive PEG-based hydrogels can also direct differentiation of pluripotent progenitor cells towards a cardiac lineage in vitro, using embryonal carcinoma cells as a model (Kraehenbuehl et al. 2008).

Another important trigger of morphogenesis and tissue regeneration is the sequestration of growth factors. Incorporation of growth factors into hydrogels can be realised by covalent attachment (Delong et al. 2002). For example, transforming growth factor beta (TGF-β) has been tethered to PEG to regulate smooth muscle cell function (Mann et al. 2001). But this can lead to a very strong attachment which in many cases interferes with the function of the effector molecule. Therefore, the noncovalent binding of growth and differentiation factors to components of biohybrid polymer materials or the entrapment of the factors within the networks are in general considered advantageous.

Hence, the rather strong electrostatically driven binding of persulfated saccharides such as heparin to various signalling molecules is a beneficial effect making heparin highly attractive for the design of different types of bioactive matrices.

Accordingly, heparin has been incorporated into noncovalently assembled, polymeric hydrogel networks based on its interactions with known heparin-interacting peptides and proteins. Poly(ethylene glycol) star polymers functionalised with heparin-binding peptide motifs were reported to assemble with heparin into viscoelastic solutions with tunable properties (Seal and Panitch 2003; Seal and Panitch 2006). These can also be mixed with star-poly(ethylene glycol)–heparin conjugates to form noncovalent hydrogels capable of growth factor delivery via hydrogel erosion (Yamaguchi and Kiick 2005; Zhang et al. 2006; Yamaguchi et al. 2005). Such erosion strategies, although passive, may offer opportunities to modulate the growth factor activity via co-release of the growth factor with the heparinised macromolecules. In addition, physical networks were formed through direct association of similar PEG-heparin conjugates with dimeric, heparin-binding growth factors (specifically vascular endothelial growth factor, VEGF) (Yamaguchi et al. 2007). These hydrogels degrade through receptor-mediated erosion as VEGF is delivered to the cells.

Other authors describe the covalent incorporation of heparin into hydrogel networks: Anseth and coworkers (Benoit and Anseth 2005; Benoit et al. 2007) have copolymerised methacrylated high-molecular-weight heparin and dimethacrylated PEG to yield hydrogels of varying composition. These gels were analysed as a possible delivery vehicle for basic fibroblast growth factor (FGF-2) and as a synthetic extracellular matrix for the osteogenic differentiation of human mesenchymal stem cells. Tae et al. (Tae et al. 2006) described a system in which heparin was modified with a dihydrazide and cross-linked to the N-hydroxysuccinimidyl

ester of PEG-bis-butanoic acid. The resulting system allowed a controllable release of bioactive vascular endothelial growth factor.

Kiick and co-workers (Nie et al. 2007; Kiick 2008) suggested the combination of noncovalent assembly strategies with covalent cross-linking methods for the formation of mechanically tunable, biodegradable, heparinised hydrogels that can be distinguished by receptor-responsive rheology and delivery profiles. Toward these ends, they investigated methods to functionalise heparin with chemically reactive groups at controlled degrees of substitution, and demonstrated the rapid in situ cross-linking of this multifunctional heparin with thiol-derivatised PEGs of various molecular weights and polymer structures. The gels can be used as a controlled delivery vehicle for growth factors with activities useful for tissue regeneration and vascularisation (e.g. basic fibroblast growth factor).

In a different approach (Freudenberg et al. 2009), the defined and systematic variation of the biomolecular complexity and the mechanical characteristics of 3D-networks were achieved by cross-linking amino end-functionalised star-PEG with 1-ethyl-3-(3-dimethylaminopropyl) carbodiimid/N-hydroxysulfosuccinimid (EDC/sulfo-NHS) activated carboxylic groups of heparin (Fig. 4). As a key feature of this system, the variation of the cross-linking degree[3] allows to define the viscoelastic characteristics and swelling: Increased cross-linking density (gel type A to C) correlates with increased storage moduli and decreased swelling in PBS (Figs. 5 and 6). Beyond that, cross-linking controls the star-PEG and heparin content of the swollen gels: Higher degrees of cross-linking produced higher star-PEG contents of the gel while the heparin content remained rather constant

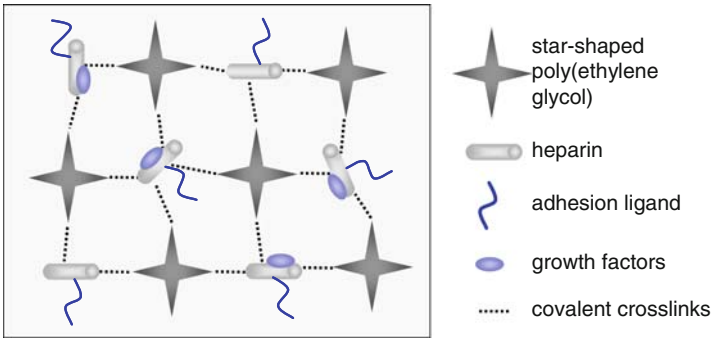

Fig. 4 Reaction of EDC/sulfo-NHS activated heparin with amine-end-functionalised star-PEG to form biohybrid gels. Gel materials are additionally modified with adhesion ligands (integrin binding RGD peptides) and loaded with soluble signalling molecules (growth factors, e.g. FGF-2). The covalent cross-links (dashed lines) could be replaced by use of enzymatically cleavable cross-links (e.g. matrix metalloprotease sensitive peptide sequences) to allow for remodelling of the matrix by invading cells

[3]The cross-linking degree of the gels was calculated based on the star-PEG and heparin amount in the rinsed gels. More precisely, the degree is counted for the heparin carboxylic acid groups assuming that in average 3 of the 4 amino groups of the remaining star-PEG molecules are bound to heparin.

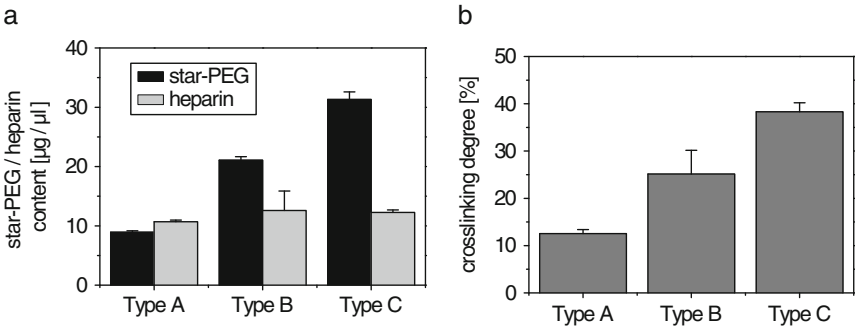

Fig. 5 Characterisation of different hydrogel materials (type A, B, C). (a) star-PEG and heparin content of the swollen gels; (b) cross-linking degree counted for the heparin carboxylic acid groups. Data are presented as mean ± root mean square deviation from $n = 4$

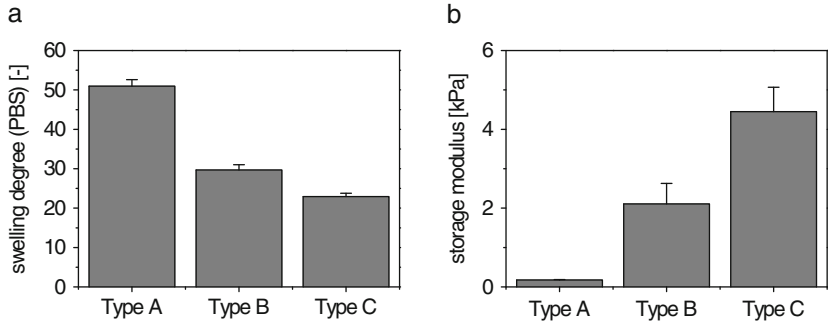

Fig. 6 Characterisation of different hydrogel materials (type A, B, C). (a) gravimetric swelling degree in PBS; (b) storage modulus of the gels obtained by rheological measurements. Data are presented as mean ± root mean square deviation from $n = 4$ (a) or $n = 3$ (b)

(Fig. 5). Furthermore, RGD peptides were covalently attached to EDC/sulfo-NHS activated carboxylic acid functionalities of heparin. A wide variety of growth factors (such as FGF-2) can be incorporated through noncovalent interactions with heparin (Freudenberg et al. 2009). Biofunctionalisation was found to correlate well with the heparin content of the structurally different materials (type A to C, Figs. 5 and 7), as shown for the attachment of adhesive ligands. This allows for an independent variation of mechanical properties at constant biomolecular characteristics.

The latter set of biohybrid gels was successfully demonstrated to stimulate growth and proliferation of different cell types in vitro and is currently applied to explore novel cell replacement strategies.

For example, the suitability of the gels to support the growth of endothelial cells was evaluated since endothelial cells play a crucial role in the sprouting of capillary blood microvascular vessels. A lack of vascularisation is a major obstacle for successful tissue engineering therapies, as it results in insufficient nutrient supply

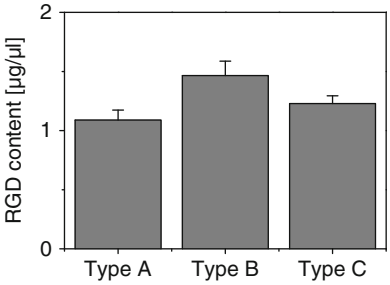

Fig. 7 Biofunctionalisation of different hydrogel materials (type A, B, C): amount of covalently attached RGD-peptides obtained by acid hydrolysis / HPLC analysis. Data are presented as mean ± root mean square deviation from $n = 4$

and waste removal, cell death as well as restricted tissue development or even loss (Boontheekul and Mooney 2003; Carmeliet 2003). The introduced biohybrid hydrogel system was considered a promising base for the adjustment of pro-angiogenic conditions as it permits a far-going structural and molecular adaptation to particular tissues and processes. In particular the materials could be used to mimic and modulate the bioadhesive nature of the ECM by incorporating RGD-peptides and to bind growth factors which control angiogenesis. Furthermore the two main building blocks heparin and star-PEG can be linked via MMP sensitive peptide units (Fig. 4). This additionally allows for the localised and enzyme controlled remodeling of the matrix by invading cells mimicking the proteolytic susceptibility of the ECM.

Human endothelial cells isolated from umbilical cord (HUVECs) were seeded on pure and RGD modified gels to determine the cell-adhesive characteristics of the compared materials. Cell adhesion and proliferation (or apoptosis) were observed by means of microscopic and colorimetric techniques.

Figure 8 shows representative bright field images of HUVECs on different gels after 4 days of culture (compared to fibronectin, FN). With increasing PEG content (Type B and Type C) cell attachment was reduced in line with the decreasing non-specific protein adsorption. However, covalent binding of RGD motifs to the materials with higher PEG-content (Type B and C) enabled cell adhesion. On the latter materials, HUVECs formed confluent cell layers which were morphologically similar to those on fibronectin coated substrates (see Fig. 8).

Live/dead staining[4] and MTT-assay[5] were used to quantify cell viability. RGD-functionalisation of gels with higher PEG content (e.g. gel Type B) resulted in an

[4]This assay is used to measure cell viability. It is a two-color fluorescence assay that simultaneously determines live (viable) and dead (nonviable) cells: Live cells have intracellular esterases that convert nonfluorescent, cell-permeable fluorescein di-O-acetate to the intensely fluorescent fluorescein (green). Cleaved fluorescein is retained within cells. Dead cells have damaged membranes; propidium iodide enters damaged cells and is fluorescent when bound to nucleic acids. It produces a bright red fluorescence in damaged or dead cells.

[5]Colorimetric MTT (tetrazolium) assay (Mosmann 1983) was used to quantify living cells. In short, yellow MTT (3-(4,5-dimethylthiazol-2-yl)-2,5-diphenyl tetrazolium bromide) is reduced to purple colored formazan in the mitochondria of living cells. The absorbance of the colored solution is analysed using a spectrophotometer allowing for quantification of living cells.

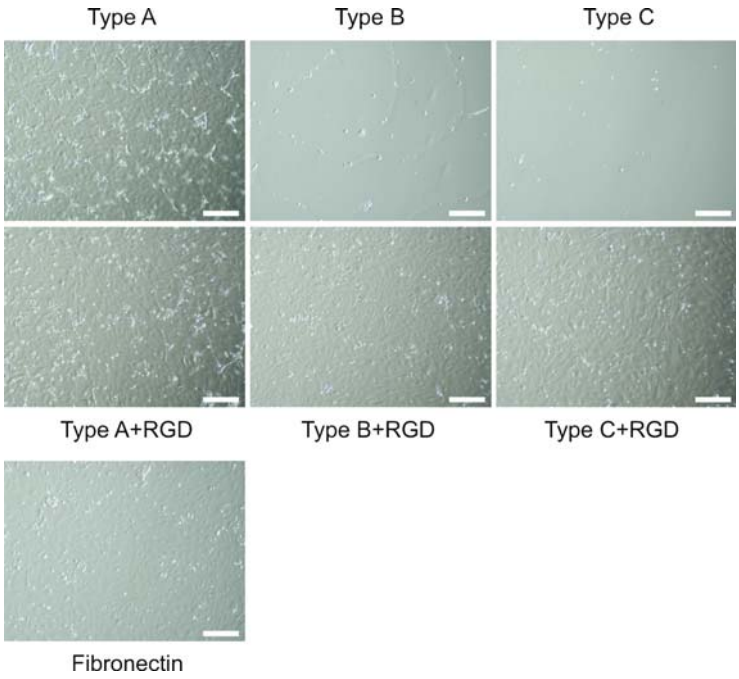

Fig. 8 Effect of PEG content and RGD modification on adhesion and proliferation of human endothelial cells: representative bright field images of 4 day old cell cultures on different substrates compared to fibronectin (FN). Scale bar 200 μm

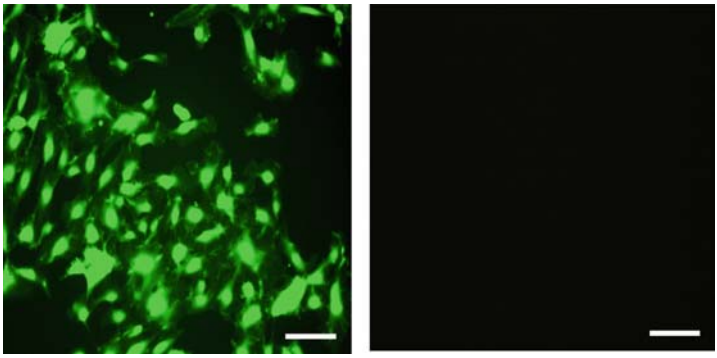

Fig. 9 Viability of human endothelial cells isolated from umbilical cord on RGD modified gels (here shown for Type B) monitored by the live/dead assay. Representative pictures shows live (fluorescein di-O-acetate, viable cells visible as light spots, left) and dead (propidium iodide, no dead cells visible, right) staining. Image after 1 day culture. Scale bar 200 μm

excellent cell viability as indicated by the bright green fluorescence produced by incorporated cleaved fluorescein (see live/dead staining, Fig. 9). No dead cells were detected. Thus, any acute toxicity of the gels could be excluded. These findings

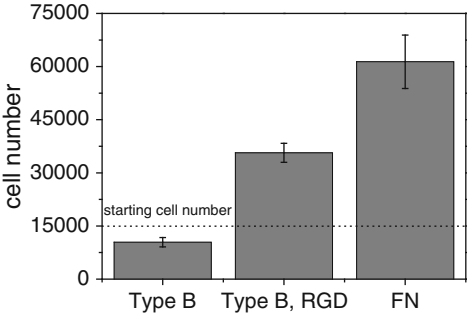

Fig. 10 Viability of human endothelial cells isolated from umbilical cord on unmodified, RGD-modified gels (here shown for Type B) and fibronectin (FN) reference monitored by the colorimetric MTT-(tetrazolium)-assay. MTT-assay was used to quantify living cells after 3 days in culture

were underpinned by data obtained from the MTT-assay for HUVECs grown for 3 days on unmodified, RGD-modified gels and fibronectin coated surfaces. While the number of living cells was decreasing in contact with the unmodified materials (see Fig. 10) functionalisation of the gels with adhesion ligands (RGD) resulted in a significant proliferation of the HUVECs (see Fig. 10).

These results clearly demonstrate how cell adhesion onto the developed set of biohybrid materials can be easily tuned through the choice of PEG-content and biomolecular functionalisation. More advanced functionalisation schemes additionally utilize non-covalent loading of growth and differentiation factors to locally induce the formation of capillary endothelial cell networks. Based on that, the novel biohybrid hydrogel can be expected to offer valuable extensions of various tissue engineering strategies.

4 Summary and Perspective

Polymer hydrogels can be instrumental for various novel therapeutic strategies which aim at exploiting the regenerative potential of cells. So far, synthetic polymer gels are utilised in that context for the design of cell culture carriers with functional thin film coatings to enable advanced culture techniques, such as harvesting cell sheets without enzymatic treatment. Beyond that, synthetic and biohybrid gels receive more and more interest as cell scaffolds for *in vivo* tissue engineering strategies, as for instance to establish injectable matrices for localised cell replacement.

Future work will concern more sophisticated polymer networks capable of switching complex sequences of developmental steps as required for the (re-) generation of specialised tissues and organs. For that aim, the structural and biomolecular complexity of hydrogel-based materials has to be increased and the characteristics of these future materials have to be temporally and spatially controlled. This will require advanced synthetic approaches which, in turn, have to be underpinned by powerful analytical strategies. Accordingly, the future research

on bioactive hydrogel materials similarly depends on progress in molecular life science and in the architecture of polymeric materials.

References

Benoit DSW, Anseth KS (2005) Heparin functionalized PEG gels that modulate protein adsorption for hMSC adhesion and differentiation. Acta Biomater 1:461–470

Benoit DSW, Durney AR, Anseth KS (2007) The effect of heparin-functionalized PEG hydrogels on three-dimensional human mesenchymal stem cell osteogenic differentiation. Biomaterials 28:66–77

Biederman H, Osada Y (1992) Plasma polymerization processes. Elsevier, Amsterdam

Boontheekul T, Mooney DJ (2003) Protein-based signaling systems in tissue engineering. Cur Opin Biotechn 14:559–565

Burdick JA, Anseth KS (2002) Photoencapsulation of osteoblasts in injectable RGD-modified PEG hydrogels for bone tissue engineering. Biomaterials 23:4315–4323

Burdick JA, Khademhosseini A, Langer R (2004) Fabrication of gradient hydrogels using a microfluidics/photopolymerization process. Langmuir 20:5153–5156

Canavan HE, Cheng XH, Graham DJ et al (2005) Cell sheet detachment affects the extracellular matrix: a surface science study comparing thermal liftoff, enzymatic, and mechanical methods. J Biomed Mater Res A 75:1–13

Capila I, Linhardt RJ (2002) Heparin-protein interactions. Angew Chem Int Ed 41:391–412

Carmeliet P (2003) Angiogenesis in health and disease. Nat Med 9:653–660

Chen GP, Imanishi Y, Ito Y (1998) Effect of protein and cell behavior on pattern-grafted thermoresponsive polymer. J Biomed Mater Res 42:38–44

Cheng XH, Canavan HE, Stein MJ et al (2005) Surface chemical and mechanical properties of plasma-polymerized N-isopropylacrylamide. Langmuir 21:7833–7841

Curti PS, de Moura MR, Veiga W et al (2005) Characterization of PNIPAAm photografted on PET and PS surfaces. Appl Surf Sci 245:223–233

Da Silva RMP, Mano JF, Reis RL (2007) Smart thermoresponsive coatings and surfaces for tissue engineering: switching cell-material boundaries. Trends Biotechnol 25:577–583

Delong SA, Mann BK, West JL (2002) Scaffolds modified with tethered growth factors to influence smooth muscle cell behavior. Faseb J 16:A36–A36

Discher DE, Janmey P, Wang YL (2005) Tissue cells feel and respond to the stiffness of their substrate. Science 310:1139–1143

Drury JL, Mooney DJ (2003) Hydrogels for tissue engineering: scaffold design variables and applications. Biomaterials 24:4337–4351

Fischbach C, Mooney DJ (2006) Polymeric systems for bioinspired delivery of angiogenic molecules. In: Werner C (ed) Polymers for regenerative medicine. Springer, Berlin Heidelberg, pp 191–221

Freudenberg U, Hermann A, Welzel PB et al (2009) A star PEG-heparin hydrogel platform to aid cell replacement therapies for neurodegenerative diseases. Biomatrials, in press, doi: 10.1016/j.biomaterials.2009.06.002

Götze T, Valtink M, Nitschke M et al (2008) Cultivation of an immortalized human corneal endothelial cell population and two distinct clonal subpopulations on thermo-responsive carriers. Graefes Arch Clin Exp Ophthalmol 246:1575–1583

Gramm S, Komber H, Schmaljohann D (2005) Copolymerization kinetics of N-isopropylacrylamide and diethylene glycol monomethylether monomethacrylate determined by online NMR spectroscopy. J Polym Sci Pol Chem 43:142–148

Hatakeyama H, Kikuchi A, Yamato M et al (2006) Bio-functionalized thermoresponsive interfaces facilitating cell adhesion and proliferation. Biomaterials 27:5069–5078

Hatakeyama H, Kikuchi A, Yamato M et al (2007) Patterned biofunctional designs of thermo-responsive surfaces for spatiotemporally controlled cell adhesion, growth, and thermally induced detachment. Biomaterials 28:3632–3643

Hern DL, Hubbell JA (1998) Incorporation of adhesion peptides into nonadhesive hydrogels useful for tissue resurfacing. J Biomed Mater Res 39:266–276

Huang J, Wang XL, Chen XZ et al (2003) Temperature-sensitive membranes prepared by the plasma-induced graft polymerization of N-isopropylacrylamide into porous polyethylene membranes. J Appl Polym Sci 89:3180–3187

Hutmacher DW, Garcia AJ (2005) Scaffold-based bone engineering by using genetically modified cells. Gene 347:1–10

Ide T, Nishida K, Yamato M et al (2006) Structural characterization of bioengineered human corneal endothelial cell sheets fabricated on temperature-responsive culture dishes. Biomaterials 27:607–614

Jia X, Kiick K (2009) Hybrid multicomponent hydrogels for tissue engineering. Macromol Biosci 9:140–156

Kanzaki M, Yamato M, Hatakeyama H et al (2006) Tissue engineered epithelial cell sheets for the creation of a bioartificial trachea. Tissue Eng 12:1275–1283

Kiick KL (2008) Peptide- and protein-mediated assembly of heparinized hydrogels. Soft Matter 4:29–37

Kolff WJ, Berk HTJ, ter Welle NM et al (1997) The artificial kidney: a dialyser with a great area. J Am Soc Nephrol 8:1959–1965

Kopecek J, Yang J (2009) Peptide-directed self-assembly of hydrogels. Acta Biomater 5:805–816

Kraehenbuehl TP, Zammaretti P, Van der Vlies AJ et al (2008) Three-dimensional extracellular matrix-directed cardioprogenitor differentiation: systematic modulation of a synthetic cell-responsive PEG-hydrogel. Biomaterials 29:2757–2766

Kwon OH, Kikuchi A, Yamato M et al (2000) Rapid cell sheet detachment from poly (N-isopropylacrylamide)-grafted porous cell culture membranes. J Biomed Mater Res 50:82–89

Kwon OH, Kikuchi A, Yamato M et al (2003) Accelerated cell sheet recovery by co-grafting of PEG with PIPAAm onto porous cell culture membranes. Biomaterials 24:1223–1232

Lai JY, Chen KH, Hsu WM et al (2006) Bioengineered human corneal endothelium for transplantation. Arch Ophthalmol 124:1441–1448

Liu YC, Cai SS, Shu XZ et al (2007) Release of basic fibroblast growth factor from a crosslinked glycosaminoglycan hydrogel promotes wound healing. Wound Repair Regen 15:245–251

Lutolf MP, Hubbell JA (2005) Synthetic biomaterials as instructive extracellular microenvironments for morphogenesis in tissue engineering. Nat Biotechnol 23:47–55

Lutolf MP, Lauer-Fields JL, Schmoekel HG et al (2003) Synthetic matrix metalloproteinase-sensitive hydrogels for the conduction of tissue regeneration: engineering cell-invasion characteristics. P Natl Acad Sci USA 100:5413–5418

Mann BK, Schmedlen RH, West JL (2001) Tethered-TGF-beta increases extracellular matrix production of vascular smooth muscle cells. Biomaterials 22:439–444

Matsuda N, Shimizu T, Yamato M et al (2007) Tissue engineering based on cell sheet technology. Adv Mater 19:3089–3099

Mosmann T (1983) Rapid colorimetric assay for cellular growth and survival- application to proliferation and cyto-toxicity assays. J Immun Met 65:55–63

Nie T, Baldwin A, Yamaguchi N et al (2007) Production of heparin-functionalized hydrogels for the development of responsive and controlled growth factor delivery systems. J Control Release 122:287–296

Nillesen STM, Geutjes PJ, Wismans R et al (2007) Increased angiogenesis and blood vessel maturation in acellular collagen-heparin scaffolds containing both FGF2 and VEGF. Biomaterials 28:1123–1131

Nishida K, Yamato M, Hayashida Y et al (2004) Functional bioengineered corneal epithelial sheet grafts from corneal stem cells expanded ex vivo on a temperature-responsieve cell culture surface. Transplantation 77:379–385

Nitschke M, Zschoche S, Baier A et al (2004) Low pressure plasma immobilization of thin hydrogel films on polymer surfaces. Surf Coat Technol 185:120–125

Nitschke M, Gramm S, Götze T et al (2007a) Thermo-responsive poly(NiPAAm-co-DEGMA) substrates for gentle harvest of human corneal endothelial cell sheets. J Biomed Mater Res A 80:1003–1010

Nitschke M, Götze T, Gramm S et al (2007b) Detachment of human endothelial cell sheets from thermo-responsive poly(NiPAAm-co-DEGMA) carriers. Express Polym Lett 1:660–666

Pan YV, Wesley RA, Luginbuhl R et al (2001) Plasma polymerized N-isopropylacrylamide: synthesis and characterization of a smart thermally responsive coating. Biomacromolecules 2:32–36

Peppas NA, Hilt JZ, Khademhosseini A et al (2006) Hydrogels in biology and medicine: from molecular principles to bionanotechnology. Adv Mater 18:1345–1360

Pratt AB, Weber FE, Schmoekel HG et al (2004) Synthetic extracellular matrices for in situ tissue engineering. Biotechnol Bioeng 86:27–36

Pridgen EM, Langer R, Farokhzad OC (2007) Biodegradable, polymeric nanoparticle delivery systems for cancer therapy. Nanomedicine 2:669–680

Rzaev ZMO, Dincer S, Piskin E (2007) Functional copolymers of N-isopropylacrylamide for bioengineering applications. Prog Polym Sci 32:534–595

Schild HG (1992) Poly (N-Isopropylacrylamide) – experiment, theory and application. Prog Polym Sci 17:163–249

Schmaljohann D, Nitschke M, Beyerlein D et al (2003a) Thermo-reversible swelling of plasma immobilized hydrogel films. Polymer Preprints 44:196–197

Schmaljohann D, Oswald J, Jorgensen B et al (2003b) Thermo-responsive PNiPAAm-g-PEG films for controlled cell detachment. Biomacromolecules 4:1733–1739

Schmaljohann D, Beyerlein D, Nitschke M et al (2004) Thermo-reversible swelling of thin hydrogel films immobilized by low-pressure plasma. Langmuir 20:10107–10114

Schmaljohann D, Nitschke M, Schulze R et al (2005) In situ study of the thermoresponsive behavior of micropatterned hydrogel films by imaging ellipsometry. Langmuir 21: 2317–2322

Seal BL, Panitch A (2003) Physical polymer matrices based on affinity interactions between peptides and polysaccharides. Biomacromolecules 4:1572–1582

Seal BL, Panitch A (2006) Viscoelastic behavior of environmentally sensitive biomimetic polymer matrices. Macromolecules 39:2268–2274

Shimizu T, Yamato M, Isoi Y et al (2002) Fabrication of pulsatile cardiac tissue grafts using a novel 3-dimensional cell sheet manipulation technique and temperature-responsive cell culture surfaces. Circ Res 90:E40–E48

Silva GA, Czeisler C, Niece KL et al (2004) Selective differentiation of neural progenitor cells by high-epitope density nanofibers. Science 303:1352–1355

Stamov D, Grimmer M, Salchert K et al (2008) Heparin intercalation into reconstituted collagen I fibrils: impact on growth kinetics and morphology. Biomaterials 29:1–14

Tae G, Scatena M, Stayton PS et al (2006) PEG-cross-linked heparin is an affinity hydrogel for sustained release of vascular endothelial growth factor. J Biomat Sci Polym E 17:187–197

Takezawa T, Mori Y, Yoshizato K (1990) Cell-culture on a thermoresponsive polymer surface. Bio-Technology 8:854–856

Tessmar JK, Gopferich AM (2007) Customized PEG-derived copolymers for tissue-engineering applications. Macromol Biosci 7:23–39

Tsuda Y, Kikuchi A, Yamato M et al (2004) Control of cell adhesion and detachment using temperature and thermoresponsive copolymer grafted culture surfaces. J Biomed Mater Res A 69:70–78

Tsuda Y, Kikuchi A, Yamato M et al (2005) The use of patterned dual thermoresponsive surfaces for the collective recovery as co-cultured cell sheets. Biomaterials 26:1885–1893
Tsuda Y, Shimizu T, Yarnato M et al (2007) Cellular control of tissue architectures using a three-dimensional tissue fabrication technique. Biomaterials 28:4939–4946
Van Tomme SR, Hennink WE (2007) Biodegradable dextran hydrogels for protein delivery applications. Expert Rev Med Devic 4:147–164
von Recum H, Okano T, Kim SW (1998) Growth factor release from thermally reversible tissue culture substrates. J Control Release 55:121–130
Werner C (ed) (2006) Polymers for regenerative medicine. Springer, Berlin Heidelberg
West JL, Hubbell JA (1999) Polymeric biomaterials with degradation sites for proteases involved in cell migration. Macromolecules 32:241–244
Wichterle O, Lim D (1960) Hydrophilic gels for biological use. Nature 185:117–118
Yamada N, Okano T, Sakai H et al (1990) Thermo-responsive polymeric surfaces; control of attachment and detachment of cultured cells. Macromol Chem Rapid Commun 11:571–576
Yamaguchi N, Kiick KL (2005) Polysaccharide-poly(ethylene glycol) star copolymer as a scaffold for the production of bioactive hydrogels. Biomacromolecules 6:1921–1930
Yamaguchi N, Chae BS, Zhang L et al (2005) Rheological characterization of polysaccharide-poly (ethylene glycol) star copolymer hydrogels. Biomacromolecules 6:1931–1940
Yamaguchi N, Zhang L, Chae BS et al (2007) Growth factor mediated assembly of cell receptor-responsive hydrogels. J Am Chem Soc 129:3040–3041
Yamato M, Akiyama Y, Kobayashi H et al (2007) Temperature-responsive cell culture surfaces for regenerative medicine with cell sheet engineering. Prog Polym Sci 32:1123–1133
Zhang L, Furst EM, Kiick KL (2006) Manipulation of hydrogel assembly and growth factor delivery via the use of peptide-polysaccharide interactions. J Control Release 114:130–142

Index